# Assessing sensorimotor plasticity with multimodal magnetic resonance imaging




**James Kolasinski**

A thesis submitted for the degree of Doctor of Philosophy

Lady Margaret Hall

University of Oxford

October 2014

# Contents

**1 Introduction** **1**

1.1 The sensorimotor network . . . . . 1

1.1.1 Divisions of the cerebral cortex . . . . . 1

1.1.2 Localisation of sensorimotor cortex . . . . . 3

1.1.3 The postcentral somatic sensory system . . . . . 7

1.1.3.1 Peripheral receptors . . . . . 7

1.1.3.2 The dorsal column pathway . . . . . 9

1.1.3.3 Remapping afferent inputs: modality and topography 10

1.1.3.4 Primary somatosensory cortex . . . . . 10

1.1.3.5 Higher order sensory areas . . . . . 12

1.1.4 The precentral motor system . . . . . 15

1.1.4.1 Primary motor cortex: Brodmann area 4 . . . . . 16

1.1.4.2 Brodmann area 6 . . . . . 17

1.1.4.3 Lateral Brodmann area 6: premotor cortex . . . . . 17

1.1.4.4 Medial Brodmann area 6: supplementary motor cortex 18

1.1.4.5 Subcortical motor control . . . . . 19

1.1.4.6 Descending motor efferents . . . . . 20

1.1.5 Concepts of somatotopy . . . . . 24

1.1.5.1 Somatotopy and the primary somatosensory cortex . 25

1.1.5.2 Somatotopy and the primary motor cortex . . . . . 29

1.1.6 The human hand: a special case . . . . . 30

1.2 Principles of plasticity . . . . . 35

1.2.1 Synaptic transmission . . . . . 35
1.2.2 Hebbian theory of synaptic plasticity . . . . . 36
1.2.3 Long term potentiation and depression . . . . . 37
1.3 Defining plastic change . . . . . 38
1.4 Plasticity and the sensorimotor network . . . . . 39
1.4.1 Normal variation in somatotopy . . . . . 40
1.4.2 Usage-dependent plasticity . . . . . 41
1.4.2.1 Plasticity and disuse . . . . . 42
1.4.3 Experience-dependent plasticity . . . . . 43
1.4.3.1 Motor learning . . . . . 43
1.4.3.2 Sensorimotor training . . . . . 44
1.5 Sensorimotor stroke . . . . . 47
1.5.1 Focal cerebral ischaemia . . . . . 47
1.5.1.1 Aetiology . . . . . 47
1.5.1.2 Pathophysiology . . . . . 47
1.5.2 Stroke recovery . . . . . 49
1.5.2.1 Mechanisms of stroke recovery . . . . . 49
1.5.2.2 Time course of stroke recovery . . . . . 50
1.5.2.3 Motor rehabilitation for stroke . . . . . 51
1.6 Aims . . . . . 52

**2 Methods of imaging the sensorimotor network 54**

2.1 Principles of nuclear magnetic resonance . . . . . 54
2.1.1 The nuclear moment . . . . . 55
2.1.2 Spin excitation and relaxation . . . . . 56
2.1.3 T1, T2 and T2* . . . . . 56
2.2 Magnetic resonance imaging acquisition . . . . . 60
2.2.1 Image contrast . . . . . 60
2.2.2 Slice selection and spatial encoding . . . . . 62

2.3 Structural MRI . . . . . 64
2.3.1 T1-weighted MRI . . . . . 64
2.3.2 T2-weighted MRI . . . . . 64
2.4 BOLD fMRI . . . . . 65
2.4.1 Neurovascular coupling . . . . . 65
2.4.2 The BOLD signal . . . . . 66
2.4.3 Components of the BOLD signal . . . . . 67
2.4.4 Echo Planar Imaging . . . . . 69
2.5 Diffusion-weighted MRI . . . . . 69
2.5.1 Diffusion artefacts . . . . . 70
2.5.1.1 Eddy currents . . . . . 71
2.5.1.2 Magnetic field inhomogeneities . . . . . 71
2.5.1.3 Gradient non-linearities . . . . . 71
2.5.1.4 Bulk motion . . . . . 72
2.5.2 Diffusion tensor imaging . . . . . 72
2.5.2.1 Fractional anisotropy . . . . . 73
2.5.2.2 Mean diffusivity . . . . . 73
2.5.2.3 Radial diffusivity . . . . . 74
2.5.3 Diffusion and neural tissue . . . . . 74
2.5.4 Diffusion-weighted MRI and non-isotropic voxel dimensions . 75
2.6 Imaging at ultra-high field . . . . . 75
2.6.1 Origins of ultra-high field imaging . . . . . 76
2.6.2 BOLD fMRI at ultra-high field . . . . . 77
2.6.3 The BOLD signal at ultra-high field . . . . . 77
2.6.4 Special considerations for ultra-high field fMRI . . . . . 78
2.6.4.1 Brain coverage . . . . . 79
2.6.4.2 Motion artefact . . . . . 79
2.6.4.3 Field inhomogeneity . . . . . 80
2.6.4.4 Specific absorption rate . . . . . 81

2.6.4.5 Participant experience . . . . . 81
2.7 MRI analysis . . . . . 84
2.7.1 fMRI preprocessing . . . . . 84
2.7.1.1 Motion correction . . . . . 84
2.7.1.2 Spatial smoothing . . . . . 84
2.7.1.3 Temporal filtering . . . . . 85
2.7.2 Task fMRI . . . . . 85
2.7.2.1 General Linear Model . . . . . 85
2.7.2.2 Phase-encoding . . . . . 87
2.7.3 Resting-state fMRI . . . . . 88
2.7.3.1 Acquisition and preprocessing . . . . . 88
2.7.3.2 Model-free analysis: MELODIC ICA . . . . . 89
2.7.4 Diffusion-weighted MRI . . . . . 89
2.7.5 Structural MRI . . . . . 90
2.7.5.1 Voxel-Based Morphometry . . . . . 90
2.7.5.2 Longitudinal within-subject VBM analysis . . . . . 91
2.7.6 MRI registration methods . . . . . 92
2.7.6.1 FLIRT . . . . . 92
2.7.6.2 FNIRT . . . . . 93
2.8 Transcranial magnetic stimulation . . . . . 96

**3 Resolving digit somatotopy in primary somatosensory cortex with fMRI at 7 tesla 97**

3.1 Introduction and rationale . . . . . 97
3.2 Methods . . . . . 100
3.2.1 Participants . . . . . 100
3.2.2 Experimental design . . . . . 100
3.2.3 MRI acquisition . . . . . 101
3.2.4 fMRI tasks . . . . . 102
3.2.5 MRI analysis . . . . . 104

3.2.5.1 Image preprocessing . . . 104
3.2.5.2 Image registration . . . 104
3.2.5.3 Phase-encoding task analysis . . . 107
3.2.5.4 Block task analysis . . . 109
3.2.5.5 Surface projection . . . 111
3.2.5.6 Statistics . . . 111
3.3 Results . . . 114
3.3.1 Phase-encoding design digit maps . . . 114
3.3.2 Block design digit maps . . . 115
3.3.3 Concurrence of phase-encoding and block maps . . . 119
3.3.4 Reproducibility of phase-encoding digit maps . . . 119
3.4 Discussion . . . 126
3.4.1 Primary somatosensory cortex maps . . . 126
3.4.2 Concurrence of maps from phase-encoding and block design tasks 127
3.4.3 Digit map reproducibility . . . 128
3.4.4 Digit mapping paradigm . . . 129
3.5 Conclusions . . . 130

**4 Mapping short-term experience-dependent plasticity in digit somatotopy 132**

4.1 Introduction and rationale . . . 132
4.2 Methods . . . 134
4.2.1 Participants . . . 134
4.2.2 Experimental design . . . 134
4.2.3 MRI acquisition . . . 135
4.2.4 Topographic mapping task . . . 135
4.2.5 MRI analysis . . . 136
4.2.5.1 Surface projection and profile plots . . . 137
4.2.5.2 Overlap measures and statistics . . . 137
4.3 Results . . . 140

4.3.1 Digit profile plots of in Brodmann area 3b . . . . . 140
4.3.2 The gluing manipulation and digit overlap . . . . . 140
4.4 Discussion . . . . . 147
4.4.1 Remapping and plasticity . . . . . 147
4.4.2 Neural mechanisms of remapping . . . . . 150
4.4.3 Excitatory and inhibitory balance and remapping . . . . . 151
4.4.4 Remapping in context . . . . . 151
4.5 Conclusions . . . . . 152

**5 Investigating maladaptive plasticity associated with chronic disuse of the upper limb 153**

5.1 Introduction and rationale . . . . . 153
5.2 Methods . . . . . 155
5.2.1 Participants . . . . . 156
5.2.2 Experimental design . . . . . 156
5.2.3 MRI acquisition . . . . . 156
5.2.4 Clinical measures . . . . . 157
5.2.5 MRI analysis . . . . . 157
5.2.5.1 Grey matter voxel-based morphometry analysis . . . 157
5.2.5.2 White matter analysis . . . . . 159
5.2.6 Statistics . . . . . 160
5.3 Results . . . . . 162
5.3.1 Native space grey matter voxel-based morphometry results . . 162
5.3.2 Grey matter voxel-based morphometry results relative to the side of tear . . . . . 166
5.3.3 White matter results . . . . . 168
5.3.4 Correspondence of grey matter and white matter results . . . 172
5.4 Discussion . . . . . 176
5.4.1 The ventral attention network . . . . . 176
5.4.2 Spatial attention and disuse . . . . . 178

5.4.3 Relating grey matter and white matter integrity . . . . . 179
5.4.4 Right posterior hippocampus and spatial localisation . . . . . 180
5.4.5 Limitations and future directions . . . . . 180
5.5 Conclusions . . . . . 182

**6 Assessing the imaging markers of functional recovery after chronic upper limb disuse 183**

6.1 Introduction and rationale . . . . . 183
6.2 Methods . . . . . 185
6.2.1 Participants . . . . . 185
6.2.2 Experimental design . . . . . 186
6.2.3 Exercise rehabilitation intervention . . . . . 187
6.2.4 MRI acquisition . . . . . 187
6.2.5 Clinical measures . . . . . 188
6.2.6 Longitudinal grey matter voxel-based morphometry . . . . . 188
6.2.7 Longitudinal white matter analysis . . . . . 189
6.2.8 Statistics . . . . . 189
6.3 Results . . . . . 189
6.3.1 Changes in clinical measures . . . . . 190
6.3.2 Grey matter changes . . . . . 190
6.3.3 Longitudinal white matter results . . . . . 194
6.3.4 Relating behavioural and grey matter changes . . . . . 194
6.4 Discussion . . . . . 196
6.4.1 Plasticity and the right ventral attention network . . . . . 197
6.4.2 Orbitofrontal cortex and sensory reinforcers . . . . . 198
6.4.3 Insular cortex and changes in pain . . . . . 199
6.4.4 Limitations and future directions . . . . . 199
6.5 Conclusions . . . . . 200

**7 Investigating candidate imaging biomarkers of motor function in**

**sub-acute stroke** **202**

7.1 Introduction and rationale . . . . . 202

7.2 Methods . . . . . 205

7.2.1 Patients . . . . . 205

7.2.2 MRI acquisition . . . . . 207

7.2.3 Motor function measures . . . . . 208

7.2.3.1 Wolf motor function test . . . . . 208

7.2.3.2 Pinch grip measures . . . . . 208

7.2.4 TMS measures . . . . . 208

7.2.5 MRI analysis . . . . . 209

7.2.5.1 Data aligment relative to stroke hemisphere . . . . . 209

7.2.5.2 Image registration . . . . . 209

7.2.5.3 Lesion masking . . . . . 210

7.2.5.4 Diffusion-weighted MRI analysis . . . . . 210

7.2.5.5 Resting state fMRI analysis . . . . . 212

7.2.6 Statistics . . . . . 213

7.3 Results . . . . . 213

7.3.1 CST-lesion overlap measures . . . . . 214

7.3.2 CST FA asymmetry . . . . . 215

7.3.3 Sensorimotor network strength . . . . . 216

7.4 Discussion . . . . . 217

7.4.1 Structural measures of CST disruption . . . . . 218

7.4.2 Sensorimotor network connectivity and stroke . . . . . 219

7.4.3 Diffusion measures of CST integrity . . . . . 221

7.4.4 Limitations and future directions . . . . . 222

7.5 Conclusions . . . . . 222

**8 Conclusions and future directions** **224**

8.1 Overview of the thesis . . . . . 224

8.2 Future directions . . . . . 227

8.2.1 Behavioural correlates of digit remapping . . . . . 227
8.2.2 Modifying digit mapping paradigms . . . . . 229
8.2.3 Spatial attention, the body schema and disuse . . . . . 229
8.3 General conclusions . . . . . 230

**Appendices** **264**

**A Edinburgh Handedness Inventory** **265**

**B Oxford Shoulder Score Questionnaire** **267**

**C Brief Pain Inventory: Short Form** **271**

# List of Figures


1.1 Brodmann's cytoarchitectonic parcellation of the human cerebral cortex 2

1.2 Major cortical components of the sensorimotor network . . . . . 3

1.3 Ferrier's proposed localisation of cortical function in humans . . . . . 6

1.4 The dorsal-column medial-lemniscal pathway . . . . . 13

1.5 The somatosensory afferent system . . . . . 14

1.6 Efferent output from the primary motor cortex . . . . . 22

1.7 Descending corticospinal motor efferents . . . . . 23

1.8 Penfield's early maps of sensory and motor somatotopy . . . . . 25

1.9 Topography of somatotosensory cortex from human surgical mapping 26

1.10 The sensory and motor homunculi . . . . . 27

1.11 Somatotopic map of Brodmann areas 3a and 1 in cynomolgus monkey 32

1.12 BOLD fMRI tactile and kinaesthetic activation maps . . . . . 33

1.13 Innervation densities of mechanoreceptive afferent fibres in the hand 34

1.14 Individual variability in microelectrode maps of primate area 3b . . . . 41

1.15 Individual variability in high-field fMRI maps of primate area 3b . . 42

1.16 Remapping of the primary motor cortex after motor learning . . . . 44

1.17 Experience-dependent remapping of area 3b digit representations . . 46

2.1 Spin alignment and precession under an applied magnetic field $B_0$ . . 58

2.2 Spin relaxation: the growth and decay of longitudinal and transverse magnetisation . . . . . 59

2.3 Recovery and decay curves of neural tissue . . . . . 63

2.4 Structural MRI: common imaging contrasts . . . . . 65
2.5 Methods of functional brain mapping . . . . . 66
2.6 The haemodynamic response . . . . . 68
2.7 Diffusion-weighted EPI sequence . . . . . 71
2.8 The growth of 7T MRI worldwide . . . . . 76
2.9 Comparing the BOLD signal at varying field strengths . . . . . 78
2.10 BOLD EPI coverage versus repetition time at 7 tesla . . . . . 80
2.11 Motion susceptibility of ultra-high resolution BOLD EPI data . . . . 82
2.12 Field inhomogeneity . . . . . 83
2.13 Overview of phase-encoding analysis . . . . . 94
2.14 Boundary-based registration in FLIRT . . . . . 95

3.1 Overview of digit topography study design . . . . . 101
3.2 Task fMRI EPI coverage . . . . . 103
3.3 Task fMRI button box . . . . . 104
3.4 Overview of fMRI phase-encoding design . . . . . 105
3.5 Overview of fMRI block task design . . . . . 106
3.6 Registration of a limited FOV BOLD EPI data to structural space . 109
3.7 Phase-encoding digit representations: volumetric space . . . . . 111
3.8 Phase-encoding digit representations: surface space . . . . . 112
3.9 BOLD signal time course from phase-encoding digit representations . 113
3.10 Phase-encoding cross-correlation as a function of lag in digit representations . . . . . 114
3.11 Comparison of phase-encoding and block task GLM-derived digit representations (i) . . . . . 116
3.12 Comparison of phase-encoding and block task GLM-derived digit representations (ii) . . . . . 117
3.13 Statistical agreement of phase-encoding and block task general linear model (GLM)-derived digit representations . . . . . 118
3.14 Comparison of phase-encoding digit representations over time . . . . 120

3.15 Assessing the reproducibility of phase-encoding derived digit representations . . . 121

4.1 Overview of digit plasticity study design . . . 135
4.2 Brodmann area 3b axes along the central sulcus . . . 138
4.3 Overview of digit profile plot overlap metrics . . . 139
4.4 Example digit profile plots across individual subjects and sessions . . . 141
4.5 Average overlap between adjacent digits . . . 142
4.6 The gluing manipulation causes changes in the overlap between adjacent digit representations . . . 144
4.7 The gluing manipulation does not affect the peak $z$-statistic of each digit profile . . . 145
4.8 The gluing manipulation does not affect the area of each digit profile 146

5.1 The anatomy of the rotator cuff . . . 155
5.2 Patients with chronic disuse of the upper limb show localised differences in grey matter density compared to control subjects . . . 163
5.3 Clusters of lower grey matter density in patients compared to control subjects . . . 164
5.4 Grey matter density in posterior right superior temporal gyrus is strongly correlated with shoulder function in patients . . . 165
5.5 Grey matter density in sensorimotor cortex contralateral to rotator cuff tear shows no difference in grey matter density in patients compared with control subjects . . . 167
5.6 Probabilistic tractography seeded in posterior right superior temporal gyrus VBM cluster . . . 169
5.7 Posterior right superior temporal gyrus VBM cluster shows strong anatomical connectivity to right superior longitudinal fasciculus . . . 170
5.8 Right superior longitudinal fasciculus shows reduced white matter integrity in patients compared with controls . . . 171

5.9 Radial diffusivity in right superior longitudinal fasciculus is strongly correlated with shoulder function in the patient group . . . . . 172
5.10 Radial diffusivity in right superior longitudinal fasciculus is correlated with grey matter density in posterior right STG in the patient group 173

6.1 Overview of the longitudinal rehabilitation study design . . . . . 186
6.2 The exercise rehabilitation intervention results in improvements in shoulder function . . . . . 191
6.3 The exercise rehabilitation intervention is associated with localised increases in grey matter density . . . . . 192
6.4 Comparison of grey matter voxel-based morphometry results identified in cross-sectional and longitudinal analysis . . . . . 193
6.5 Greater improvements in shoulder function are associated with greater increases in right superior temporal gyrus grey matter density in rehabilitation responders . . . . . 195

7.1 Overview of candidate imaging markers in the sensorimotor network 206
7.2 Overview of the ischaemic lesion location in the patient group . . . . 213
7.3 Correlations between CST-lesion cross-section and motor function . . 214
7.4 Correlations between CST-lesion overlap and motor function . . . . . 215
7.5 Correlations between CST FA asymmetry and measures of motor function 216
7.6 Correlations between the strength of the sensorimotor network and measures of motor function . . . . . 217

# List of Tables


1.1 Overview of peripheral mechanoreceptors . . . . . 8

1.2 Overview of peripheral proprioceptors . . . . . 9

2.1 Overview of relative T1 and T2 values of different tissue components . 61

3.1 $z$-statistic thresholds for the phase-encoding digit representations . . 123

3.2 $z$-statistic thresholds for the block design digit representations . . . . 124

3.3 Comparison of phase-encoding and block task digit representations . 125

4.1 The gluing manipulation and overlap between adjacent digits: post-hoc paired samples $t$-tests . . . . . 143

5.1 Summary of patient and control subject demographic information and clinical scores . . . . . 161

5.2 Summary of significant clusters from grey matter VBM analysis . . . 166

5.3 Partial correlations: relating behavioural measures and MRI-derived metrics . . . . . 175

6.1 Actual and projected scan figures for longitudinal exercise rehabilitation study . . . . . 185

6.2 Summary of significant clusters from longitudinal grey matter VBM analysis . . . . . 194

6.3 Summary of OSS changes associated with exercise rehabilitation intervention . . . . . 196

# Acronyms

| | |
|---|---|
| ATP | adenosine trisphosphate. |
| BBR | Boundary Based Registration. |
| BET | Brain Extraction Tool. |
| BOLD | blood oxygenation level dependent. |
| BPI | Brief Pain Inventory. |
| CIMT | constraint induced motor therapy. |
| CMRR | Centre for Magnetic Resonance Research. |
| COPE | contrast of parameter estimate. |
| CSF | cerebrospinal fluid. |
| CST | corticospinal tract. |
| DOF | degrees of freedom. |
| DTI | diffusion tensor imaging. |
| EMG | electromyography. |
| EPI | echo planar imaging. |
| EPSP | excitatory postsynaptic potentials. |
| FA | fractional anisotropy. |
| FAST | FMRIB's Automated Segmentation Tool. |
| FDR | false discovery rate. |
| FDT | FMRIB's Diffusion Toolbox. |
| FEAT | fMRI Expert Analysis Tool. |
| FID | free induction decay. |
| FILM | FMRIB's Improved Linear Model. |

| | |
|---|---|
| FLIRT | FMRIB's Linear Image Registration Tool. |
| fMRI | functional magnetic resonance imaging. |
| FNIRT | FMRIB's Nonlinear Image Registration Tool. |
| FOV | field of view. |
| FSE | fast spin echo. |
| FSL | FMRIB Software Library. |
| FSPGR | fast spoiled gradient echo. |
| FST | functional strength training. |
| FWHM | full-width half-maximum. |
| GABA | gamma-aminobutyric acid. |
| GE | gradient echo. |
| GIFTI | Geometry Informatics Technology Initiative. |
| GLM | general linear model. |
| GM | grey matter. |
| GRF | Gaussian random field. |
| HHb | deoxyhaemoglobin. |
| HR | haemodynamic response. |
| HRF | haemodynamic response function. |
| ICA | Independent Components Analysis. |
| ICMS | intracortical microstimulation. |
| ILF | inferior longitudinal fasciculus. |
| LTD | long term depression. |
| LTP | long term potentiation. |
| $M_0$ | net magnetisation. |
| MCFLIRT | Motion Correction using FMRIB's Linear Image Registration Tool. |
| MD | mean diffusivity. |
| MDM | magnetic dipole moment. |
| MEG | magnetoencephalography. |

| | |
|---|---|
| MELODIC | Multivariate Exploratory Linear Optimized Decomposition into Independent Components. |
| MEMPRAGE | multi echo magnetisation prepared rapid gradient echo. |
| MEPs | motor evoked potentials. |
| MIRCT | massive irreparable rotator cuff tear. |
| MNI | Montreal Neurological Institute. |
| MP2RAGE | magnetization prepared 2 rapid acquisition gradient echo. |
| MPRAGE | magnetisation prepared rapid gradient echo. |
| MRI | magnetic resonance imaging. |
| NHS | National Health Service. |
| NMDA | *N*-methyl-D-aspartate. |
| NMR | nuclear magnetic resonance. |
| NO | nitric oxide. |
| $O_2Hb$ | oxyhaemoglobin. |
| OFC | orbitofrontal cortex. |
| OSS | Oxford Shoulder Score. |
| PE | parameter estimate. |
| PET | positron emission tomography. |
| RCT | randomised control trial. |
| RD | radial diffusivity. |
| RF | radio frequency. |
| ROI | region of interest. |
| rTMS | repetitive transcranial magnetic stimulation. |
| SAR | specific absorption rate. |
| SE | spin echo. |
| SLF | superior longitudinal fasciculus. |
| SMG | supramarginal gyrus. |
| SNARE | soluble *N*-ethylmaleimide-sensitive factor attachment protein receptor. |
| SNR | signal-to-noise ratio. |

| | |
|---|---|
| STG | superior temporal gyrus. |
| STS | superior temporal sulcus. |
| TE | echo delay time. |
| TMS | transcranial magnetic stimulation. |
| TPJ | temporoparietal junction. |
| TR | repetition time. |
| UHF | ultra-high field. |
| USFDA | United States Food and Drugs Administration. |
| VA | ventroanterior nucleus of the thalamus. |
| VBM | voxel-based morphometry. |
| VFC | ventral frontal cortex. |
| VL | ventrolateral nucleus of the thalamus. |
| VPL | ventro-posterolateral nucleus of the thalamus. |
| WM | white matter. |
| WMFT | Wolf motor function test. |

# Publications arising and supplementary work

During the first year of my doctoral studies I undertook a period of nine months as the von Clemm fellow at Harvard University. During this period I worked in the Laboratory for Computational Neuroimaging at Massachusetts General Hospital, supervised by Dr Lilla Zollei and Dr Bruce Fischl, in collaboration with Dr P. Ellen Grant and Dr Emi Takahashi at Boston Children's Hospital. I worked on a project applying post-mortem diffusion-weighted MRI to study human fetal neurodevelopment.

This period of study in a different laboratory setting was extremely useful in terms of developing new image analysis skills, and bridging the gap between undergraduate and graduate studies. The manuscript arising from this period was published in the journal Neuroimage, where it featured on the cover in October 2013. The fetal imaging data contained in this manuscript are not in keeping with the general theme of this thesis, and have therefore been omitted. The data and supplementary material are available in published form under the following citation:

Kolasinski, J., Takahashi, E., Stevens, A. A., Benner, T., Fischl, B., Zollei, L., Grant, P. E. (2013). Radial and tangential neuronal migration pathways in the human fetal brain: Anatomically distinct patterns of diffusion MRI coherence. NeuroImage, 79, 412?422. doi:10.1016/j.neuroimage.2013.04.125

The data presented in chapters 3 to 5 are currently being prepared for submission for publication in peer-reviewed journals.

# Acknowedgements

My DPhil thesis would not have been possible without the continued support of a great many people, both in Oxford and elsewhere. My sincere thanks go to the following:

Most importantly to the individuals who agreed to be scanned as a part of the various studies presented in this thesis, many of whom willingly allowed me to glue together their fingers in the name of science.

To my truly wonderful co-supervisors, Heidi Johansen-Berg and Charlotte J. Stagg.

To Heidi in particular for offering enthusiastic and constructive ideas every step of the way, for understanding my own data better than I do within the first five minutes of a meeting, and for forgiving me for losing my laptop!

To Charlie in particular for her ongoing support, enthusiasm, and critical eye. And more importantly, for sending me an email on 10th February 2010, asking if I "might be interested in doing some imaging". Exactly 56 months later, still under her guidance, I am submitting my doctoral thesis.

To the Nuffield Department of Clinical Neurosciences, Lady Margaret Hall, the Martin Wronker/Cephalosporin scholarship, and the Wellcome Trust for funding my studies.

To Veronica Conboy, Bobby Ainsworth, Douglas Natusch and Claire Burcham in Torbay for acquiring the data presented in chapters 5 and 6.

To Torbay Hospital Charitable Trust for funding the research presented in chapters 5 and 6.

To the many people involved in the multi-centre FAST INdICATE trial for collecting the data presented in chapter 7.

To Adam Thomas for being an all-round analysis guru, and a fellow gin enthusiast.

To Tamar Makin for introducing me to somatosensory cortex, though I fear I will never be ready to let go of motor cortex altogether.

To Nancy Rawlings for for diligently proof-reading my entire thesis, and for keeping everyone in the plasticity lab organised and on-track.

To Mike Sanders and Jon Campbell for dealing with my awkward scan protocol and very specific slice placement needs.

To Stuart Clare for his help in setting up the fMRI protocols for chapters 3 and 4, and for his ready advice ever since.

To Saad Jbabdi for his assistance with the surface-based analysis of the fMRI data presented in chapters 3 and 4.

To Pierre Vila for his assistance with stroke lesion masking.

To Paul McAllister (1970 - 2014), for his generosity, enthusiasm, and for being a true inspiration.

To Robert Wilkins for his enduring friendship, mentorship and support.

To Candy and Milly Kolasinski for their stimulating discussion of the literature.

To my parents, Sandra and Pete, for their continued faith in my career choices, and for supporting me without question in everything I have ever done.

*To my parents*

Assessing sensorimotor plasticity with multimodal magnetic resonance imaging

**James Kolasinski**

**Trinity Term 2014** **Lady Margaret Hall**

**A thesis submitted in partial fulfillment of the requirements for the degree of Doctor of Philosophy in the University of Oxford.**

## Abstract

The sensorimotor network receives a rich variety of somesthetic afferents and outputs considerable motor efferents, both of which drive experience-dependent plasticity in the system. It remains unclear to what extent subtle changes in somaesthesis and motor function extrinsic to the brain drive plasticity in the functional organisation and anatomy of the sensorimotor network. This thesis contains a series of multimodal MRI experiments to investigate how altered-use and disuse can induce plastic changes in the sensorimotor network of the human brain.

In Chapter 3, a method of mapping digit somatotopy in primary somatosensory cortex at the single-subject level using 7.0 tesla fMRI was developed and applied for a study of healthy participants. Using a phase-encoding paradigm, digit representations were accurately mapped in under 10 minutes. These maps were reproducible over time and comparable to a standard block design.

In Chapter 4, a further fMRI study assessed the potential for short-term reorganisation of digit representations in primary somatosensory cortex following a manipulation whereby the right index and right middle fingers were glued together for 24 hours. There was a marked shift in the cortical overlap of adjacent digits after the glued manipulation, not seen across an equivalent control period, providing strong evidence for short-term remapping of primary somatosensory cortex.

In Chapter 5, a patient study investigated plasticity associated with chronic unilateral disuse of the upper limb. A cross-sectional comparison with control participants showed reduced grey matter density in the posterior right temporoparietal junction, and increased radial diffusivity in the white matter of the right superior longitudinal fasciculus, consistent with change in the right ventral attention network. A complementary longitudinal study in Chapter 6 investigated structural plasticity associated with rehabilitation of the disused limb. There were localised increases in grey matter density, notably in the right temporoparietal junction, further implicating a potential role for regions responsible for egocentric attention in regaining upper limb use.

In Chapter 7, a further patient study investigated candidate predictive biomarkers at the sub-acute stage of stroke recovery, identifying CST-lesion cross-section and sensorimotor network strength as correlates of motor function, which warrant further study.

The results of the studies presented in this thesis provide a novel insight into the nature and time frame of functional and structural plasticity associated with altered use and disuse. Further study of how subtle changes in our sensory and motor use shape the sensorimotor network is warranted, particularly in the context of disuse in non-neurological clinical populations.

**This thesis contains approximately 45 000 words**

# 1 Introduction

*This chapter provides an overview of the anatomy and function of the sensorimotor network. It goes on to focus on the topographic organisation of the primary motor cortex and the primary somatosensory cortex. The principles of plasticity in the brain are then reviewed, including a discussion of the specific examples of sensorimotor plasticity pertinent to the thesis. Finally the chapter outlines the overall aims of the thesis.*

## 1.1 The sensorimotor network

### 1.1.1 Divisions of the cerebral cortex

The human cerebral cortex is a highly convoluted laminar structure broadly considered to bestow advanced cognitive function in humans. The left and right cortical hemispheres are further divisible into four major lobes. Beyond these gross anatomical divisions, the cortex can be further parcellated on the basis of its microstructure. The classic description from Brodmann (Brodmann, 1909) parcellates the cortex into distinct cytoarchitectonic areas on the basis of different cellular and laminar structure (Figure 1.1). This map has been further refined on the basis of other anatomical features such as myeloarchitecture, (Vogt and Vogt, 1919; Economo and Koskinas, 1925; Sarkisov et al., 1949), and functionally validated using electrical stimulation techniques in neurosurgical patients (Foerster, 1926). The functional relevance of

these cytoarchitectonic regions has resulted in their continued use in modern neuroscience, in spite their obvious limitations such as inter-subject variability and the inability to accurately define their borders on the basis of cortical surface landmarks alone (Zilles and Amunts, 2010).



Figure 1.1: *Brodmann's cytoarchitectonic parcellation of the human cerebral cortex.* Of particular interest in the sensorimotor network are areas 4 (Primary motor cortex) and 6 (Dorsal and ventral premotor cortex; supplementary motor cortex), which subserve motor function, and areas 1, 2, 3a and 3b (Primary somatosensory cortex), which function in somaesthesis. Figure from Brodmann, 1909.

The sensorimotor network consists of both cortical and subcortical structures, which collectively confer the broad functions of somaesthesis and voluntary movement. The

major cortical components of the sensorimotor network are schematically depicted in Figure 1.2.

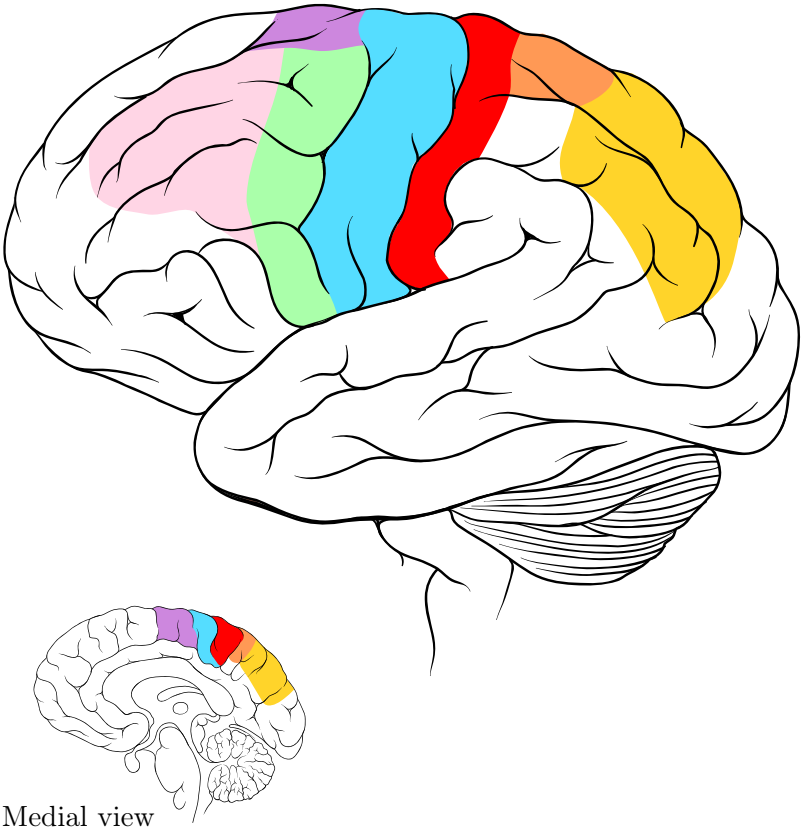


Figure 1.2: *Major cortical components of the sensorimotor network.* Pink: Dorsolateral prefrontal cortex. Green: Premotor cortex. Purple: Supplementary motor cortex. Blue: Primary motor cortex. Red: Primary somatosensory cortex. Orange/Yellow: Area 5 and 7 of posterior parietal cortex. Adapted from background image outline by Lynch and Jaffe, n.d.

### 1.1.2 Localisation of sensorimotor cortex

*"The cortical glandule is the last boundary where sensations terminate and the last prison house whence the actions break forth; for the fibres, both sensory and motory, begin and end in these glandules."*

SWEDENBORG, 1669-1672

Despite a somewhat grandiloquent tone, renowned polymath and seer Emanuel Swedenborg accurately assigned higher order motor and sensory function to the cerebral cortex in the mid-seventeeth century (Swedenborg, 1672). Further advances in the localisation of cortical sensorimotor function were largely hampered in the nineteenth century by arguments of equipotency in the brain, which postulated functionality as a unitary whole (Flourens, 1846; Tyler and Malessa, 2000). Only in the late nineteenth century did evidence from the seminal patient lesion studies of Broca and Wernicke provide strong support for the general theory of cortical localisation (Broca, 1861; Wernicke, 1874).

David Ferrier became a major proponent of cortical localisation (Figure 1.3), specifically in the control of the peripheral musculature. He demonstrated clear contralateral motor deficits following the selective unilateral ablation of precentral gyrus, as well as a pattern of ensuing Wallerian degeneration visible to the naked eye in the descending motor tract (Ferrier, 1875). Furthermore, Ferrier produced convincing evidence from lesion studies that motor and sensory function were controlled by differing cortical regions, on the basis of hemianaesthesia without hemiplegia and vice versa (Ferrier, 1886). Early work from Charles Sherrington examined the sensorimotor connections between the brain and spinal cord, similarly observing that shallow surface lesions in the precentral gyrus induced "a wide scatter of degenerated fibres all through the pyramid" (Sherrington, 1889). Alfred Campbell went further, building upon the observations of Betz (Betz, 1874) to demonstrate histologically in human tissue that large pyramidal cells of layer V of precentral gyrus are chief among those damaged following amputation of the upper limb. He remarked that the pattern was similar to patients suffering from amytrophic lateral sclerosis, further implicating the "intermediate precentral area" as a major output of cortical motor function (Campbell, 1905).

Our current understanding of cortical localisation relies heavily upon the early experiments observing the behavioural effects of natural or induced cortical lesions.

As a result, we now view the cortex as a distributed system in which architectonically individual functional units perform highly specialised roles.

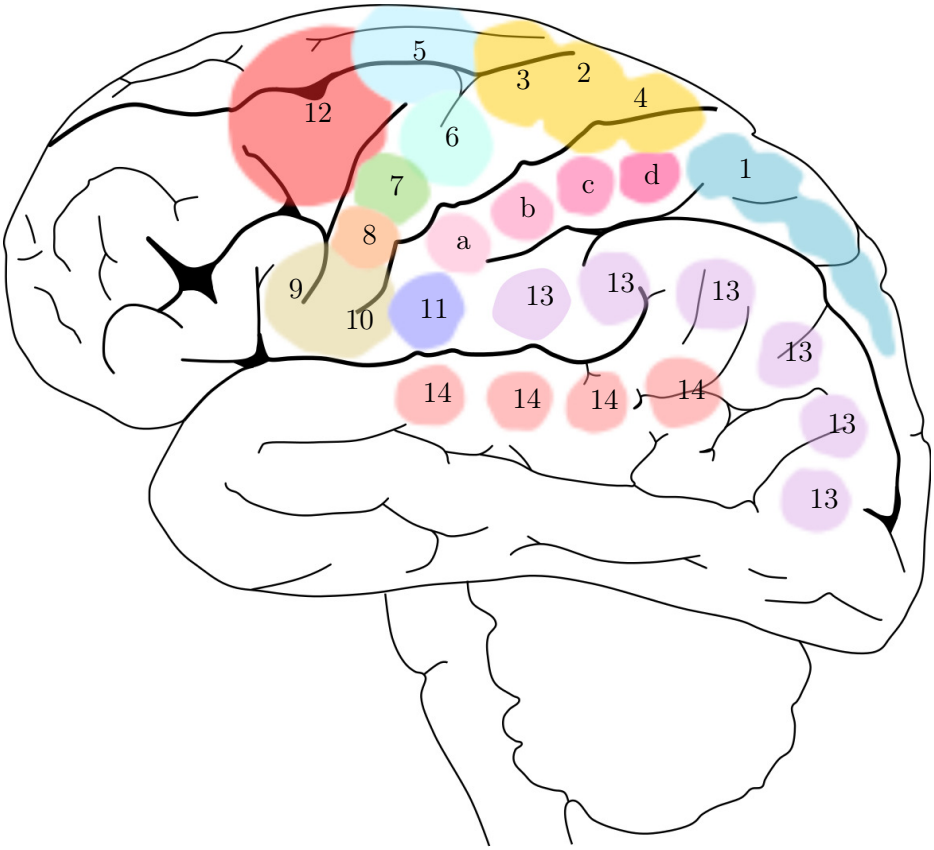


Figure 1.3: *Ferrier's proposed localisation of cortical function in humans.* Based on experimental studies in non-human primates. 1) Movement of contralateral lower limb. 2-4) Complex movements of the arms and legs (for example, as used in climbing or swimming). 5) Extension forwards of the upper limb. 6) Movement of the hand and forearm involving the biceps. 7) Elevation of the angle of the mouth. 8) Depression of the angle of the mouth. 9-10) Centre of movement of the lips and tongue. Region in which disease causes aphasia. 11) Centre of the plastysma, refraction of the angle of the mouth. 12, a-d) Centres of movement of the hand and wrist. 13) Centre of vision. 14) Centre of hearing. Adapted from Tyler and Malessa, 2000.

### 1.1.3 The postcentral somatic sensory system

*"...Every ruder touch whatever springs up from the surface of the whole, through the medium of the nerves in the medulla spinalis or medulla oblongta, and so into the high active cineritious [grey] substance and the circumambient cortex of the brain."*

Swedenborg, 1669-1672

Swedenborg's early description of the pathway conveying mechanoreceptive *"ruder touch"* information from the peripheral tissue to the cerebral cortex is broadly accurate. The brain is dependent upon signals from peripheral receptors to derive information about the external environment. Somaesthesis refers to the sensory experience elicited by mechanical stimulation of peripheral tissue, which encompasses touch-pressure, form-pressure, texture, flutter-vibration and proprioception (Mountcastle, 2005). Mechanoreceptive information from the periphery is projected principally by the dorsal-column medial-lemniscal pathway summarised in Figure 1.4. Thermal and nociceptive information is conveyed peripherally by the small fibre system: polymodal A-delta and C-fibre afferents, continuing centrally via the anterolateral system.

#### 1.1.3.1 Peripheral receptors

Somethesis arises from the stimulation receptors located in the deep and superficial peripheral tissues. The various modalities of somethesis are conveyed by different peripheral receptors, as summarised in tables 1.1 and 1.2, though most natural peripheral stimuli recruit a number of these receptors simultaneously. Mechanoreceptors provide a very direct link between peripheral mechanical stimulation and discharge of the associated primary sensory neuron. Receptors often rely on a multicellular corpuscle, which determines their particular subtype of mechanical sensitivity. All mechanoreceptors operate at a low threshold given the innocuous stimuli they relay.

Table 1.1: Overview of peripheral mechanoreceptors

| Class | Fibre type | Stimulus | Adaptation rate | Sensory experience evoked |
|---|---|---|---|---|
| *Glabrous skin* | | | | |
| Meissner corpuscle | A-beta | Movement, displacement, velocity | Rapid | Velocity, horizontal movement contact, low frequency flutter |
| Pacinian corpuscle | A-beta | Contact, vibration, lateral movement | Rapid | Contact, movement, high frequency vibration |
| Merkel cell neurite-complex | A-beta | Contact, pressure, lateral movement | Slow | Contact, pressure, texture, two-dimensional form |
| Ruffini corpuscle | A-beta | Contact, displacement, skin stretch | Slow | Not perceived in humans; speculative: proprioception in motor control |
| *Hairy skin* | | | | |
| G-1/G-2 hair follicle | A-beta | Contact movement/ Displacement | Rapid | Contact, movement and flutter |
| Field skin surface | A-beta | Contact movement | Rapid | Contact and movement |
| Pacinian corpuscle | A-beta | Transient/ mechanical oscillation | Rapid | Vibration/tickle |
| Merkel cell axon-complex | A-beta | Contact pressure | Slow | None reported |
| Ruffini corpuscle | A-beta | Contact pressure | Slow | Touch/pressure |
| D-hair follicle | A-delta | Slowly moving displacement | Slow | Movement and contact |
| C-mech unencapsulated | Unmyelinated C-fibre | Low-threshold distortion | Intermediate | Mechanical sensitivity / 'pleasant' touch |

Table 1.2: Overview of peripheral proprioceptors

| Class | Fibre type | Sensitivity |
|---|---|---|
| *Muscle spindles* | | |
| Primary endings: Intrafusal fibres | Type Ia | Muscle length and rate of change |
| Secondary endings: Nuclear bag and chain | Type II | Muscle length |
| Golgi tendon organs | Type Ib | Muscle tension |
| Non-spindle endings | Type II | Deep pressure |
| Joint receptors | Mixed | Joint position at limit of range |

#### 1.1.3.2 The dorsal column pathway

Suprathreshold sensory stimulation of peripheral mechanoreceptors induces a series of action potentials passing through the myelinated neurite of dorsal root ganglion cell and directly into the dorsal columns of the spinal cord, without a synapse or decussation. The dorsal columns can be divided into the medial funiculus gracilis and the lateral funiculus cuneatus, both visible at the upper cervical level, broadly conveying information from the lower and upper limbs respectively (Figure 1.4). The primary afferents continue in the dorsal columns to the medullary dorsal column nuclear complex (DCNC), where they synapse for the first time. Second order relay neurons decussate in the medulla as the internal arcuate bundle, thereafter forming the medial lemniscus, which ascends through the pons and midbrain. Second-order neurons synapse once again in the ventral-posterior lateral nucleus of the thalamus, whence third-order neurons project principally to the primary somatosensory cortex. Mechanoreceptive primary-afferents from the head and face synapse first in the principal nucleus of the trigeminal complex prior to decussation and passage in the medial lemniscus, with second-order neurons synapsing in the ventral posterior medial nucleus of the thalamus.

#### 1.1.3.3 Remapping afferent inputs: modality and topography

The dorsal column system acts as more than a simple white matter conduit for mechanoreceptive information; it also remaps primary afferent fibres. Evidence from axonal degeneration studies in non-human primates (Walker and Weaver, 1942) and topographical studies of human tissue (Smith and Deacon, 1984) demonstrates that inputs to the dorsal column at each spinal level form successive lamina containing *"the full complement of large-fibred mechanoreceptive afferents . . . arranged one after another from caudal to rostral in a medial to lateral dimension"* (Mountcastle, 2005). Reorganisation occurs for both modality and topography in the dorsal columns. At the level of input, mechanoreceptive afferents demonstrate dermatomal topography based on peripheral innervation patterns, and are not divided on the basis of their somatosensory modality. At the level of the DCNC, remapping has occurred such that afferent fibres are organised somatotopically on the basis of body form, and further segregated on the basis of somatosensory modality (Whitsel et al., 1972a; Whitsel et al., 1972b; Werner and Whitsel, 1973). This remapping persists into the DCNC (Florence et al., 1988) through to the ventral posterior nucleus of the thalamus (Jones et al., 1982).

#### 1.1.3.4 Primary somatosensory cortex

Somatic sensory regions of the cerebral cortex can be defined as those with *1)* direct thalamocortical projections from the somatic sensory nuclei of the thalamus, *2)* a representation of the sensory surface, *3)* a specific response profile to stimuli at the single neuron level, *4)* unique cortical and subcortical connectivity, and *5)* distinct sensory deficits following removal or damage (Kaas, 1983; Mountcastle, 2005). The classic somatic sensory area of the human cortex is located in the postcentral gyrus: the primary somatosensory cortex. The primary somatosensory cortex acts broadly as both a processing region for afferent sensory inputs, as well as a more central node in the redirection of incoming sensory information across the sensorimotor network

(Figure 1.5). In fact, the primary somatosensory cortex is composed of four strip-like cortical areas, broadly running laterally, in line with the postcentral cytoarchitectonic divisions proposed by Brodmann, 1909, which are functionally distinct. Early evidence from single unit recording demonstrated a correlation between response properties and cytoarchitectonic organisation in the primate postcentral gyrus (Powell and Mountcastle, 1959). Area 3a, 3b, 1 and 2 each receive thalamocortical inputs representing a distinct subset of the somatosensory modalities, in keeping with the parallel processing of these modalities both peripherally and in the dorsal column medial-lemniscal system (Clark and Powell, 1953; Jones et al., 1979; Friedman and Jones, 1980; Friedman and Jones, 1981; Maendly et al., 1981; Nelson and Kaas, 1981).

The functional parcellation of the primary somatosensory cortex has led many to question the validity of considering these areas as an amalgam, when despite their obvious cortico-cortical links, they perform distinct modality-specific roles, as summarised by Jon Kaas: *"three zones were clearly distinguished on the basis of markedly different response properties alone: a rostral 3a region activated from subcutaneous receptors, a middle area 3b plus area 1 region activated from cutaneous receptors, and a caudal area 2 region activated by deep receptors. These response tendencies changed sharply at the architectonic borders."* (Kaas, 1983). Further work has surmised that area 3a receives input predominantly from muscle spindles afferents; area 3b receives input from both rapidly and slowly adapting cutaneous receptors; area 1 mainly receives input from rapidly adapting cutaneous receptors, and area 2 responds to stimulation of joint receptors (Kaas, 1993; Grefkes et al., 2001).

The areas display markedly different cytoarchitecture. Area 3b has densely packed layers III and IV, while area 3a displays a less granular structure, with a thinner layer IV than area 3b, and a more pronounced layer V, though not comparable to that of the primary motor cortex. Area 1 is generally less densely packed than area 3b, and as a result shows a less marked pattern of lamination. Progressing caudally to area 2, a more distinctive layer IV and VI develops.

There is clear separation of information encoding different somatosensory modalities throughout the dorsal column system, medial lemniscus and thalamus. It is only at the level of the primary somatotosensory cortex and beyond that corticocortical connections between different Brodmann areas suggest a degree of integration between somesthetic submodalities. Most striking is the degree of connectivity between area 3b and 1, with the interconnection of homologous body representations (Kaas, 1983). Area 2 makes strong connections with area 3a and area 5 (Vogt and Pandya, 1978). Area 3a appears to make strong connections with rostral motor cortex, and area 1 (Strick and Preston, 1978; Jones et al., 1979). The connections of the primary somatosensory cortex are summarised schematically in figure 1.5.

#### 1.1.3.5 Higher order sensory areas

The feed-forward efferent connections of the primary somatosensory cortex suggest a serial approach to the processing of sensory stimuli. The processing streams for somatic sensory information can be divided broadly into two separate but highly interconnected systems on the basis of function and anatomy. The parietal-frontal system consists of Brodmann areas 5 and 7 of the parietal lobe, and various frontal motor areas in the sensorimotor network (Figure 1.2), which is involved in sensory abstraction required for object recognition, the sense of body position and body form, and the integration of sensory information with movements undertaken in the immediate environment. The lateral system consists of regions of the insula and areas directly adjacent to the Sylvian fissure, such as secondary somatosensory cortex. The lateral system is a gateway for sensory information to the frontal and temporal lobes, integrating sensory information with cognitive and limbic responses, as well as memory.

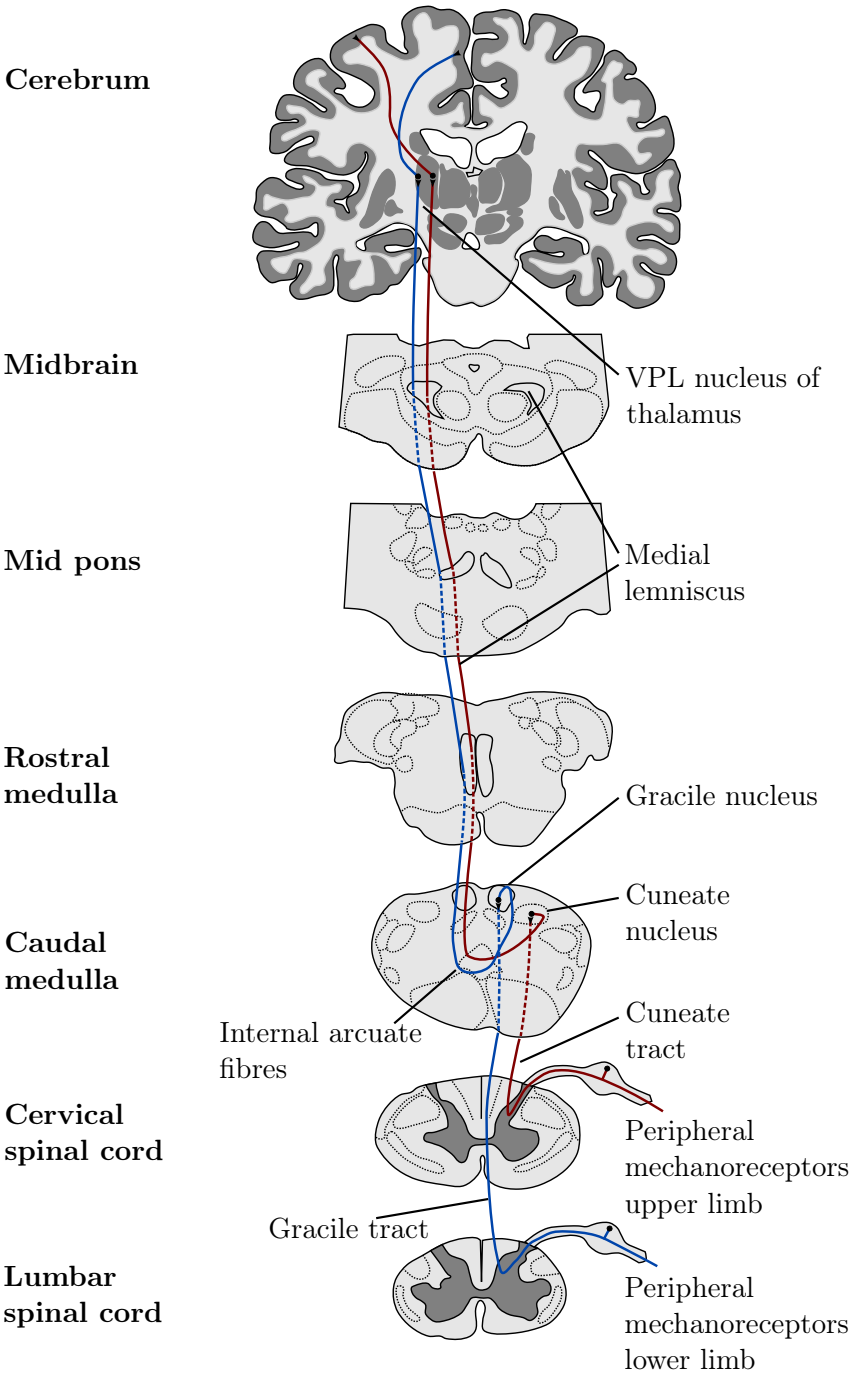


Figure 1.4: *Overview of the dorsal-column medial-lemniscal pathway.* Red: afferents from the upper limb. Blue: afferents from the lower limb.

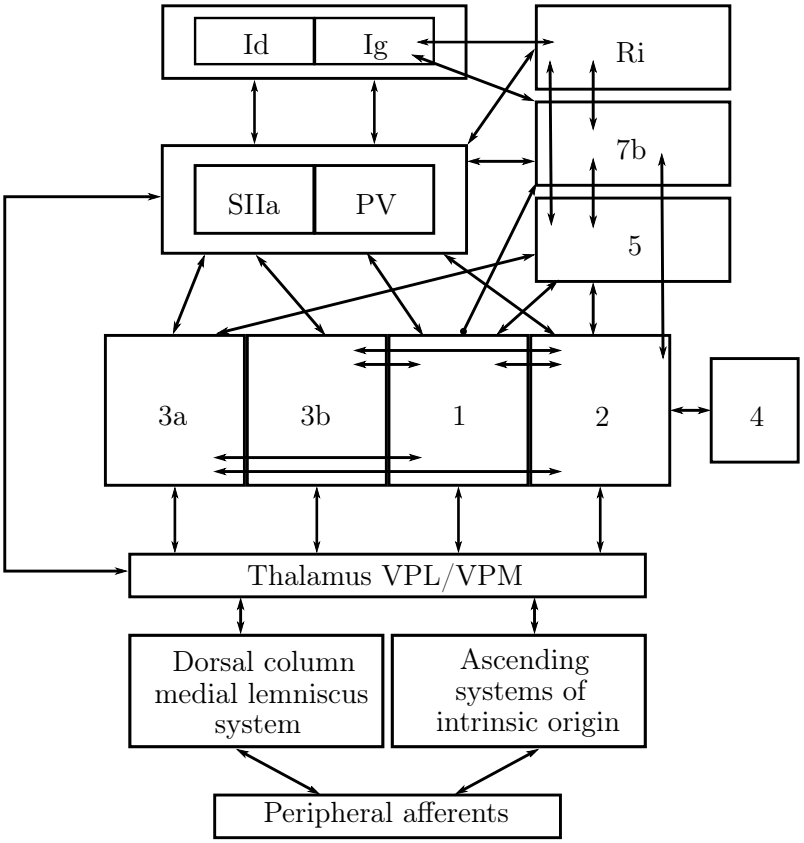


Figure 1.5: *Schematic of the somatosensory afferent system including higher order cortical areas of the lateral and parietal-frontal system.* VPL: ventro-posterolateral nucleus; VPM: ventropostero-medial nucleus; SII: secondary somatosensory cortex; PV: parietal ventral area; Id: dysgranular insula; Ig: granular insula. Ri: rostral interstitial nucleus of medial longitudinal fasciculus. Numbers refer to Brodmann areas. Reproduced from Mountcastle, 2005.

### 1.1.4 The precentral motor system

*"From each cortical gland proceeds a single . . . nerve fibre; this is carried down into the body, in order that it may . . . produce some action . . ."*

Swedenborg, 1669-1672

The major regions involved in human motor function are located principally in the frontal lobe. A classic view of the cortical motor system encompassed two key regions. The first of these regions is the primary motor cortex, the dominant region of corticospinal motor output (Nudo and Masterton, 1990), anatomically located at Brodmann area 4 on the precentral gyrus bordering the central sulcus. The second region is the supplementary motor area, a relatively smaller region of the frontal lobe located on the medial aspect within Brodmann area 6, and classically implicated in coarser axial and proximal movements (Penfield and Welch, 1951; Woolsey et al., 1952).

Evidence from non-human primate studies has demonstrated a more expansive agranular frontal region implicated in movement, which encompasses both Brodmann areas 4 and 6 (Matelli et al., 1985; Matelli et al., 1991). These studies posit a more complex parcellation of the cortical motor system, implicating up to seven different regions of motor cortex. While Brodmann area 4 is well established as the primary motor cortex, Brodmann area 6 has been subdivided into a variety of functionally distinct areas (Rizzolatti et al., 1998). Rizzolatti proposes three key broad functions of the motor areas beyond the primary motor cortex: *1)* Sensory-motor transformations involving visual and somatosensory inputs, *2)* a mirror mechanism underlying motor mimicry, *3)* motor decision making and action initiation (Rizzolatti and Luppino, 2001). The broader function and the extensive prefrontal and parietal connections of these motor areas demonstrate the importance of considering the precentral cortical motor system in the context of the sensorimotor network (Matsumura and Kubota, 1979; Muakkassa and Strick, 1979; Luppino et al., 1993) (Figure 1.2), rather than as an isolated system of descending cortical output.

#### 1.1.4.1 Primary motor cortex: Brodmann area 4

The primary motor cortex is the major, but not sole, source of descending corticospinal motor fibres in the human brain (Nudo and Masterton, 1990), predominantly supplying the contralateral musculature. It is located on the precentral gyrus of the frontal lobe, caudal to the central sulcus, and rostral to the precentral sulcus, described by Brodmann as *"an almost vertically disposed, wedge-shaped field with its apex directed inferiorly, although slanting slightly posteriorly, that sits astride the dorsal margin of the cortex and whose wider base stretches more or less onto the medial surface"* (Brodmann, 1909).

Area 4 shows the classic laminar cytoarchitecture of other cortical regions, though is agranular: lacking an distinguishable layer IV. The area has a cortical thickness 1.6 times thicker than the average across the human brain (Rockel et al., 1980). Furthermore, it is somewhat atypical in its *"widely-spaced neurones are separated by large masses of neuropil, which could provide very rich synaptic connections between neurones"* (Phillips, 1981). Area 4 is in fact readily identifiable on the basis of the large pyramidal Betz cells found most densely in layer V, whose soma can attain a diameter of up to 120 micrometres (Betz, 1874; Meyer, 1987), with characteristic apical and basal dendrites. Non-pyramidal neurons include stellate and basket cells, the latter implicated in inhibitory GABAergic interactions with pyramidal cells (Jones, 1983).

Area 4 shows thalamocortical afferent connectivity, mainly excitatory to layer III pyramidal cells (Amassian and Weiner, 1966; Sloper and Powell, 1979), as well as extensive cortico-cortical connectivity via callosal projections (Meyer et al., 1995; Meyer et al., 1998). The primary motor cortex is a major output of corticofugal fibres, providing efferent signals to the contralateral musculature from both layer III and layer V. Those fibres originating superficially are destined for proximal structures, and those originating deeper in layer V destined for more distant targets, for example cortico-motorneuronal fibres and corticorubral fibres (Jones, 1984) (Figure 1.6).

#### 1.1.4.2 Brodmann area 6

The study of Brodmann area 6 is complicated by a lack of clear homology in this region between humans and non-human primates. Evidence from a variety of studies in both groups suggests that Brodmann area 6 can be subparcellated into a number of functionally and structurally distinct regions (Rizzolatti et al., 2002). Currently in the human literature, these are commonly considered to be dorsal and ventral premotor cortex, the supplementary motor area, and the pre-supplementary motor area (Vorobiev et al., 1998).

#### 1.1.4.3 Lateral Brodmann area 6: premotor cortex

The first description of the premotor cortex came from Campbell, who described an "intermediate precentral region", which he felt well delineated cytoarchitectonically (Campbell, 1905). It is now increasingly clear than both dorsal and ventral subdivisions exist within the human brain, which were previously identified in non-human primates (Barbas and Pandya, 1987; Davare et al., 2006; Tomassini et al., 2007).

The dorsal premotor cortex has been strongly implicated in motor planning, and "is activated when a new motor program is established ... or when the motor program is changed on the basis of sensory stimulation." (Roland et al., 1980). Evidence from single unit recording studies implicates the dorsal premotor cortex in voluntary movement, as in the primary motor cortex, but with a higher-threshold for movements using microstimulation techniques, and a timecourse showing activity prior to and during a cued movement (Weinrich and Wise, 1982; Wise, 1985). The area shows strong connectivity with visual and sensory regions (Caminiti et al., 1996; Matelli et al., 1998; Fogassi et al., 1999) to integrate body-part and target information (Hoshi and Tanji, 2000; Hoshi and Tanji, 2007). The dorsal premotor cortex has also been implicated in mental rehearsal without subsequent motor action (Cisek and Kalaska, 2004). Studies of limb immoblisation have demonstrated alterations in motor planning abilities, as well as the level of cortical excitability during motor

rehearsal (Bassolino et al., 2012; Kaneko et al., 2003), suggesting a role for the dorsal premotor cortex in maladaptive changes to the cortical motor system following peripheral dysfunction.

The ventral premotor cortex is involved in visuomotor integration, specifically in target or object oriented movement of the hand and mouth and the immediate surroundings (Rizzolatti et al., 2002). Located on the ventral border of Brodmann area 6 and Brodmann area 44, the region exhibits a predominantly agranular cytoarchitecture, with prominent layer III pyramidal cells (Binkofski and Buccino, 2006). Evidence from the non-human primate literature implicated the ventral premotor cortex in the control of grip and grasp in the hand through dense connections to the hand region of the primary motor cortex, rather than via its direct corticospinal efferents (Shimazu et al., 2004; Dum and Strick, 2005; Prabhu et al., 2009), though these corticospinal connections are thought to be involved in action suppression during observation in non-human primates (Kraskov et al., 2009). The ventral premotor cortex exerts both excitatory and inhibitory influences on the primary motor cortex, which seems to be relevant in behavioural responses to stimuli, action reprogramming and action suppression (Rushworth et al., 2001; Rushworth et al., 2005; Buch et al., 2010).

#### 1.1.4.4 Medial Brodmann area 6: supplementary motor cortex

The supplementary motor area is located in the dorsomedial frontal cortex, corresponding to the medial aspect of Brodmann area 6, dorsal to the cingulate sulcus and gyrus. The region shows mixed functional properties; evidence from surgical resections shows deficits in the initiation and sustenance of contralateral movement, which presents as motor neglect (Laplane et al., 1977; Krainik et al., 2001). Some patients demonstrate recovery in the long term, but with persistent defects in complex movement of the hand and digits. Early cerebral blood flow studies identified the supplementary motor cortex as a "supramotor" region consistently activated during complex but not simple movements (Orgogozo and Larsen, 1979).

Stimulation studies of the supplementary motor cortex have yielded mixed results, reporting responses ranging from complex postural or limb based movements, inhibition of movement, or an urge to move (Nachev et al., 2008). The supplementary motor cortex shows strong reciprocal connectivity with the primary motor cortex, as well as contributing up to 10 percent of the corticospinal motor outflow (Dum and Strick, 1991; Wise, 1996; Johansen-Berg et al., 2004; Takada et al., 2004).

Evidence from primate and human imaging studies has also been mixed. Some studies have implicated the supplementary motor cortex in the initiation of internally cued movement (Deecke and Kornhuber, 1978; Jahanshahi et al., 1995), reporting a so-called readiness potential therein. Further work has suggested a role for the supplementary motor cortex in motor sequence movement; the planning and ordering multiple movements ahead to perform complex tasks (Tanji and Shima, 1994; Clower and Alexander, 1998; Shima and Tanji, 2000). The supplementary motor cortex has consistently been associated with a role in complex hand and finger movements (Laplane et al., 1977; Shibasaki et al., 1993; Gerloff, 1997; Sadato et al., 1997; Rogers et al., 2004).

#### 1.1.4.5 Subcortical motor control

The basal ganglia, the cerebellum and the thalamus are all involved in the subcortical control of motor function. The basal ganglia are an amalgam of subcortical grey matter structures, which function broadly in action selection and inhibition (Mink, 1996). The basal ganglia has a recurrent connection to a variety of cortical regions (Hoover and Strick, 1999; Middleton and Strick, 2000), including motor, premotor and prefrontal cortex, exerting control over systems beyond the sensorimotor network. In brief, the cortico-basal loop is thought to function using a reinforcement learning model.

In contrast, the cerebellum plays a role in the online fine-tuning of motor function, as well as broader cognitive functions (Thach et al., 1992). The cerebellum can be broadly

separated into three divisions. The vestibulocerebellum receives inputs from the ipsilateral vestibular nuclei and reticular formation; it is involved in the maintenance of balance. The pontocerebellum receives inputs from the contrlateral pons and motor cortex; it is involved in motor coordination. Finally the spinocerebellum receives ascending spinal input from the spinocerebellar tracts and the red nucleus, which support its role in the maintenance of posture and muscle tone.

The thalamus shows extensive connections with both the basal ganglia and the cerebellum. The motor thalamus consists of the ventrolateral nucleus of the thalamus (VL), the ventro-posterolateral nucleus of the thalamus (VPL) and the ventroanterior nucleus of the thalamus (VA), with recent evidence suggesting a role for the mediodorsal thalamus in eye movement (Lynch et al., 1994; Sommer, 2003). Cerebellar efferents send signals to the VL and VPL thalamic nuclei. Evidence from studies of non-human primates suggests that these components of the motor thalamus are involved in the initiation of visually cued movement, but not movement that is self-initiated (Donkelaar et al., 1999). A cerebello-thalamic-cortical loop involving the primary motor cortex also suggests a role for the thalamus in the production of micromovements, which collectively form the larger smooth movements we that we produce (Gross et al., 2002). The thalamus also plays a role in cortico-basal loops, acting as a relay between the globus pallidus interna and various motor and cognitive regions of the frontal cortex (McFarland and Haber, 2002).

#### 1.1.4.6 Descending motor efferents

The corticospinal tract is the predominant output from the cerebral cortex involved in voluntary movement (Figure 1.7). Corticospinal fibres originate predominantly from the primary motor cortex (Nudo and Masterton, 1990), but other contributions also come from frontal and parietal regions, including supplementary motor area rostrally, and area 3a caudally (Dum and Strick, 1991; Jones and Porter, 1980). Corticospinal fibres are formed from the axonal projections of layer V pyramidal cells, which form

well-described clusters within the cortex (Murray and Coulter, 1981), with the size of pyramidal cell soma clearly proportional to the length of the axonal projection coursing into the spinal cord. Corticospinal fibres descend in the internal capsule and cerebral peduncle. At the level of the medullary pyramid, 80 to 90 percent of corticospinal fibres decussate, descending in the lateral funiculus of the spinal cord. A small minority of uncrossed fibres descend in the ventromedial spinal cord. Corticospinal fibres synapse with spinal motoneurons in the ventral horn of the spinal cord, with a medial to lateral representation of proximal to distal muscles. Spinal motoneurons project via the ventral root into a mixed spinal nerve, from which they pass to form a neuromuscular interaction with their target.

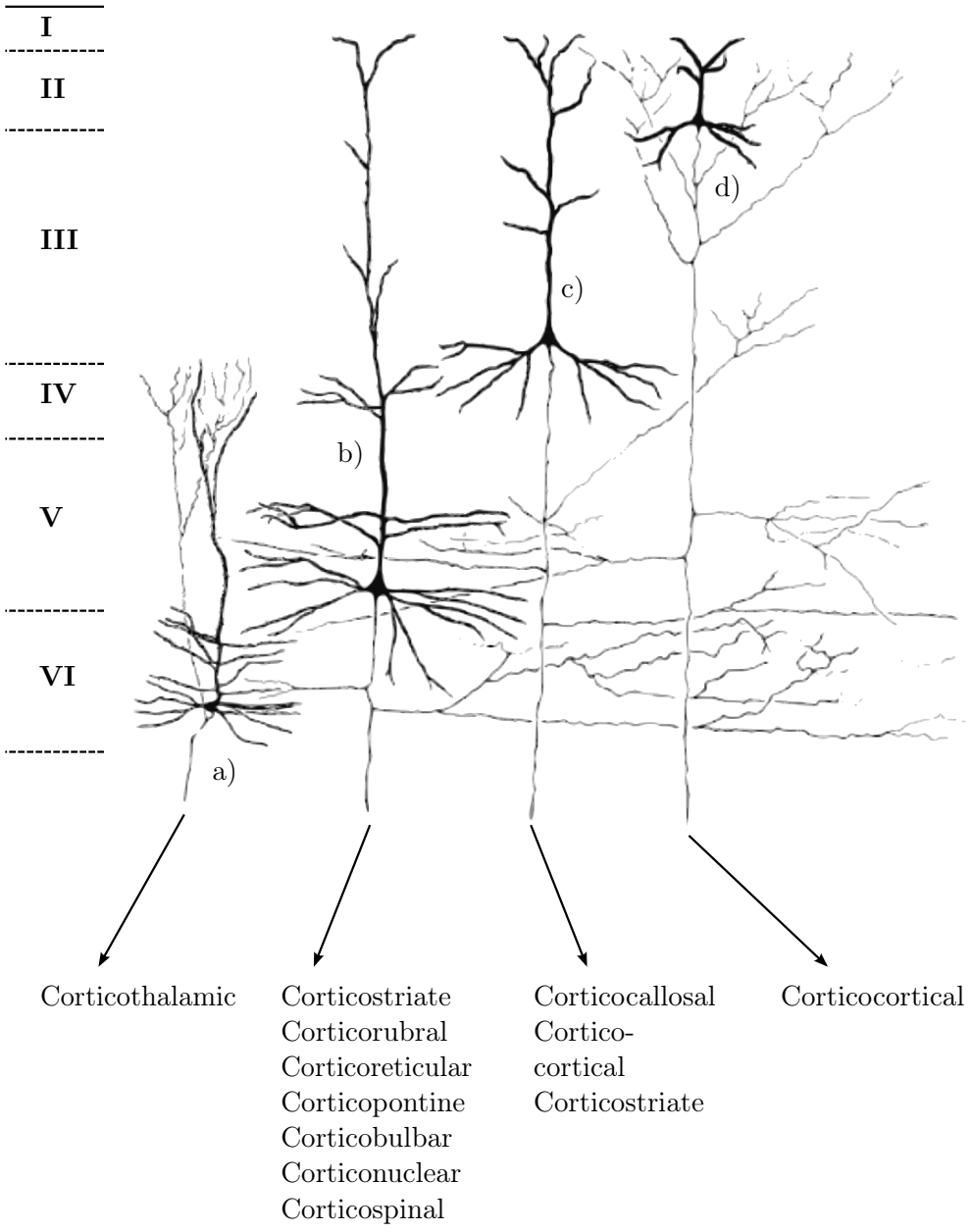


Figure 1.6: *Overview of efferent output from lamina of the primary motor cortex.* Dendritic output from pyramidal neurons of: a) layer VI; b) layer V; c) layer III; d) layer II. Adapted from Jones and Wise, 1977 and Jones, 1984.

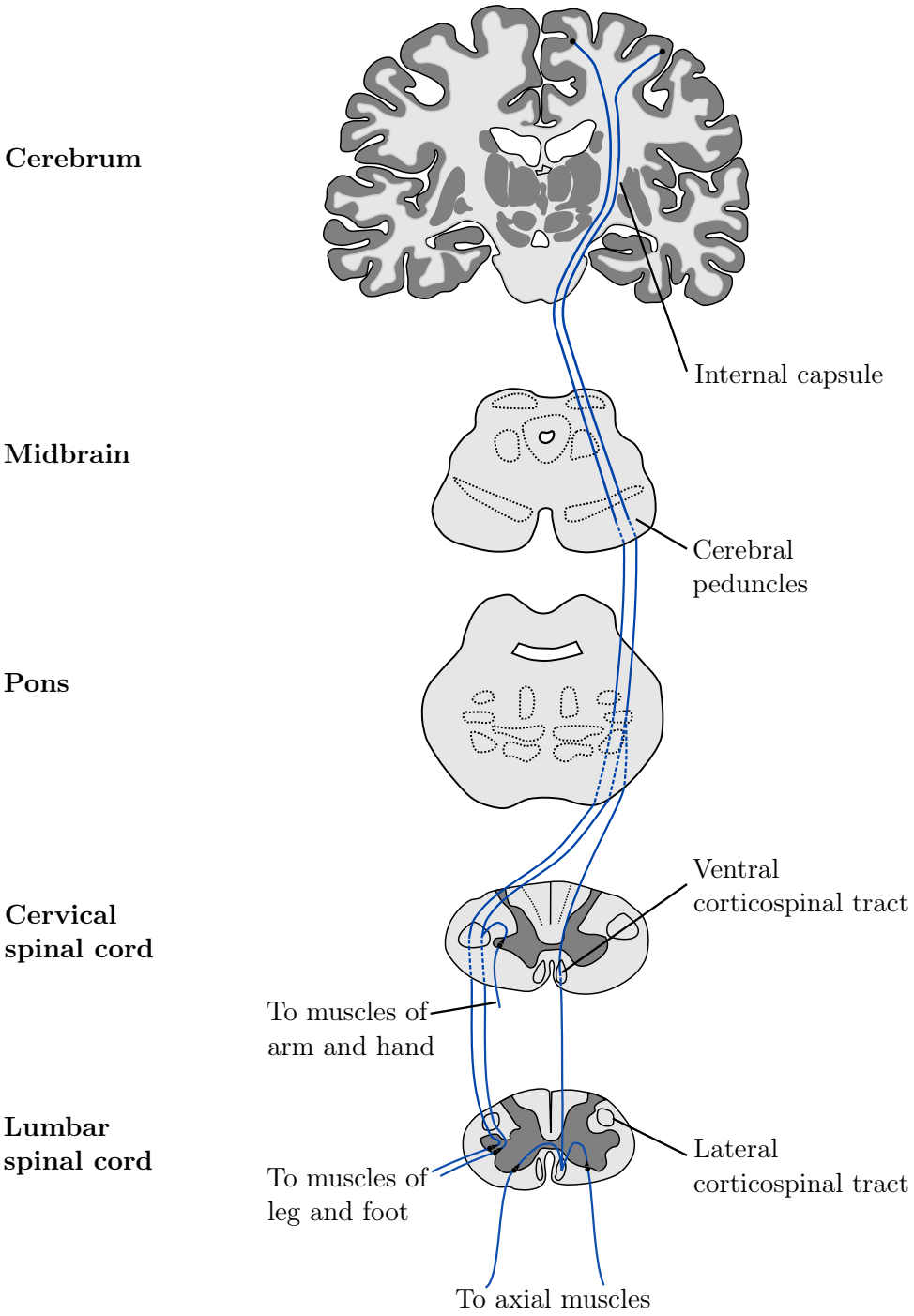


Figure 1.7: *Overview of descending corticospinal motor efferents.* The principal corticospinal motor output originates from the primary motor cortex, with the majority of fibres decussating at the medullary pyramids to form the lateral corticospinal tract, and an uncrossed minority forming the ventral corticospinal tract supplying the axial musculature.

### 1.1.5 Concepts of somatotopy

*"The muscle and actions which are in the ultimates of the body or in the soles of the feet depend more immediately upon the higher parts; upon the middle lobe the muscles which belong to the abdomen and thorax, and upon the third lobe those which belong to the face and head; for they seem to correspond to one another in an inverse ratio."*

SWEDENBORG, 1669-1672

Swedenborg provides a highly accurate description of somatotopy in his extensive study on the cerebrum published in the mid-seventeenth century (Swedenborg, 1672), although this was not widely translated or distributed until the early twentieth century. The term *somatotopic* refers to a scheme of organisation in which neighbouring peripheral sensory fields are mapped to neighbouring regions in their representation in the central nervous system, save some discontinuities or distortions (Mountcastle, 2005). This effectively yields a neural representation based around a body map. The term somatotopy is commonly misused to describe topographic organisation based generally on some form of body map across the sensorimotor system of the brain, referring to regions receiving sensory afferent information, and projecting motor efferent information.

The study of body maps in the primary sensory and motor cortices of the human brain was pioneered by Wilder Penfield in the mid-twentieth century using intra-surgical micro stimulation and recording techniques to derive detailed maps of the cortical surface in neurosurgical patients, yielding the now ubiquitous caricature images of the sensory and motor homunculi (Figures 1.8 to 1.10). It is now clear that body map topography is a common feature across the primary sensory and motor cortices, their subcortical connections (Whitsel et al., 1969; Jones et al., 1982; Florence et al., 1988; Brown et al., 1989; Mitz and Wise, 1987; Dykes and Craig, 1998), and in other cortical sensory and motor region across the brain (Romani et al., 1982; Grill-Spector and Malach, 2004; Silver and Kastner, 2009). However, the existence of true somatotopy

beyond the primary somatosensory cortex in the cortical motor regions is a matter of some debate.

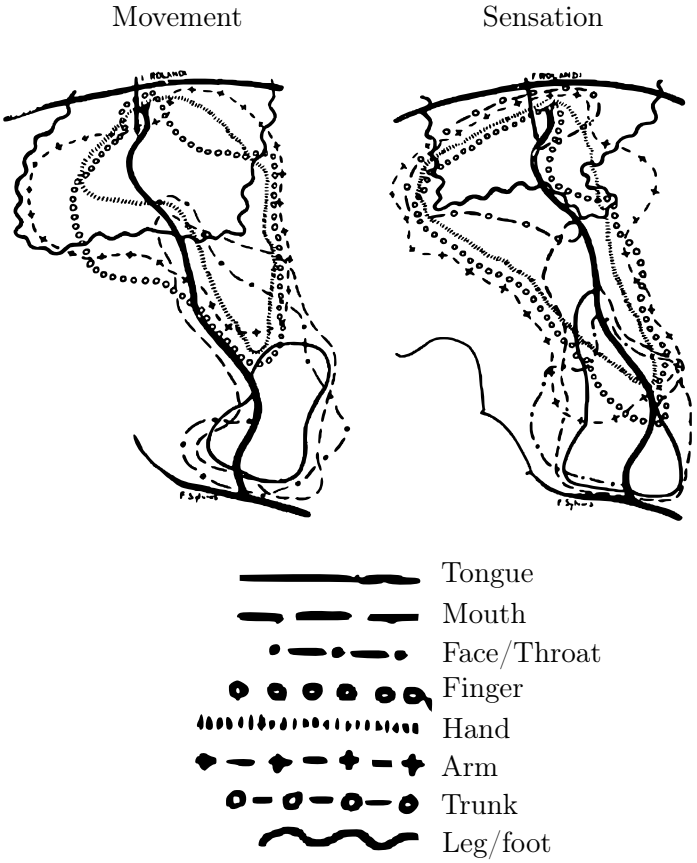


Figure 1.8: *Overview of early somatotopy findings in Penfield and Boldrey, 1937.* Lines enclose the areas in which responses were recorded for different regions of the body in any subject, with overlap demonstrating the considerable inter-subject variability. Schematic figures both show dorsolateral view of the right precentral and postcentral gyri. The central sulcus is shown as the curved bold line running top to bottom. Reproduced from Penfield and Boldrey, 1937.

#### 1.1.5.1 Somatotopy and the primary somatosensory cortex

Beyond the seminal work of Penfield, studies of somatotopy continued to focus on the primary somatosensory cortex. While the sensory homunculus demonstrates the concept of somatotopic organisation, even Penfield himself described it as a

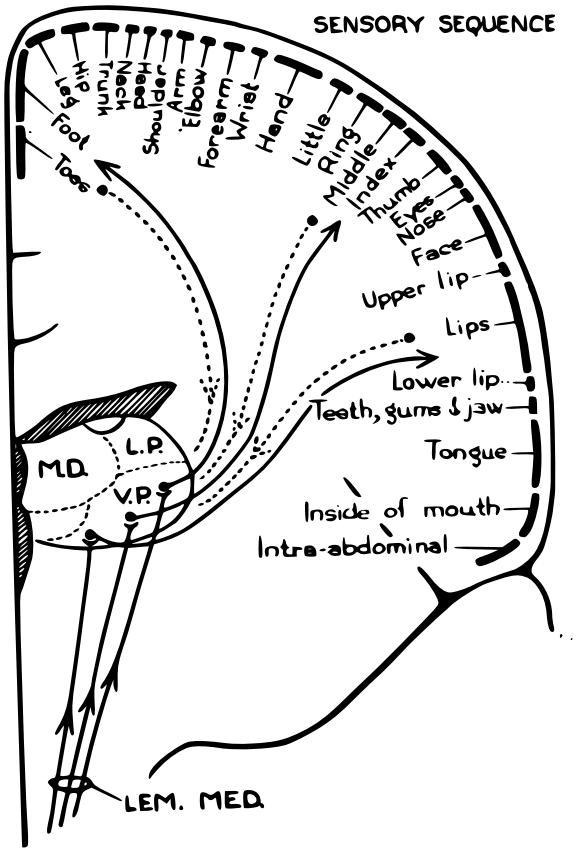


Figure 1.9: *Summary of electrical stimulation studies of the primary somatosensory cortex in awake human subjects, presented in Penfield and Jasper, 1954.* Results based on verbal reports of somethesis during surgical following cortical stimulation. Sulcal patterns mean stimulation sites were predominantly located in Brodmann area 1. Reproduced from Mountcastle, 2005.

caricature, demonstrating only the general pattern of representation. As discussed in section 1.1.3.4, the primary somatosensory cortex is further subdivided into four functionally and cytoarchitectonically distinct subregions corresponding to Brodmann areas 3a, 3b, 1 and 2. Early studies of somatotopic representations in non-human primates suggested a single map which spans the entire postcentral gyrus (Paul et al., 1972a; Paul et al., 1972b). In the late 1970s, an extensive microelectrode mapping study across 4400 sites in the postcentral gyrus of the New World monkey reported distinct contralateral body maps in area 3b and 1, though these were mirror images in certain regions, including the hand and finger representations (Kaas et

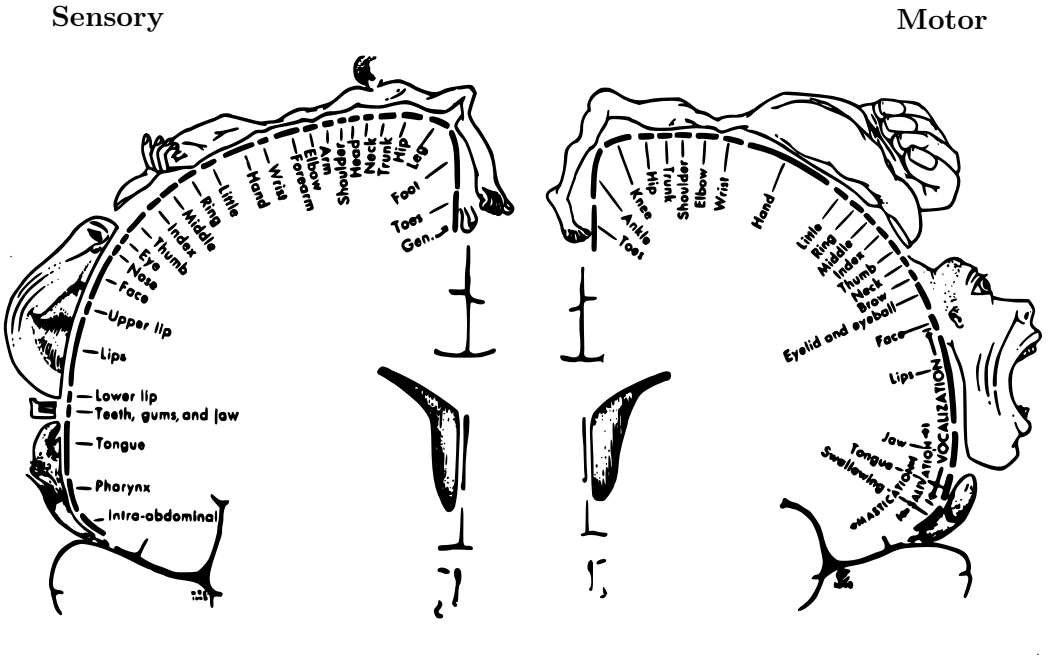


Figure 1.10: *The sensory and motor homunculi proposed originally in Penfield and Rasmussen, 1950.*

al., 1979; Nelson et al., 1980). Similar maps have since been identified in area 2 and area 3a (Pons and Kaas, 1986; Huffman and Krubitzer, 2001). Area 3a does not display the same level of intricate topography as areas 3b and 1, though its strong connectivity with the primary motor cortex may explain this observation (Section 1.1.5.2). Area 2 is characterised by distinct multi-digit receptive fields, supporting recent evidence for its involvement in sensory integration in the primary somatosensory cortex (Mountcastle et al., 1975; Yau et al., 2013). Somatotopic maps derived from microelectrode studies in the primary somatotosensory cortex display considerable inter-subject variability (Merzenich et al., 1987). Detailed studies of area 3b have suggested that the representation of individual digits are subdivided further into regions showing differential responses to slowly and rapidly adapting peripheral mechanoreceptors (Sur et al., 1982) (Section 1.1.3.1).

Efforts to map somatotopy in the human primary somatosensory cortex have applied a range of experimental approaches, from invasive electrophysiology paradigms performed during neurosurgery to the use of non-invasive techniques such as positron

emission tomography, magnetoencephalography (MEG), and optical functional mapping (Fox et al., 1987; Wood et al., 1988; Mogilner, 1993; Sato et al., 2005; Koch et al., 2010).

Functional magnetic resonance imaging (fMRI) provides a unique opportunity to assess patterns of brain activity non-invasively in human subjects (Section 2.4). fMRI has been applied extensively to the study of somatotopy in the primary somatotosensory cortex of the brain, assessing patterns of activation associated with sensory stimulation across the body, with an increasing focus on the fine-grain topography, which is well reported in microelectrode mapping studies (Jack et al., 1994; Puce et al., 1995; Yousry et al., 1995; Pujol et al., 1996; Lee et al., 1998; Stippich et al., 1999; Maldjian et al., 1999). Work aiming to further replicate microelectrode mapping studies in primates has considered differential activation of the Brodmann areas which collectively constitute primate somatosensory cortex (Figure 1.12), using a combination of tactile and kinaesthetic stimuli to demonstrate a differential activation of area 3a during the latter condition, with activation of areas 3b, 1 and 2 for both stimuli. This finding is consistent with the strong connection between area 3a and the primary motor cortex and the selective response of area 3a to stimulation of subcutaneous and joint receptors (Moore et al., 2000) (Section 1.1.3.4).

Current efforts seek to refine fMRI-derived somatotopic maps using a variety of approaches, particularly in order to resolve representations of individual digits, which are disproportionately represented in the primary somatotosensory cortex. First, stimulus type and delivery pattern is increasingly considered: pure tactile stimuli are most commonly applied in fMRI mapping paradigms, but these can vary from vibrotactile, air-puff or even soft-touch delivered during scan sessions (Overduin and Servos, 2004; Sanchez-Panchuelo et al., 2010; Besle et al., 2013b). Furthermore, ultra-high field (UHF) imaging is increasingly exploited to enable both increased signal-to-noise ratio (SNR) and improved resolution of the maps recorded (Further details in section 2.6). The ability to derive robust and reproducible maps of topography in

the primary somatosensory cortex has yet to be demonstrated at the single subject level in humans.

#### 1.1.5.2 Somatotopy and the primary motor cortex

The term somatotopy is now broadly applied in discussions of the primary motor cortex, referring to a form of body map representation in this agranular region, analogous to the neighbouring postcentral gyrus. While it has been clear for some time that coarse topography exists in the primary motor cortex (Penfield and Boldrey, 1937; Penfield and Jasper, 1954), resolving true somatotopy in the primary motor cortex has been more challenging. There are numerous reasons why a one-to-one representation of individual body regions in the primary motor cortex would be disadvantageous, and hence why the organisation of motor efferents from precentral gyrus may not be synonymous with the postcentral system. *1)* Muscles function in synergies rather than individually to achieve movement, for example, muscles of the shoulder, arm and hand are all recruited in common tasks using the upper limb. *2)* To achieve individuated movement, for example in the digits, isometric contraction of neighbouring muscles is frequently required: a different kind of synergy. *3)* The nature of peripheral myotendinous and bony anatomy places physical constraints of the movement of highly individuated regions, such that these cannot be achieved naturally (Schieber and Santello, 2004).

Evidence from both the primate electrophysiology and human imaging literature cannot clearly demonstrate fine-grain somatotopy in the primary motor cortex without considerable overlap or multiple representations (Kwan et al., 1978; Nudo et al., 1996; Dechent and Frahm, 2003; Olman et al., 2011). While coarse representations of individual limbs and body parts undoubtedly exist, the representation of smaller body parts therein is unclear, with increasing evidence supporting organisation driven by muscle synergies and the motor repertoire of individual subjects (Schieber, 2001; Meier et al., 2008; Overduin et al., 2012).

### 1.1.6 The human hand: a special case

*"That which the delicate yellow spot is to the sentifacient sheet of the retina, may the thumb and index be said to constitute in the great sentifacient field of the limb "*

Sherrington, 1906

The primate hand is a special case in terms of sensorimotor function: the proverbial fovea of the somatosensory system, acting as an exquisite sensory organ, as well as possessing unrivalled motor abilities. These two roles are intimately linked in the day-to-day dextrous uses of the hand, for example in common acts such as palpation using the palm and fingertips in order to derive sensory information regarding object characteristics: *"Without eye movements, vision fades, and the immobile hand is an impoverished sensory organ as regards the complex somesthetic perceptions"* (Mountcastle, 2005).

Bipedalism freed the hand for this sensorimotor role in our hominid predecessors around 3.5 million years ago (Leakey, 1981). Analysis of primate hand structure in the intervening period saw a gradual shift from features adapted for arboreal living, to the eventual emergence of the opposability and evidence of tool use in *H. habilis* (Leakey et al., 1964). It is arguable that the evolution of structure in the primate hand itself drove the development of its extensive neural representation: many structural adaptations present in the primate hand predate the emergence of the extensive functional repertoire seen in *H. Sapiens* (Walker and Leakey, 1993).

In terms of sensory function, the hand shows considerable structural adaptation. Papillary ridges and grooves increase the sensory surface area and show limited motility, which may play a role in sensory function. A high density of sensory afferents, both bare and associated with multicellular mechanoreceptive organs, underlie the unparalleled two-point touch and point localisation thresholds seen in the region,

specifically in the tips of the digits (Figure 1.13). Even the vascular supply is adapted to compensate for frequent indentation of the glabrous skin, with a double capillary loop protecting the vascular supply from crush forces. In terms of motor adaptation, the range of movements possible in the hand are underpinned by the actions of 44 muscles controlling the movement of 27 bones, yielding around 25 degrees of freedom, which permit precision dexterity.

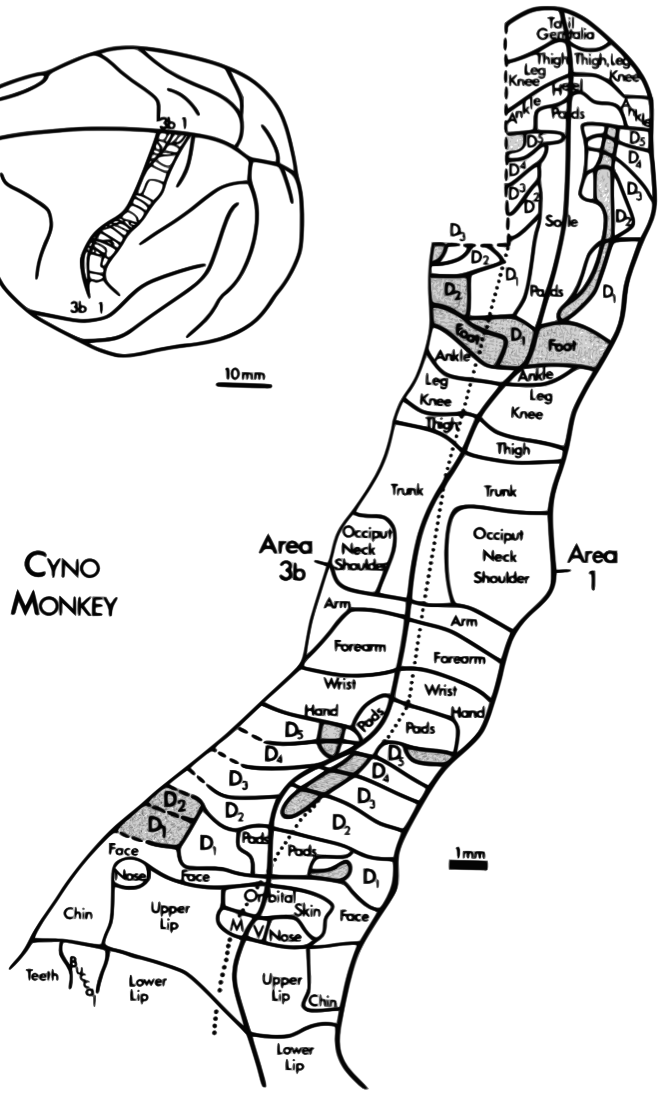


Figure 1.11: *Somatotopic map of Brodmann areas 3a and 1 from microelectrode mapping in cynomolgus monkey.* Dorsolateral view of unfolded cortical surface. The representation of individual digits of the hand and foot are numbered (D1-D5).Shaded regions represent hairy skin. Heavy line: border of area 3b and area 1. Dotted line: central sulcus. Diagram represents summary based on the overlap of maps from several subjects. Reproduced from Nelson et al., 1980.

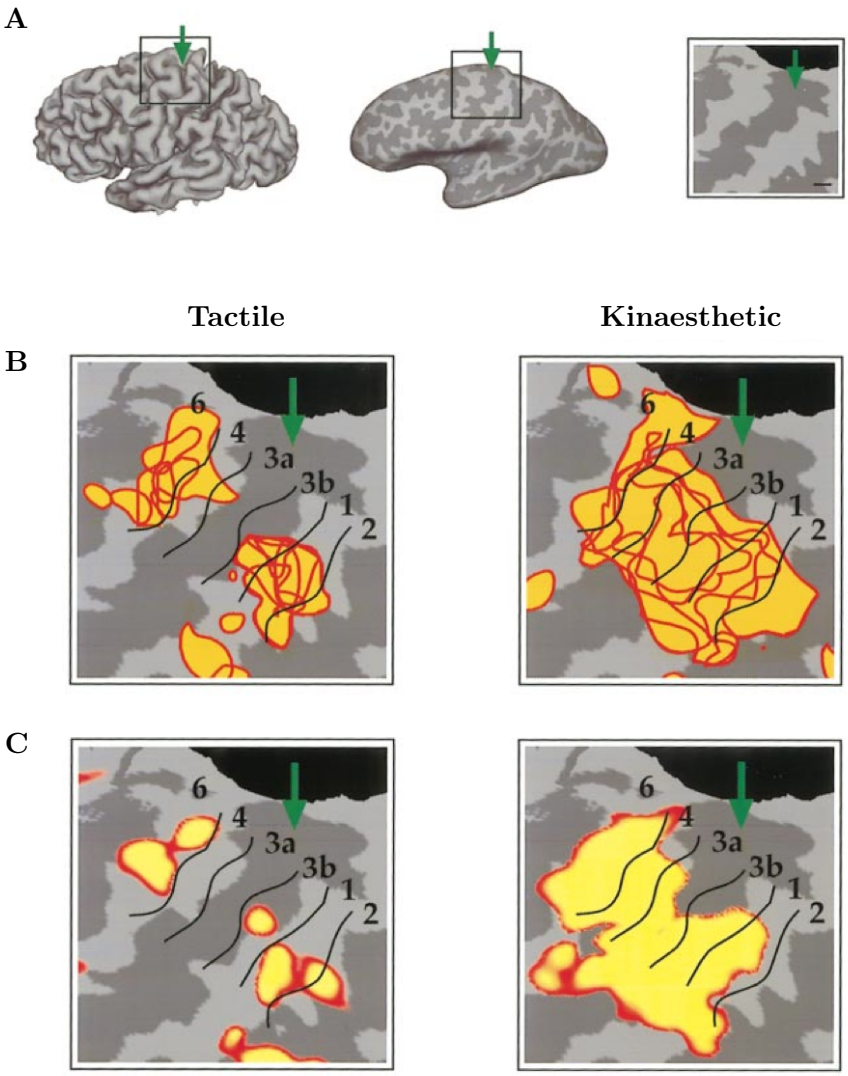


Figure 1.12: *BOLD fMRI tactile and kinaesthetic activation maps presented in Moore et al., 2000.* A: a grey-white boundary reconstruction (left); an inflated pial surface reconstruction (centre); an enlargement of hand knob region on inflated pial surface (right). Scale bar: 1 cm. B: activation maps from five subjects registered into common space and projected onto flattened pial surface representation. (red lines with yellow fill, *t*-test analysis). Tactile activation (left) and kinesthetic/motor activation (right). Solid black lines show anatomically defined borders of Brodmann areas in region of interest. C: the average tactile (left) and kinesthetic/motor (right) activation patterns are projected onto the same brain as in B. Figure and caption reproduced and adapted from Moore et al., 2000.

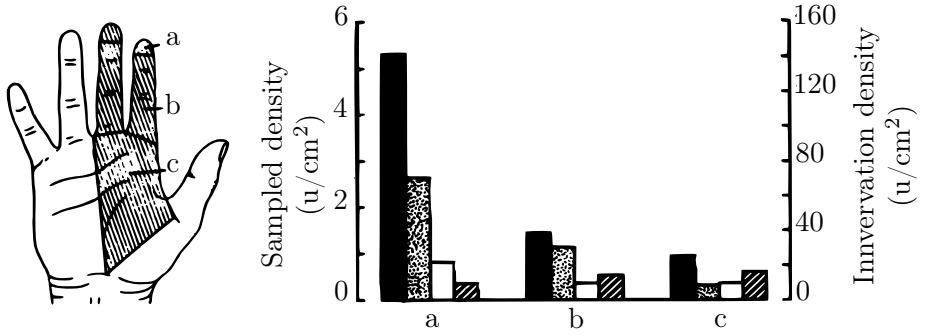


Figure 1.13: *Innervation densities of mechanoreceptive afferent fibres in the glabrous skin of the human hand.* Results of microelectrode recording from the median nerves of waking humans. Filled bars: Rapidly adapting; Stippled bars: Slowly adapting type I; Open bars: Pacinian corpuscles; Hatched bars: Slowly adapting type II. Sampled density: number of fibres per unit squared. Innervation density: absolute number of terminated fibres per unit squared. From Johansson and Vallbo, 1979.

## 1.2 Principles of plasticity

*"When two elementary brain-processes have been active together or in immediate succession, one of them, on reoccurring, tends to propagate its excitement into the other. "*

William James, 1890

Plasticity in the context of neuroscience refers to the inherent ability of the brain to exhibit enduring structural and functional changes on the basis of experience. In this context the term experience is considered broadly, from activities which stimulate learning and memory, to pathological changes both intrinsic and extrinsic to the central nervous system, which can drive both damaging and compensatory plastic changes.

### 1.2.1 Synaptic transmission

The basis of synaptic transmission was investigated initially at the neuromuscular junction peripherally (Claude, 1856; Sherrington, 1897). Chemical synapses use a system of neurotransmitter signalling to transfer electrical impulses from a presynaptic to a postsynaptic neuron across the synaptic cleft.

In brief, the process of synaptic transmission begins with an action potential reaching a bouton in a presynaptic neuron, with resulting depolarisation and opening of voltage-gated $Na^+$ channels. The shift in membrane potential prompts the opening of voltage-gated $Ca^{2+}$ channels in the presynaptic membrane (Augustine et al., 1985), leading in an initially slow influx in $Ca^{2+}$ locally in the bouton due to the limited electrochemical gradient in the depolarised state, followed by a more rapid influx at the bouton begins to hyperpolarise (Geiger and Jonas, 2000; Schneggenburger and Neher, 2000). $Ca^{2+}$-synaptotagamin binding prompts activation of soluble *N*-ethylmaleimide-sensitive factor attachment protein receptor (SNARE) complexes associated with

the release of vesicles of neurotransmitter (Geppert et al., 1994; Südhof, 2004). The ensuing binding of the vesicle and presynaptic membrane produces a fusion pore, through which neurotransmitter is released into the synaptic cleft. Diffusion of the neurotransmitter across the cleft and binding to ionotropic or metabotropic post-synaptic receptors results in a post-synaptic response, leading to direct or indirect depolarisation of the post-synaptic neuron, and an ensuing excitatory postsynaptic current (Lisman et al., 2007).

### 1.2.2 Hebbian theory of synaptic plasticity

Although plasticity frequently manifests as a structural or functional change in the brain on a network level, the underlying mechanism is grounded in synaptic connections and changes therein. It was Ramón Y Cajal who first proposed a dominant role for dynamic neural connections in the process of learning in adulthood, rather than an ongoing process of neurogenesis (Cajal, 1894). While others had also considered a synaptic mechanism for changes in the brain (James, 1890), it was not until the mid-twentieth century that this theory was meaningfully expanded by Canadian physiologist Donald Hebb.

Concerned with the challenging role of the psychologist in reducing the complexities of human behaviour to mechanistic physiological processes, Hebb proposed his now ubiquitous theory of synaptic plasticity in the book: The Organisation of Behaviour (Hebb, 1949). Hebb postulated that *"when an axon of cell A is near enough to excite cell B or repeatedly and consistently take part in firing it, some growth process or metabolic changes take place in one or both cells such that A's efficiency, as one of the cells firing B, is increased."* Hebbian plasticity is now more broadly considered to refer to the phenomenon of long lasting synaptic change driven by correlated pre-synaptic and post-synaptic activity in two connected neurons (Abbott and Nelson, 2000).

### 1.2.3 Long term potentiation and depression

Long term potentiation (LTP) and long term depression (LTD) refer to the phenomena by which specific patterns of activity in neuronal cells, which are in synaptic contact, can elicit prolonged enhancement or diminishment in their synaptic communication (Malenka and Nicoll, 1999; Ito, 1989). Initial evidence of LTP came from studies of the rabbit hippocampus, wherein short bursts of high frequency electrical stimulation were shown to produce increased synaptic strength persisting over the ensuing hours and days (Lømo, 1966; Bliss and Lømo, 1973). The mechanism underlying LTP has been the subject of intense investigation (Malenka and Bear, 2004), most using in vitro hippocampal preparations, studying the synapses between Schaffer collaterals and the commisural axons of CA1 pyramidal cells; these findings appear to translate to excitatory synapses in the cerebral cortex (Kirkwood et al., 1993). However, it is increasingly clear that LTP is mechanistically variable depending on the anatomical region, the initial trigger and the developmental period under study. *N*-methyl-D-aspartate (NMDA) receptor-dependent LTP is one of the most intensely studied of these synaptic processes, with a clear role for intracellular $Ca^{2+}$ in the induction phase (Malenka et al., 1992), and a multitude of downstream presynaptic and postsynaptic intracellular signalling cascades implicated in the sustained effects (Kirkwood et al., 1997; Yasuda et al., 2003), which promote structural growth and changes in synaptic contact and dendritic spine formation over the long term (Lüscher et al., 2000; Lisman and Zhabotinsky, 2001; Ju et al., 2004).

LTD is classically induced following longer periods of low frequency presynaptic stimulation, and like LTP, is reliant on NMDA signalling postsynaptically, with a characteristic pattern of increased intracellular $[Ca^{2+}]$ recruiting a range of downstream processes to alter postsynaptic receptor frequency and dynamics, as well as feedback signalling to alter neurotransmitter release (Collingridge et al., 2010). It is important to consider LTP and LTD occurring at the single synapse level in the broader context of neuronal networks, which display remarkable stability in the face

of highly dynamic neuronal interactions. There is increasing evidence that a collection of homeostatic processes function to regulate levels of neuronal activity at a network level through mechanisms such as activity-dependent regulation of neuronal firing, changes in the threshold for LTD and LTP on the basis of prior activity, or even scaling of synaptic responses to equilibrate global profiles of activity (Turrigiano, 2012).

## 1.3 Defining plastic change

Discussion of plasticity encompasses a broad range of related phenomena in the brain. Although we typically consider changes in synaptic signalling as the irreducible unit of plasticity, this can be considered at a number of different levels. While it is possible to observe functional or structural changes in the human brain using tools such as magnetic resonance imaging (MRI), the cellular underpinnings of these changes are likely diverse (Zatorre et al., 2012). At the synaptic level, changes in grey matter may encompass axonal sprouting, dendritic branching with synaptogenesis, and neurogenesis. In white matter, observed structural changes may be underpinned by fibre reorganisation and the formation or remodelling of myelin. In additional plastic change across the brain may be underpinned by glial changes or angiogenesis. This range of potential mechanisms bestows an immense plastic potential in the brain, not only enabling the formation of new synapses or myelin, but also the taking advantage of the degenerate pattern of connectivity in the brain by potentiating or uncovering pre-existing silent or weak connections (DeFelipe et al., 1986; Recanzone et al., 1992).

In studying plasticity in the human brain with non-invasive tools, it is not possible to directly observe these microstructural phenomena. It is therefore commonly necessary to use markers of functional and structural plasticity as surrogates of the diverse range of microstructural plastic phenomena ongoing in the human brain. In the context of short-term plasticity over the order of days to weeks, functional measures

of brain activity are frequently used as markers. However, with the ever increasing resolution and specificity of structural imaging, it is possible to resolve markers of structural change over short periods (Johansen-Berg et al., 2012).

## 1.4 Plasticity and the sensorimotor network

The sensorimotor network receives a rich variety of afferent signals providing peripheral sensory input, as well as considerable efferent output in motor control. Hence there is obvious scope for plasticity in the system, with sensory and motor events acting as the experience that drives adaptation and changes in the system. At the cellular level, the animal literature provides clear evidence of LTP in the sensorimotor network, both from in vitro slice preparations assessing connections between the primary sensory and the primary motor cortex (Sakamoto et al., 1987) and within the primary motor cortex (Hess and Donoghue, 1994), as well as using microelectrode stimulation in vivo (Iriki et al., 1989; Monfils et al., 2004). Similarly, prolonged low-frequency stimulation of sensorimotor afferents has induced a measurable pattern of synaptic depression therein (Froc et al., 2000; Werk et al., 2006). The sensorimotor system continues to form an ideal model system through which studies of peripheral manipulations can be used to study the dynamics of plastic changes (Jones, 2000). Further, an ability to redress the balance between maladaptive and adaptive plasticity in the sensorimotor network has enormous therapeutic potential in the treatment of diseases with aetiology both intrinsic and extrinsic to the brain (Nudo et al., 2001; Nava and Röder, 2011). For the purposes of this thesis, I refer to two different forms of plasticity in the sensorimotor system:

> *Usage-dependent*: functional or structural alterations in the sensorimotor network driven by changes in the level of sensory afferent input or motor output, for example following deafferentation or in cases of chronic disuse following injury.

*Experience-dependent*: functional or structural alterations in the sensorimotor network driven by a change in a pattern sensorimotor activity, including the learning of a new motor skill or some kind of sensory training.

### 1.4.1 Normal variation in somatotopy

The degree of individual variability in the fine grain somatotopy of maps in the brain is quite striking in cross-sectional studies of the primary somatosensory cortex. Early work applying metabolic labelling techniques with [$^{14}$C]-2-deoxyglucose demonstrated this variability between macaques (Juliano and Whitsel, 1985), further supported by microelectrode recording studies (Merzenich et al., 1987) (Figure 1.14), both arguing that while the broad lateral to medial representation of digits two to five was consistent across individuals, the size, shape and orientation of individual digit representations differed considerably. This consensus has been further supported by recent work applying UHF fMRI to map digit representations in the primary somatosensory cortex of New World monkeys (Figure 1.15) (Zhang et al., 2010). Merzenich argues that while this variability in individual digits may seem surprising, given the highly reproducible patterning seen in human hand development, the neural representations of the digits may be changed developmentally through some kind of experience based plasticity (Merzenich et al., 1987). More recent work studying the development of somatotopy in rats reported particularly early and isolated development of topography in barrel cortex: a region organised with a fine degree of topography (Seelke et al., 2012). The apparently precocious development of over-represented regions exhibiting detailed somatotopy is perhaps a driving force behind the variability seen therein in adulthood, with sensory and motor experiences during development potentially shaping representations.

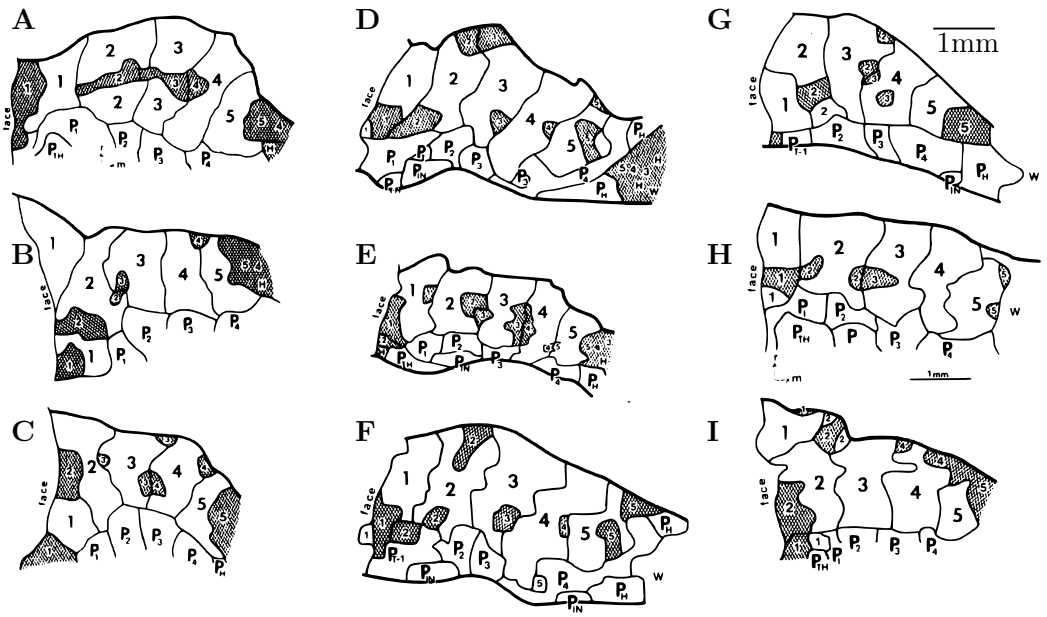


Figure 1.14: *Individual variability in microelectrode maps of primate area 3b.* Representations of individual digits (1-5) in nine owl monkeys (A-I). P: pads. Hatched regions: dorsal skin. W: wrist. Adapted from Merzenich et al., 1987.

### 1.4.2 Usage-dependent plasticity

Much early work on usage-dependent plasticity focused on studies of peripheral deafferentation. As a continuation of their detailed microelectrode mapping in the primary somatosensory cortex, Kaas and Marezenich began to consider the variable effects of deafferentation: from nerve transection to digit amputation (Merzenich et al., 1983; Merzenich et al., 1984). These considerable insults to the peripheral nervous system prompted rapid plastic changes in the primary somatosensory cortex. In the case of transection of the median nerve, microelectrode mapping directly following the deafferentation showed large silenced regions, unmasking minor supply from the radial nerve, and a reorganisation of the silenced site over period of weeks to months, with similar patterns seen following amputation. The long term effects of this reorganisation, assessed in primates 12 years after initial deafferentation, showed a considerable potential for usage-dependent plasticity to drive remapping on a scale which sees the face region expand into that previously representing the

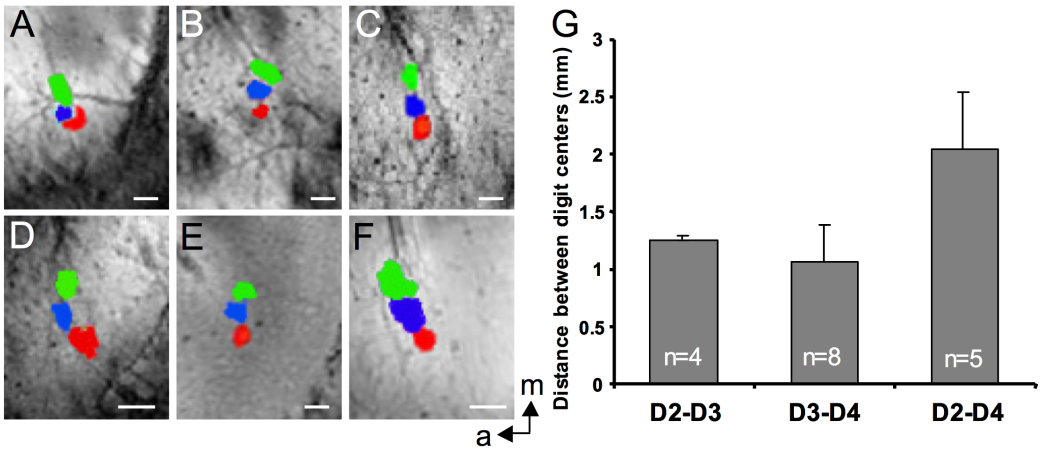


Figure 1.15: *Individual variability in high-field fMRI maps of primate area 3b.* Representations of D2 (red), D3 (blue) and D4 (green) in six New World monkeys (A-F). P: pads. Reproduced from Zhang et al., 2010.

limb (Pons et al., 1991). Our understanding of usage-dependent plasticity remains incomplete, with this rapid reorganisation also associated with maladaptive features such as phantom pain (Mountcastle, 2005). Recent work assessing this phenomenon in amputees suggests an inherent change in the cortical region initially silenced, which prompts an altered sensory experience in the body region it represents, rather than a simple regression of its cortical representation (Makin et al., 2013).

#### 1.4.2.1 Plasticity and disuse

Beyond examples of usage-dependent plasticity *in extremis*, such as amputation or denervation, the same underlying processes have been implicated in a number of pathological conditions. Chronic disuse of a limb over a prolonged period has been shown to induce rapid changes in cortical structure over a period of two weeks (Langer et al., 2012), as well as changes in the excitability of the primary motor cortex (Facchini et al., 2002). Sensory deafferentation over the short term through local anaesthesia has demonstrated measurable benefit when used as an adjunct in stroke rehabilitation, associated with disinhibition in the primary motor cortex

and alterations in topographic organisation therein (Weiss et al., 2004; Björkman et al., 2009; Weiss et al., 2011; Sens et al., 2012). Cortical changes resulting from deprivation of sensory input have implicated so-called silent neurons in redistribution of cortical representation (Margolis et al., 2012).

### 1.4.3 Experience-dependent plasticity

In contrast to the drastic reduction or cessation of afferent and efferent sensorimotor activity described in section 1.4.2, studies considering experience-dependent plasticity consider much more subtle effects. These studies can be broadly subdivided into those considering motor learning: the acquisition of a new skill through training, and those considering a peripheral manipulation which alters both sensory afferent and motor efferent activity.

#### 1.4.3.1 Motor learning

Plastic reorganisation of topography in the primary motor cortex following motor learning is thought to be driven by training of new muscles synergies, whose repeated use drives some form of motor memory mechanism (Latash, 2010). Short periods of motor training involving digit movement have demonstrated measurable digit-specific behavioural changes in the primary motor cortex using transcranial magnetic stimulation (TMS) methods and measuring motor end plate potentials (Pascual-Leone et al., 1995; Classen et al., 1998). The underlying changes in the primary motor cortex which drive this behavioural effect were first comprehensively investigated in squirrel monkeys (Nudo et al., 1996). This study applied microelectrode mapping of the primary motor cortex before and after a number motor learning paradigms using the upper limb. It demonstrated a task-specific reversible remapping of motor topography, which persisted over several days. Training on a small object retrieval task drove expansion in regions response for digit movement (Figure 1.16), while a bolt turn task involving unilateral pronation prompted expansion of the region

responsible for movement of the forearm. These findings have since been supported by studies applying fMRI, which demonstrate rapid changes after only a few trials of a motor training task (Karni et al., 1998). Recent evidence from intracortical recordings in the rat shows that this remapping phenomenon is essential for the acquisition of motor skills, but is not required for motor skills to be sustained, suggesting an alternative mechanism of motor memory (Molina-Luna et al., 2008).

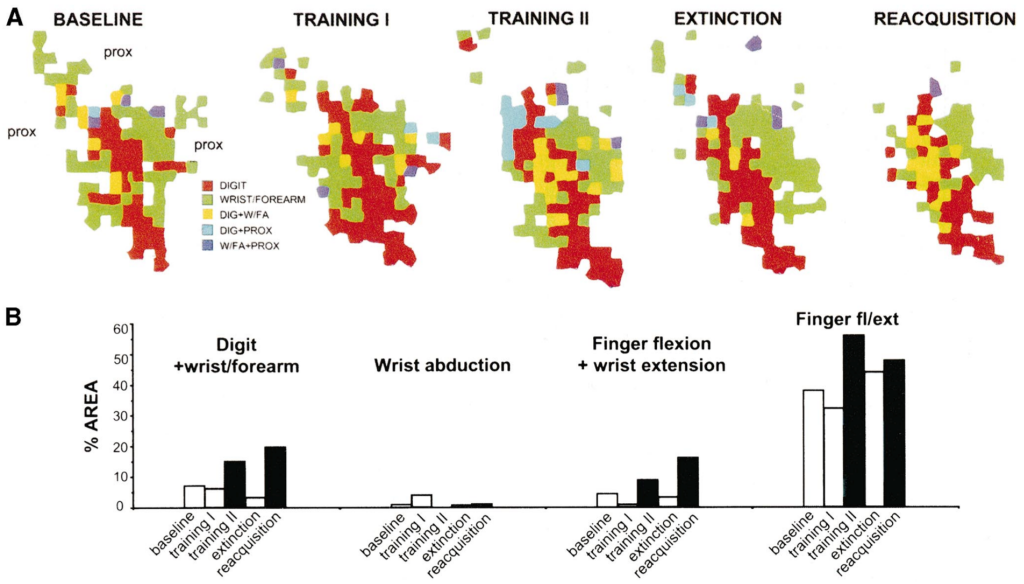


Figure 1.16: *Topographic remapping of the primary motor cortex after motor learning in the squirrel monkey.* A. Baseline: initial microelectrode map of forelimb representation. Training I: Microelectrode mapping after 11 days of Kluver board training. Training II: Microelectrode mapping after an additional 39 days of Kluver board training: marked increase in distal forelimb representations. Extinction: Microelectrode mapping after 4 months with no practice: reversal of remapping effect. Reacquisition: Microelectrode mapping on reacquisition of motor skill after 30 days of Kluver board training; similar remapping observed as seen in Training II. B. Bar charts display breakdown of overall distal forelimb representation at each time point. Reproduced from Schieber, 2001. Adapted from Nudo et al., 1996.

#### 1.4.3.2 Sensorimotor training

Plasticity-induced reorganisation of somatotopy in the primary somatosensory cortex has principally been investigated through manipulation or training that will alter

afferent input. This idea can be explained in the context of Hebbian plasticity, such that if signals from previously unrelated peripheral regions become temporally correlated, this will drive synchronous activity in cortical neuronal populations, driving synaptic changes which will affect neuronal networks and cortical maps. The effects of such peripheral manipulations were well described in a microelectrode mapping study of somatosensory study, which considered the effects of surgical attachment of digits three and four on the primary somatosensory cortex in the adult owl monkey (Allard et al., 1991). This study demonstrated that over a period of months this induced syndactyly caused previously discontinuous representations of digits three and four in area 3b to develop considerable overlap (Figure 1.17). This finding was reproduced in a similar study of raccoons (Zarzecki et al., 1993). Further experiments considered the effects of tasks involving synchronous and asynchronous sensory stimuli to the digits, demonstrating that these tasks respectively drove integration and separation of cortical digit representations in area 3b of the owl monkey (Wang et al., 1995). These findings have prompted investigation of somatosensory remapping in humans, with an MEG study measuring the short-term effects of finger webbing over several hours showing a reduction in the separability of digit representations using electrical stimulation (Stavrinou et al., 2007).

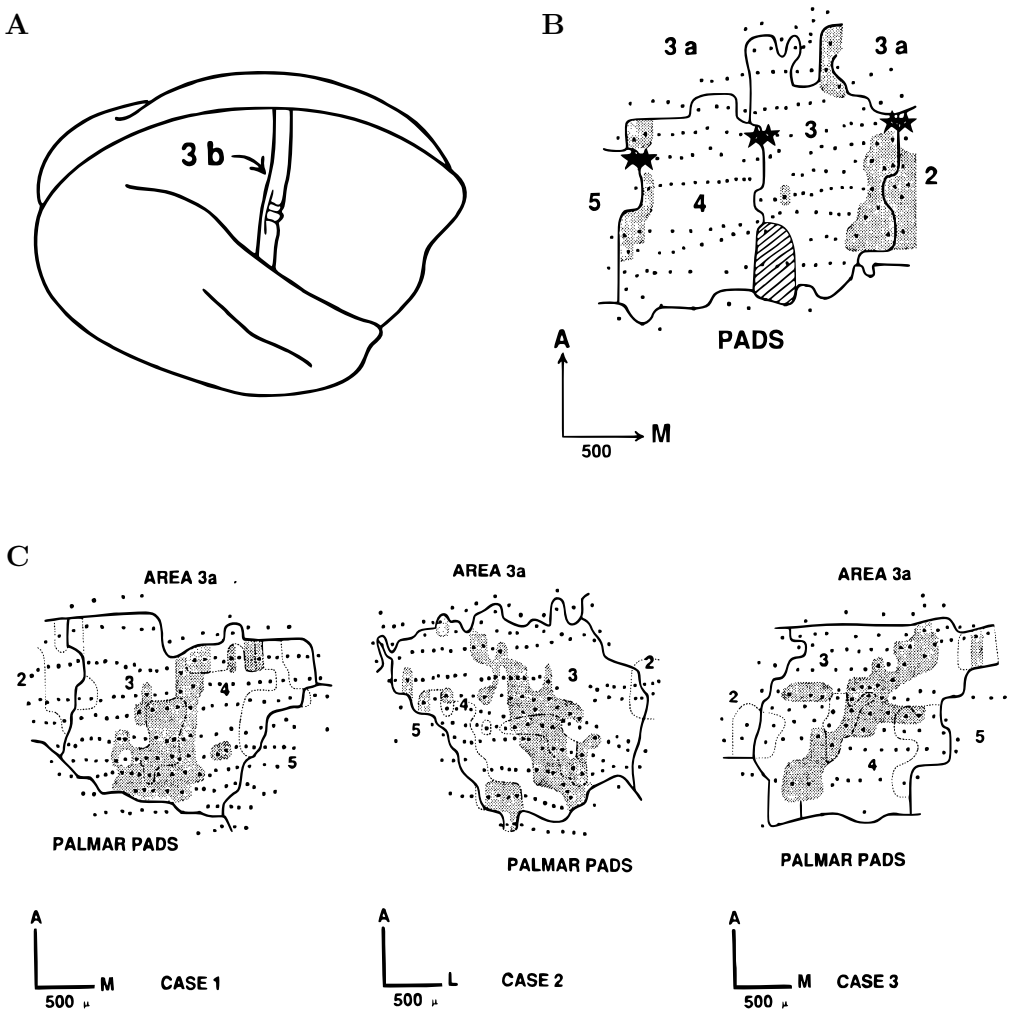


Figure 1.17: *Experience-dependent remapping of area 3b digit representation in the owl monkey.* A: dorsolateral view of the right hemisphere of the owl monkey brain, highlighting area 3b and the digit representations therein. B. Typical microelectrode mapping representation of digits three and four in area 3b; P: palm. Shaded regions: dorsal skin. C. Microelectrode mapping representation of digits three and four 5.5 months, 7.5 months and 3 months following surgery (left to right). Shaded regions: dual receptive fields from digits three and four. Adapted from Allard et al., 1991.

## 1.5 Sensorimotor stroke

Stroke refers to a spectrum of cerebrovascular disease broadly characterised by interruption to blood supply the brain, both transient and prolonged, which result in tissue hypoxia and ensuing damage. There are around 111 000 instances of first stroke in the United Kingdom each year (Scarborough, 2009), of which 80 percent are ischaemic, and the remaining 20 percent are haemorrhagic. In the United Kingdom, around 300 000 people are living with moderate or severe disability as a result of stroke (Adamson et al., 2004), many with persistent deficits in sensory and motor function.

### 1.5.1 Focal cerebral ischaemia

#### 1.5.1.1 Aetiology

Focal cerebral ischaemia is characterised by the occlusion of a blood vessel in the brain, leading to local hypoxia and tissue damage, rather than global ischaemia. The location and duration of this occlusion dictates the severity and symptomatology of each individual stroke. The major causes of vascular occlusion are in situ thrombosis and embolism. Atherosclerosis is a leading cause for vessel occlusion, forming a prothrombotic surface, as well as a potential source of fatty emboli. The anatomical extent of damage caused by occlusion is highly variable. The extent of collateral flow is a major factor determinant of hypoxic damage, and is particularly poor in deep subcortical structures, and arterial borderzones in the cerebral cortex. Emboli commonly lodge in the middle cerebral artery, particularly on the left hand side, as it forms a direct continuation of the internal carotid artery (Kumar et al., 2009).

#### 1.5.1.2 Pathophysiology

The brain is exquisitely sensitive to ischaemic insults. Although it typically accounts for between one and two percent of body mass in humans, it consumes around 20

percent of oxygen and glucose intake. Any interruption in blood supply perturbs the highly aerobic metabolic processes occurring in the brain. A lack of oxygen and glucose in the brain impairs major metabolic pathways, resulting in a reduction in the production of adenosine trisphosphate (ATP). When this reduction in ATP production reaches a critical point, cells enter a state of energy failure. The severity and effect of this energy failure differ across the affected region of brain tissue. The severely affected ischaemic core passes a threshold at which individual neurons can no longer support their membrane potential, leading to terminal depolarisation, and irreversible damage. Depolarisation leads to uncontrolled release of excitatory neurotransmitters such as glutamate, and a failure in reuptake mechanisms. A process of excitotoxicity ensues, whereby a high concentration of extracellular glutamate promotes an influx of $Ca^{2+}$ into neurons via postsynaptic receptor binding, leading to further intracellular $Ca^{2+}$ release (Lo et al., 2005). Intracellular $Ca^{2+}$ concentration is maintained at micromolar concentrations, and subject to careful homeostatic regulation. An excessive concentration of intracellular $Ca^{2+}$ activates the intrinsic apoptotic pathway, leading to the activation of $Ca^{2+}$-dependent proteases, initiator caspases, and eventually executioner caspases. These enzymes promote cytoskeletal breakdown, and activate endonucleases which degrade nuclear DNA (Kumar et al., 2009).

The tissue surrounding the ischaemic core is known as the penumbra (Astrup et al., 1981). The penumbra exhibits perturbations in metabolic processes, but energy production and membrane potential are not critically affected. However, as metabolic demands increase disproportionate to perfusion in the penumbra, a process of spreading ischaemia occurs, leading to expansion of the irreversibly damaged core (Petzold et al., 2003). The therapeutic window to prevent this expansion lasts only three hours from the initial vascular insult. Current clinical approaches aim to reduce depolarisation, reduce metabolic tissue demands through hypothermia, and increase collateral blood supply (Rogalewski et al., 2006). Although these methods have proved very effective in preventing ongoing damage, they provide questionable benefit

beyond the initial three hours post-stroke (Hossmann, 2012).

### 1.5.2 Stroke recovery

Stroke recovery is clinically divided into three distinct periods: the acute phase from three to seven days post stroke, the sub-acute phase from one to six months post stroke; and the chronic phase from six months onwards (Teismann et al., 2011). Functional recovery post-stroke spans the acute and chronic periods, with some patients exhibiting behavioural improvements years after the initial vascular insult (Cramer, 2008). Functional recovery consists of elements of behavioural adaptation or compensation, as well as true recovery driven by plastic changes in the brain (Levin et al., 2009; Moon et al., 2009). The post-stroke brain exhibits a unique signature of plasticity. Current research efforts seek to understand both the timeframe of this plastic state, and strategies through which it might be extended or rekindled in chronic stroke patients.

#### 1.5.2.1 Mechanisms of stroke recovery

Stroke recovery is facilitated by both the nature of brain connectivity, and the inherent plastic ability of the brain to remap (Section 1.2). In terms of connectivity, the brain functions through distributed networks subserving given functions, meaning focal damage typically does not compromise an entire neural system. Furthermore, the brain shows a degree of degeneracy in its connectivity, with large numbers of diffuse connections. Evidence from the barrel cortex in mouse shows that minor sensory stimuli rapidly induce activity across the sensorimotor network (Ferezou et al., 2007). Similarly, sensory afferents from individual digits in the raccoon have been show to display widely distributed low-level activation across the primary somatosensory cortex, despite the fine grain topography seen therein (Smits et al., 1991). These diffuse connections can offer a valuable link between compromised penumbral regions following a stroke, and related healthy cortical tissue. The diffuse

connections likely act in combination with the brain's inherent ability to adapt and remap. Such remapping has been observed to a varying extent, from reorganisation with primary somatosensory cortex (Winship and Murphy, 2008), to more extensive shifts, for example in non-human primate stroke models where damage to the hand representation in the primary motor cortex has been shown to prompt an enlargement of the equivalent representation in ventral premotor cortex, proportional to the degree of connectivity between these two regions prior to the stroke (Frost et al., 2003). Similarly, evidence from two-photon microscopy in murine stroke models suggests the potential for remapping of forelimb sensory function to the primary motor cortex after an ischaemic stroke and other more distant sites, implying a functional shift at the level of network activity in response to a focal lesion (Brown et al., 2009). This enhanced plasticity post-stroke might impair previously described mechanisms of experience-dependent plasticity seen in the healthy brain, suggesting a stroke-specific plastic state during recovery (Jablonka et al., 2007).

#### 1.5.2.2 Time course of stroke recovery

The potential for a unique signature of plasticity post-stroke raises questions regarding the time-frame in which the potential for recovery is optimal. Transcriptome analysis in a rat ischaemic stroke model shows a peri-infarct pattern of gene expression consistent with enhanced synaptogenesis, dendritic spine production, growth and proliferation seven days after the vascular insult (Carmichael et al., 2005). Work in rats has investigated the effects of varying the delay between stroke and rehabilitation using an endothelin-1 model of stoke affecting the primary sensorimotor cortex (Biernaskie et al., 2004). This study demonstrated that an enriched recovery program starting at five or 14 days post-stroke promoted significant recovery of motor function, and was associated with enhanced dendritic branching of layer V pyramidal neurons in the primary motor cortex. In contrast, the same rehabilitation paradigm applied at 30 days produced no measurable recovery compared to the control condition . This finding has been broadly mirrored in studies of early versus delayed rehabilitation

in the hospital setting (Weinrich et al., 2004). It therefore seems that although functional recovery can clearly be attained in the chronic stages of stroke recovery (Ward and Cohen, 2004), there is evidence for a unique window early after stroke upon which specifically designed rehabilitation approaches could capitalise.

#### 1.5.2.3 Motor rehabilitation for stroke

Beyond the timing of stroke rehabilitation, the rehabilitation intervention applied remains an issue of some debate. Stroke patients frequently suffer from long term sensory and motor deficits which impair their ability for independent living. At six months post-stroke, only 38 percent of those receiving rehabilitation recover functional dexterity in their hand (Kwakkel et al., 2003). It is increasingly clear that rehabilitation paradigms incorporating repetitive movements akin to those used in everyday tasks seem to stimulate improvements in motor function (Bütefisch et al., 1995).

A common variety of rehabilitation is constraint induced motor therapy (CIMT) which involves forced use the the compromised limb through restraint of the unaffected limb. The rationale behind CIMT comes from evidence of learned non-use in chronic stroke patients who become reliant on their heathy limb, a phenomenon linked with maladaptive plasticity in the cerebral cortex (Wolf et al., 1989). CIMT has been shown to promote motor reorganisation and expansion of the motor representation in the brain of chronic stroke patients (Wolf et al., 2006; Sawaki et al., 2008). However, early after stroke, CIMT has not demonstrated any benefit over standard therapies, perhaps because it requires a high degree of baseline dexterity in the digits of the affected hand (Fritz et al., 2005; Boake et al., 2007). CIMT is therefore unsuitable for the majority of acute stroke patients, which is unfortunate given the evidence for a potential early surge in post-stroke plasticity (Section 1.5.2.2).

Other approaches are increasingly targeting the acute stage of stroke rehabilitation. Functional strength training (FST) involves both task-specific exercises and strength

training for patients with moderate to severe paresis (Kamper et al., 2006; Ada et al., 2006), with potential gains of standard therapy (Donaldson et al., 2009). FST focuses specifically on strengthening muscles in the shoulder girdle and around the elbow to facilitate stable placement of the hand, as well as the production of appropriate grasp strength for different tasks.

## 1.6 Aims

The primary aim of this thesis is to investigate experience-dependent and usage-dependent plasticity in this sensorimotor network of the human brain. I aim to use a variety of MRI modalities to investigate the propensity for both short-term and long-term neuroplastic phenomena in both healthy control participants and patient populations. The plastic processes under study are principally in the context of altered use or disuse, which causes changes in both sensory afferent and motor efferent activity. I seek to understand how deficits or alterations in the periphery can shape or shift structure and function in the sensorimotor network, whether these changes are an adaptive or a maladaptive, and whether they occur in health or disease . Finally, I aim to contrast the studies of plasticity driven by factors extrinsic to the brain with a study of sub-acute stroke, in order to assess how deficits in the sensorimotor network reflect motor function in the periphery.

In Chapter 2 I will outline details of the imaging methods and analysis applied in this thesis, with specific detail on the special considerations relevant when imaging at UHF. In Chapter 3 I will develop a paradigm to rapidly and reproducibly map digit somatotopy in the primary somatosensory cortex at the single subject level. I will build upon this work in Chapter 4, where I will apply the digit mapping paradigm to study the effects on digit somatotopy of a peripheral manipulation where the right index and right middle finger are glued together for a period of 24 hours. In contrast, the experiments described in Chapters 5 and 6 will aim to investigate the plasticity of long-term disuse, specifically assessing structural brain changes associated with

long-term unilateral disuse of the upper limb in patients with massive irreparable rotator cuff tear in a cross-sectional study (Chapter 5), and the extent to which rehabilitation of limb use is associated with brain change in a longitudinal study Chapter 6. Finally in Chapter 7 I will assess how deficits within the sensorimotor network in subacute stroke patients relate to motor function in the early stages of recovery.

# 2 Methods of imaging the sensorimotor network

*This thesis uses MRI to study plasticity in the sensorimotor network of the human brain. MRI provides a useful means of investigating brain structure and function non-invasively without exposure to ionising radiation. The work presented in this thesis uses a combination of MRI modalities acquired on both clinical systems and ultra-high field research systems. In this chapter I provide an overview of the basic principles of nuclear magnetic resonance and how it is applied in medical imaging. I go on to discuss the benefits and limitations of imaging at ultra-high field. Finally I discuss the MRI analysis of structural, functional and diffusion-weighted MRI pertinent to the thesis.*

## 2.1 Principles of nuclear magnetic resonance

Nuclear magnetic resonance (NMR) results from the interaction between certain nuclei within a sample under study and an applied magnetic field. These nuclei are able to absorb and emit, or resonate, energy on the radio frequency (RF) range of the electromagnetic spectrum. The ability to detect this RF signal following the application of an RF pulse can be tuned to yield a range of information regarding the sample in question. The observation of resonance and ensuing investigation of NMR formed the basis of the 1952 Nobel Prize for Physics, awarded to Edward Purcell and Felix Bloch. The principles of NMR are now applied broadly in the physical

sciences, and since the late 1970s, have formed the basis of MRI (Mansfield, 2013). MRI is a non-invasive medical imaging technique, applied broadly in both clinical and research settings, favoured for its versatility and underlying mechanism, which does not involve exposure to ionising radiation.

### 2.1.1 The nuclear moment

Early investigations of NMR observed that charged nuclei, such as the hydrogen nucleus $H^+$, themselves produce an electromagnetic field. MRI is specifically concerned with hydrogen nuclei due to their relative abundance in both water and fat in biological systems. According to quantum theory, every species of atomic nuclei has a given number of energy states. The proton of a hydrogen nucleus possesses one of two energy states denoted -$^1/_2$ and $+^1/_2$, referring to species spinning in opposite directions and producing opposite electromagnetic fields. As the $H^+$ proton is unpaired, it yields a net magnetic field, known as a magnetic dipole moment (MDM).

In the absence of a magnetic field, the axes of each MDM is oriented randomly, resulting in no net magnetisation ($M_0$). When a static magnetic field is applied ($B_0$), the axes of each MDM realigns, half with the direction of the $B_0$, and half opposing the direction of the $B_0$ (Figure 2.1). The number of MDMs aligned with the $B_0$ increases exponentially over a period of time, leading to an increasing $M_0$ at a rate dependent of the strength of the applied magnetic field and the properties of the sample being imaged. Protons also precess about the axis of the $B_0$, as well as spinning on their own axis, though the $M_0$ remains in the direction of the $B_0$ . The rate of precession defined by the angular precessional frequency (Larmor frequency $\omega$) is dictated by the strength of the external field ($B_0$) and the gyromatic ratio of the nuclei in question ($\gamma$):

$$\omega = \gamma B_0$$

### 2.1.2 Spin excitation and relaxation

When an external magnetic field is applied to a sample, the nuclei therein are aligned with and precess about the direction of this magnetic field, yielding a $M_0$ in the direction of the $B_0$, which by convention is considered the z-axis of the imaging coordinate system. In order to derive a signal from the nuclei, a second magnetic field ($B_1$) must be applied in the form of an RF pulse, an electromagnetic wave. This pulse is applied along the x-axis, perpendicular to the $B_0$ field (Figure 2.2B). The application of this weaker oscillating $B_1$ field flips the nuclei into the x-y plane, as the nuclei precess about both the $B_0$ and $B_1$ fields. As $B_0 >> B_1$ and therefore $\omega_0 >> \omega_1$, the nuclei precess more slowly about the $B_1$ field, resulting in a spiral motion of procession known as nutation.

However, this secondary resonance about $B_1$ is dependent on the RF pulse transferring energy to the nuclei. Resonance is only achieved when the frequency of the applied RF pulse matches the Larmor frequency of the nuclei precessing in the $B_0$ field. If these two frequencies are matched, the nuclei are flipped into the x-y plane and precession about $B_1$ ensues. Precession about the $B_1$ results increasing phase coherence in the precessing nuclei, leading to an increased transverse magnetisation in the x-y plane ($M_{xy}$) and a reduction in the magnetisation in the z-axis ($M_z$) (Figure 2.2).

### 2.1.3 T1, T2 and T2*

Once the RF pulse is switched off, a process of relaxation occurs, such that the nuclei in the sample realign with the $B_0$ field in the z-axis, yielding $M_0$ as they return to a low energy state in which the nuclei are out of phase with one another. The relaxation process is characterised by a gradual increase in $M_z$, and a reduction in $M_{xy}$. The pattern of relaxation is dependent on the environment of the nuclei. The rate of $M_z$ growth and $M_{xy}$ decay are not directly related (Figure 2.2A), and therefore they both provide distinct information regarding the sample under study.

The rate of $M_z$ growth is reflected in the time constant T1, referred to as the longitudinal relaxation time, or spin-lattice relaxation time. This represents the loss of RF pulse energy from the nuclei to their surroundings, known as the lattice. The rate of $M_{xy}$ decay is reflected in the time constants T2 and T2*. T2 is referred to as the transverse relaxation time, or spin-spin relaxation time and is dependent upon the gradual decay of $M_{xy}$ driven by the transfer of energy between adjacent nuclei; so-called spin-spin interactions. T2* is dependent upon the gradual decay of $M_{xy}$ driven by both spin-spin interactions, and inhomogeneities in the $B_0$ field, which lead to individual nuclei experiencing slightly different field strength, leading to dephasing. The characteristics of T2 and T2* signals are exploited during fMRI acquisition, as changes in blood oxygenation cause alterations in the magnetic susceptibility of the blood vessel and surrounding tissue, driving changes in the local field gradient. The intravascular and extravascular effects of blood oxygenation changes on T2/T2* signal are discussed in more detail in section 2.4.

The decay of $M_{xy}$ can be measured as a signal through a process of magnetic induction, such that an oscillating field will produce a current and voltage in a wire. Following the application of the RF pulse, the precession of nuclei about $B_1$ is able to induce a large current in a coil of wire. Due to an ongoing process of dephasing during relaxation, this oscillating signal becomes increasingly weak after the RF pulse, a phenomenon known as free induction decay (FID) (Figure 2.2C).

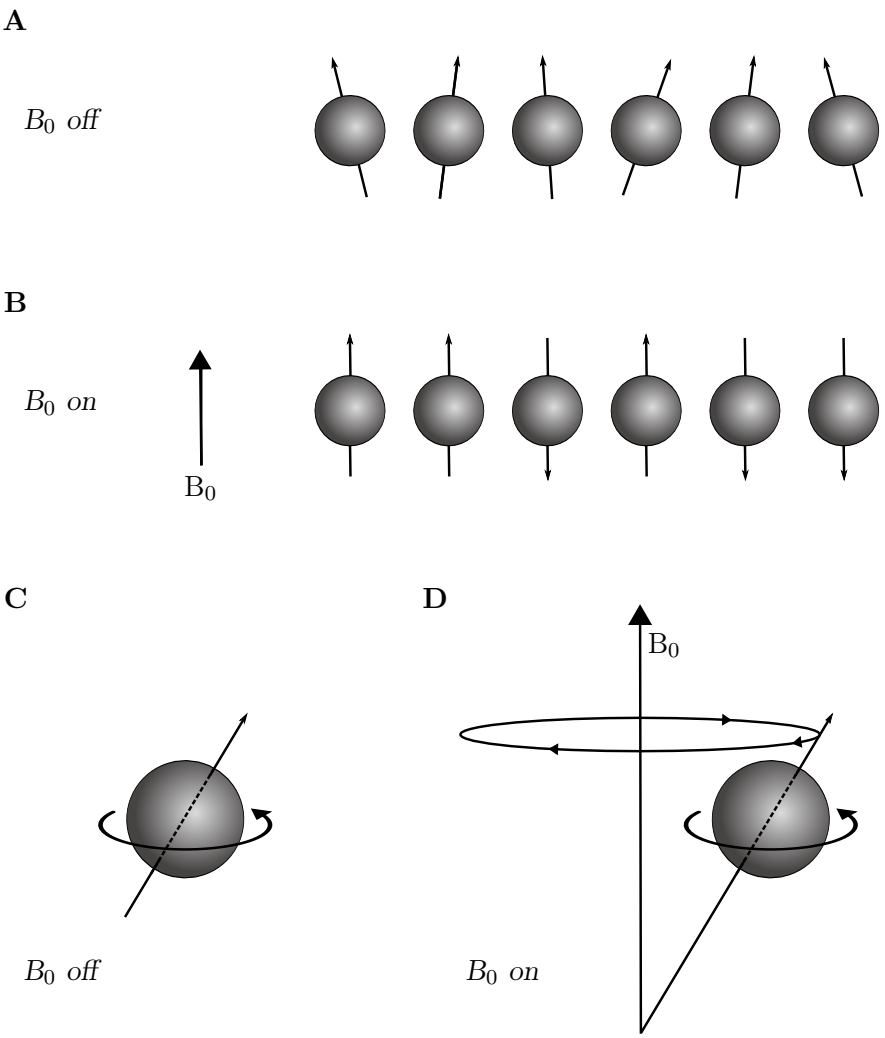


Figure 2.1: *Spin alignment under an applied magnetic field ($B_0$).* In the absence of the $B_0$ field, the axis of each magnetic dipole moment (MDM) is oriented randomly (A), about which it rotates (C), yielding no $M_0$. Under an applied $B_0$ field, the axis of each MDM is aligned with the direction of the $B_0$ field, or aligned in the opposite direction (B), both rotating on its own axis, and precessing about the axis of the $B_0$ field (D). The $M_0$ increases over time as a majority of the magnetic dipoles become aligned with the $B_0$. Adapted in part from (Hashman Hashemi et al., 2010).

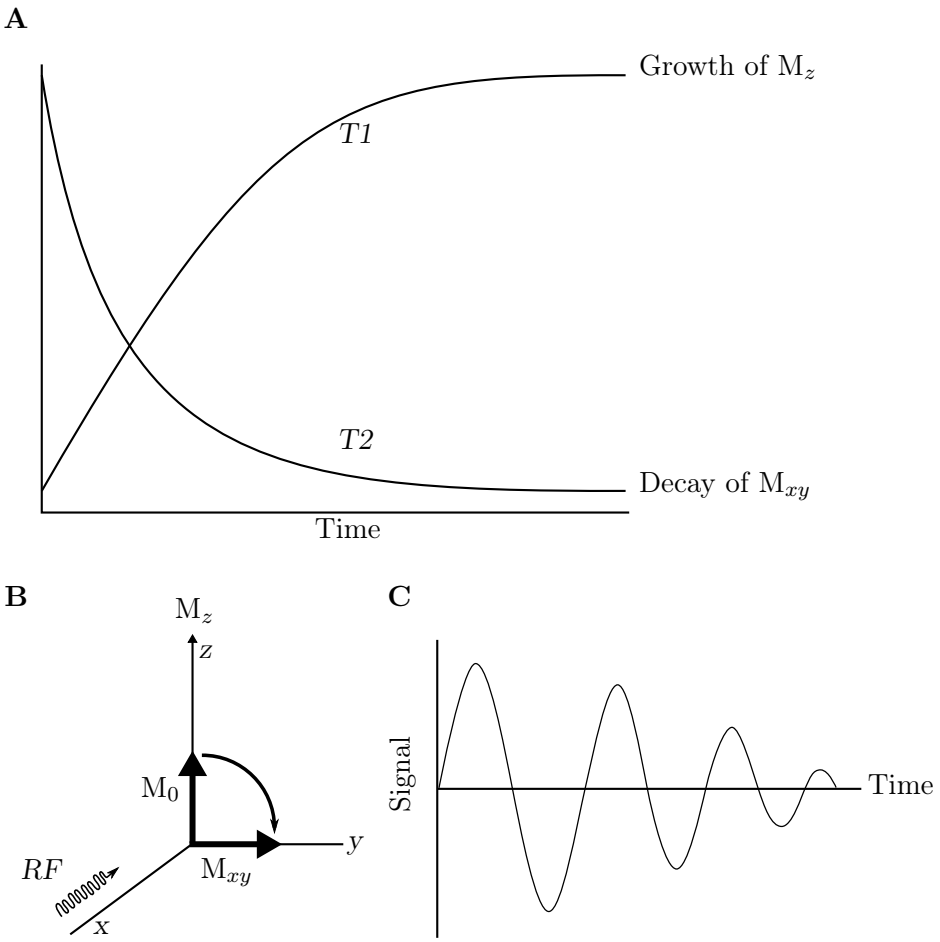


Figure 2.2: *The changes in transverse and longitudinal magnetisation during spin relaxation.* A. The exponential pattern of change in $M_{xy}$ and $M_z$ during spin relaxation do not share the same rate. B. Application of an RF pulse in the x-axis flips nuclei into the xy plane. C. The ongoing process of dephasing during spin relaxation results in a decaying sinusoidal signal pattern over time: FID. Adapted in part from (Hashman Hashemi et al., 2010).

## 2.2 Magnetic resonance imaging acquisition

The general principles of NMR are applied broadly to medical imaging in the form of MRI. In general MRI scanners are composed of a number of magnetic fields. The static magnetic field ($B_0$) is typically provided by a large superconducting system, supercooled to operate at a temperature around absolute zero. The resulting reduction in electrical resistance allows for high currents to be used, inducing a field of 1.5-3.0T in the clinical setting, though UHF research systems operating at 7T and above are now used for research (Section 2.6). Gradient coils provide a rapidly adjustable field, which is used to enable the spatial encoding of data to form images (Section 2.2.2). Finally an RF coil transmits the RF pulse ($B_1$), and is frequently combined with a receive coil to detect the resulting signal induced by $M_{xy}$ (Figure 2.2C).

### 2.2.1 Image contrast

T1 and T2 are dictated by the environment of the nuclei in the sample under study, and thus in human imaging vary between tissue subtypes. The values of T1 and T2 vary depending on tissue composition (Table 2.1). It is possible to manipulate certain parameters of the MRI acquisition sequence in order to weight the signal more strongly towards T1 or T2, frequently to gain contrast between two tissue types. The repetition time (TR) of an acquisition refers to the interval between two RF pulses. The echo delay time (TE) of an acquisition refers to the delay between the RF pulse and measurement of the signal. The recovery and decay curves of neural tissue subtypes demonstrate how varying TR and TE can alter the signal recorded and result in different image contrast (Figure 2.3). A T1-weighting is attained from a short TR and a short TE, while a T2-weighting is attained from a long TR and a long TE. A proton-weighted image can also be acquired using a long TR and short TE.

Table 2.1: Overview of relative T1 and T2 values of different tissue components

| Time constant | Water | Solids | Fat and proteinaceous material |
|---|---|---|---|
| **T1** | Very long T1: inefficient spin-spin transfer | Long T1: inefficient spin-spin transfer | Short T1: efficient spin-spin transfer |
| **T2** | Long T2: low dephasing | Short T2: high dephasing | Intermediate T2: moderate dephasing |

### 2.2.2 Slice selection and spatial encoding

In order to derive a meaningful image from a recorded RF signal, it must be possible to localise the origin of that signal from the sample in question. Applying an RF pulse without some kind of localisation would yield a single FID signal from the entire sample. The gradient coils of the MRI scanner provide the ability to localise the signal by limiting the excitation induced by a given RF pulse to a certain region. The gradient coils are able to produce rapidly changing magnetic fields, which can induce controlled non-uniformity in the $B_0$ field. This linear non-uniformity makes it possible to manipulate the Larmor frequency of the nuclei across a sample, such that an applied RF pulse will only achieve resonance in a given region of tissue. In order to image a specific slice, the $G_z$ gradient is applied, and a range of frequencies are applied in each RF pulse, inducing resonance in a given slice tissue. The range of frequencies is defined by the image bandwidth, which determines the thickness of each image slice. In order to spatially encode data within a given slice the $G_x$ and $G_y$ gradients are applied. The signal acquired during the repeated image cycles is subject to a series of complex Fourier transforms to yield an output image.

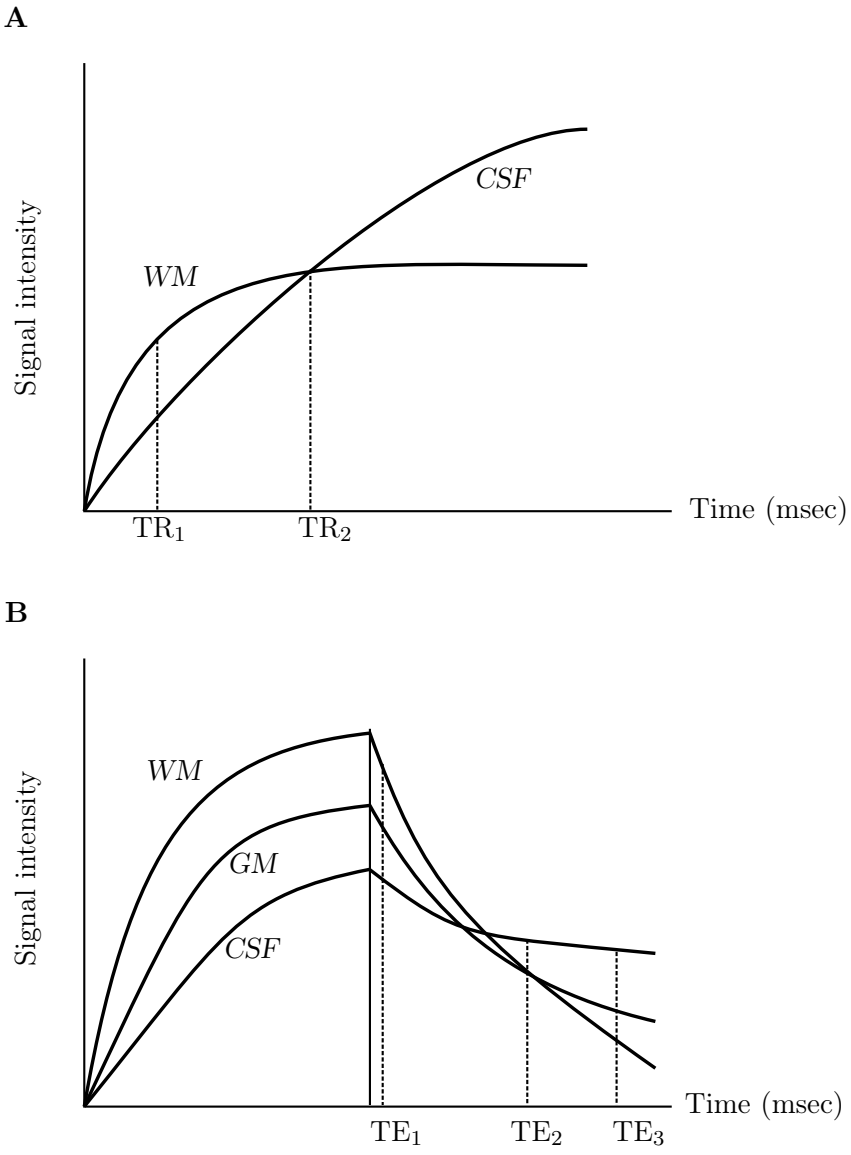


Figure 2.3: *Recovery and decay curves of grey matter, white matter and cerebrospinal fluid.* The timing of the TR and TE can alter tissue contrast. A. The T1 of white matter and cerebrospinal fluid differ considerably. By selecting a shorter TR ($TR_1$) it is possible to maximise T1 contrast. B. By changing the delay between the RF pulse and recording the signal TE, differing contrast can be attained. At a short ($TE_1$) we achieve a T1-weighting (white matter intense). At a long TE ($TE_3$) we achieve a T2-weighting (grey matter intense). An intermediate TE ($TE_2$) can yield isointense grey matter and white matter. WM: white matter, GM: grey matter, CSF: cerebrospinal fluid, TE: echo delay time, TR: repetition time. Adapted from (Hashman Hashemi et al., 2010).

## 2.3 Structural MRI

Structural images of the brain seek to provide anatomical detail to evaluate brain structure and the presence of pathology. Commonly applied structural sequences for brain imaging include T1-weighted, T2-weighted and proton density weighted images, capturing the unique properties of neural tissue subtypes discussed in section 2.2.1.

### 2.3.1 T1-weighted MRI

T1-weighted images are achieved by using a short TR to maximise the T1 effect on the signal, and a short TE to minimise, but not eradicate the T2 effect. A common sequence used in the acquisition of T1-weighted images is the magnetisation prepared rapid gradient echo (MPRAGE) (Mugler and Brookeman, 1990), which achieves good contrast between grey matter (GM), white matter (WM) and cerebrospinal fluid (CSF) (Figure 2.4A). T1-weighted images are frequently used for segmentation of these tissue subtypes for quantitative analysis and cortical surface reconstruction (Section 2.7.5).

### 2.3.2 T2-weighted MRI

T2-weighted images are achieved by using a long TR and a long TE to maximise the T2 contrast in the neural tissue. T2-weighted images provide good anatomical detail, but are primarily used to detect pathological lesions in the brain due to their ability to differentiate tissue and water. T2-weighted images therefore provide good definition of ischaemic lesions, particularly in the acute and subacute stages where they are used in preference to T1-weighted images (Pineiro et al., 2000; González et al., 2010).

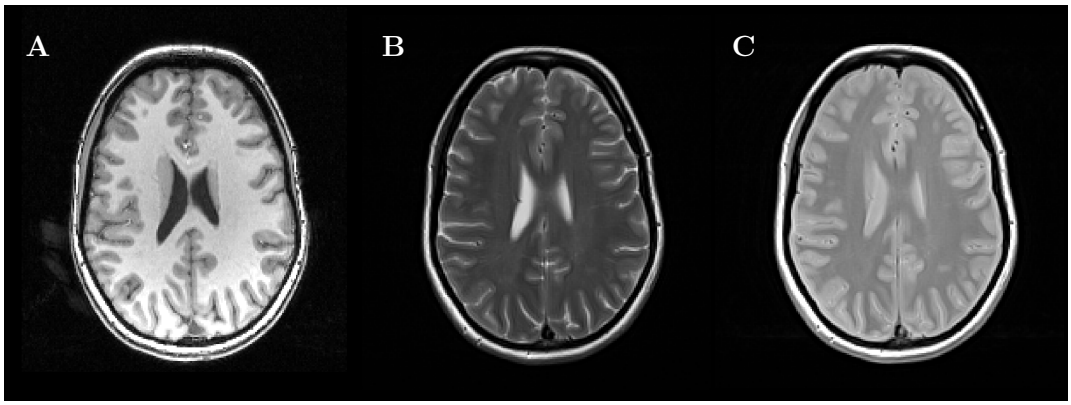


*T1-weighted* *T2-weighted* *Proton-density weighted*

Figure 2.4: *Structural MRI: common imaging contrasts.*

## 2.4 BOLD fMRI

The concept of blood oxygenation level dependent (BOLD) fMRI was first demonstrated by Ogawa and colleagues in rats, providing a means of non-invasively imaging local changes in blood oxygenation, and proposing this as a measurement linked to regional neuronal activity (Ogawa et al., 1990). fMRI is now applied broadly in the field of neuroscience to study patterns of activation during specific tasks and at rest (Sections 2.7.2 and 2.7.3). The technique is entirely based upon the high degree of neurovascular coupling present in the human brain, such that local increases in neuronal activity drive local haemodynamic changes, the time course of which can be captured using specific MRI sequences. fMRI provides a useful compromise between image resolution and invasiveness, which makes it a useful technique for functional brain mapping (Figure 2.5).

### 2.4.1 Neurovascular coupling

The brain exerts a high degree of metabolic demand on the body, accounting for an average 2% of body mass, but consuming 20% of oxygen and glucose intake. This expenditure contributes constitutive activities, such as maintaining the resting membrane potential, as well as processes associated with electrical and chemical

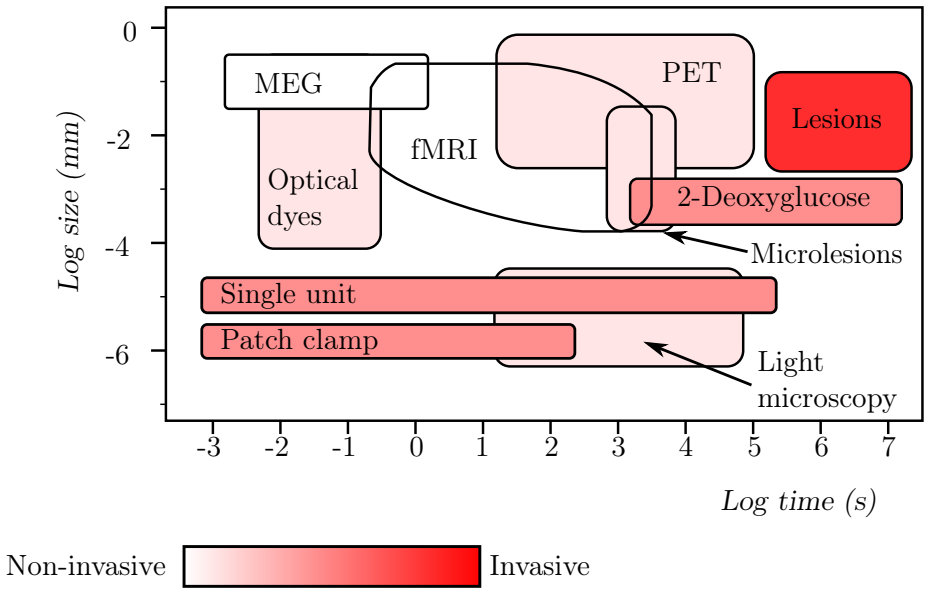


Figure 2.5: *Methods of functional brain mapping.* fMRI offers a balance in terms of spatial and temporal resolution, providing a non-invasive means of brain mapping. Adapted from Jezzard et al., 2001.

neurotransmission. In order to meet the changing regional metabolic demands of the brain, regulation of vascular supply is tightly coupled to local neuronal activity, yielding a haemodynamic response to neural activity (Figure 2.6). The exact mechanism of this coupling remains unclear, but appears to be driven principally by activity and the resultant metabolic activity at synapses in the grey matter, with candidate signals including nitric oxide (NO), $K^+$, and the cerebral response to hypercapnia (Filosa et al., 2006; Iadecola and Nedergaard, 2007; Paulson et al., 2009).

### 2.4.2 The BOLD signal

The BOLD signal is derived from changes in the relative concentrations of deoxyhaemoglobin (HHb) and oxyhaemoglobin ($O_2$Hb), which are associated with local changes in brain activity. As activity increases, the relative local concentration of HHb increases. BOLD fMRI is based around the idea of magnetic susceptibility: the degree to which the material being imaged is able to distort the applied magnetic

field ($B_0$). HHb and $O_2$Hb exhibit different magnetic susceptibility properties. $O_2$Hb is diamagnetic, meaning when placed in the $B_0$ field, it induces a small field in the opposite direction, leading to a distortion due to the local reduction in the effective magnetic field. In contrast HHb is paramagnetic, meaning that in the presence of the $B_0$ field it induces a small field in the same direction, locally strengthening the effective magnetic field. Therefore changes in the relative concentrations in of HHb and $O_2$Hb lead to changes in the distortion of the local field, which impact the local T2 and T2* signal in distinct ways.

The BOLD response to a given stimulus remains an indirect measure of neuronal activity. The haemodynamic response function (HRF) in the BOLD response illustrates the signal change resulting from a given stimulus (Figure 2.6). Following stimulus onset, there is an initial dip in the signal (0.5-1.0s), followed by a positive BOLD response peaking at around 5-8s, with signal change of 1-2% at a field strength of 1.5 T. After the stimulus end point there is a return to baseline, preceded by a signal undershoot. As the haemodynamic response (HR) does not directly mirror neuronal activation, it forms the basis of modelling neuronal activation in fMRI analysis (Section 2.7.2). Characteristics of the HR signal change varies with field strength (Zwaag et al., 2009), which is discussed in more detail in section 2.6.

### 2.4.3 Components of the BOLD signal

The changes in magnetic susceptibility associated with changes in the relative concentration of HHb and $O_2$Hb have both intravascular and extravascular effects. Within the vessel itself, hydrogen nuclei are effectively in a single compartment, with no appreciable diffusion out of the vessel possible during the duration of a single TE. The hydrogen nuclei therefore experience the field distortions resulting from the relative concentrations of HHb and $O_2$Hb. As regional activity increases and the relative concentration of HHb increases accordingly, there is a distinct shift from a diamagnetic to a paramagnetic susceptibility state, yielding an apparent reduction in the recorded MRI signal: a T2 effect.

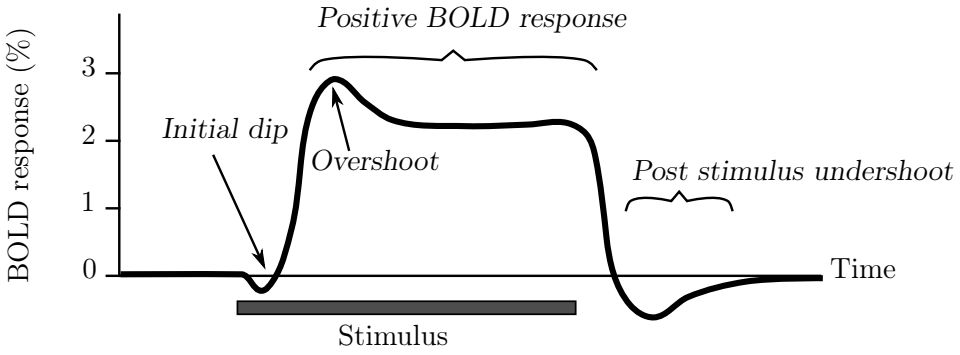


Figure 2.6: *The haemodynamic response to a given stimulus.* Adapted from Jezzard et al., 2001.

The extravascular signal contribution results from the effect of local field distortions induced by the changing relative concentrations of HHb and $O_2$Hb within an adjacent vessel. An increase in the local concentration of HHb induces local signal dephasing due to field distortions, leading to a reduction in the T2* signal.

The magnitude of the changes in T2 and T2* signal recording during fMRI experiments increase with increasing field strength. While the magnitude of the intravascular signal increases linearly with field strength, the extravascular signal increases exponentially (Ogawa et al., 1993; Gati et al., 1997). As such, with increasing field strength there is an increasing contribution of signal derived from extravascular tissue, and a diminishing intravascular contribution from large vessels to the BOLD signal. Therefore while at 1.5T, the BOLD fMRI appears to be dominated by intravascular venous signal (Lai et al., 1993; Hoogenraad et al., 2001), at UHF this signal is much reduced, favouring an extravascular signal dominated by the effects of the microvasculature, with the potential for increased signal specificity (Ugurbil et al., 1999; Yacoub et al., 2001). The effect of field strength on the nature of the BOLD signal must therefore be considered in the application of UHF imaging.

### 2.4.4 Echo Planar Imaging

Echo planar imaging (EPI) refers to an MRI sequence used to rapidly achieve whole brain images. It is applied widely in fMRI acquisitions where it is necessary to sample the BOLD signal across the entire brain with every TR. Single-shot EPI sequences achieve this by sampling the signal across the entire brain after a single RF excitation pulse. The ability to sample signal across the entire brain with this degree of rapidity necessitates the use of the high performance gradients. After the RF excitation pulse, a series of rapidly oscillating gradient pulses are applied, producing multiple gradient echoes in a single shot. The demanding nature of EPI sequences renders them particularly affected by magnetic susceptibility artefacts. Typical BOLD EPI sequences provide a resolution of 3mm x 3mm x 3mm, though the increasing application of UHF imaging provides potential for improved spatial resolution (Section 2.6).

## 2.5 Diffusion-weighted MRI

Diffusion can be defined as the perpetual mixing of molecules caused by thermal motion, which occurs even at thermodynamic equilibrium. This constant movement is ongoing in the fluid component of living tissue, including free water present in neural tissue. By capturing information regarding the direction and magnitude of this diffusion, it is possible to infer information regarding the overlying structure of tissue, which constrains the movement of water molecules. Diffusion-weighted MRI applies a specific pulse sequence that is able to quantify the degree of water diffusion in different regions of the brain, from which it is possible to infer information regarding brain microstructure.

As discussed in section 2.1, MRI involves the initial excitation of spins with a 90°RF pulse, followed by precession at the Larmor frequency, with dephasing due to magnetic field inhomogeneity and dipole-dipole interactions. A variant of this process, the spin

echo (SE) sequence applies a second, refocusing 180°RF pulse to negate this dephasing. The SE sequence is highly sensitive to diffusion, resulting from dephasing due to translational movement of spins (Hahn, 1950). It is the phenomenon of translational diffusion leading to dephasing that forms the basis of diffusion-weighted MRI. The precessional frequency of a given spin is determined by its local magnetic field. By applying a magnetic field gradient, spins at different positions experience different magnetic fields. The translational displacement of diffusion causes phase shifts, which can then be quantified through the signal measured. The stronger the gradients, the more defined the phase shift observed. The strength of the gradient applied is referred to as the b-value: a measure proportional to the square of the gradient strength.

Typical diffusion-weighted sequences apply a bipolar gradient after excitation and before signal measurement. The first gradient adds a positive phase, the magnitude of which is dependent on its position in space. The second gradient applies a negative phase, again proportional to the position in space. In a static system the positive and negative phase applied to a given spin would be balanced, yielding no net effect; the spins would be perfectly in phase. However, in reality, motion of the spin due to diffusion yields a net effect of the bipolar gradient (Figure 2.7). The resulting dephasing has an exponential effect on signal, measurement of which can yield information regarding the diffusion in a given region of the brain. The gradients applied in this case have a given direction. By acquiring signal after applying diffusion gradients in multiple directions and when no gradient is applied, it is possible to model the characteristics of diffusion in a given region of the brain.

### 2.5.1 Diffusion artefacts

Diffusion-weighted MRI acquired using single-shot EPI (Figure 2.7) is associated with a number of specific artefacts, which must be taken into consideration during image preprocessing.

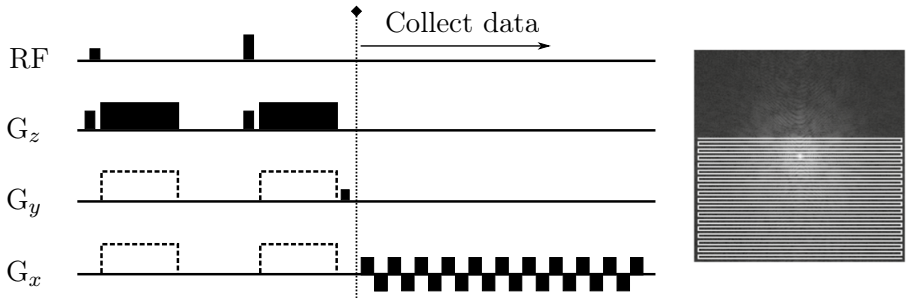


Figure 2.7: *Diffusion-weighted EPI sequence.* (A) Diffusion-weighted pulse sequence. (B) An example acquisition trajectory. Adapted from Pipe, 2009.

#### 2.5.1.1 Eddy currents

The bipolar gradients applied during diffusion-weighted MRI sequences require large and rapid changes in the gradient coils. The activity of the gradient coils is therefore capable of inducing currents in other components of the magnet. These eddy currents cause a slowing of the gradient rapid gradient changes used during diffusion-weighted MRI pulse sequences, causing the effects of a given gradient to persist beyond the period in which it was truly applied. Eddy currents can induce image artefact and warping. A combination of actively-shielded scanners and pulse-sequences designed to compensate for eddy currents has lessened their effect.

#### 2.5.1.2 Magnetic field inhomogeneities

Tissue/air boundaries can induce marked inhomogeneity in the static $B_0$ field of the magnet, leading to alterations in frequency of spin precession, leading to off-resonance phase. This can lead to geometric distortions in diffusion-weighted EPI acquisitions. Correction for such inhomogeneities is discussed in section 2.7.4.

#### 2.5.1.3 Gradient non-linearities

The basis of diffusion-weighted MRI sequences is founded upon the ability to induce a linearly increasing magnetic field across the brain to assess patterns of water diffusion.

These gradients must also diminish outside of the imaging volume so as to decrease the potential for peripheral nerve stimulation. This trade-off leads to non-linearities in the magnetic field induced by the gradients, leading to spatial variation in the actual diffusion weighting. Gradient non-linearity is not routinely corrected or accounted for.

#### 2.5.1.4 Bulk motion

Motion in the direction of a given diffusion gradient will alter the phase of a given voxel in space, and affect the diffusion signal. Such bulk motion is typically induced by movement of the subject in the scanner, as well as cardiac pulsations. It is important to assess for high levels of motion during diffusion-weighted MRI acquisitions; motion can have a marked effect on group comparisons of diffusion data (Yendiki et al., 2014).

### 2.5.2 Diffusion tensor imaging

In order to characterise Gaussian diffusion in three dimensions, the most simplistic model applied is known as diffusion tensor imaging (DTI), in which the components of diffusion along the three orthogonal axes is broken down, including their off-diagonal elements combining diffusion in two of these directions. The diffusion tensor model can be summarised as follows:

$$\begin{pmatrix} D_{xx} & D_{xy} & D_{xz} \\ D_{xy} & D_{yy} & D_{yz} \\ D_{xz} & D_{yz} & D_{zz} \end{pmatrix}$$

The diffusion tensor model is typically thought of as an ellipsoid, representing the nature of diffusion from a central origin. The orthogonal axes of this ellipsoid represent the eigenvectors $\varepsilon_x$, $\varepsilon_y$ and $\varepsilon_z$, along which the diffusion magnitude is characterised

by three eigenvalues $\lambda_1$, $\lambda_2$ and $\lambda_3$, sorting by magnitude ($\lambda_1 \geq \lambda_2 \geq \lambda_3$). The signal attenuation calculated after the application of a bipolar gradient in multiple directions is used to estimate the diffusion tensor using linear regression (Basser et al., 1994). From the modelled diffusion tensor, with its eigenvectors and eigenvalues, it is possible to calculate rotationally invariant metrics of diffusion anisotropy.

#### 2.5.2.1 Fractional anisotropy

Fractional anisotropy (FA) is a metric of diffusion anisotropy: the extent to which diffusion is directional. FA is calculated voxel-wise as a measure of the variance of three eigenvalues from their collective mean, normalised by the magnitude of diffusion, as show in the formula below, where $\lambda$ represents an eigenvalue, representing the magnitude of diffusion in the direction of the three eigenvectors($\varepsilon_1$, $\varepsilon_2$ and $\varepsilon_3$):

$$FA = \sqrt{\frac{3}{2}} \frac{\sqrt{(\lambda_1 - \langle\lambda\rangle)^2 + (\lambda_2 - \langle\lambda\rangle)^2 + (\lambda_3 - \langle\lambda\rangle)^2}}{\sqrt{\lambda_1^2 + \lambda_2^2 + \lambda_3^2}}$$

FA is less susceptible to artefacts induced by noise metrics derived from simple ratios of eigenvalues. FA is used widely in the study of white matter, both in relation to adaptive plastic changes in health (Scholz et al., 2009), as well as a measure of white matter integrity in complex pathology (Le Bihan and Johansen-Berg, 2012) (Section 2.5.3).

#### 2.5.2.2 Mean diffusivity

mean diffusivity (MD) is a metric which reflects the overall amount of diffusion within a voxel, calculated as the average of the three eigenvalues as follows:

$$MD = \frac{\lambda_1 + \lambda_2 + \lambda_3}{3}$$

MD is a widely favoured diffusion metric applied broadly in the field. However, given the desire to relate changes or differences in diffusion metrics to underlying tissue microstructure, there is an increasing emphasis on considering specific eigenvalues independently.

#### 2.5.2.3 Radial diffusivity

radial diffusivity (RD) is a metric reflecting the average of the second and third eigenvalues of a given voxel:

$$RD = \frac{\lambda_2 + \lambda_3}{2}$$

RD is often referred to an index of perpendicular diffusion. Building on studies of axial diffusivity (the magnitude of the first eigenvalue), radial diffusivity is often thought more sensitive to changes in myelination, with supporting evidence from imaging in animal models of demyelination (Song et al., 2002; Song et al., 2005; Budde et al., 2007; Budde et al., 2009; Klawiter et al., 2011). However, given the potential for shifts in the direction of the principal eigenvectors as a result of isolated tissue pathology, it is important to apply caution when interpreting the meaning of changes or differences in these more directional diffusion metrics (Wheeler-Kingshott and Cercignani, 2009). Furthermore, in regions of complex fibre architecture, it is no longer possible to interpret changes in RD directly in the context of myelin (Johansen-Berg and Behrens, 2009).

### 2.5.3 Diffusion and neural tissue

The ability to model patterns of water diffusion in the brain enables us to infer information regarding underlying tissue microstructure. An early study applying

diffusion-weighted MRI to the brain remarked that water diffusion in white matter was more anisotropic, while water diffusion in grey matter was more isotropic (Moseley et al., 1990). This is in keeping with the anatomy of white matter fibre bundles, which constrain water diffusion perpendicularly, inducing anisotropic movement of water molecules.

The exact structural underpinning of white matter diffusion anisotropy has been a subject of considerable investigation (Beaulieu, 2002). While myelin undoubtedly plays a role in white matter diffusion anisotropy (Hajnal et al., 1991), similar patterns are observed during neurodevelopment prior to myelination (Beaulieu et al., 1998). There is also thought to be a contribution from extracellular water, whose diffusion is constrained or hindered parallel to axonal fibre bundles (Le Bihan et al., 1993). It is now broadly viewed that patterns of membrane organisation induce diffusion anisotropy in white matter, with a contribution from the myelin sheath (Le Bihan and Johansen-Berg, 2012).

### 2.5.4 Diffusion-weighted MRI and non-isotropic voxel dimensions

The acquisition of diffusion-weighted MRI data with an in-plane resolution that differs from the slice thickness yields image voxels with non-isotropic dimensions. Such an acquisition is sometimes applied to achieve whole brain coverage in a shorter period of time, which may reflect either a limitation of the MRI system, or the need to minimise scan duration in certain patient populations. However, non-isotropic voxels introduce a number of limitations, including an increase in partial voluming in the direction with the larger voxel dimension. Furthermore, more complex diffusion analysis such as probabilistic tractography would be beyond the remit of images with non-isotropic voxel dimensions, which could bias fibre tracking in a given direction.

## 2.6 Imaging at ultra-high field

Since the advent of MRI in the clinical setting, the imaging technology applied for diagnostic purposes has continued to develop. While early systems operated at a

field strength of 0.6 tesla, these were rapidly superseded by 1.5 tesla in the mid 1980s, which still accounts for over 90% of MRI systems worldwide. In the early 2000s, high field systems operating at 3.0 tesla received approval for clinical use from the United States Food and Drugs Administration (USFDA) (Salvolini and Scarabino, 2006). MRI systems operating beyond 3 tesla are said to operate at UHF. While UHF systems are approved for human imaging (*International Electrotechnical Commission* 2002; *United States Food and Drug Administration* 2003), they are not currently licensed for routine diagnostic purposes. A growing number of 7.0 tesla MRI systems are being used for research and experimental clinical studies worldwide (Figure 2.8) (Ugurbil, 2012), though they represent the vast minority of systems operational worldwide.

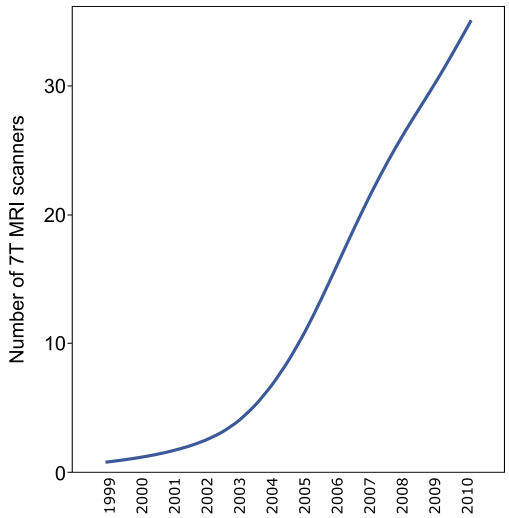


Figure 2.8: *The number of 7T MRI systems ordered worldwide.* Data collected in April 2010. Adapted from Ugurbil, 2012.

### 2.6.1 Origins of ultra-high field imaging

Early efforts to harness the potential of UHF systems came from the MRI 'big three': Siemens, Philips and General Electric, in the mid 1980s. However, early research and development of these systems, all operating at 4.0 tesla, experienced limited success (Barfuss et al., 1988). It was in the late 1980s that a number of academic

labs developed an interest in UHF imaging, led by groups at the Centre for Magnetic Resonance Research (CMRR) at the University of Minnesota. The CMRR pioneered UHF brain imaging, with a 4.0 tesla system operational in 1992, followed in 1999 by the first human MRI system operating at 7.0 tesla (Vaughan et al., 2001). There are currently around forty 7.0 tesla MRI systems operational or planned across the world, with efforts to develop imaging at 9.4 tesla and beyond (Vaughan et al., 2006).

### 2.6.2 BOLD fMRI at ultra-high field

Early efforts in BOLD fMRI development arguably first began at UHF, with fMRI at the CMRR beginning at 4.0 tesla. Initially believing BOLD contrast to be driven solely by a susceptibility effect, the CMRR group did not investigate fMRI at 1.5 tesla. It is now clear that the BOLD signal is composed of a number of contributing factors, not just the extravascular susceptibility driven component considered by early investigators (Section 2.4.3). However, the issue of draining veins and intravascular signal contributions at lower field strength became increasingly evident at 1.5 tesla; a contribution seen to diminish in proportion to magnetic field strength (Turner et al., 1993; Gati et al., 1997), prompting more recent investigation of BOLD fMRI at UHF.

### 2.6.3 The BOLD signal at ultra-high field

The development of scanners of field strengths of 7.0 tesla has enabled us to push the limits of MRI acquisition in terms of SNR, spatial resolution and sensitivity. In terms of BOLD fMRI, there are various interrelated gains associated with imaging at 7.0 tesla. Firstly, the susceptibility difference between $O_2$Hb and HHb scales linearly with field strength (Ogawa et al., 1993; Gati et al., 1997), permitting improved spatial resolution, or a reduction in the number of trials required to robustly demonstrate the effects seen at lower field strengths. Secondly, the short T2 of blood at 7.0 tesla yields an attenuated signal when using the short TE required for BOLD EPI, leading to a

reduced intravascular contribution to the BOLD signal, and an associated increase in spatial sensitivity.

Comparative studies across field strengths have demonstrated that these gains translate into an increase in the magnitude of the relative signal change associated with a given task (finger tapping), and an earlier onset of the BOLD signal response compared to that seen at lower field strengths (Figure 2.9) (Zwart et al., 2005; Zwaag et al., 2009). Comparisons of BOLD EPI resolution at 7.0 tesla have demonstrated that the potential for gains in timecourse SNR are associated with the acquisition of data at higher spatial resolution, with an associated reduction in physiological noise contributions (Triantafyllou et al., 2005).

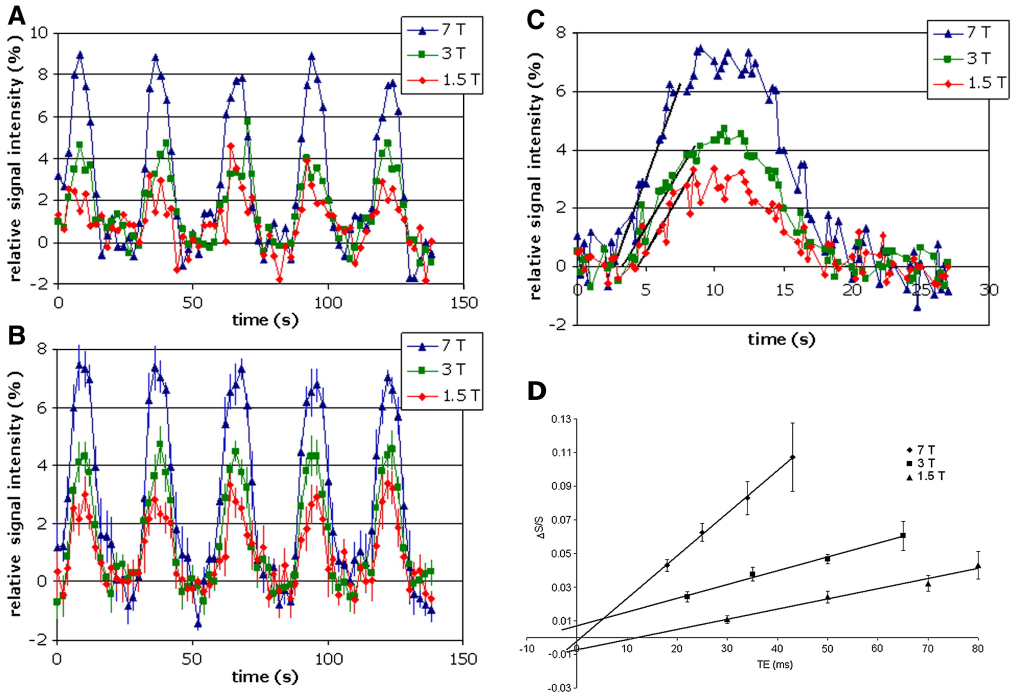


Figure 2.9: *Comparing the BOLD response at 1.5, 3.0 and 7.0 tesla during a finger tapping task.*. Reproduced from Zwaag et al., 2009.

### 2.6.4 Special considerations for ultra-high field fMRI

Although BOLD fMRI benefits from improvements in image contrast and spatial specificity at 7.0 tesla, with associated increases in the feasibility of higher resolution

imaging, the application of UHF imaging is not necessarily always a logical progression from imaging at 3 tesla. The choice of field strength and imaging resolution depend on the question under study. In particular it should be emphasised that the marked benefits of imaging at 7.0 tesla have some associated costs or caveats, which must be considered carefully.

#### 2.6.4.1 Brain coverage

When acquiring BOLD EPI data, we typically seek a combination of maximal spatial and temporal resolution. Currently, using a standard 2D gradient echo EPI sequence at 3.0 tesla, a state-of-the-art system can achieve an isotropic resolution of 2mm with a TR of 3 seconds. At 7.0 tesla, we often wish to capitalise on SNR gains to reduce voxel sizes further. Imaging resolutions approaching or surpassing 1mm isotropic are associated with a markedly increased matrix size, meaning more read-out points per line, placing greater demands on the gradients and the data acquisition rate. Furthermore, the long read-out time required at this resolution has the potential to blur data in the phase-encoding direction, reducing the effective resolution. These limitations with a standard 2D gradient echo (GE)-EPI sequence dictate a trade-off between spatial and temporal resolution, which is typically mitigated by reductions in brain coverage to reduce the TR to an acceptable level for the paradigm in question (Figure 2.10). The acquisition of a limited field of view (FOV) requires a clear hypothesis and region of interest (ROI), raising issues of consistent slice placement and analysis approaches that will likely differ from a standard group-based GLM.

#### 2.6.4.2 Motion artefact

Motion is a potential cause of imaging artefact in fMRI data acquired at any field strength. As resolution approaches 1mm isotropic, motion artefacts are increasingly problematic, even in data from experienced or expert participants (Olman and Yacoub,

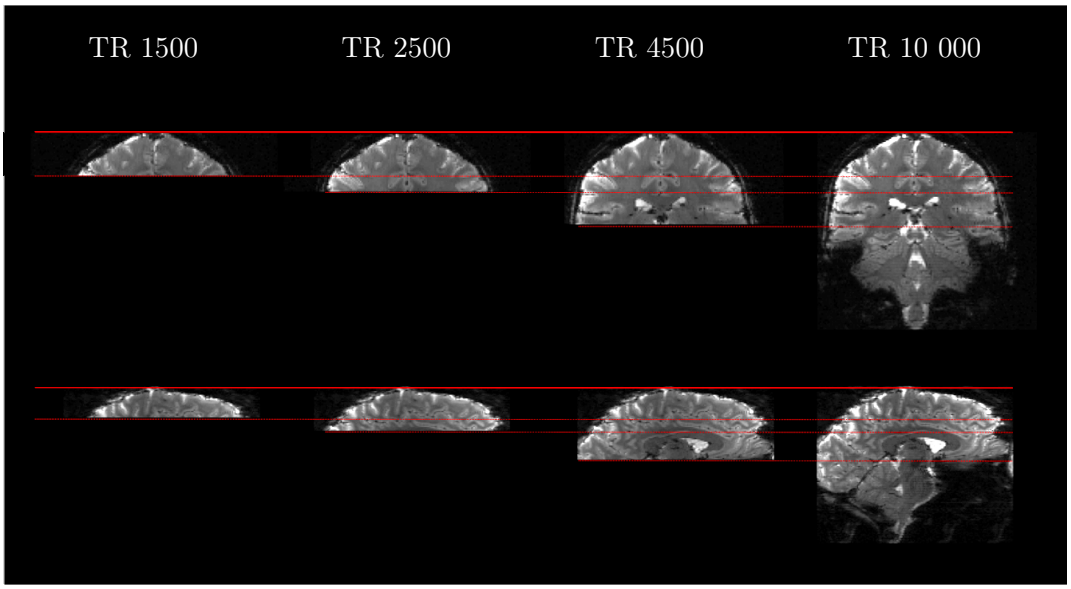


Figure 2.10: *BOLD EPI coverage versus TR at 7 tesla.* Two-dimensional BOLD EPI acquisition brain coverage is constrained by the temporal sampling resolution, dictated by the TR. Top row: coronal slices. Bottom row: sagittal slices. Data acquired in Oxford, September 2012 by Stuart Clare and James Kolasinski.

2011). Rapid, relatively small movements during image acquisition at high resolution can readily induce spin history artefact in slice interleaved sequences. Slice acquisition is typically interleaved for BOLD EPI to reduce the cross-talk between adjacent slices. If a subject suddenly moves during an interleaved acquisition in the slice direction, there is the potential for slices which have just been excited to move into the space of those which have not been excited, and vice versa. Higher resolution increases the susceptibility for such a movement. The different degree of excitation in adjacent slices will result in a difference in signal intensity, manifesting as a striping or banding (Figure 2.11). After motion has stopped, equilibrium is regained and signal intensity returns to normal.

#### 2.6.4.3 Field inhomogeneity

The relative similarity between the RF wavelength applied during MRI acquisition and the size of the human head leads to dielectric effects, which at UHF in particular leads to non-uniformity in the RF $B_1$ field, producing variation in signal intensity across

the brain (Figure 2.12A/B). Inhomogeneity in white matter signal is problematic for cortical surface reconstruction, which requires accurate segmentation of the white matter across the entire brain (Fujimoto et al., 2014). At 7.0 telsa, white matter uniformity can be attained using a sequence such as the magnetization prepared 2 rapid acquisition gradient echo (MP2RAGE), which acquires two images with separate inversion times, using the latter to normalise the former, reducing the bias in the resulting image (Figure 2.12C/D) (Marques et al., 2010). Another alternative is to acquire MPRAGE T1-weighted structural images at lower field strengths where field inhomogeneity is less marked and easily corrected during pre-processing (Figure 2.12E/F).

#### 2.6.4.4 Specific absorption rate

Specific absorption rate (SAR) refers to the rate at which the pulse sequence used to acquire MRI images deposits thermal energy into the scan participant. The SAR limits become increasingly relevant at UHF where the RF pulses with higher energy are used. The scanner console is able to calculate and enforce SAR limits, which are dictated by guidelines from the USFDA and equivalent bodies.

#### 2.6.4.5 Participant experience

At 7.0 tesla there is an increased incidence of scan participants reporting sensory phenomena as they are moved in and out of the scanner bore. These phenomena are induced only when participants move through the magnetic field, and typically subside quickly. Sensory experiences can include dizziness as a result of vestibular overcompensation, phosphenes, and a metallic taste in the mouth (Schenck et al., 1992; Theysohn et al., 2014).

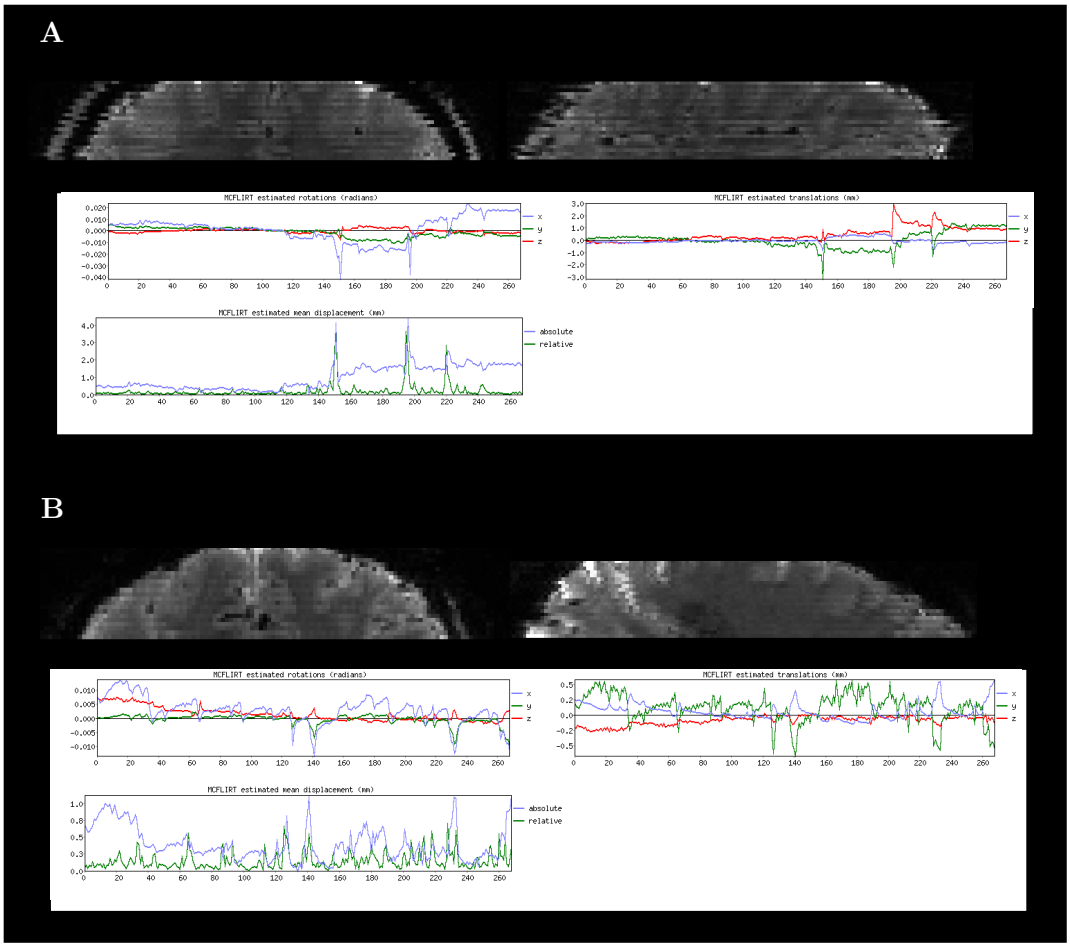


Figure 2.11: *Motion susceptibility of ultra-high resolution BOLD EPI data.* Images show characteristic spin history artefact banding in the coronal (A/B: left), and sagittal (A/B: right) plane. Motion parameter graphs show the output from FSL motion correction undertaken using MCFLIRT, with estimates of rotation and translation in three orthogonal planes, and the overall mean displacement. Both moderate (A: mean displacement of up to 4mm) and relatively low (B: mean displacement of up to 1mm) levels of sudden rapid motion cause marked artefact in associated volumes of four-dimensional BOLD EPI datasets. Data acquired in Oxford, October 2012 by James Kolasinski.

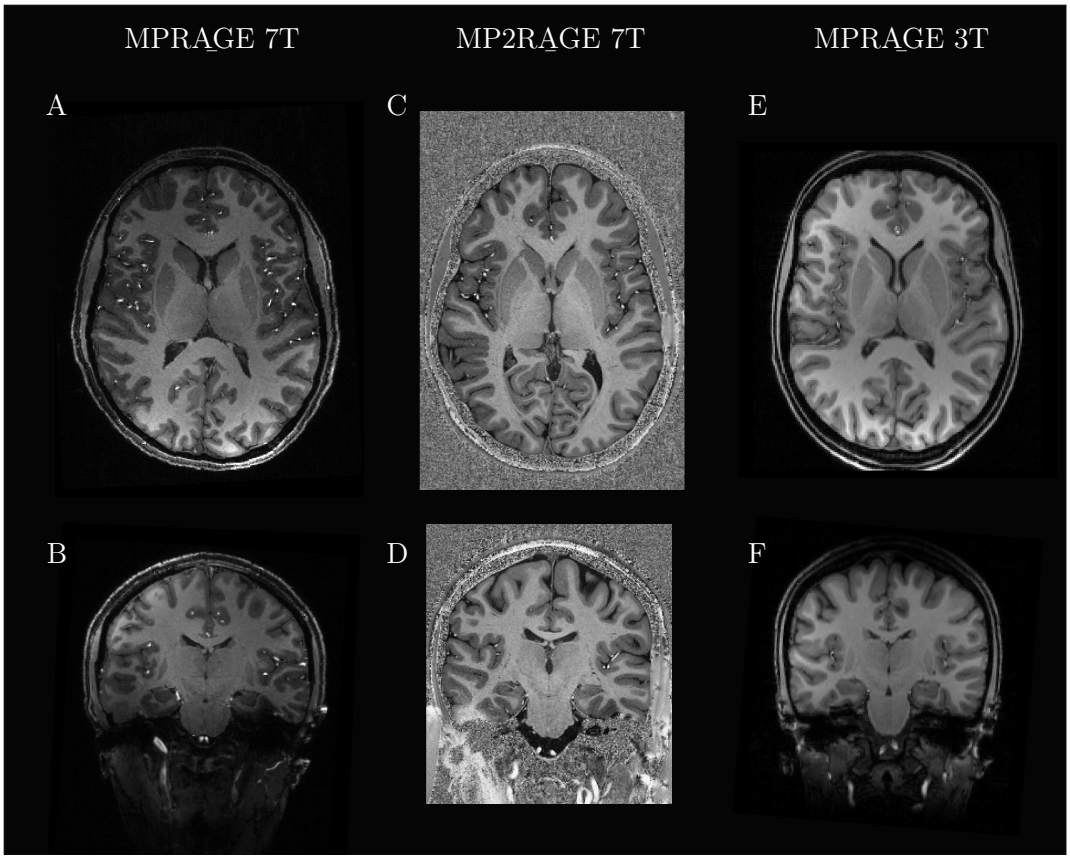


Figure 2.12: *Field inhomogeneity.* A traditional T1-weighted MPRAGE image acquired at 7.0 tesla (A/B) displays a considerable degree of regional signal variation as a result of inhomogeneity in both the $B_0$ and $B_1$ fields. Many image analysis approaches, including cortical surface reconstruction are dependent upon homogenous signal intensity within a given tissue compartment (e.g. white matter). At 7T, such homogeneity can be attained using an MP2RAGE sequence (C/D) that acquires two images with different inversion times for signal normalisation purposes. This can lead to problems with image preprocessing, such as brain extraction, due to the resulting signal outside the skull (C/D). A final solution is to acquire structural T1-weighted images at a lower field strength, where inhomogeneity is less pronounced and more easily corrected during preprocessing (E/F). Data acquired in Oxford, October 2012 by James Kolasinski.

## 2.7 MRI analysis

All image analysis was undertaken using components of the FMRIB Software Library (FSL)(Smith et al., 2004; Woolrich et al., 2009; Jenkinson et al., 2012), unless otherwise specified. This is a comprehensive library of analysis tools for fMRI, structural MRI and diffusion MRI brain imaging data.

### 2.7.1 fMRI preprocessing

#### 2.7.1.1 Motion correction

Head motion is unavoidable in human MRI studies, despite efforts to position participants as comfortably as possible on the scanner bed, particularly when undertaking a task involving movements. Motion correction aims to realign all image volumes in a four-dimensional fMRI run to a single volume. If motion is low this realignment can improve data quality and the statistical power of subsequent analysis. However, rapid or large motion can be a particular problem, diminishing the homogeneity of the magnetic field established by shimming based on the initial head position in the scanner, the effects of which cannot be rectified by pre-processing. Motion artefact at UHF can be considerable, resulting from relatively small movements, necessitating careful inspection of the data (Section 2.6.4.2).

In FSL preprocessing is undertaken by MCFLIRT, resampling each slice to the middle volume of the fMRI run using trilinear interpolation. MCFLIRT provides an estimate of motion during the fMRI acquisition, as shown in figure 2.11. Further details of linear registration are discussed in section 2.7.6.1.

#### 2.7.1.2 Spatial smoothing

A Gaussian smoothing kernel is applied to the raw four-dimensional fMRI data in order to average out noise in the data. In principle by removing noise and retaining genuine activation-related signal, smoothing increases SNR. Spatial smoothing also ensures a Gaussian spatial distribution in the signal, which is an assumption of later GLM analysis (Section 2.7.2.1).

#### 2.7.1.3 Temporal filtering

Low frequency changes in signal are frequently visible in raw BOLD EPI data. While these fluctuations were originally ascribed to subject motion or physiological noise, they appear to result mainly from scanner instabilities or changes during the course of image acquisition, such as heating (Smith et al., 1999). These signals are removed using a temporal high-pass filter.

### 2.7.2 Task fMRI

#### 2.7.2.1 General Linear Model

The GLM has formed the cornerstone of fMRI analysis for the past 20 years (Poline and Brett, 2012). The concept of the GLM was first applied to fMRI data in the mid-1990s (Friston et al., 1995). The GLM provides a conceptually simple means of interrogating fMRI data to model task-related activation in response to given stimuli or instructions.

**Model design** The GLM applied in fMRI Expert Analysis Tool (FEAT) takes a univariate approach, fitting a model to each voxel individually, using pre-whitening of the data with the FMRIB's Improved Linear Model (FILM) tool to account for time series autocorrelation. In fMRI studies, stimuli are commonly modelled as boxcars, with 'off' and 'on' periods. These boxcar models are convolved by a HRF to account for the general pattern vascular response and the lag between almost instantaneous neuronal activation and the neurovascular changes identifiable with BOLD fMRI. The GLM seeks to assess the degree to which a voxel's timecourse matches the individual regressors in the model, and therefore the association between activity therein and the task or stimulus modelled. The GLM applies the following approach:

$$y = \beta_0 x_0 + \beta_1 x_1 + ... + \beta_p x_p + \epsilon$$

For the timecourse of each voxel (y), a goodness of fit ($\beta$) is estimated for the regressors (x) in the model, plus the error ($\epsilon$). This yields a voxelwise map of the parameter estimate (PE) ($\beta$ equivalent), which can be further processed to $t$-values by dividing the PE map by the error estimate, with further standard statistical transformations into $z$-statistic or $p$-value maps. The goodness of fit can be summarised not only for individual regressors, but also for the contrast between these regressors, by subtracting one parameter estimate from the other, and dividing by a combined standard error to give a voxelwise map of the contrast of parameter estimate (COPE). This provides the opportunity to locate regions which whose activation was significantly greater during one condition compared with another.

**Statistical thresholding** The GLM provides voxelwise maps reflecting the fit of a model to the BOLD fMRI data. These maps must be thresholded to ascertain which regions of the brain show significant results based on the initial model and the specified contrasts. As a result of the univariate approach of the GLM, there is a clear multiple comparisons issue in thresholding the statistical maps, with each voxel having been considered independently in the model fit. It is therefore necessary to adjust the statistical threshold for significance accordingly in order to avoid type I error. Given the number of voxels under consideration, Bonferroni corrections or equivalent are too conservative for the thresholding of activation maps. FEAT applies a cluster-based approach to thresholding statistical maps. This approach assesses for the presence of contiguous clusters spanning a number of voxels, and uses Gaussian random field (GRF) theory to estimate the significance level of each cluster, and compare this to the cluster probability threshold. The resulting map of significant clusters is then used to mask the raw $z$-statistic map produced from the original COPEs. Cluster-based thresholding provides a more relevant means of thresholding voxelwise data, accounting for the fact that brain activation in response to a given stimulus typically spans across many adjacent voxels.

#### 2.7.2.2 Phase-encoding

Phase-encoding paradigms and analysis differ from the typical block designs and GLM approach applied in the majority of fMRI studies. Phase-encoding provides a powerful means of mapping regions in the brain which show topographic patterns of organisation, such as early visual cortex or the primary somatosensory cortex (Engel, 2012). Phase-encoding is very simply based upon the idea that activation in response to continuous but shifting stimuli can be visualised as a travelling wave of BOLD signal change in topographically organised regions, which allows us to visualise maps on the cortical surface.

**Origins** The application of phase-encoding designs originates from the use of fMRI to study retinotopy in early visual cortex. Primary visual cortex is organised retinotopically: a specific location in the cortex maps to a region in visual field, with adjacent regions in space mapped broadly to adjacent regions in the cortex. In its original form, phase-encoding involved the presentation of visual stimuli shifting continuously in the visual field. Analysis fitted multiple sinusoids each with a different phase to the BOLD fMRI data in order to assess which sinusoid best fit the pattern of activation at each point (Sereno et al., 1995; Engel et al., 1997). Plotting this phase as a function of location on the cortex provides a robust means of topographically mapping visual cortex (Sereno et al., 1995; Engel et al., 1997; Wandell et al., 2007; Huang and Sereno, 2007).

**Theory and approaches** In this thesis, phase-encoding analysis is undertaken using a cross-correlation approach. This analysis involves the correlation of the raw BOLD timecourse from each voxel (Figure 2.13A) against a range of models. The models applied all follow the same pattern (Figure 2.13B), but shifted by a range of time lags, sufficient to cover the entire course of the task (Figure 2.13C). By correlating each of these models against the raw BOLD signal, it is possible to plot

lag against correlation value for a given voxel (Figure 2.13D), effectively producing a tuning curve for each voxel, which show clear shifts in phase (Figure 2.13E). By subdividing these lags on the basis of the task in question, it is possible to isolate activation maps associated with a given task or stimulus, the $r$-values from which can be transformed to $z$-statistics and thresholded to produce activation maps.

### 2.7.3 Resting-state fMRI

While at rest, the brain exhibits spontaneous patterns of activity. Data from the fMRI literature have demonstrated that these spontaneous fluctuations in activity occur in functionally connected regions of the brain (Raichle et al., 2001; Vincent et al., 2007), such that related areas show similarities in the timecourse of their activity. Although the physiological role of this network activity remains unclear, the study of this phenomenon has become increasingly prevalent, and has identified changes in the profile of resting state activity in a number of disease states, including stroke and other movement disorders (Park et al., 2011; Poston and Eidelberg, 2012).

#### 2.7.3.1 Acquisition and preprocessing

During a resting state scan, participants are instructed to relax, to allow their mind to wander, and either to close their eyes, or to focus on a fixation cross. As well as being subject to the standard preprocessing steps for fMRI analysis generally (Section 2.7.1), resting state analysis also requires particularly careful denoising and artefact removal, to which the analysis is particularly sensitive. Common artefact corrections include the addition of motion parameters as confound regressors in analysis. Many investigators also include the global signal as a confound regressor in resting state analysis: this practice is somewhat crude and renders the interpretation of final results difficult (Smith et al., 2013). The two principal analysis options for resting state data are functional connectivity analysis using predefined seed ROIs, or a more data-driven multivariate independent components analysis. In this thesis, only the latter analysis is applied.

#### 2.7.3.2 Model-free analysis: MELODIC ICA

The major limitation of model-based analysis is the potential for significant patterns of activation that do not fit the model-specified timecourse to be overlooked in analysis. In the context of resting state fMRI, this is well illustrated by the discovery of various anatomically and functionally separable resting state networks (Beckmann et al., 2005). Independent Components Analysis (ICA) can be used to resolve these resting-state networks in the human brain; simplistically this analysis approach searches for regions of the brain with similar patterns of resting-state activity. Regions of the brain that exhibit common resting-state activation patterns are then assigned to a component or network. Once these components or networks have been derived, it is possible to undertake statistical analyses to compare them across different groups. It is also possible to derive a measure of the strength or connectivity within a given network.

In the context of this thesis, ICA is used to assess the strength or connectivity of the sensorimotor network. Full details of the analysis approach used to calculate this metric are provided in section 7.2.5.5.

### 2.7.4 Diffusion-weighted MRI

All diffusion-weighted MRI data presented in this thesis are undertaken using FMRIB's Diffusion Toolbox (FDT), a component of FSL (Behrens et al., 2003). Data preprocessing includes eddy current correction and brain extraction, following by the fitting of a diffusion tensor model at each voxel to derive measures of the three principal eigenvalues and eigenvectors, as well as diffusion metrics such as FA, MD and RD.

Probabilistic tractography in FDT allows for the estimation of anatomical connectivity between two regions on the basis of diffusion-weighted MRI data, from which parameters regarding local fibre orientation can be estimated. By assessing the local fibre orientation serially across a number of voxels, it is possible to quantify the likelihood of an anatomical connection between two regions.

### 2.7.5 Structural MRI

Structural MRI sequences provide a means of visualising various subcomponents of brain tissue (Section 2.3). Structural MRI is broadly limited to signal contrast between cell-rich grey matter, both cortical and subcortical, myelin and axon-rich white matter, and CSF. As discussed in section 2.2.1, the sequence parameters of a scan can weight the image, such that different contrasts are attained. T1-weighted scans such as the MPRAGE and multi echo magnetisation prepared rapid gradient echo (MEMPRAGE) provide good contrast between grey matter and white matter, and are therefore valuable for cortical reconstruction, as well as quantitative analysis of grey matter and white matter structure. T2-weighted scans provide very different contrast, and in the context of this thesis are valuable for the identification and labelling of ischaemic and haemorrhagic stroke lesions (Section 2.3.2).

#### 2.7.5.1 Voxel-Based Morphometry

Structural MRI has long been used as a tool to compare groups of subjects. While comparisons of metrics such as grey matter signal intensity are possible using ROI analysis of well-defined structures in the brain, a more data-driven, hypothesis-free approach is necessary to identify more subtle structural changes. Voxel-based morphometry (VBM) provides a means of comparing the signal intensity of a certain tissue type, typically grey matter, in a voxelwise fashion across groups of participants. This is an automated, systematic and whole-brain method, providing the ability to produce statistical maps of group differences across the entire brain (Ashburner and Friston, 2000; Good et al., 2001).

In this thesis, VBM analyses are undertaken using FSL-VBM (Douaud et al., 2007), an optimised VBM protocol (Good et al., 2001). First, structural images are brain-extracted and grey matter-segmented before being registered to the Montreal Neurological Institute (MNI) standard space comprised of 152 control brain images using non-linear registration (Andersson et al., 2007b). The resulting images are averaged

and flipped along the x-axis to create a left-right symmetric, study-specific grey matter template, composed equally from the participants of each group. Second, all native grey matter images are non-linearly registered to this study-specific template and "modulated" to correct for local expansion (or contraction) due to the non-linear component of the spatial transformation. The modulated grey matter images are then smoothed with an isotropic Gaussian kernel with a sigma of 2mm. Finally, voxelwise GLM is applied using permutation-based non-parametric testing, correcting for multiple comparisons across space.

#### 2.7.5.2 Longitudinal within-subject VBM analysis

A within-subject design provides a powerful means of addressing questions regarding plasticity in the human brain. Such analysis provides a means of reducing the effect of inter-subject variance, making comparisons within the same subject, across a number of different time points. Structural MRI analysis can be adapted in this way to make comparisons within-subject over a period of time, for example, before or after a period of training or a therapeutic intervention. While this approach is attractive in terms of its greater statistical power, there are specific considerations in the scan acquisitions and analysis approaches. Longitudinal designs are more susceptible to experimental biases than the more standard cross-sectional designs commonly applied.

Firstly, a bias in the MRI acquisition introduced at a certain point in time has the potential to markedly impact the results. A classic example might be a change in contrast induced by an MRI scanner upgrade. In a cross-sectional design inter-subject variance would far outweigh such a subtle difference induced by scanner hardware changes, in a longitudinal design this bias may introduce a marked effect on the results.

A second bias is commonly introduced in the analysis of longitudinal data. In the case of structural data and VBM, this can be in the creation of a subject-specific template. The first stage in VBM analysis requires the within-subject alignment of

MRI data from multiple time points. The resampling and interpolation of data from one time point into another time point has the potential to introduce a systematic bias, as the resampled data will be inherently smoother than the data that has not been resampled. It is therefore important to produce an unbiased template using MRI data from all time points under study, which acts as a common space into which all data is resampled for longitudinal analysis (Thomas et al., 2009).

### 2.7.6 MRI registration methods

In the context of MRI analysis, registration refers to the process of aligning or matching two images, to produce a matrix or warp, which maps the transformation. Resampling or warping an image refers to the application of a registration matrix or warp to remap an image from one space into another.

In this thesis, there are two distinct situations in which image registration is important. The first is the intra-subject registration of task BOLD EPI data into a common space, such as a whole brain EPI image, or a T1-weighted structural image using linear registration implemented with FMRIB's Linear Image Registration Tool (FLIRT) (Jenkinson and Smith, 2001; Jenkinson et al., 2002). The second is inter-subject registration, or more commonly, the alignment of single subject data to a common space or template such as the MNI-152 standard space, or equivalent, using non-linear registration implemented with FMRIB's Nonlinear Image Registration Tool (FNIRT) (Andersson et al., 2007a; Andersson et al., 2007b).

#### 2.7.6.1 FLIRT

FLIRT is a tool that performs linear (affine) registration of one image to another. FLIRT has the potential to allow 12 degrees of freedom (DOF), incorporating rotations, scalings, skews and translations. In the context of this thesis, FLIRT is used for intra-subject registration of limited FOV BOLD EPI data to a T1-weighted structural image, with 7 DOF: three translations, three rotations and a single global scaling.

In this context, Boundary Based Registration (BBR) is used, meaning that a white matter segmentation of the target T1-weighted structural image is used to inform the registration. As both BOLD EPI and T1-weighted images have clear boundaries between cortical grey matter and white matter, in simple terms the BBR approach attempts to align the grey-white matter boundary derived from the BOLD EPI data with the boundary calculated from the T1-weighted white matter segmentation (Greve and Fischl, 2009) (Figure 2.14). BBR is particularly effective at high-quality registration of BOLD EPI data with a limited FOV.

#### 2.7.6.2 FNIRT

Individual subjects develop a degree of heterogeneity in brain morphology and atrophy. While these do not preclude inter-subject or group comparison, registration into a standard or template space is necessary to do so. Non-linear registration techniques provide a robust means of inter-subject registration based on a warp, offering a registration superior even to a 12 DOF linear registration (Section 2.7.6.1). In the context of this thesis, non-linear registration is implemented using FNIRT in order to register data from single subjects into a standard space or subject average, particularly important to account for regions of focal atrophy frequently seen in older participants.

In scans where obvious pathology is present, such as lesions in stroke, it is important to down weight or exclude these regions from the calculation of a non-linear registration matrix into standard space, where the pathological lesion would not be present. Registration of brain including such pathology therefore includes a lesion mask, which downweights the contribution of the lesion voxels to the calculation of a non-linear warp. During resampling, the lesion will still be warped into standard space, but will not have biased the calculation of the warp itself.

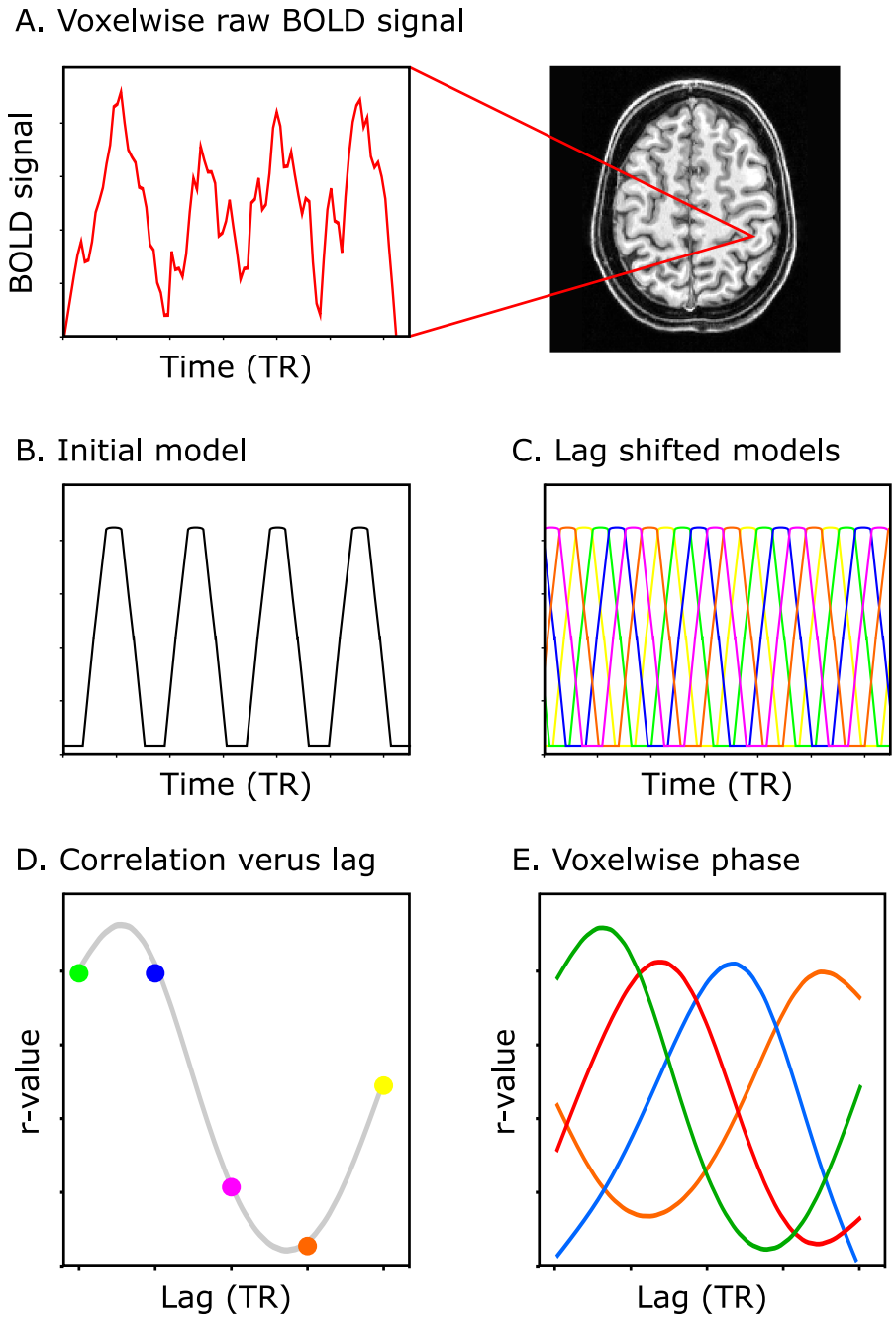


Figure 2.13: *Overview of phase-encoding analysis.* Phase-encoding analysis involves cross-correlating the BOLD signal in each voxel (A), with a model (B) shifted by a given lag over a number of interations (C). By cross-correlating the BOLD signal with the HRF-convolved model at each lag, it is possible to plot correlation values as a function of the lag by which the model has been shifted (D). By assessing the phase of the resulting curve, for each voxel it is possible to ascertain the given lag or shift of the model that the BOLD activity most closely matched (E: colours represent different example voxel timecourse correlation plots). This approach increases sensitivity to track a wave of activation associated with the repeated cycles of a given stimulus, such as a rotating wedge in retinotopy, or sequential sensory stimulation of successive adjacent digits.

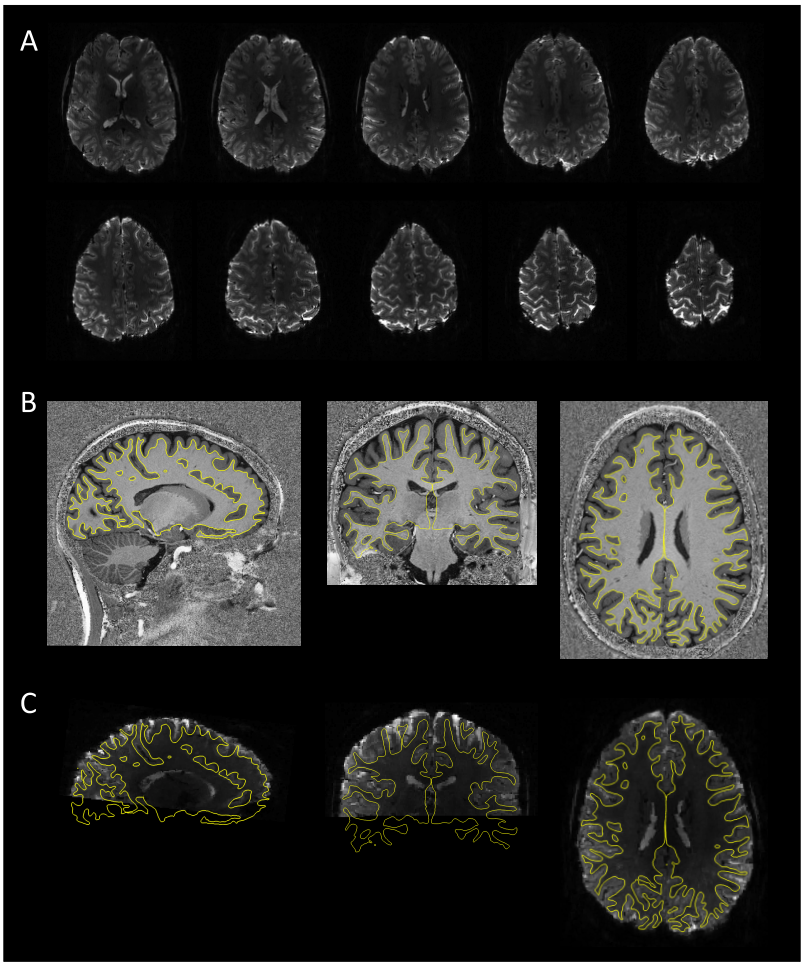


Figure 2.14: *Boundary-based registration in FLIRT.* A. Axial slices of raw BOLD EPI data to be resampled to structural space. B. T1-weighted MP2RAGE data showing grey/white matter boundary (yellow). C. BOLD EPI data resampled into structural space using BBR, visually demonstrating the high degree of concordance with the grey/white matter boundary derived from the structural data (yellow).

## 2.8 Transcranial magnetic stimulation

Transcranial magnetic stimulation (TMS) is a broadly applied neurophysiological technique that has developed over the past 25 years (Barker et al., 1985). In the context of the sensorimotor system, TMS is offers a means of investigating cortical excitability and the integrity of the descending corticospinal tract responding for motor outflow.

The basis principle of TMS is based around electromagnetic induction: a sudden rapidly-induced magnetic field applied to the scalp is able to induce a current into the brain, and at the correct magnitude is able to induce neuronal firing. TMS equipment is typically composed of a stimulator and a figure of eight coil. The figure of eight coil is placed on the scalp, overlying a region of interest, at which point the stimulator capacitors discharge a brief current into the coil, inducing a local magnetic field, which induces a current in the underlying brain tissue. It is possible to modulate the stimulator output to alter the magnitude of the stimulation.

In the context of this thesis, simple monophasic TMS is applied to the ipsilesional motor region of stroke patients in combination with electromyography (EMG) motor evoked potentials (MEPs) from the hand, to assess the integrity of the descending corticospinal tract (CST). This measurement is based on the principle that greater disruption to the CST will necessitate a greater magnitude of stimulation to elicit MEPs in the hand, if this is possible at all. The minimum magnitude of the stimulation required to induce such a movement is referred to as the motor threshold, and can be induced with participants at rest, or during isometric contraction of a muscle. Single pulse TMS measurements used in combination with the recording of MEPs have been shown previously to provide a useful measure of corticospinal tract integrity and motor excitability (Ridding and Rothwell, 1997; Ward et al., 2003).

# 3 | Resolving digit somatotopy in primary somatosensory cortex with fMRI at 7 tesla

*As discussed in Chapter 1, it is well established in the non-human primate literature that the primary somatosensory cortex exhibits somatotopy, with representations of the individual digits, and a degree of variability between individuals. fMRI at 7.0 tesla provides a unique opportunity to investigate this organisation in humans. To date, efforts to map the individual digits in the primary somatosensory cortex have required complex stimulation equipment or manual stimulation, and have often necessitated long scan duration. Furthermore, little work has been done to investigate the reproducibility of these high resolution maps. This chapter therefore outlines part of a large longitudinal fMRI study undertaken at 7.0 tesla, which sought to rapidly map digit topography at the single-subject level, and to investigate to spatial reproducibility of these maps over 24 hours and again over four weeks.*

## 3.1 Introduction and rationale

As described in section 1.1.5.1, the concept of somatotopy in the primary somatosensory cortex is well established, from Penfield's early intra-surgical recordings (Penfield and Boldrey, 1937) to more detailed systematic mapping performed in non-human primates (Kaas et al., 1979; Nelson et al., 1980). Within these maps exist disproportionately large representations of the contralateral digits. The microelectrode mapping studies discussed in section 1.1.5.1 have provided valuable insight into the

nature of somatotopy in the primary somatosensory cortex in non-human primates, demonstrating a considerable degree of inter-subject variability (Section 1.4.1).

It is increasingly evident that the somesthesis plays a considerable role in the control of movement, both in the context of motor learning (Ostry et al., 2010; Vidoni et al., 2010) and motor rehabilitation (Xerri et al., 1998; Celnik et al., 2007). The hand and dexterity therein are central to many skilled movements in humans, therefore considerable efforts have been made to map the sensory representations of the digits in the brain. The ability to readily map the sensory representations of individual digits in the human brain could offer insights into the link between the inter-individual variability in both somatotopic organisation and dexterity, as well as the potential to investigate how these somatotopic maps change, both in a use-dependent fashion, and in response to pathological insults such as stroke.

fMRI offers a unique opportunity to non-invasively investigate patterns of brain activation in humans participants. As outlined in section 2.4, fMRI relies upon the phenomenon of neurovascular coupling in the brain, inferring changes in neuronal activity from local changes in the relative concentrations of HHb and $O_2$Hb, which drive focal alterations in magnetic susceptibility.

In the context of somatotopy in the primary somatosensory cortex, fMRI studies have built upon the positron emission tomography (PET) literature (Fox et al., 1987). Early fMRI data reported multiple foci of activation in the primary somatosensory cortex in response to tactile stimulation (Lin et al., 1996), with subsequent work demonstrating crude topographic activation associated with stimulation of individual digits (Gelnar et al., 1998). Subsequent studies demonstrated patterns consistent with ordered digit somatotopy in the primary somatosensory cortex (Overduin and Servos, 2004; Huang and Sereno, 2007). However, the majority of studies to date have been performed at field strengths ranging from 1.5-4.0 tesla, meaning SNR constraints place digit representations in the primary somatosensory cortex at or around the realistic limit of resolution for BOLD fMRI. Most studies are therefore

unable to uniformly resolve digit representations at the single subject level (Maldjian et al., 1999; Schweizer et al., 2008), and are limited by low resolution (Overduin and Servos, 2004; Duncan and Boynton, 2007), a reliance on group analysis of data (Maldjian et al., 1999; Nelson and Chen, 2008) or mapping only a limited number of digits (Francis et al., 2000).

Recent studies have taken advantage of the increased availability of UHF MRI systems, mapping digit topography in the primary somatosensory cortex at 7.0 tesla. As outlined in section 2.6, beyond an increase in SNR and associated improvements in spatial resolution, the nature of the BOLD signal is inherently different at UHF compared with 1.5 or 3.0 tesla systems, with a reduction in intravascular signal, resulting in greater spatial specificity. Various groups have mapped complete digit somatotopy in the primary somatosensory cortex at the single subject level using passive tactile stimulation in an event-related or phase-encoding paradigm (Sanchez-Panchuelo et al., 2010; Stringer et al., 2011; Sanchez-Panchuelo et al., 2012; Besle et al., 2013a; Martuzzi et al., 2014; Stringer et al., 2014). The ability to undertake mapping in the individual has applications for both studies of neuroplasticity and clinically for pre-surgical planning. However, current approaches are limited by the requirement for specialist stimulation equipment and the need for a considerable number of repeated fMRI runs, with a duration of as much as 20 minutes of data to derive maps. There are also issues of variability in stimulus perception, and maintenance of attention. As such, these approaches are potentially unfeasible for multimodal imaging studies where time is limited or where only shorter duration scans are possible, such as in patient studies or work with older participants. Furthermore the majority of these stimulation approaches activate only a subset of peripheral glabrous mechanoreceptors and proprioceptors (Tables 1.1 and 1.2), while natural sensory stimulation of the hand associated with movement typically recruits a combination thereof. In this chapter, I refer to somatosensory cortex as comprising Brodmann areas 2, 1, 3a and 3b, which are involved in the process of both tactile and pressure information, as well as deeper proprioceptive information.

In the present chapter, I have developed a rapid and easily-implemented paradigm to map digit topography in the primary somatosensory cortex of the human brain at the single-subject level using fMRI at 7.0 tesla. Specifically, I sought to assess the robustness of this mapping technique in comparison to more traditional block-design approaches applied commonly in the fMRI literature. Further, I investigated the reproducibility of these maps over time to validate their stability and their potential use in studies of neuroplasticity.

## 3.2 Methods

### 3.2.1 Participants

Thirteen healthy control participants [Mean age: 27.8 ± 6.08; six female] were recruited in accordance with local central university research ethics committee approval (University of Oxford MSD-IDREC-C2-2013-05). All participants were right handed according to the Edinburgh Handedness Inventory (Oldfield, 1971). A full version of the Edinburgh Handedness Inventory can be found in Appendix A.

### 3.2.2 Experimental design

The data discussed in the current chapter were acquired as a part of a larger project summarised in figure 3.1, and described further in Chapter 4. The current analysis considers three of the acquired scan sessions: two sessions separated by a period of 24 hours, and a third session four weeks prior to, or following the other two sessions (-4 weeks: six participants; +4 weeks: seven participants). During each session subjects undertook a one hour fMRI scan. One of the sessions also involved an additional scan to acquire a structural image.

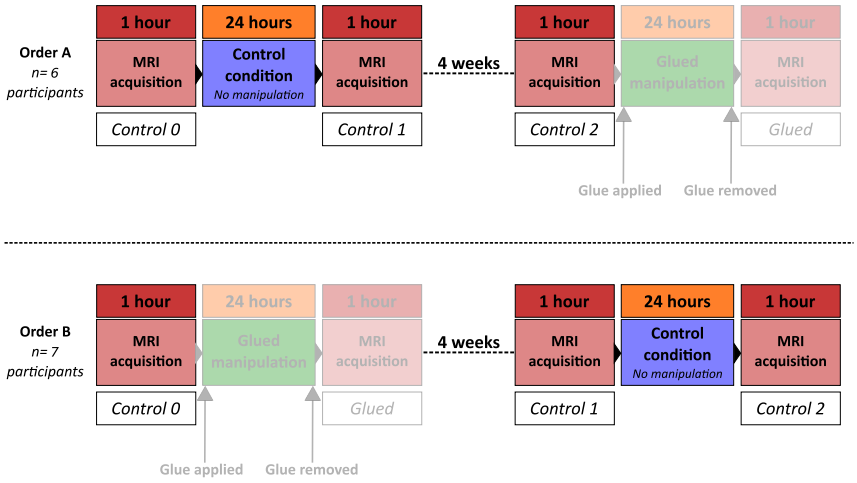


Figure 3.1: *Overview of digit topography study design.* Participants attended four scan sessions in total. The current chapter considers the three control scans: two sessions separated by a period of 24 hours, and a third session four weeks prior to, or following the other two sessions. The scans not considered in this chapter are shown with increased transparency.

### 3.2.3 MRI acquisition

fMRI data were acquired using a Siemens 7T Magnetom system and a 32-channel head coil. A functional localiser scan was used to aid slice placement (Multislice gradient echo EPI, TR: 3000ms, TE: 25ms, flip angle: 90, bandwidth: 1568Hz, 43 axial slices, 2x2x2mm resolution, GRAPPA factor = 2). Task fMRI data were acquired using a FOV on the basis of the functional localiser results (Figure 3.2), with true axial slices centred on the hand knob activation in the z-axis of the left hemisphere (Multislice gradient echo EPI, TR: 1500ms, TE: 25ms, flip angle: 90°, bandwidth: 1562Hz, 22 axial slices, 1.2x1.2x1.2mm resolution, GRAPPA factor = 2).

For image registration purposes, a single volume partial FOV high-saturation EPI image with the same scan parameters as the task fMRI was acquired, along with a single-volume high-saturation whole brain EPI scan (Multislice gradient echo EPI, TR: 8490ms, TE: 25ms, flip angle: 90°, bandwidth: 1562Hz, 128 axial slices, 1.2x1.2x1.2mm resolution, GRAPPA factor = 2) (Figure 3.2). T1-weighted MEMPRAGE structural

scans were acquired during one of the three sessions using a 3T Siemens Trio system (TR: 2530ms, TE: 1.69, 3.55, 5.41 and 7.27ms, 1x1x1 mm, GRAPPA factor = 2).

### 3.2.4 fMRI tasks

Participants performed a series of tasks involving visually-cued movements of individual digits in the scanner: digit 2 (D2: index finger), digit 3 (D3: middle finger), digit 4 (D4: ring finger) and digit 5 (D5: little finger). During the three minute functional localiser scan, subjects were instructed to appose their right thumb and each of the digits of their right hand sequentially during 15 second movement blocks, contrasted with equivalent periods of rest.

All subsequent task fMRI involved individual digit movements in the form of button presses using an MRI-compatible button-box resting on the participant's right thigh during the scan (Figure 3.3). Subjects were presented with four white circles, corresponding to the four digits of the right hand, shown on a visual display projected into the scanner bore. The displayed circles flashed individually at a constant frequency in order to cue subjects to make button presses at the specified rate. A phase-encoding task (Section 2.7.2.2) was used, which involved continuous button presses at a rate of 1Hz with no rest periods. The phase forward task cycled through D2-D5 and consisted of sequential 8 second blocks of button presses at 1Hz per digit (i.e. D2 x 8, D3 x 8, D4 x 8, D5 x 8, D2 x 8 ...), as shown in figure 3.4A. The phase backward task cycled through D5-D2, as shown in figure 3.4B. In both the phase forward and backward tasks, each cycle through the digits was repeated eight times (8 mins 50s).

A block task was also undertaken, in which participants were instructed to perform individual digit button presses at 1Hz (e.g. D2, D2, D2, D2 ...) during 12 second task blocks, which alternated with 12 second blocks of rest. Four blocks of movement were collected per digit, giving 16 button press movement blocks and 16 rest blocks in total, presented in one of two counterbalanced orders, randomised across visits (6 mins 24s) (Figure 3.5).

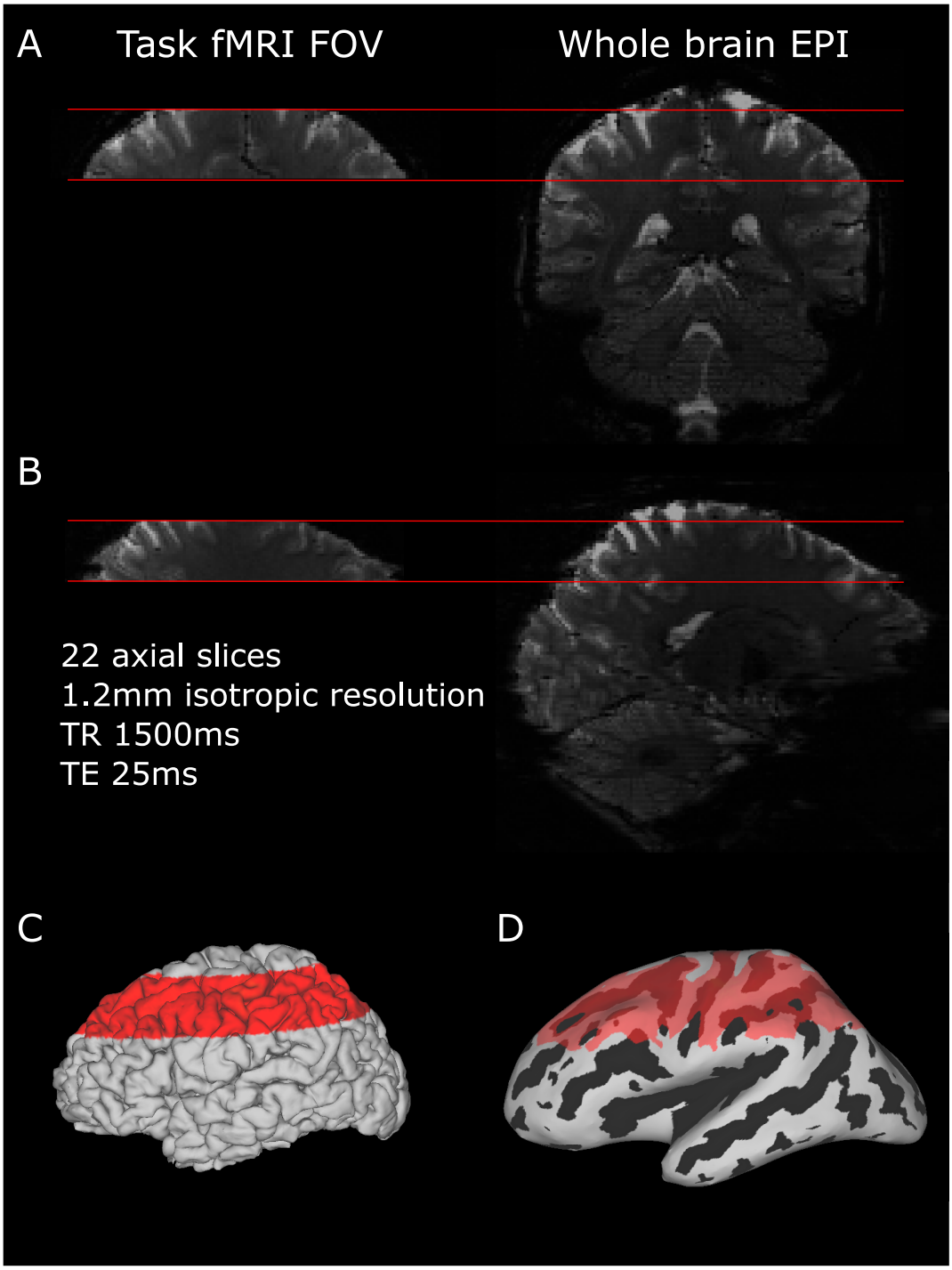


Figure 3.2: *Task fMRI EPI coverage centred around the sensorimotor hand knob.* Coronal (A) and sagittal (B) slices of EPI coverage (left) and whole brain EPI data for registration purposes (right). The extent of coverage is displayed on the pial surface (C: red) and on a representation of the pial surface inflated (D: red).




Figure 3.3: *Task fMRI button box.*

### 3.2.5 MRI analysis

MRI analysis was undertaken using tools from FSL (www.fmrib.ox.ac.uk/fsl) (Smith et al., 2004; Woolrich et al., 2009; Jenkinson et al., 2012). MRI data were visualised on cortical surface reconstructions produced using FreeSurfer (www.freesurfer.net) (Dale et al., 1999; Fischl et al., 2001) viewed in Connectome Workbench (Marcus et al., 2011).

#### 3.2.5.1 Image preprocessing

All fMRI data were subject to the following preprocessing steps: motion correction using MCFLIRT (Jenkinson et al., 2002); removal of non-brain tissue using the Brain Extraction Tool (BET) (Smith, 2002); spatial smoothing with a Gaussian kernel of 1.5mm full-width half-maximum (FWHM); high pass temporal filtering (Gaussian-weighted least squares straight line fitting with sigma = 100 seconds).

#### 3.2.5.2 Image registration

All image registration was undertaken within subject using FLIRT (Jenkinson and Smith, 2001; Jenkinson et al., 2002). Four-dimensional task fMRI data were first

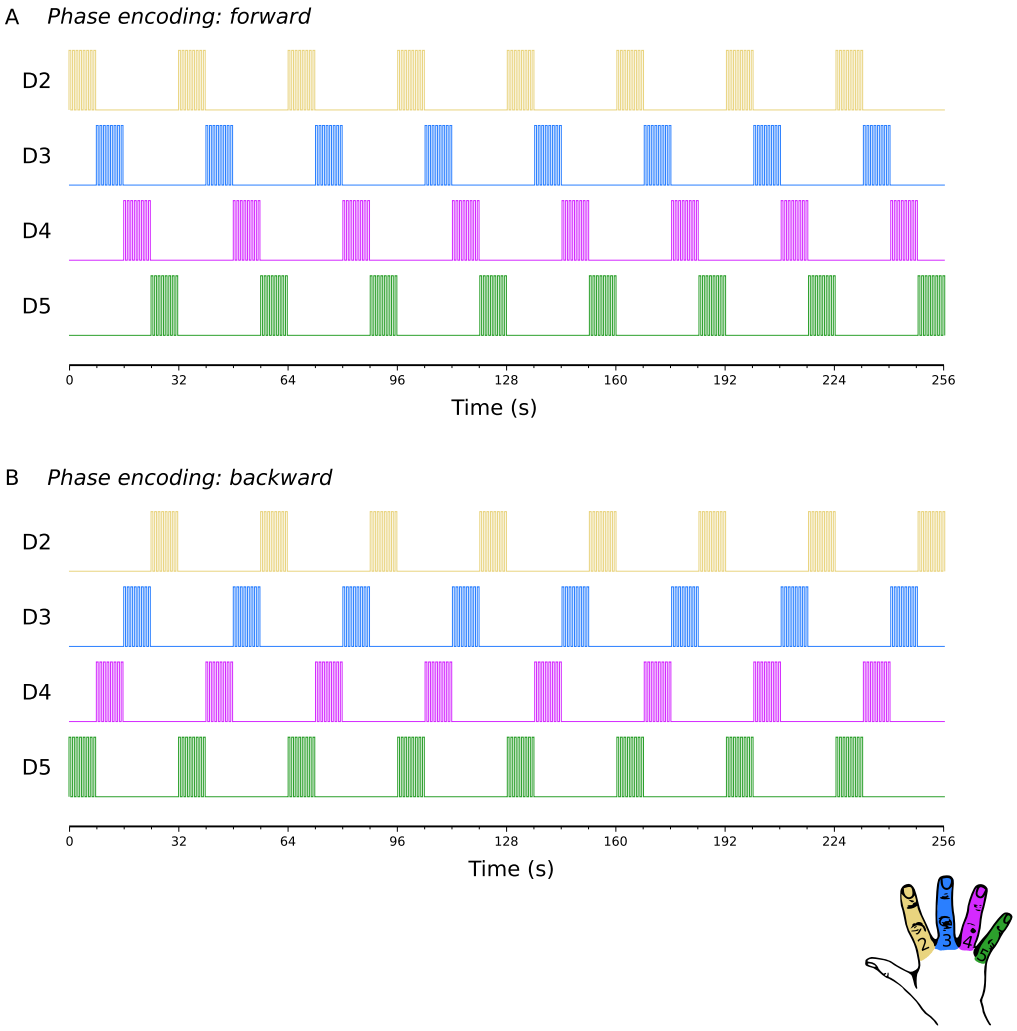


Figure 3.4: *Overview of fMRI phase-encoding design.* Two phase-encoding runs were acquired at each time point: forward (A), and backward (B). Boxcar peaks represent movement of digit 2, 3, 4 or 5 (D2, D3, D4, D5). Each coloured boxcar peak represents eight movements of the specific digit, at a rate of 1Hz. Across each 32 second cycle, the task progress from D2-D5 in the forward order (A), and D5-D2 in the backward order (B).

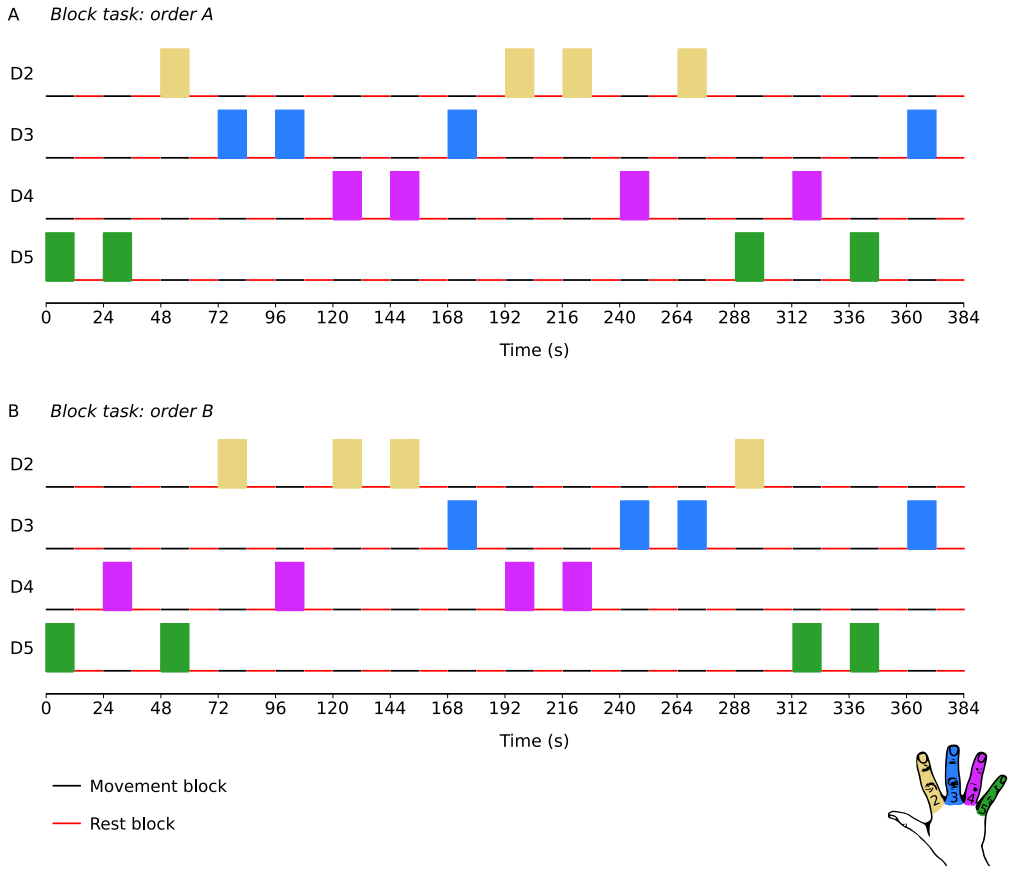


Figure 3.5: *Overview of fMRI block task design.* One run of block task data were acquired at each time point, either order A (A) or order B (B). Boxcar peaks represent movement of digit 2, 3, 4 or 5 (D2, D3, D4, D5). The block task contrasts 12 second periods of movement (black) with 12 second periods of red (red). Each coloured boxcar peak represents twelve movements of a specific digit in a movement block, at a rate of 1Hz. The order of movement blocks was counterbalanced.

registered to the single volume partial FOV high-saturation EPI image acquired during that session (Degrees of freedom: 6, cost function: normalised correlation). The single volume partial FOV high-saturation EPI image was registered to the T1-weighted MEMPRAGE image using BBR (Degrees of freedom: 6, FMRIB's Automated Segmentation Tool (FAST) white matter segmentation, no search) (Greve and Fischl, 2009), initialised with an affine registration matrix. The initialisation matrix was the sum of the following registrations: the single volume partial FOV high-saturation EPI image to the single-volume high-saturation whole brain EPI scan (Degrees of freedom: 6, cost function: normalised correlation, no search); the single-volume high-saturation whole brain EPI scan to the T1-weighted structural MEMPRAGE image (Degrees of freedom: 6, cost function: mutual information).

#### 3.2.5.3 Phase-encoding task analysis

The phase-encoding task fMRI data were analysed using an approach previously applied in retinotopy, and more recently for body mapping (Orlov et al., 2010; Sanchez-Panchuelo et al., 2010), as outlined in section 2.7.2.2. This analysis used cross-correlation to find the time point in the phase forward (D2-D5) and phase backwards (D5-D2) tasks at which each cortical voxel responded maximally.

To achieve this, the preprocessed BOLD EPI data were correlated against a series of reference models, as in figure 2.13C. The model was composed of a gamma HRF convolved boxcar: 8 second 'on' and 24 second 'off', repeated eight times, mirroring the eight cycles of the phase forward and phase backward tasks. The model was shifted in time iteratively so that activity at each TR could be modelled. This approach increases sensitivity to track a wave of activation associated with the cycles of movement which progress either from D2-D5, or D5-D2. A correlation was calculated between the raw BOLD signal of each voxel and the reference model at each lag. Each iteration of the model shifted the boxcar by one TR (1.5s), with sufficient shifts to cover one 32 second cycle through D2-D5 or D5-D2. Each boxcar model

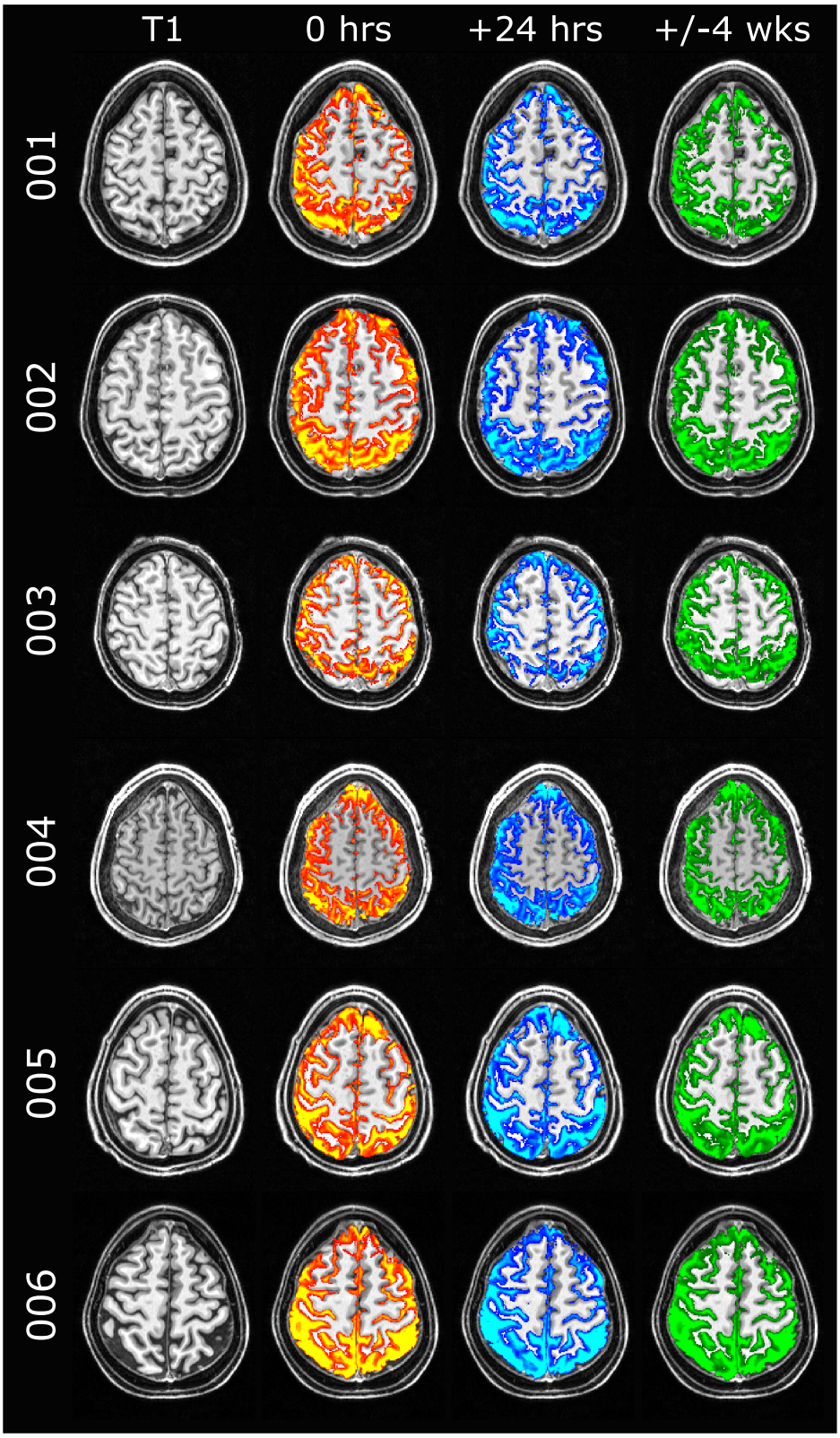
T1
0 hrs
+24 hrs
+/-4 wks
001
002
003
004
005
006

was assigned to a given digit in the cycle, taking into account the haemodynamic delay with a time to peak of 4.5 seconds. The boxcar models corresponding to a given digit in both the phase forward and phase backward tasks were resampled to the single volume partial FOV high-saturation EPI space (spline interpolation) and averaged to give one $r$-value map per digit. These soft-edged maps were further masked using a winner-takes-all approach to produce $r$-value maps in which each voxel was assigned exclusively to one digit. Both the soft-edged and winner-takes-all $r$-value maps were converted into a corresponding $z$-statistic on the basis of the distribution of values within the brain tissue of the FOV for which BOLD EPI data were acquired. $z$-statistic maps were converted to uncorrected p-values using fslmaths. Individual digit maps were thresholded using FDR to determine a corrected p-value threshold on the basis of the observed $p$-value distribution within the data ($\alpha$=0.001) (Genovese et al., 2002).

#### 3.2.5.4 Block task analysis

The block task fMRI data were analysed using a GLM in FEAT. All analysis was undertaken on the single-subject level, using FILM to estimate timeseries autocorrelation and pre-whiten each voxel. Each digit (Figure 3.5) was modelled with a separate boxcar regressor with gamma HRF convolution and its temporal derivative, giving a total of four regressors. FEAT was used to produce activation maps corresponding to all four digits by contrasting a given digit regressor to the rest blocks (e.g. D2 > rest), or contrasting a given digit to blocks representing other digits (D2 > D3, D4, D5). Each of these contrasts yielded activation maps for each individual participant; these $z$-statistic images were thresholded at $Z$ >2.3 with a corrected cluster extent

---

Figure 3.6 *(preceding page)*: *Registration of a limited FOV BOLD EPI data to structural space.* The results of boundary based registration and the resampling of BOLD EPI data to the structural space. Six representative participants (rows), showing BOLD EPI data in structural space, thresholded and coloured to emphasise the sulcal patterns and demonstrate overlap with structural images at the three scan time points (0 hrs: orange/yellow; +24 hrs: blue; ± 4 wks: green.)

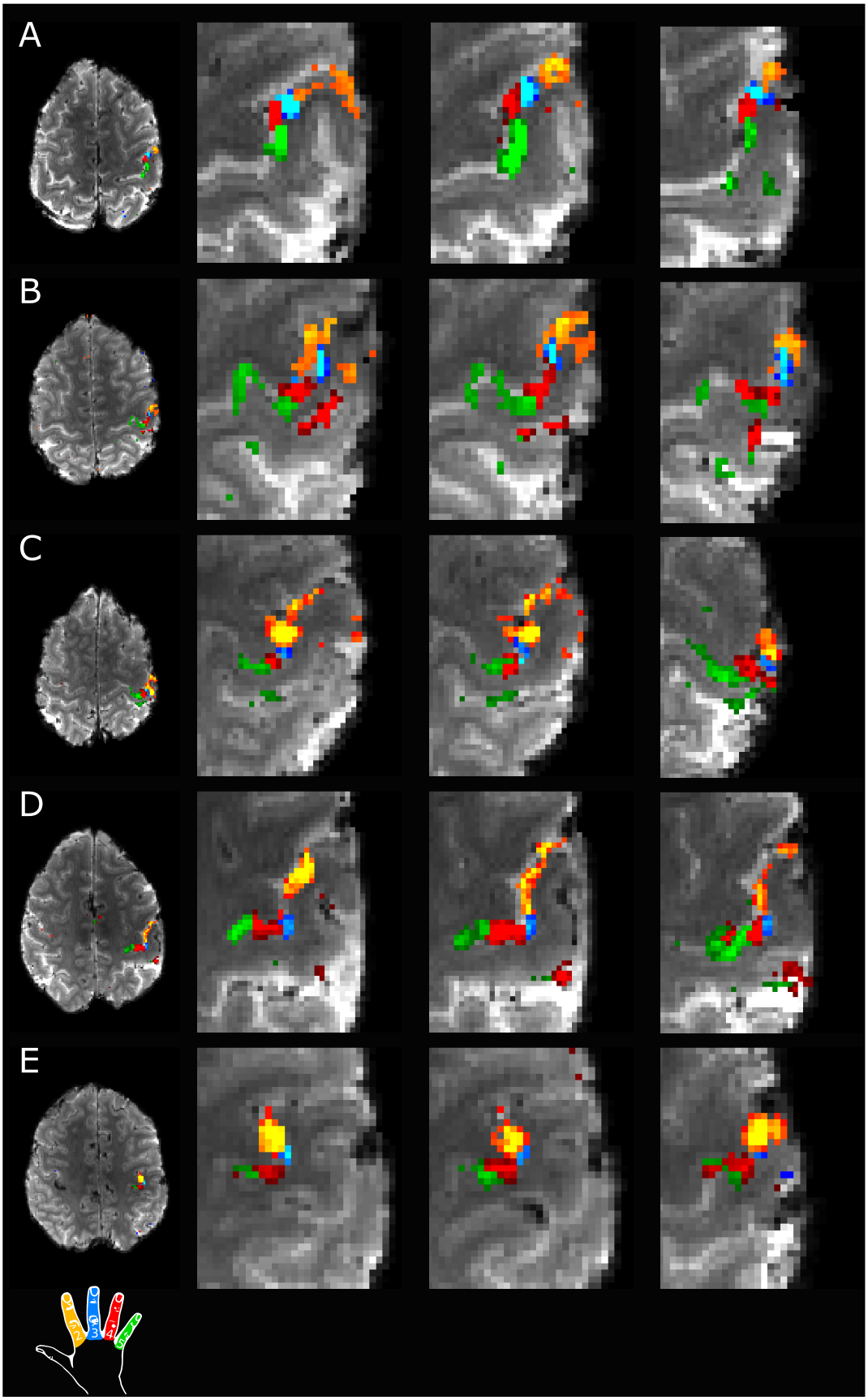
A
B
C
D
E

threshold of $p < 0.05$. Thresholded digit maps were resampled into the single volume partial FOV high-saturation EPI space (spline interpolation).

#### 3.2.5.5 Surface projection

Cortical surface reconstructions were generated from T1-weighted MEMPRAGE scans for each subject, resampled to native structural space, and converted to Geometry Informatics Technology Initiative (GIFTI) format. Both block-task and phase-encoding task digit maps were resampled from the single volume partial FOV high-saturation EPI space to native structural space (spline interpolation). Digit maps were projected from three-dimensional volume space to two-dimensional surface space.

#### 3.2.5.6 Statistics

All statistical analysis and graphing were undertaken using JMP (Version 11.0, SAS Institute, Cary, NC, USA) and Statistics Package for the Social Sciences (Version 19.0, IBM Corporation, Armork, NY, USA).

---

Figure 3.7 *(preceding page)*: *Phase-encoding digit representations: volumetric space.* Activation maps for individual digits from phase-encoding data analysis. Data from five representative subjects (A-E), showing one whole brain axial slice (Column 1), and three axial slices through the anatomical hand knob (Columns 2-4). Individual digit representations were derived from a winner-takes-all approach, and were thresholded using FDR ($\alpha$=0.001), colour coded to correspond to the colours of the digits on the hand schematic. All data overlaid on individual subject BOLD EPI axial slices.

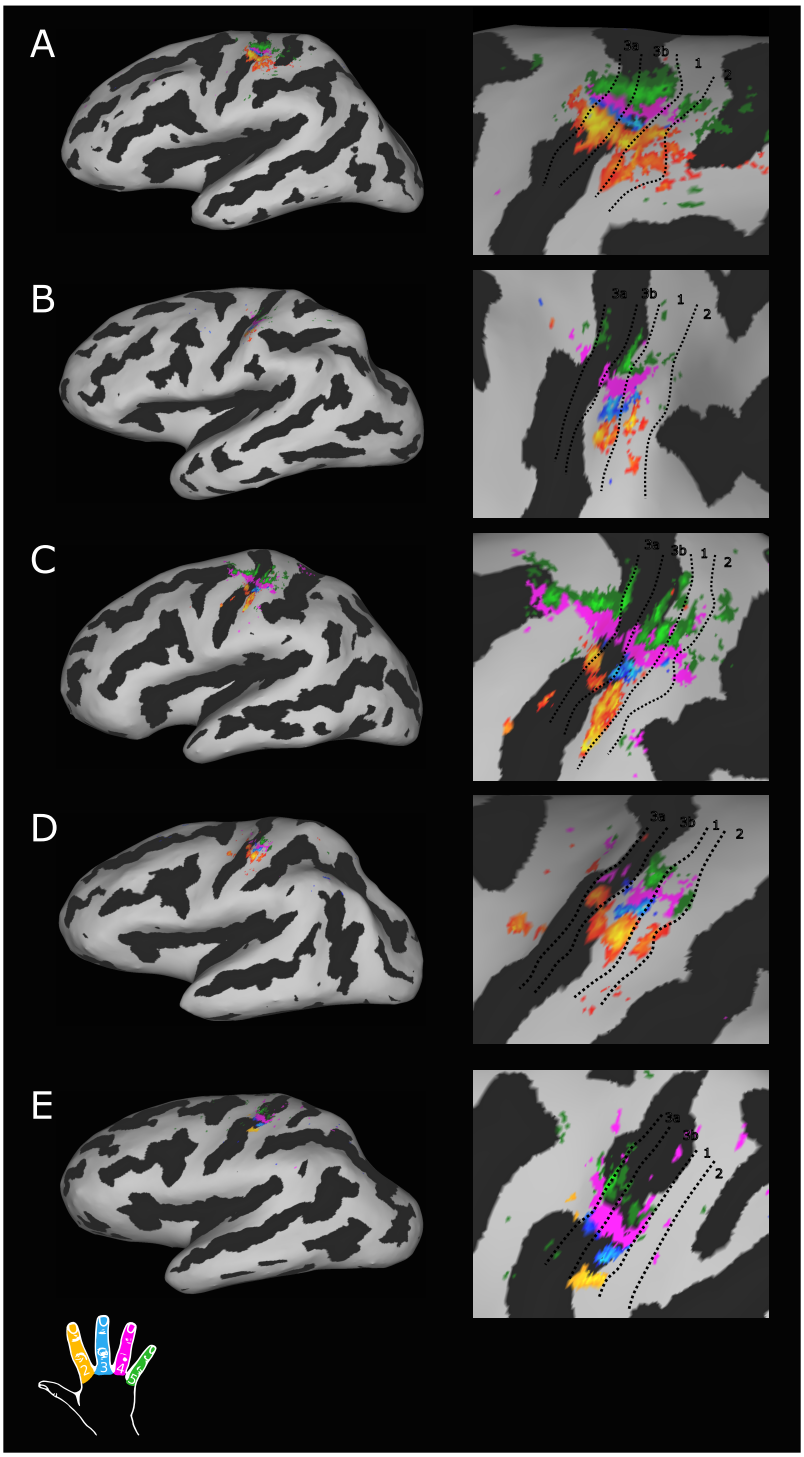


Figure 3.8: *Phase-encoding digit representations: surface space.* Activation maps for individual digits from phase-encoding data analysis projected onto the inflated cortical surface reconstructions of individual subjects (A-E). Digit representations overlaid with Brodmann area estimated boundaries (Area 3a, 3b, 2 and 1) from single-subject FreeSurfer cortical parcellation. Inflated cortical surfaces display the gyral pattern of the brain, with sulci shown in black and gyri in grey.

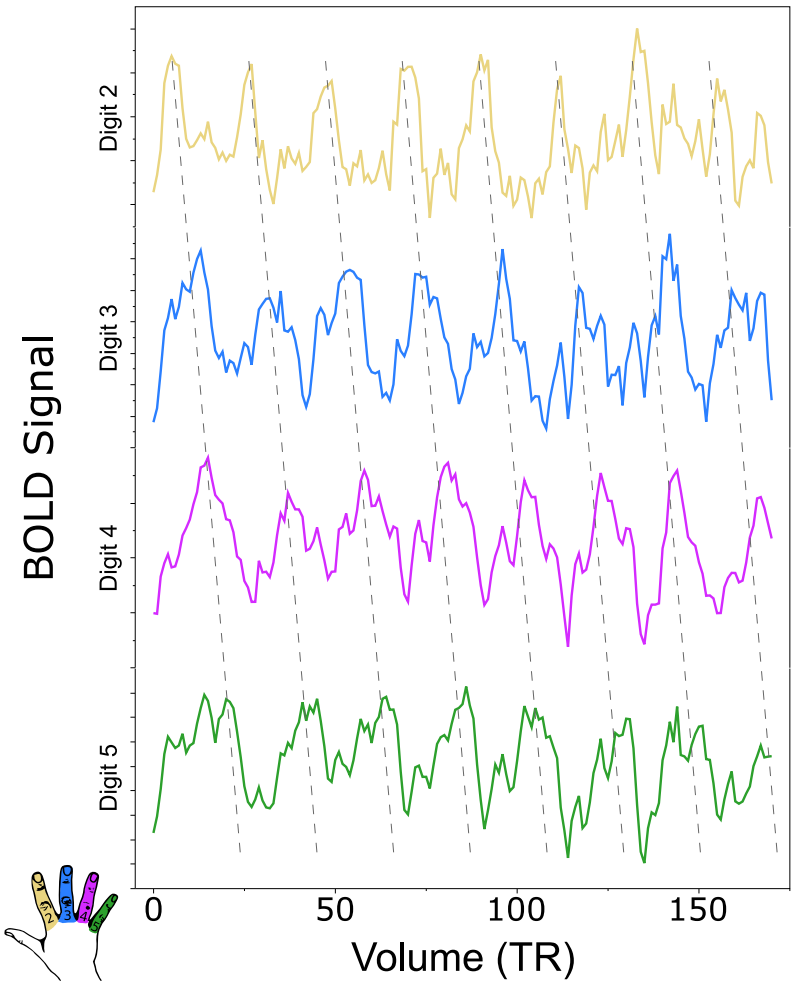


Figure 3.9: *BOLD signal time course from phase-encoding digit representations.* The BOLD time course averaged within the four phase-encoding derived digit representations, from a single representative subject and time point. The grey dashed lines intersect each BOLD trace at the TR corresponding to the end of each sequence of eight button presses for that digit. The sequential signal peaks from digit 2 to digit 5 consistent with the phase forward task (Section 3.2.4 and figure 3.4).

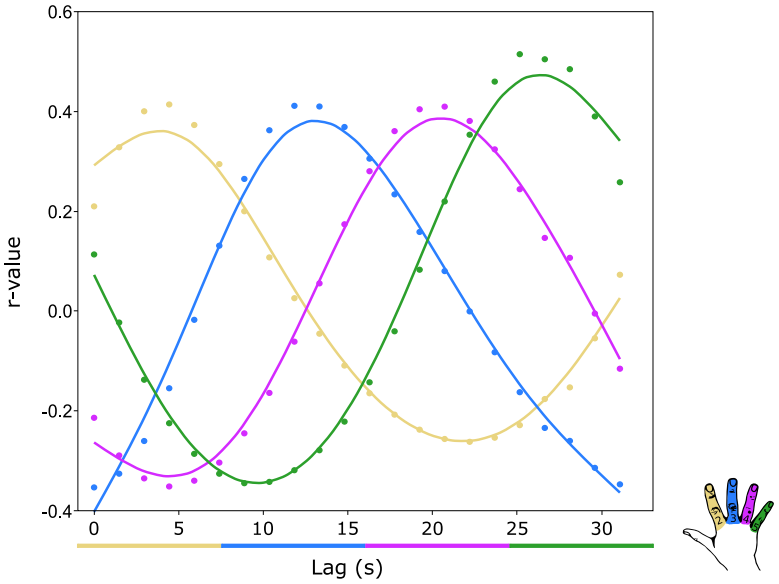


Figure 3.10: *Phase-encoding cross-correlation as a function of lag in digit representations.* Average *r*-value within each phase-encoding derived digit representation across a range of phase-encoding cross-correlation lags. Data shown represent a single representative subject and time point.

## 3.3 Results

All BOLD EPI data were assessed for excessive motion both visually and using motion estimate outputs from MCFLIRT (Section 2.6.4.2): data from three subjects exhibited visible spin history motion artefact as a result of sharp motion during one or more scan sessions (greater than 1mm of absolute mean displacement in fewer than five volumes); these participants were excluded. One further subject was excluded on the grounds of an incidental finding. Nine subjects were considered in further analysis [Mean age: 29.2 ± 6.43; five female; -4 weeks: four participants; +4 weeks: five participants]. High quality image registration between BOLD EPI images and structural images was achieved for all subjects (Figure 3.6).

### 3.3.1 Phase-encoding design digit maps

The thresholded activation maps from the phase-encoding analysis displayed a clear ordered digit topography in the postcentral gyrus around the anatomical hand knob,

broadly consistent with the estimated location of Brodmann area 3b (Figures 3.7 and 3.8). There was a progression parallel to the central sulcus along the gyrus from digit two ventrally and laterally, through to digit five dorsally and medially. The maps demonstrated a smooth continuous progression between adjacent digits. Patterns of activation are isolated to the primary somatosensory cortex on the postcentral gyrus, with minimal extraneous activation within the FOV in which BOLD EPI data were acquired (Figures 3.7 and 3.8). The digit maps display a degree of inter-subject variability, with some participants displaying maps extending to regions including Brodmann area 3a more rostrally, and Brodmann area 2 more caudally (Figure 3.8).

To explore the signal underlying these maps, I performed a post-hoc ROI analysis. I extracted the average BOLD signal time course within each FDR-corrected digit representation (Figure 3.9). These showed specific activation patterns in a sequence consistent with the task digit order (Figure 3.4). A post-hoc ROI analysis plotting $r$-value of the correlation between BOLD EPI data and the model as a function of the model shift (Section 2.7.2.2) showed a shift in phase of each digit (Figure 3.10).

### 3.3.2 Block design digit maps

The thresholded activation maps from the block task GLM analysis (Figures 3.11 and 3.12) show ordered digit topography around the anatomical hand knob, consistent with the estimated location of Brodmann area 3b and the phase-encoding derived maps. Activation maps derived from contrasting one digit with all others displayed more discrete focal clusters for the individual digits, while contrasting individual digits with rest periods yielded larger more broadly overlapping clusters for the individual digits. Qualitatively the block maps displayed a degree of inter-subject variability, similar to the results of the phase-encoding paradigm.

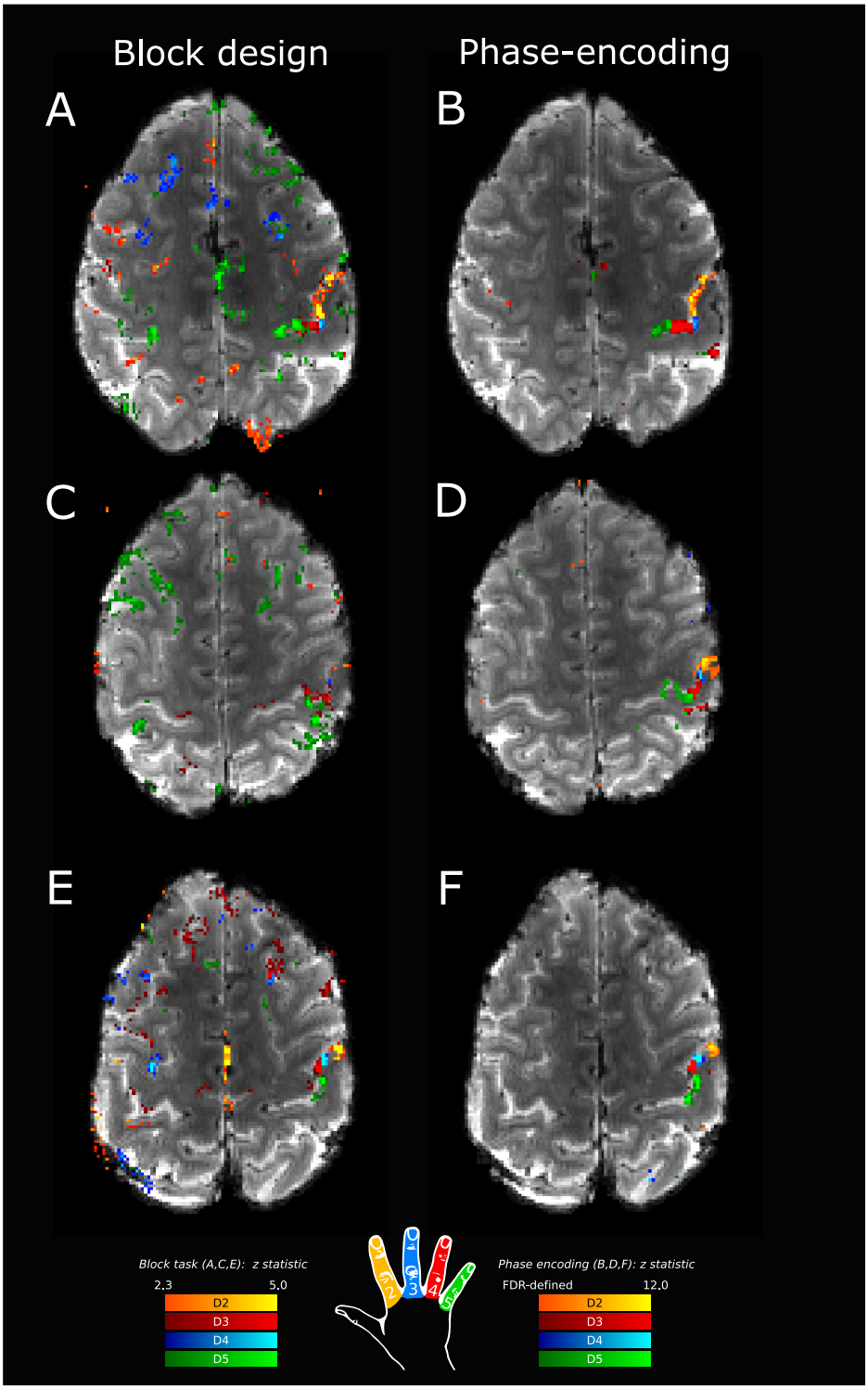


Figure 3.11: *Comparison of phase-encoding and block task GLM-derived digit representations (i).* Activation $z$-stat maps shown for GLM-derived digit representations (left column; contrast: digit $>$ other digits), and for phase-encoding derived digit representations (right column) for three individual subjects. Activation maps overlaid on axial slices of BOLD EPI data, allowing for within subject comparison of maps (A/B; C/D; E/F). Full details of $z$-statistic thresholds are shown in tables 3.1 and 3.2 (Subjects 1-3).

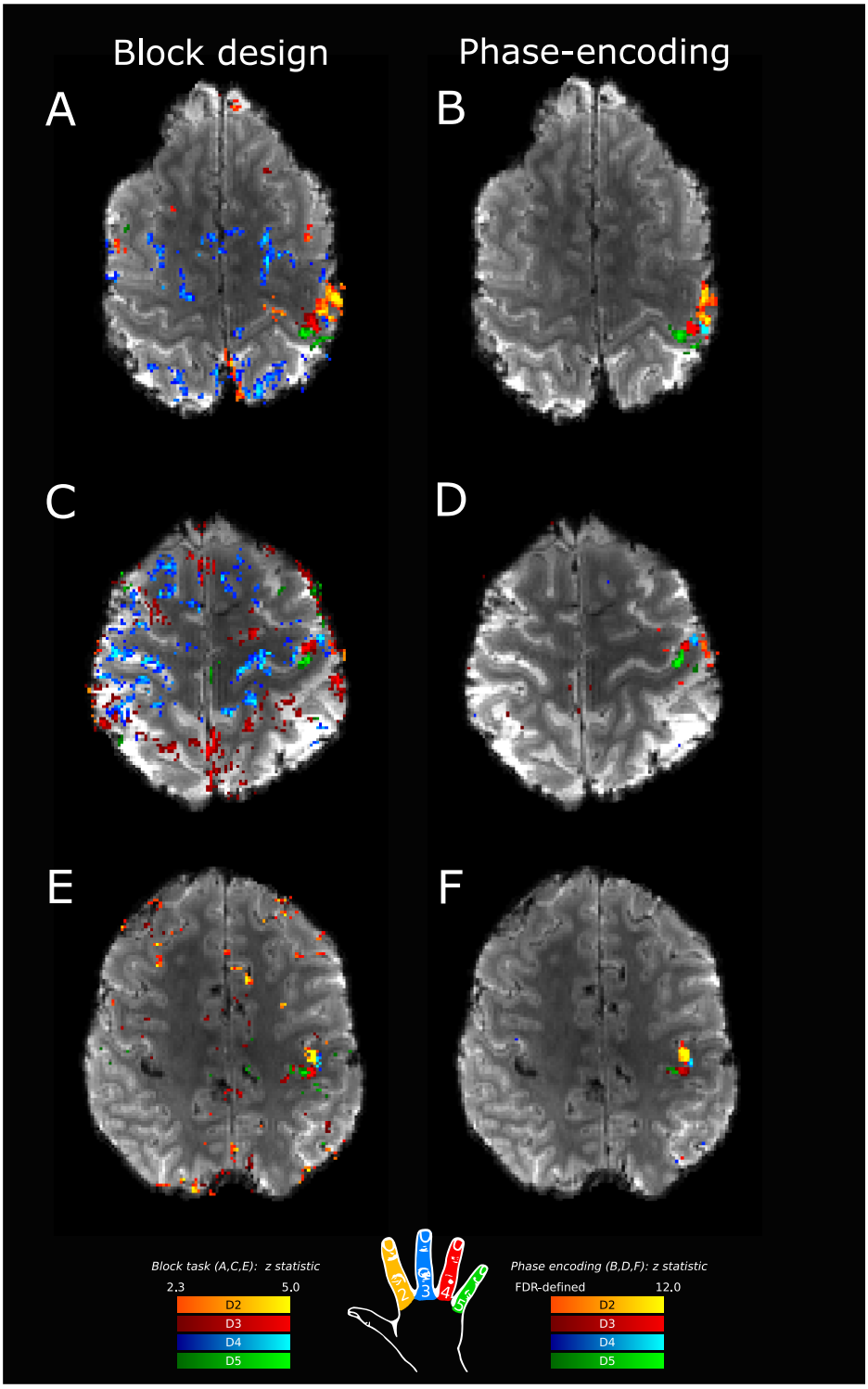


Figure 3.12: *Comparison of phase-encoding and block task GLM-derived digit representations (ii).* Data from three further subjects, as presented in figure 3.11. Full details of *z*-statistic thresholds are shown in tables 3.1 and 3.2 (Subjects 4-6).

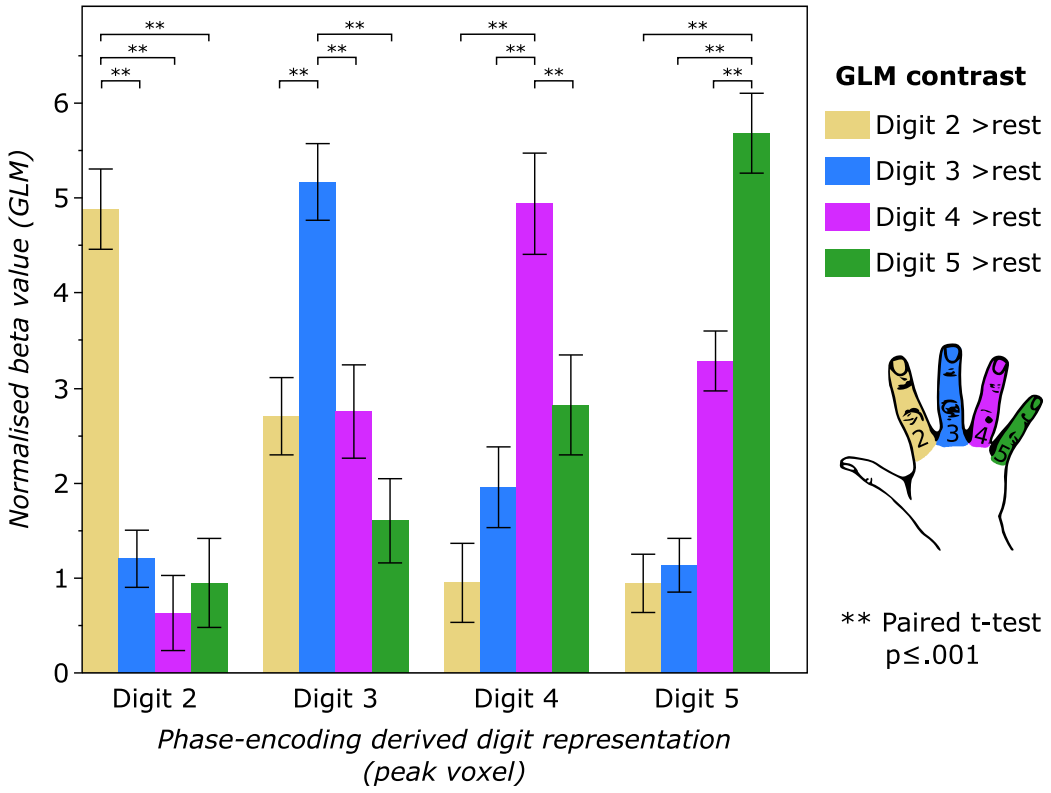


Figure 3.13: *Comparison of phase-encoding and block task GLM-derived digit representations in the primary somatosensory cortex.* At the peak voxel of each phase-encoding derived digit representation, extracting the beta values from each block task GLM contrast demonstrates a maximal value for homologous pairings (e.g. D2 phase-encoding vs. D2 > rest GLM contrast), which are significantly greater than non-homologous pairings (e.g. D2 phase-encoding vs. D4 > rest GLM contrast). RM-ANOVA: significant interaction between phase-encoding digit representation and the digit contrast of the block design GLM on the normalised beta value: $F(9,72) = 69.15$, $p < .001$; post-hoc paired t-tests shown in table 3.3.

### 3.3.3 Concurrence of phase-encoding and block maps

In order to validate the phase-encoding analysis with the more traditional block task GLM analysis, I sought to assess the agreement between the independently derived sets of digit representations. In order to do this, the normalised beta values from the GLM contrasts comparing each digit to rest (e.g. D2 > rest) were extracted at the peak voxel of each phase-encoding derived digit representation (Figure 3.13). These values were averaged for each digit across the three scan sessions for each subject.

A repeated measures ANOVA was performed with one factor of phase-encoding digit representation (D2-D5) and one factor of block design digit representation (D2-D5). As predicted there was a significant interaction between phase-encoding digit representation and block design digit representation on the normalised beta value: $F(9,72) = 69.15$, $p < .001$, sphericity assumed. Post-hoc paired samples t-tests demonstrated a significantly stronger relationship between the phase-encoding and block design digit representations for homologous digits compared with non-homologous digits (Table 3.3). For example, phase-encoding D2 has larger beta value for the D2 > rest block task contrast compared with other digit contrasts from the block design (e.g. the D4 > rest GLM contrast). These results indicate an agreement between the two mapping methods: the peak voxel from the phase-encoding-derived map of a given digit shows a maximal normalised beta value for the GLM contrast specific to the same digit.

### 3.3.4 Reproducibility of phase-encoding digit maps

Surface-projections of digit maps derived from phase-encoding analysis qualitatively display a clear degree of reproducibility within subject (Figure 3.14). To quantitatively assess the reproducibility of the phase-encoding approach to mapping digit representations in the primary somatosensory cortex, a spatial cross-correlation

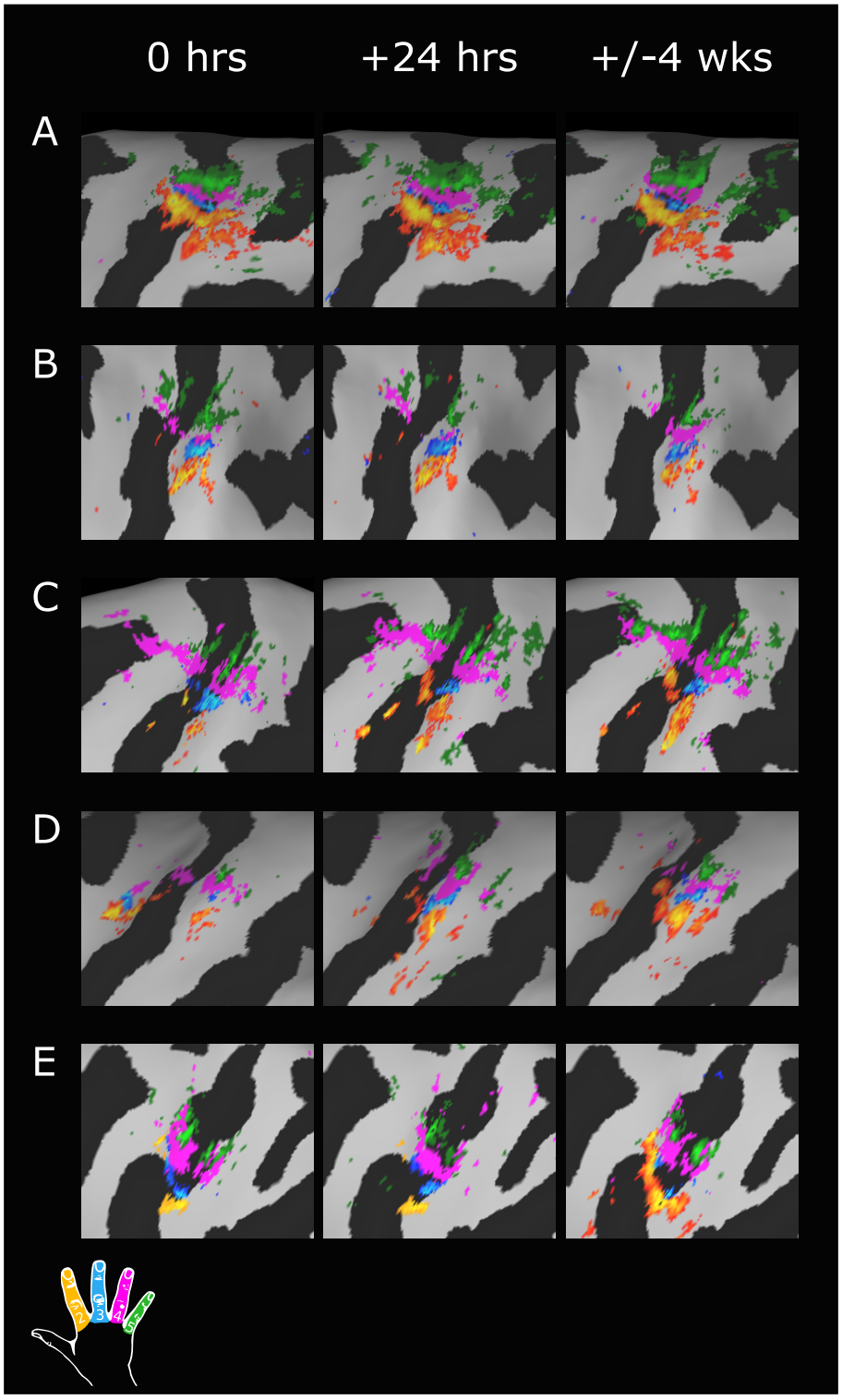


Figure 3.14: *Comparison of phase-encoding digit representations at three scan intervals.* Phase-encoding derived digit representations projected to the cortical surface. Data from five subjects presented (A-E) across three time points. Although there is a high degree of between-subject variability (as shown by the large differences between rows), there is far less within-subject variability over time (as shown by the small differences between the columns).

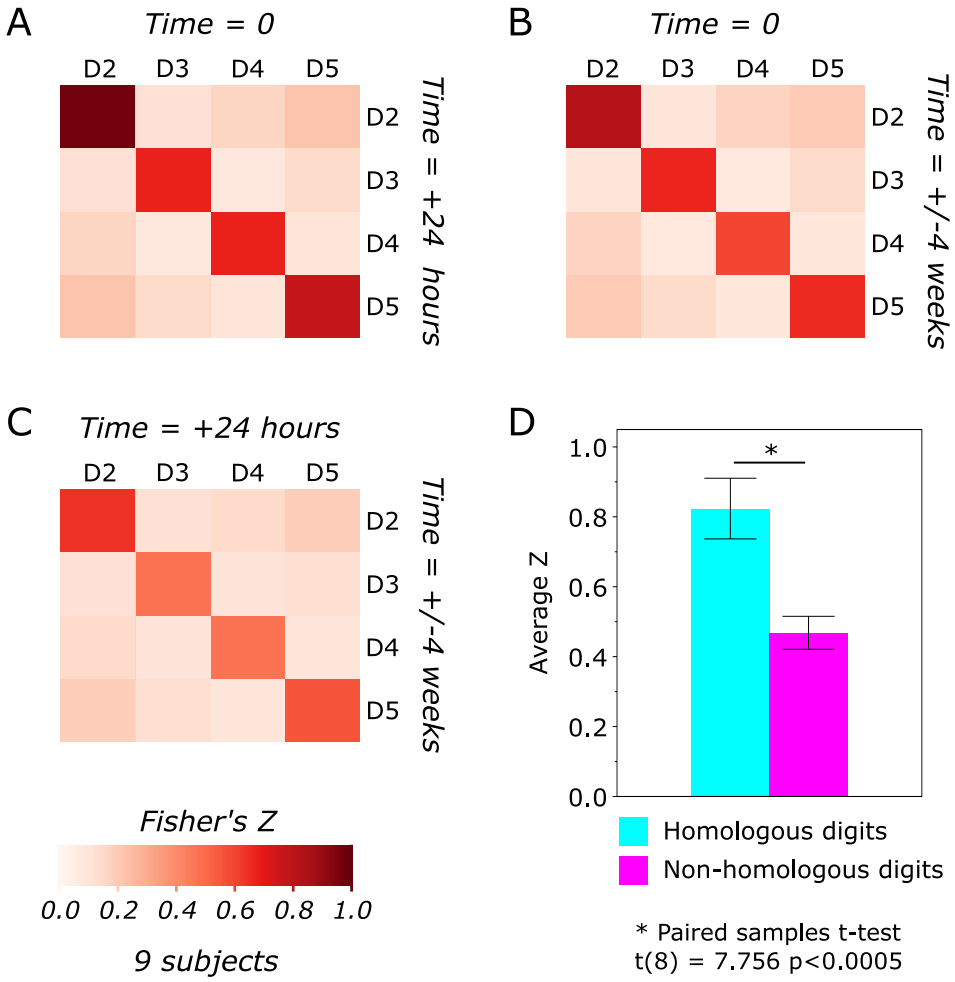


Figure 3.15: *Assessing the reproducibility of phase-encoding derived digit representations in the primary somatosensory cortex.* A-C: Correlation matrices represent spatial cross-correlation within Brodmann area 3b between digit representations. Each matrix shows data for a different pair of time points. Cells within each matrix represent $z$-transformed correlation coefficients calculated between each pair of digit representations. The presence of higher correlation along the diagonal confirms a high degree of voxel-wise reproducibility in phase-encoding derived digit representations across the three map-remap intervals. D: Cross-correlation values between homologous digits across these intervals were significantly greater than between non-homologous digits.

approach was used to compare the soft-edged digit maps within an anatomically defined three-dimensional ROI of Brodmann area 3b across the 24-hour and 4-week map-remap intervals (Figure 3.15). This analysis demonstrated a high degree of spatial concordance between the digit maps across both time intervals. Comparison of $z$-transformed $r$-values using a paired samples t-test show that the cross-correlation between homologous digits which was significantly greater than the cross-correlation between non-homologous digits: $t(8) = 7.756$, $p < 0.001$.

| Phase-encoding digit representations | | | | | | | | | | | | |
|---|---|---|---|---|---|---|---|---|---|---|---|---|
| | Digit 2 | | | Digit 3 | | | Digit 4 | | | Digit 5 | | |
| Subject | *FDR Threshold* | *R.Max* | *Max* | *FDR Threshold* | *R.Max* | *Max* | *FDR threshold* | *R.Max* | *Max* | *FDR threshold* | *R.Max* | *Max* |
| 1 | 4.89 | 10.58 | 12.48 | 4.89 | 12.69 | 15.19 | 4.82 | 10.02 | 11.24 | 4.97 | 9.60 | 11.28 |
| 2 | 4.97 | 12.39 | 14.74 | 4.85 | 19.40 | 23.41 | 5.06 | 11.24 | 12.25 | 5.01 | 12.26 | 13.43 |
| 3 | 4.89 | 8.72 | 9.48 | 4.77 | 19.21 | 23.03 | 4.82 | 11.41 | 13.23 | 4.81 | 9.88 | 13.48 |
| 4 | 4.81 | 15.45 | 17.98 | 4.97 | 10.65 | 12.81 | 4.94 | 15.13 | 17.31 | 4.74 | 11.06 | 12.51 |
| 5 | 4.82 | 13.15 | 15.82 | 5.23 | 9.67 | 10.72 | 4.78 | 14.79 | 17.40 | 4.77 | 12.41 | 15.10 |
| 6 | 4.89 | 13.75 | 14.64 | 4.81 | 8.56 | 11.42 | 4.98 | 10.06 | 11.30 | 5.01 | 9.94 | 11.57 |
| 7 | 4.89 | 10.47 | 12.43 | 4.98 | 9.88 | 11.61 | 4.89 | 10.54 | 13.93 | 5.06 | 12.74 | 13.33 |
| 8 | 4.91 | 11.87 | 13.62 | 5.01 | 11.64 | 13.14 | 4.91 | 12.69 | 14.75 | 4.78 | 9.31 | 10.26 |
| 9 | 4.81 | 11.19 | 14.17 | 4.89 | 9.22 | 12.81 | 4.94 | 11.10 | 12.89 | 4.78 | 7.38 | 8.29 |

Table 3.1: *z-statistic thresholds for the phase-encoding digit representations.* Details of FDR *z*-statistic thresholds, *z*-statistic robust maxima (R.max) and *z*-statistic maxima for winner-takes-all digit phase-encoding digit representations. Maps for subjects 1-3 are shown in figure 3.11B/D/F. Maps for subjects 4-6 are shown in figure 3.12B/D/F.

| Block design digit representations | | | | | | | | | | | | |
|---|---|---|---|---|---|---|---|---|---|---|---|---|
| | Digit 2 | | | Digit 3 | | | Digit 4 | | | Digit 5 | | |
| Subject | *Threshold* | *R.Max* | *Max* | *Threshold* | *R.Max* | *Max* | *Threshold* | *R.Max* | *Max* | *Threshold* | *R.Max* | *Max* |
| 1 | 2.30 | 4.43 | 7.40 | 2.30 | 4.61 | 6.34 | 2.30 | 4.38 | 5.95 | 2.30 | 4.89 | 7.78 |
| 2 | 2.30 | 4.58 | 9.87 | 2.30 | 5.35 | 7.34 | 2.30 | 4.39 | 5.88 | 2.30 | 4.16 | 5.79 |
| 3 | 2.30 | 2.44 | 11.64 | 2.30 | 5.55 | 7.54 | 2.30 | 4.72 | 6.65 | 2.30 | 4.48 | 5.70 |
| 4 | 2.30 | 5.85 | 8.91 | 2.30 | 2.53 | 8.89 | 2.30 | 4.90 | 8.61 | 2.30 | 6.49 | 10.69 |
| 5 | 2.30 | 5.42 | 9.36 | 2.30 | 4.40 | 7.50 | 2.30 | 6.50 | 8.19 | 2.30 | 6.11 | 10.34 |
| 6 | 2.30 | 5.59 | 9.26 | 2.30 | 4.88 | 6.11 | 2.30 | 4.75 | 6.65 | 2.30 | 5.07 | 7.94 |
| 7 | 2.30 | 6.79 | 8.57 | 2.30 | 4.83 | 7.06 | 2.30 | 4.70 | 6.60 | 2.30 | 4.32 | 5.71 |
| 8 | 2.30 | 5.45 | 6.97 | 2.30 | 5.99 | 8.54 | 2.30 | 4.45 | 5.61 | 2.30 | 2.56 | 7.23 |
| 9 | 2.30 | 4.57 | 8.20 | 2.30 | 4.39 | 6.07 | 2.30 | 4.37 | 5.71 | 2.30 | 5.43 | 7.88 |

Table 3.2: *z-statistic thresholds for the block design digit representations.* Details of $z$-statistic thresholds, $z$-statistic robust maxima (R.max) and $z$-statistic maxima for digit representations derived from GLM analysis of the block-design data, contrasting a given digit to blocks representing other digits (for example, D2 > D3, D4, D5) . Maps for subjects 1-3 are shown in figure 3.11A/C/E. Maps for subjects 4-6 are shown in figure 3.12A/C/E.

| *Homologous pairing (Phase digit: GLM contrast)* | *Non-homologous pairing (Phase digit: GLM contrast)* | $t$ | *df* | Sig. ($p$ (2-tail) |
|---|---|---|---|---|
| Digit 2: Digit 2 > rest | Digit 2 : Digit 3 > rest | 9.561 | 8 | <.001 |
| | Digit 2 : Digit 4 > rest | 9.294 | 8 | <.001 |
| | Digit 2 : Digit 5 > rest | 8.376 | 8 | <.001 |
| Digit 3 : Digit 3 > rest | Digit 3 : Digit 2 > rest | 9.076 | 8 | <.001 |
| | Digit 3 : Digit 4 > rest | 5.184 | 8 | 0.01 |
| | Digit 3 : Digit 5 > rest | 7.133 | 8 | <.001 |
| Digit 4 : Digit 4 > rest | Digit 4 : Digit 2 > rest | 8.151 | 8 | <.001 |
| | Digit 4 : Digit 3 > rest | 6.644 | 8 | <.001 |
| | Digit 4 : Digit 5 > rest | 7.996 | 8 | <.001 |
| Digit 5 : Digit 5 > rest | Digit 5 : Digit 2 > rest | 7.020 | 8 | <.001 |
| | Digit 5 : Digit 3 > rest | 8.245 | 8 | <.001 |
| | Digit 5 : Digit 4 > rest | 5.855 | 8 | <.001 |

Table 3.3: *Comparison of phase-encoding and block task digit representations.* Results of post-hoc t-tests shown in figure 3.13 which demonstrate significant differences in beta values between homologous pairings of phase-encoding digit representations and digits contrasts from the block design GLM and non-homologous pairings. Bonferroni significance threshold $p$ <.0041.

## 3.4 Discussion

In this chapter I sought to map the representations of individual digits in the primary somatosensory cortex at the single-subject level using UHF fMRI at 7 tesla. More specifically, I aimed to develop a paradigm that would enable digit representations to be mapped rapidly, using non-specialist equipment, in a reproducible fashion across different scan sessions. The data presented in this chapter report the results of a phase-encoding paradigm, which produces a clear pattern of digit topography in the postcentral gyrus, around the anatomical hand knob (Figures 3.7 and 3.8), with under 10 minutes of BOLD fMRI data acquisition. The more novel phase-encoding maps spatially concur with maps derived from more traditional block design data acquired in the same subjects (Figure 3.13), though the latter maps show significantly less specificity for the anatomical hand knob (Figures 3.11 and 3.12). Finally these phase-encoding maps show a high degree of reproducibility within-subject, across session, with an inter-scan interval of up to four weeks (Figures 3.14 and 3.15). Taken together, these results suggest that the paradigm implemented in this chapter provides a rapid, robust and reproducible means of mapping digit representations in the primary somatosensory cortex at the single subject level.

### 3.4.1 Primary somatosensory cortex maps

Maps of digit topography from the phase-encoding analysis showed a clear and specific pattern of activation in the left post central gyrus at the characteristic point of the anatomical hand knob (Figure 3.7) (Yousry et al., 1997). All subjects show a consistent pattern of progression, from the lateral-most representation of digit 2, to the medial most representation of digit 5. However, the maps show qualitative differences in shape and orientation, in keeping with reports of inter-subject variability from the non-human primate literature (Merzenich et al., 1987).

The Brodmann areas that constitute the primary somatosensory cortex cannot be defined accurately from gross anatomy alone: any attempts to define the borders are

therefore an estimate. Broadly speaking, Brodmann area 3a falls in the nadir of the central sulcus, with a gradual progression to Brodmann area 3b on the posterior bank of the central sulcus, with Brodmann area 1 at the apex of the postcentral gyrus, and Brodmann area 2 at the nadir of the postcentral sulcus. Given these anatomical definitions, all subjects show a map consistent with the location of Brodmann area 3b (Figures 3.7 and 3.8), with some subjects displaying an additional more anterior map consistent with Brodmann area 3a, and some a more posterior map consistent with Brodmann area 1.

The presence of well-delineated maps in Brodmann area 3b is well described in microelectrode mapping studies of individual digits in non-human primates, representing input from low threshold cutaneous fine touch receptors (Kaas et al., 1979; Merzenich et al., 1987). Digit maps in Brodmann area 3a and 2 are less discrete (Pons and Kaas, 1986; Huffman and Krubitzer, 2001). As outlined in section 1.1.3.4, different Brodmann areas in the primary somatosensory cortex receive inputs from specific somesthetic submodalities. Brodmann area 3b, in which maps were consistently clear, receives input from slowly adapting cutaenous receptors, which might be more sensitive to a slow frequency stimulus, as was applied during the fMRI task. Brodmann area 3a receives input from muscle spindle afferents, which might have been stimulated by small movements performed in the scanner. In contrast, Brodmann area 1 and 2 respond to rapidly adapting cutaneous receptors and deep joint receptors respectively; the low frequency, small finger movements made in the scanner are unlikely to induce considerable response in these somesthetic submodalties, and it is therefore unsurprising that maps in these regions were not routinely observed.

### 3.4.2 Concurrence of maps from phase-encoding and block design tasks

As outlined in section 2.7.2.2, phase-encoding designs have been applied broadly in the field of retinotopic mapping. Given their relative novelty in other sensory mapping

modalities, I assessed the robustness of this mapping technique by comparing the maps derived using phase-encoding to an independently acquired and analysed block design task, acquired in the same subjects. Qualitatively, comparison of the two mapping techniques show a concordance in the pattern of digit representations around the postcentral gyrus in the anatomical hand knob (Figures 3.11 and 3.12). Statistical analysis found that the peak voxel of each phase-encoding digit representation showed a maximal block design derived beta value for the GLM contrast relevant to the digit in question (Figure 3.13). For example, the peak voxel from digit two phase-encoding masks showed a maximal beta value for the contrast D2 $>$ rest. Previous work in digit mapping has made comparisons between phase-encoding maps and event related design data, demonstrating both a qualitative and statistical agreement between the two techniques (Besle et al., 2013a). The agreement between the two mapping modalities provides compelling evidence this approach provides a useful means of resolving patterns of smooth topography in the primary somatosensory cortex.

### 3.4.3 Digit map reproducibility

fMRI is increasingly applied in settings where reproducibility is important: from complex longitudinal studies to the clinical setting (Bosnell et al., 2008; Gountouna et al., 2010; Kristo et al., 2014). At the single subject level, the BOLD signal affected by a number of different factors. These can range from the effects of caffeine (Behzadi and Liu, 2006) or sleep-deprivation (Chee and Choo, 2004), to more subtle variables such as attention level or motion in the scanner (Johansen-Berg et al., 2000). At UHF, hardware considerations are also a considerable potential source of inter-scan variability, from a difference in head position within the field to differing shim quality (Smith et al., 2005). Given the fine scale of the digit maps reported in this chapter, and the potential use of the mapping technique in studies of plasticity, inter-scan reproducibility is a major consideration. Qualitatively, the maps show a high degree of concordance across the four week interval under study here (Figure 3.14). Further statistical quantification of this reproducibility

showed a high degree of spatial cross-correlation within an anatomically defined ROI of Brodmann area 3b, an area in which all subjects showed a complete map (Figure 3.15A-C). The high degree of cross correlation seen for homologous digits provides reassuring evidence for the reproducibility of the mapping technique. The cross-correlation values between homologous digits were significantly greater than those of non-homologous digits (Figure 3.15D). This difference demonstrates that the high correlation values seen for homologous digits were not a general characteristic of the maps seen within the anatomically-defined ROI, but in fact affected by the digit maps involved in the correlation. The degree of reproducibility seen at the single-subject level across considerable periods of time provides encouraging evidence for the utility of the mapping paradigm presented in this chapter for use in studies of neuroplasticity.

### 3.4.4 Digit mapping paradigm

This study aimed to develop a paradigm to map robust and reproducible digit somatotopy in the primary somatosensory cortex using a rapid and easily implemented approach. As discussed in section 1.1.5.1, there have been considerable efforts to undertake such mapping, with evidence from multiple paradigms of the ability to resolve individual digit representations (Sanchez-Panchuelo et al., 2010; Stringer et al., 2014; Martuzzi et al., 2014). In designing the paradigm presented in this study, I sought to address a number of limitations seen in previous work, which could render digit mapping a more useful tool for further imaging studies.

Previous digit mapping studies have applied passive stimulation approaches with some kind of isolated tactile stimulation, whether in the form of air puffs (Stringer et al., 2014), piezoelectric stimuli (Sanchez-Panchuelo et al., 2010; Besle et al., 2013a) or manually delivered passive stimulation (Martuzzi et al., 2014). Passive stimulation techniques offer greater uniformity in stimulus intensity and duration, however, they necessitate a greater number of scan repeats or long runs of fMRI acquisition to

produce maps of all digits. Furthermore, such passive stimulation approaches typically only activate a subset of the peripheral receptors in the hand, which is a sharp contrast to typical sensory stimulation of multiple receptor subtypes concurrently when paired with movement. By adopting an active motor task in the paradigm presented in this chapter, not only was it possible to resolve maps with under ten minutes of fMRI acquisition, but furthermore, the stimulation was more naturalistic and representative of sensory experiences during hand use.

The logistical considerations for this paradigm also differ considerably from previous work. An active button press task does not require any specialist or expensive MRI-compatible equipment. The task can be performed with simple visual instructions, and the ten minute scan to achieve maps of four digits renders it a useful adjunct in other multimodal studies of the sensorimotor system, where somatotopic mapping is not the primary goal of the study. This consideration is especially relevant in patient studies, where long scan duration will limit compliance, and potentially increase the incidence of motion artefact.

Finally, this paradigm shows a high degree of spatial specificity over both a shorter period or 24 hours, and a longer period of four weeks. While other work has quantified reproducibility based on peak voxel measures (Martuzzi et al., 2014), the data presented in this chapter demonstrate a high degree of concordance in the spatial distribution of the digit maps across time. A combination of the easily-implemented setup, short scan duration and reproducibility of the resulting maps renders the digit mapping paradigm a valuable tool, which could be applied broadly in the study of the human sensorimotor system.

## 3.5 Conclusions

The study presented in this chapter demonstrates an easily implemented, rapid means of mapping digit topography in the primary somatosensory cortex at the single

subject level. This phase-encoding paradigm shows a high concordance with the more traditional block designs applied previously, but shows greater specificity in resolving the smooth topography present in the sensory regions of the anatomical hand knob. The maps show a high degree of spatial reproducibility in both the short and long term. This paradigm provides a valuable and practical means to map digit topography in single subjects, both in longitudinal studies of neuroplasticity, as well as in clinical studies involving patient populations.

# 4 | Mapping short-term experience-dependent plasticity in digit somatotopy

*As discussed in Chapter 1, non-human primate studies of experience-dependent plasticity have demonstrated that peripheral manipulations, which alter sensory afferent and motor efferent activity, can drive changes in somatotopic maps in the primary somatosensory cortex. The work presented in Chapter 3 reports a rapid and reproducible means of mapping digit somatotopy in the primary somatosensory cortex with fMRI at 7.0 tesla. In this chapter, I present a continuation of the study presented in Chapter 3, considering the longitudinal changes in digit topography in the primary somatosensory cortex induced by a manipulation in which participants have the index and middle fingers of their right hand glued together for a period of 24 hours.*

## 4.1 Introduction and rationale

As outlined in sections 1.1.5.1 and 1.1.6, the hand is a special case in the context of the sensorimotor network. Firstly, it exhibits a highly exaggerated cortical representation in both the primary motor cortex and the primary somatosensory cortex relative to its actual size. Further, the hand embodies a unique interplay between sensory and motor function, to yield the dexterity upon which we are reliant in day-to-day life. As discussed in section 1.4, the rich afferent and efferent connections of the sensorimotor network have the propensity to drive considerable plastic change therein.

Studies in non-human primates have provided evidence for remapping in the hand representations of both the primary motor cortex and the primary somatosensory cortex, in the context of both activity-dependent and experience-dependent plasticity (Merzenich et al., 1983; Merzenich et al., 1984; Allard et al., 1991; Zarzecki et al., 1993). In the latter case, the potential for remapping in some usage-dependent fashion raises a fundamental question as to the driving-forces behind brain organisation. These studies show that beyond crude insults such as deafferentation or amputation, there is a potential for subtle behavioural changes in the use of the hand to drive central adaptive reorganisation. In the context of the sensory system, such adaptive remapping has been shown over a period of months (Allard et al., 1991; Zarzecki et al., 1993), whereas in the motor system, experience-dependent reorganisation has been shown more rapidly (Nudo et al., 1996). In the context of the somatosensory system, it has been argued that such remapping stems from network level changes and a process of unmasking existing anatomic connections which leads to a shift in the local excitatory/inhibitory balance, and a change in receptive field organisation (Doetsch et al., 1988b; Doetsch et al., 1988a; Doetsch et al., 1992).

The potential for such short-term remapping in sensorimotor network has not been fully investigated in the human brain. Data from the non-human primate literature would suggest that changes in coincident sensory input and alterations in the synergistic use of muscle groups may drive central remapping.

In this study, I sought to build upon the data presented in Chapter 3, using the paradigm developed to map digit topography in the primary somatosensory cortex with fMRI to investigate the potential for short-term experience-dependent plasticity in these maps. I undertook an experiment considering the longitudinal changes in digit topography in the primary somatosensory cortex induced by a manipulation in which participants had the index and middle fingers of their right hand glued together for a period of 24 hours.

## 4.2 Methods

### 4.2.1 Participants

Thirteen healthy control participants [Mean age: 27.2 ± 5.81; five female] were recruited in accordance with local central university research ethics committee approval (University of Oxford MSD-IDREC-C2-2013-05) as an extension to the study presented in Chapter 3. All participants were right handed according to the Edinburgh Handedness Inventory (Oldfield, 1971).

### 4.2.2 Experimental design

The data discussed in the current study were acquired as a part of a larger project summarised in figure 4.1, and referred to in Chapter 3. Participants attended four scan sessions in total: two sets of two scans, each separated by 24 hours. Between two of the scans (control 0 and control 1) was a control period in which subjects did not experience any manipulation. Between the remaining two scans (control 2 and glued) was a glued manipulation. During the glued condition, the right index and right middle digit of each subject were attached using a surgical grade cyanoacrylate skin glue (Derma+flex, Chemence Medical Products Inc., Alpharetta, GA, USA), applied to the lateral aspects of the fingers, leaving the finger tips and pads of the digits exposed. The order in which the participants undertook the control and glued condition was counterbalanced across the group.

The control 1, control 2, and glued scans were used for analysis (Figure 4.1). Control 0, the first scan all subjects undertook, was treated as an habituation scan, to allow participants to get used to the magnet and the scan task. In analysis, there were therefore two control scans, which followed a period of normal hand use, and a glued scan, which followed a 24 period of the gluing manipulation described above.

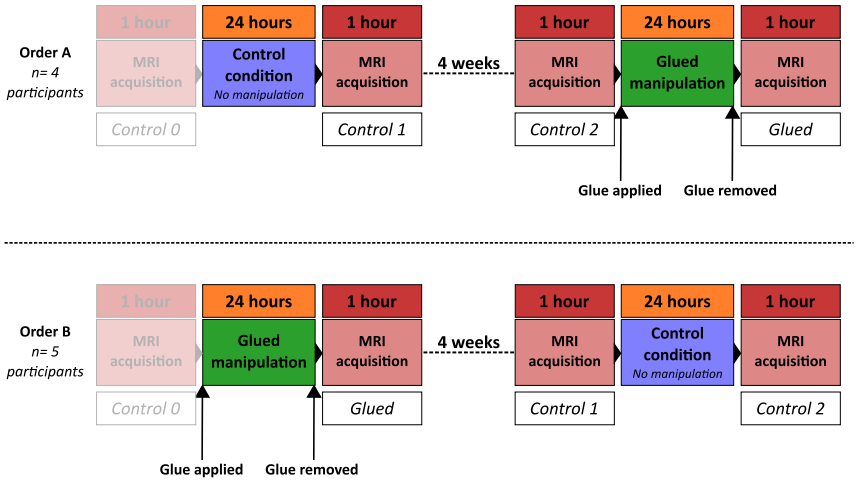


Figure 4.1: *Overview of digit plasticity study design.* Participants attended four scan sessions in total. Two scan sessions were separated by a 24 hour control period in which no manipulation was used. An additional two scans were acquired, separated by a period of 24 hours of glued manipulation, in which the index and middle fingers of the right hand were glued together. The order of the control and glued conditions was counterbalanced across the groups: order A/B. The scans not considered in this chapter are denoted by increased transparency.

### 4.2.3 MRI acquisition

fMRI data were acquired using a Siemens 7T Magnetom system and a 32-channel head coil. Full details of the imaging acquisition parameters are outlined in section 3.2.3.

### 4.2.4 Topographic mapping task

As described in Chapter 3, participants performed a series of tasks involving visually-cued movements of individual digits in the scanner: digit 2 (D2: index finger), digit 3 (D3: middle finger), digit 4 (D4: ring finger) and digit 5 (D5: little finger). During the three minute functional localiser scan, subjects were instructed to appose their right thumb and each of the digits of their right hand sequentially during 15 second movement blocks, contrasted with equivalent periods of rest.

All subsequent task fMRI data followed the phase-encoding design task outlined in section 3.2.4. Briefly, this involved continuous button presses at a rate of 1Hz with

no rest periods. The phase forward task cycled through D2-D5: 8 seconds of button presses at 1Hz per digit (i.e. D2 x 8, D3 x 8, D4 x 8, D5 x 8, D2 x 8 ...). The phase backward task cycled through D5-D2. In both the phase forward and backward tasks, each cycle through the digits was repeated eight times.

### 4.2.5 MRI analysis

Image preprocessing and registration were undertaken using the methods outlined in sections 3.2.5.1 and 3.2.5.2. Phase-encoding data were analysed using a cross-correlation approach detailed in section 3.2.5.3. The preprocessed BOLD EPI data were correlated against a reference model as a function of time lag, in units of TR. The model was composed of a gamma HRF convolved boxcar: 8 second 'on' and 24 second 'off', repeated eight times, mirroring the eight cycles of the phase forward and phase backward tasks. A correlation was calculated between the raw BOLD signal of each voxel and the reference model for each lag. Each lag shifted the reference model by one TR (1.5s), with sufficient lags to cover one 32 second cycle through D2-D5 or D5-D2. Each lag was assigned to a given digit in the cycle, taking into account the haemodynamic delay with a time to peak of 4.5 seconds. The lags corresponding to a given digit in both the phase forward and phase backward tasks were resampled to the single volume partial FOV high-saturation EPI space (spline interpolation) and averaged to give one $r$-value map per digit.

These soft-edged maps were not processed using a winner-takes-all approach. Instead the overlap between the individual digit maps was retained. These soft-edged maps were converted into a corresponding $z$-statistic on the basis of the distribution of values within the brain tissues of the FOV for which BOLD EPI data were acquired. $z$-statistic maps were converted to uncorrected p-values using fslmaths. Individual digit maps were thresholded using FDR to determine a corrected p-value threshold on the basis of the observed p-value distribution within the data ($\alpha = 0.001$) (Genovese et al., 2002).

#### 4.2.5.1 Surface projection and profile plots

Soft-edged digit maps were projected onto two-dimensional cortical surface reconstructions, as outlined in section 3.2.5.5. The inflated cortical surface, and sulcal pattern of each participant was used to manually define the axis of Brodmann area 3b along the length of the central sulcus using FreeSurfer segmentations (Figure 4.2) in Connectome Workbench (Marcus et al., 2011). As discussed in section 3.4.1, any definitions of the Brodmann areas from gross anatomy are an estimate. Brodmann area 3b is well described to broadly follow the posterior bank of the central sulcus. Manual definitions of the axis of the central suclus along Brodmann area 3b followed the midline of the probabilistically thresholded area 3b segmentation from FreeSurfer in order to maximise the likelihood of a true area 3b ROI. The axis of the central sulcus along Brodmann area 3b was used to further collapse the digit map data from two-dimensions into one dimension: the dorsal-ventral axis of the central sulcus. Using in-house Matlab scripts, the average value of each soft-edged digit map was taken at each z-coordinate down the axis of the central sulcus, to produce a profile plot of the *z*-statistics of each digit map (Figure 4.3). The profile plot for each digit was processed with robust local regression smoothing using weighted linear least squares and a 2nd degree polynomial model, which down-weights statistical outliers (Span: 15% of data points). Smoothed digit profile plots were then filtered to retain the single largest positive peak, representing the maximal *z*-statistic activation down the axis of the central sulcus, corresponding to Brodmann area 3b.

#### 4.2.5.2 Overlap measures and statistics

The cross-sectional area of the overlap between each pair of adjacent digits (Figure 4.3A) and the overall area of each digit representation (Figure 4.3B) were calculated using trapezoidal numerical integration. Overlap values were normalised by the sum of the overall area of the two contributing digit plots.

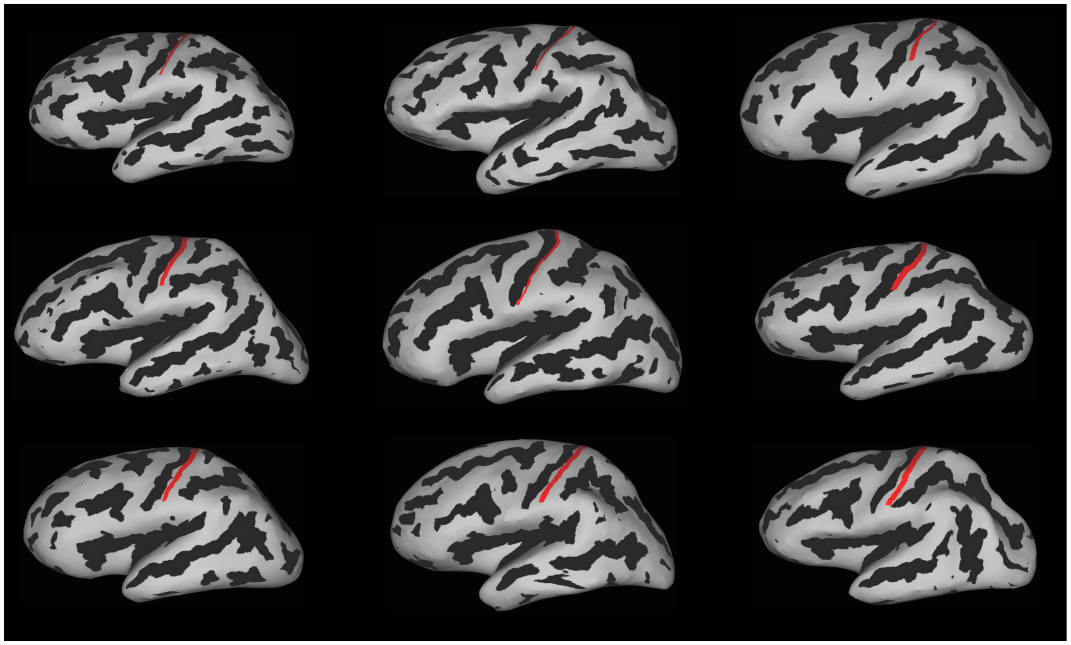

Figure 4.2: *Brodmann area 3b axes along the central sulcus.* Axes of Brodmann area 3b defined manually in single subjects using FreeSurfer segmentations. These axes were used for analysis at all time points to produce digit profile plots down the central sulcus.

In the longitudinal analysis, the control 0 time point was used as an habituation session to acclimatise subjects to the task and scanner. All inter-session intra-subject comparison therefore considers only the control 1, control 2 and glued scans (Figure 4.1).

Profile plot data processing was undertaken in Matlab (Version 2012a, Mathworks, Natick, MA, USA). All statistical analysis and graphing were undertaken using JMP (Version 11.0, SAS Institute, Cary, NC, USA) and Statistics Package for the Social Sciences (Version 19.0, IBM Corporation, Armork, NY, USA).

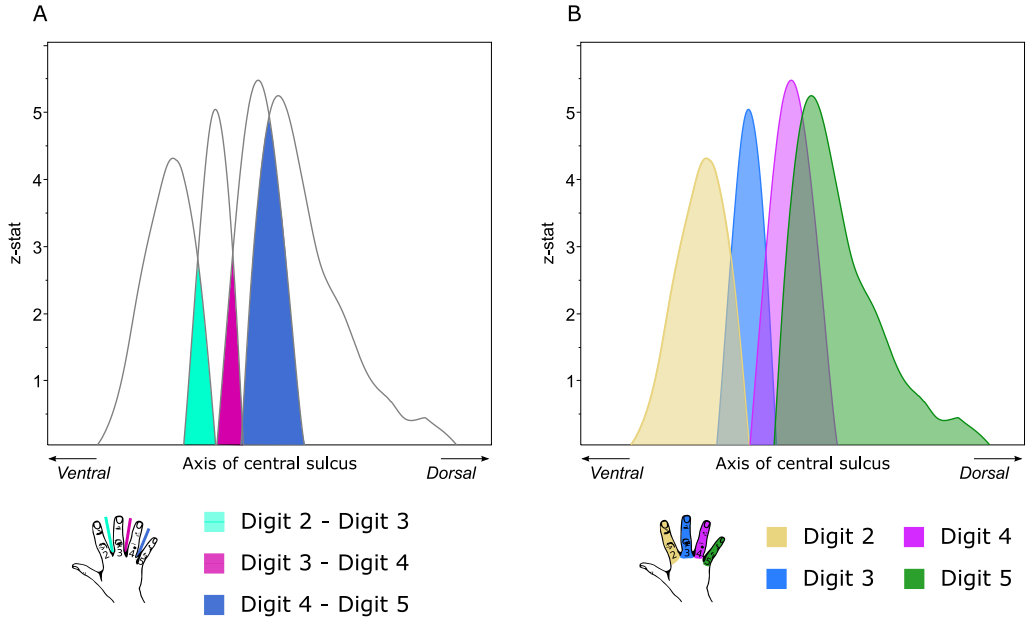


Figure 4.3: *Digit profile plots: overlap metrics.* Smoothed and filtered profile plots were used to calculate the overlap between adjacent digits (A), and the overall area of each digit representation (B). All metrics were calculated using trapezoidal numerical integration. Example profile plot from single subject and time point shown for illustration purposes.

## 4.3 Results

Data from three subjects exhibited visible spin history motion artefact as a result of sharp motion during one or more scan sessions (>1mm absolute mean displacement in < five volumes); these participants were excluded. One further subject was excluded on the grounds of an incidental finding. Nine subjects were considered in further analysis [Mean age: 27.5 ± 6.40; five female].

### 4.3.1 Digit profile plots of in Brodmann area 3b

The digit profile plots produced by further flattening the surface data into one dimension show a clearly ordered set of peaks along the axis of the central sulcus (Figure 4.4). There are clear peaks for digits two, three, four and five, progressing in a ventral to dorsal direction along the central sulcus. Quantification of the normalised digit overlap for adjacent digits shows a clear difference in the degree of overlap between the different digit pairings, with the smallest overlap between digits two and three, and the greatest overlap between digits four and five (Figure 4.5). This difference was quantified with a repeated measures ANOVA, with one factor of digit pair (D2-D3, D3-D4, D4-D5) and a dependent variable of normalised digit overlap. There was a significant main effect of digit pairing on normalised digit overlap, $F(2,16) = 21.81$, $p < 0.001$, $\eta = 0.732$. Post-hoc paired samples $t$-tests demonstrated significant differences in normalised digit overlap between the three pairings (Figure 4.5, all $p$ <0.05.)

### 4.3.2 The gluing manipulation and digit overlap

Normalised overlap between adjacent digits was compared across the control 1, control 2 and glued scans (Figure 4.1). A repeated measures ANOVA was performed with one factor of condition (control 1, control 2, glued) and one factor of digit pair (D2-D3, D3-D4, D4-D5), and a dependent variable of normalised digit overlap. There was a

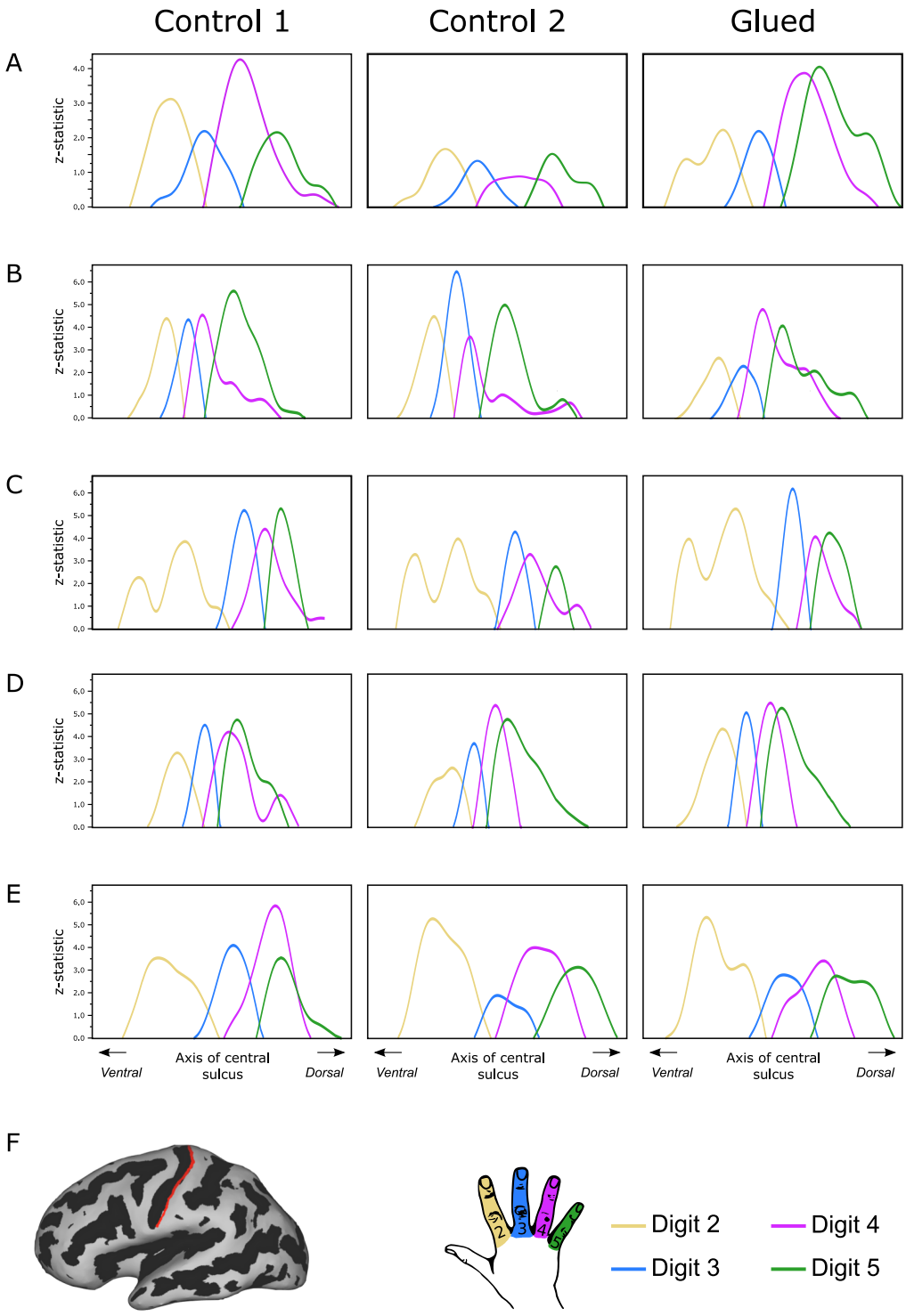


Figure 4.4: *Example digit profile plots across individual subjects and sessions.* Individual profile plots show *z*-statistic maps for each digit representation collapsed along the axis of the central sulcus (F). Data shown for five example subjects (A-E), across the three conditions analysed: control 1, control 2 and glued.

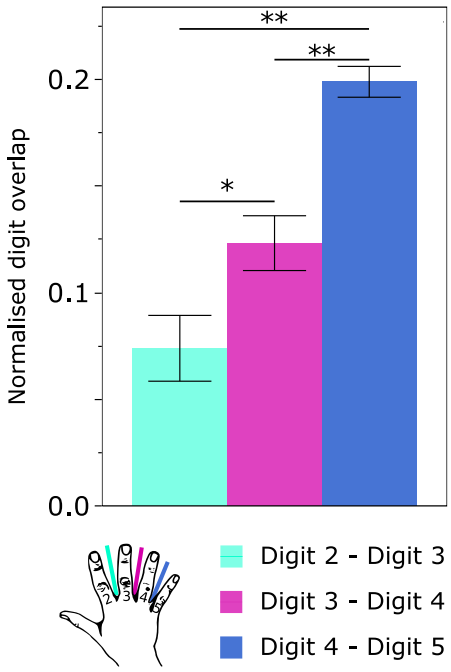


Figure 4.5: *Average overlap between adjacent digits.* Data presented represent the average normalised digit overlap from the control 1 and control 2 scans. n=9; error bars display the standard error of the mean. A repeated measures ANOVA with one factor of digit pair (D2-D3, D3-D4, D4-D5) and a dependent variable of normalised digit overlap showed significant main effect of digit pairing on normalised digit overlap, $F(2,16) = 21.81$, $p < 0.001$, $\eta = 0.732$. Post-hoc paired samples $t$-tests showed significant differences between all three digit pairings: D2-D3/D3-D4: $t(8) = 2.16$, $p = 0.03$; D3-D4/D4-D5: $t(8) = 3.83$, $p = 0.005$; D2-D3/D4-D5: $t(8) = 8.35$, $p < 0.001$. *:$p < 0.05$, **:$p < 0.01$.

significant interaction between condition and digit pair on normalised digit overlap, $F(4,32) = 7.96$, $p < 0.001$, $\eta = 0.499$. Post-hoc paired samples $t$-tests demonstrated significant differences in the overlap of digit three and digit four, and digit four and digit five when comparing the glued condition to the control 1 and control 2 conditions (Figure 4.6). The gluing manipulation induced a reduction in the overlap of digits 3 (middle) and 4 (ring), and an increase in the overlap of digits 4 (ring) and 5 (little). These changes were not seen across the equivalent control scans.

Further repeated measures ANOVAs were performed to assess for an interaction between condition and digit on the profile-plot defined area or peak $z$-statistic (Figure 4.3). There was no such interaction, suggesting that there was no significant difference in the profile plot defined area or peak $z$-statistic of each digit representation over the three sessions under study: all $p > 0.05$ (Figures 4.7 and 4.8).

| Digit overlap | Comparison | $t$ | $df$ | $p$ |
|---|---|---|---|---|
| Digit 3:Digit 4 | Glued vs. Control 1 | 3.064 | 8 | 0.0155 |
| | Glued vs. Control 2 | 2.360 | 8 | 0.0460 |
| Digit 4:Digit 5 | Glued vs. Control 1 | -3.996 | 8 | 0.0040 |
| | Glued vs. Control 2 | -3.489 | 8 | 0.0080 |

Table 4.1: *The gluing manipulation and overlap between adjacent digits: post-hoc paired samples t-tests.* Results of post-hoc paired samples $t$-tests shown in figure 4.6.

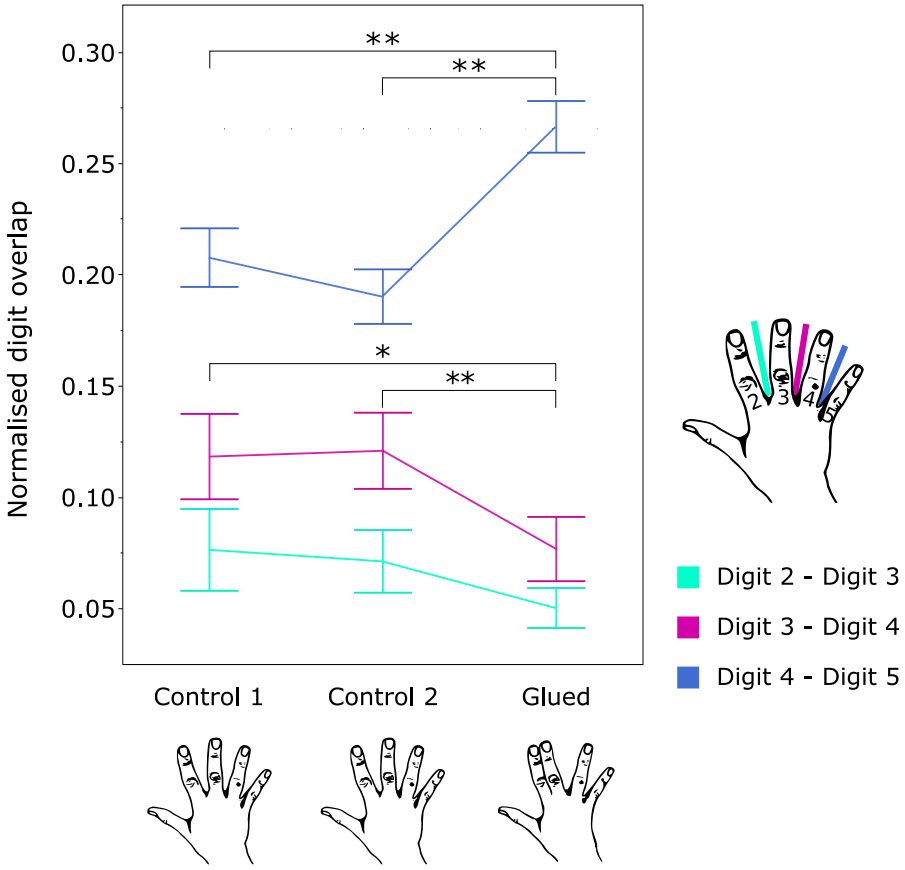


Figure 4.6: *The gluing manipulation causes changes in the overlap between adjacent digit representations.* Comparison of normalised overlap between adjacent digits demonstrates a significant increase in D4/D5 overlap, and a significant reduction in D3/D4 overlap, in response to the glued manipulation. RM ANOVA: significant interaction between condition and digit overlap: $F(4,32) = 7.96$, $p < 0.001$, $\eta = 0.499$. Post-hoc paired samples $t$-tests presented in table 4.1. *:$p$ <0.05, **:$p$ <0.01. The order of the conditions is counterbalanced across participants.

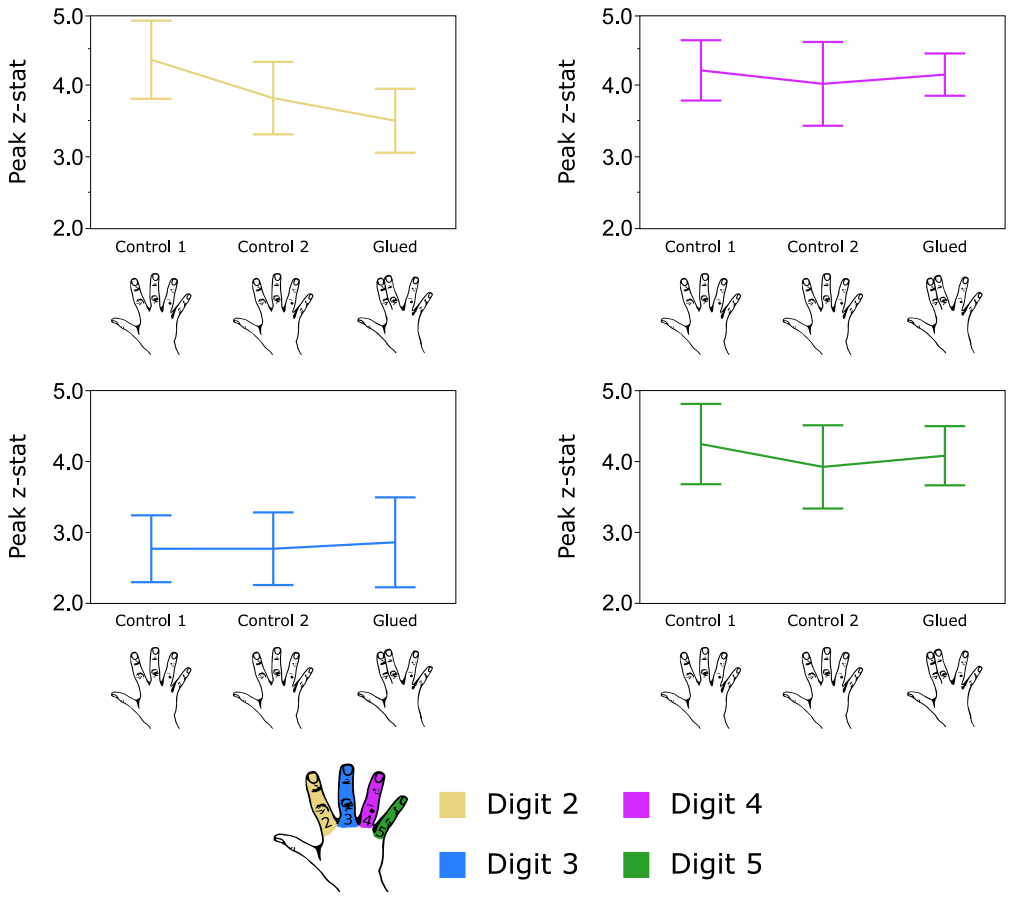


Figure 4.7: *The gluing manipulation does not affect the peak z-statistic of each digit.* No significant difference was observed in the profile plot peak $z$-statistic across the sessions under study.

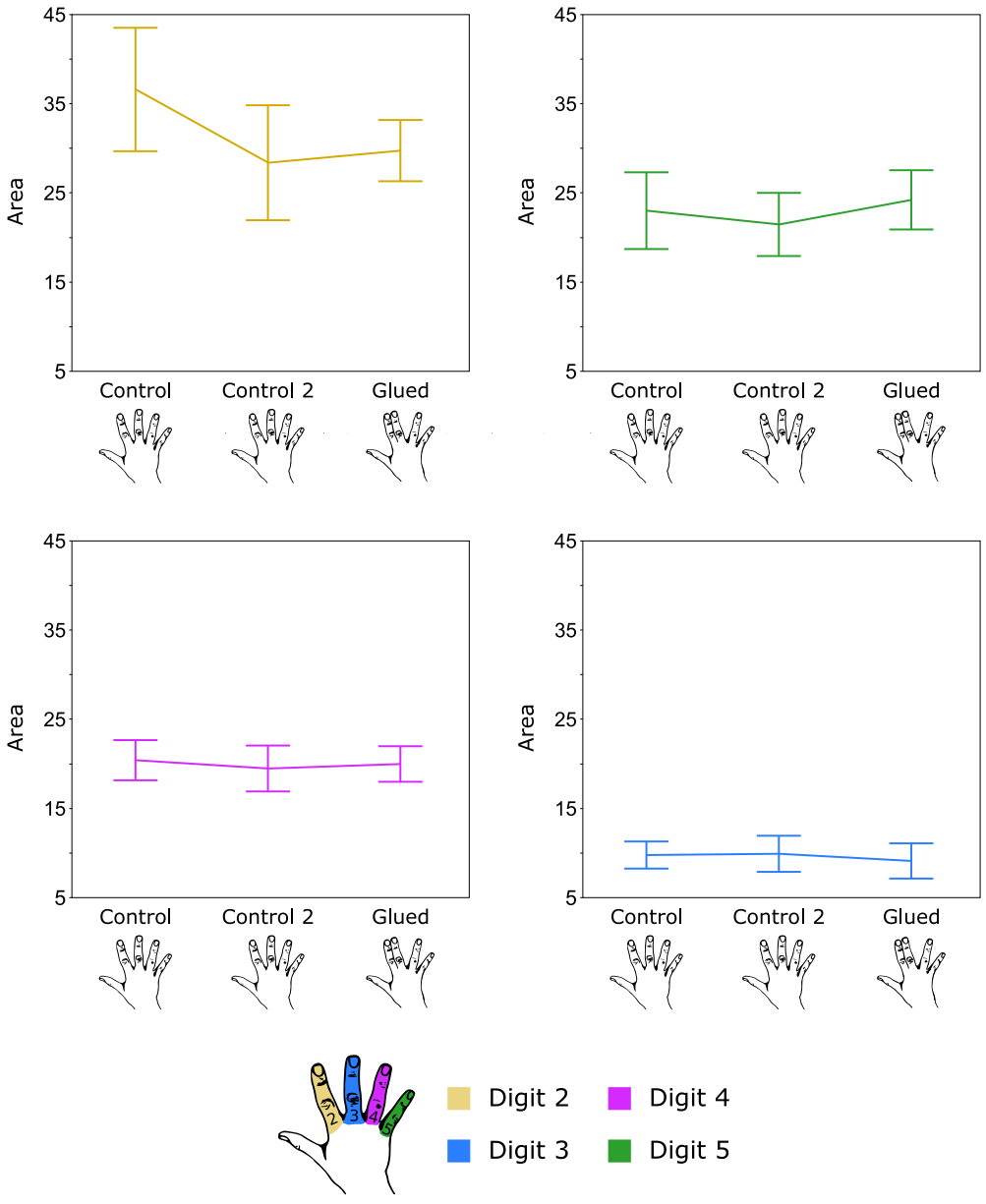


Figure 4.8: *The gluing manipulation does not affect the area of each digit profile.* No significance difference was observed in the profile plot area of each digit representation across the sessions under study.

## 4.4 Discussion

In this study I sought to investigate the potential for short-term experience-dependent plasticity in the topographic representations of individual digits in the primary somatosensory cortex. More specifically I used the fMRI digit mapping paradigm presented in Chapter 3 to investigate the topographic effects of a peripheral manipulation in which two digits of the subjects' right hand were glued together for a period of 24 hours. The data presented in this chapter demonstrate a marked shift in the cortical overlap of adjacent digits after the glued manipulation, which was not seen across the control condition. Specifically, gluing together digit two (index finger) and digit three (middle finger) induced a reduction in the cortical overlap of the digit three (middle finger) and digit four (ring finger) representations, and an increase in the cortical overlap of the digit four and digit five (little finger) representations. No change was seen in the overlap between the glued digit representations (digits two and three). These data demonstrate the propensity for functional reorganisation of fine-grain primary somatosensory cortex topography over a period of just 24 hours in response to a manipulation affecting sensorimotor function in the hand. This finding provides a fundamental insight into the nature of cortical plasticity, demonstrating a potential for a short-term experience-dependent change in the sensory representation of the digits.

### 4.4.1 Remapping and plasticity

The phenomenon of adjustment or remapping in fine-grain somatosensory topographic maps has been described previously in the non-human primate literature. Work from Merzenich's group has demonstrated that following a period of surgically-induced syndactyly (fusing of the digits), microelectrode mapping reveals the emergence of cortical somatosensory receptive fields responsive to both of the fused digits (Allard et al., 1991). Further work from Zarzecki and colleagues assessed a similar phenomenon in the primary somatosensory cortex of the raccoon (Zarzecki et al., 1993). This study

measured the frequency of corticocortical and somatosensory excitatory postsynaptic potentials (EPSP) across the cortical digit representations in response to stimulation of different digits. At baseline they reported that 20% of cells within a given digit representation respond to both the digit in question as well as its adjacent digits; after a period of surgically-induced syndactyly this figure rose to around 85%. In contrast to these studies, work assessing somatosensory digit maps in human subjects after the surgical release of congenital syndactyly has demonstrated a marked reduction in digit overlap, and the development of more organised representations of individual digits (Mogilner et al., 1993). Merzenich remarks that despite the inter-subject variability in digit maps, the degree of overlap in receptive fields across digits representations at baseline shows considerable consistency (Merzenich et al., 1987). He argues that this consistency is founded in "the maintenance of overlap ... controlled by temporal synchronisation or sequencing of inputs" (Merzenich et al., 1983; Merzenich et al., 1984; Merzenich et al., 1987). Reports of long-term experiments assessing the effects of surgically-induced syndactyly argue that the intervention modifies the temporal structure of afferent inputs, such that the attached digits experience greater coincident sensory inputs as they are forced to function together (Allard et al., 1991). Changes in afferent inputs may result from both altered use of the manipulated digits, as well as adaptive behaviour involving other digits or body parts (Florence and Kaas, 1995). The work of Merzenich and colleagues has focused on the effects of surgically-induced syndactyly on the representations of the fused digits; other work suggests evidence for off-target changes in digits adjacent to those involved in the manipulation (Allard et al., 1991; Zarzecki et al., 1993). In fact, EPSP recordings from Zarzecki and colleagues provide evidence for marked off-target changes in cortical responses to stimulation of digits unaffected by the syndactyly intervention (Zarzecki et al., 1993).

In the present study, we report an off-target remapping effect of the short-term glued intervention on remapping of digit representations in the primary somatosensory cortex. The glued intervention involved the attachment of digit two (index finger)

and digit three (middle finger) on the right hand, inducing a short-term artificial form of the syndactyly discussed above for a period of 24 hours. The attachment of digit two and digit three prompted a short term remapping, resulting in a reduction in the overlap between digit three (middle finger) and digit four (ring finger), and an increase in the overlap between digit four (ring finger) and digit five (little finger). This change in the overlap of cortical digit representations following artificial syndactyly is in keeping with reports from studies of long-term interventions in non-human primates reporting off-target effects (Allard et al., 1991; Zarzecki et al., 1993). However, in contrast to studies in non-human primates reporting effects on the attached digits (Allard et al., 1991; Zarzecki et al., 1993), no changes in the overlap of digit two and digit three, the glued digits, was found here. Therefore, in this very short-term study the changes in overlap were off-target, manifesting in digit pairs not directly affected by the gluing intervention.

In the context of evidence for both on-target and off-target effects of induced syndactyly from the non-human primate literature, I hypothesise that the short-term remapping reported in the current study reflects changes in the sensorimotor function of the hand, which drive changes in other digit representations in the short term. The gluing intervention attaches digits two and three of the right hand: this will prompt an increased physical separation of digit three and four, which are typically anatomically enslaved by one another (Li et al., 2004; Kim et al., 2008), freeing digit four to function more synergistically with digit five. This is in keeping with the observed phenomenon of reduced shared cortical representation between digit three and digit four, and an increased in shared representation of digit four and digit five. Further, I argue that the mechanisms underpinning the changes reported in this study are likely distinct from those seen following longer-term manipulations in non-human primates. Evidence for distinct short-term and long-term mechanisms of topographic remapping is discussed below.

### 4.4.2 Neural mechanisms of remapping

Early evidence for short-term remapping came from studies of denervation, which revealed rapid shifts in cortical maps immediately after the nerve was cut (Merzenich et al., 1983). Such immediate and dramatic changes were beyond the timeframe of synaptic plasticity or axonal sprouting. It is now apparent that denervation unmasked and potentiated existing silent or weak connections via horizontal intracortical fibres between different regions of the primary somatosensory cortex (DeFelipe et al., 1986). Further relevance for the role of intracortical connections in remapping phenomena came from the observation that intracortical microstimulation (ICMS) can increase receptive field size in the primary somatosensory cortex of non-human primates (Recanzone et al., 1992). It seems that the extent of short-term expansion in the cortical representation of a given body part may be constrained by the anatomy of horizontal intracortical connectivity, with greater local connectivity associated with greater short-term plasticity (Huntley, 1997). The dependence upon pre-existing intracortical connections is thought to underpin the cortical distance limit of 1.0-1.5mm: the maximum distance of representation shifts seen in the very short term.

In the medium term, mechanisms of remapping are thought to be underpinned by the uncovering or potentiation of divergent connections. Thalamocortical connections projecting to regions of the primary somatosensory cortex that are somatotopically inappropriate have also been reported (Snow et al., 1988; Waldron et al., 1989; Jones, 1996). Such divergence in thalamocortical projections from individual neurons or adjacent regions of the thalamus have the potential to be unmasked and drive rapid reorganisation in cortical maps. In the longer term, it is thought that the pre-existing silent connections supporting remapping are reinforced by sprouting of new connections (Darian-Smith and Gilbert, 1994; Florence et al., 1998).

### 4.4.3 Excitatory and inhibitory balance and remapping

The inhibitory neurotransmitter gamma-aminobutyric acid (GABA) has been implicated in remapping at the cortical level. The application of bicuculline, a $GABA_A$ receptor antagonist, causes an increase in local receptive field size (Alloway and Burton, 1986; Alloway and Burton, 1991), resulting in the hypothesis that reduced inhibition is partly responsible for the rapid remapping phenomena observed in denervation or amputation studies. Changes in GABAergic signalling have also been observed in the dorsal column nuclei (Schwark et al., 1999) and thalamus (Hicks et al., 1986). Excitatory glutamatergic signalling is also thought to play a role in remapping phenomena, with reports of long term NMDA receptor anatagonist pre-treatment negating rapid remapping and expansion of somatotopic representations after median nerve transection in non-human primates (Garraghty and Muja, 1996). It has been argued that changes in excitatory/inhibitory balance play a key role in the plastic response, but might function at the level of single cells, rather than reflecting a broad chemical change in the cortical milieu (Jones, 2000).

### 4.4.4 Remapping in context

Remapping or alterations in digit topography have been widely reported in focal hand dystonia: a condition characterised by muscle weakness and fatigue in the hand, leading to reduced precision and dexterity (Torres-Russotto and Perlmutter, 2008). This dystonia encompass conditions known as writer's cramp and musician's cramp (Breakefield et al., 2008). Focal hand dystonia has been investigated in group fMRI studies, with strong evidence for somatotopic reorganisation or blurring of cortical representations (Elbert et al., 1998; Bara-Jimenez et al., 1998; Meunier et al., 2001; McKenzie et al., 2003; Granert et al., 2011). The observation that short-term reorganisation can occur over the course of 24 hours raises further questions as to the driving force behind dystonia associated remapping, and argues for the potential investigation of targeted rapid-interventions in dystonia to negate or limit maladaptive

remapping processes which occur in this state. In the stroke literature, fMRI data have argued for the adaptive remapping of the entire hand knob region to a more posterior cortical region in response to ischaemic damage (Pineiro et al., 2001). Given the propensity for short-term remapping of the hand representation shown in this study, and evidence of plastic remapping of the entire sensorimotor hand representation after stroke, the question of post-stroke remapping of digit representations is of potential interest. Only 38% of stroke survivors receiving rehabilitation recover functional dexterity in their hand (Kwakkel et al., 2003). Understanding the extent of remapping and topographic organisation within the reorganised area post-stroke could provide a potential insight into the differences between those individuals who regain manual dexterity after stroke, and those who do not.

## 4.5 Conclusions

The study presented in this chapter investigated the potential for short-term experience-dependent plasticity in the topographic representations of individual digits in the primary somatosensory cortex. The data presented herein demonstrate the propensity for functional reorganisation of fine-grain primary somatosensory cortex topography over a period of just 24 hours in response to a manipulation involving the gluing of the right index and right middle fingers. This finding provides an interesting insight into the nature of short-term cortical plasticity, demonstrating the potential for topographic change in response to a peripheral manipulation, as reported previously over longer periods in non-human primates. The work raises further questions in patient populations where topographic digit representations may occur, both in a maladaptive sense in ageing or focal hand dystonia, and a more adaptive sense in chronic stroke patients.

# 5 | Investigating maladaptive plasticity associated with chronic disuse of the upper limb

*The studies presented in the previous chapters of this thesis have investigated the fine-grain organisation of the sensorimotor network, and the propensity for short-term experience-dependent plasticity therein. In this chapter, I consider the potential for usage-dependent plasticity in the long-term in patients with chronic disuse of the upper limb following massive irreparable rotator cuff tear. The work presented here was undertaken in collaboration with Torbay Hospital, where the data were acquired. This chapter outlines a cross-sectional study comparing patients to control subjects in order to investigate plasticity associated with chronic upper limb disuse.*

## 5.1 Introduction and rationale

As discussed in section 1.4.2, data from the non-human primate literature shows the potential for considerable remapping of the primary somatosensory and motor cortex in response to peripheral deafferentation or amputation (Merzenich et al., 1983; Merzenich et al., 1984). Beyond these experimental interventions, such activity-dependent plasticity is also relevant in the context of neurorehabilitation and motor disuse. Immobilisation of a limb has both behavioural and neural consequences that persist beyond the period of disuse (Roll et al., 2012). Behavioural studies have demonstrated a persisting deficit in the ability to make anticipatory postural

adjustments involving the arm and shoulder after just 12 hours of wrist and finger splinting (Bolzoni et al., 2012). Further work has shown the potential for short-term structural reorganisation following disuse associated with both orthopaedic injury and writer's cramp, with evidence of changes in the contralateral primary sensorimotor cortex, contralateral corticospinal tract and right superior temporal gyrus (Granert et al., 2011; Langer et al., 2012). However, it remains unclear to what extent these short-term neuroplastic phenomena progress in the context of long-term motor immobilisation or disuse over the course of years.

Massive irreparable rotator cuff tear (MIRCT) is a chronic upper-limb musculoskeletal condition predominantly affecting the older population (Clement et al., 2012). The rotator cuff is a group of four muscles in the shoulder girdle, which function to stabilise the head of the glenohumeral joint during shoulder movement, controlling the translation of the humeral head in the relatively shallow glenoid fossa (Figure 5.1). A "rotator cuff tear" refers to a tear in one of the tendons of these four shoulder muscles. Full thickness tears are one of the most common causes of shoulder pain and disability (Bunker, 2002). Surgically irreparable tears can frequently present in older patients with no history of acute trauma, often with progressive degeneration and dysfunction of the muscle involved. They are commonly associated with atrophy and myotendinous retraction, as well as fatty infiltration of the muscle (Neri et al., 2009; Khair and Gulotta, 2011; Delaney et al., 2012). In the case of massive tears (greater than 5cm), the degree of retraction and size of tear frequently make a surgical intervention unfeasible. Patients with MIRCT experience considerable motor deficits in the affected upper limb during tasks requiring active shoulder stabilisation. However, there is a sparing of fine dextrous movements in the hand, which do not typically require rotator cuff contraction. Such a trauma therefore represents a unique isolated model of disuse affecting a specific subset of upper limb functionality.

In the present work I present a multi-modal cross-sectional study aiming to investigate the imaging markers of plasticity associated with chronic unilateral disuse of the upper limb. In particular, I apply structural MRI to compare the grey matter structure of

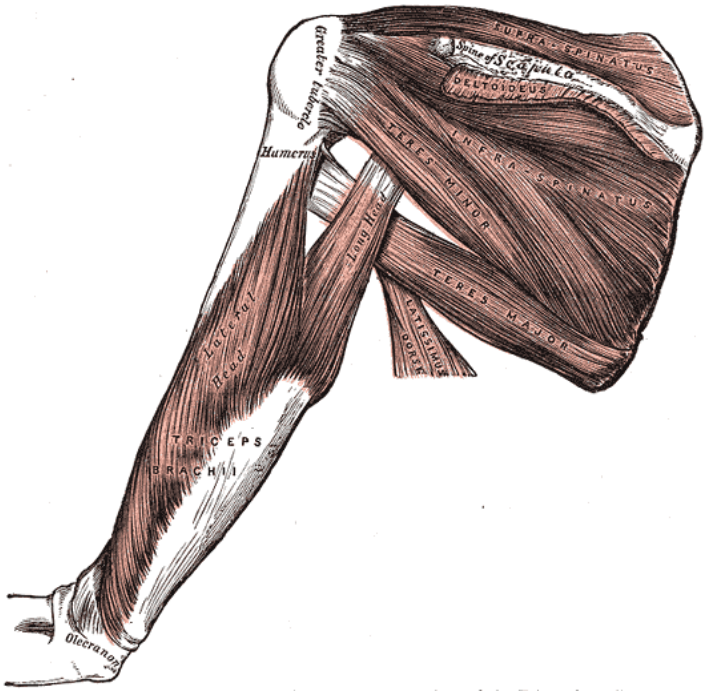


Figure 5.1: *The anatomy of the rotator cuff.* The rotator cuff comprises the four muscles and their associated tendons: infraspinatus, supraspinatus, subscapularis and teres minor. The image depicts the posterior aspect of the left shoulder girdle. Image adapted from Gray, 1918.

orthopaedic patients with MIRCT to healthy age-matched control participants using a whole-brain approach. Further, I seek to interrogate the relevance of observed grey matter differences between patients and control participants using a more focused approach, employing diffusion-weighted MRI to assess structural integrity within white matter tracts local to any observed grey matter differences. Finally I attempt to relate any observed differences in imaging metrics to clinical measures of upper limb use in the patient group under study.

## 5.2 Methods

This study was undertaken as part of a collaboration between the University of Oxford and Torbay Hospital, South Devon Healthcare NHS Foundation Trust.

### 5.2.1 Participants

Twenty-one patients with MIRCT were recruited from the orthopaedics outpatient clinic at Torbay Hospital in accordance with local NHS Research Ethic Committee approval [South-West NRES REC: 10/HO102/35; Mean age: 76.3 ± 7.68; three female; three left-handed]. All patients were more than 18 years of age, with a radiological diagnosis of a full thickness tear of more than 5cm in length confirmed by surface ultrasound. Exclusion criteria included the presence of any neurological condition, contraindication for MRI, involvement of individuals in industrial claims or litigation related to shoulder injury, history of recent shoulder trauma, or the presence of a rotator cuff tear considered to be repairable by a consultant orthopaedic surgeon.

Sixteen control participants were also recruited [Mean age: 72.8 ± 6.01; six female; two left-handed], matched for age. Exclusion criteria included the presence of any neurological condition, contraindication for MRI and the presence of any shoulder pathology or rotator cuff tear. All control participants were screened for the presence of shoulder pathology with a clinical examination and an ultrasound scan. Details of patient and control subject demographics are shown in table 5.1.

### 5.2.2 Experimental design

All patients and control participants attended an initial screening session, followed by an MRI scan session. The screening consisted of a clinical examination of the shoulder, including an ultrasound to confirm or rule out the presence of a rotator cuff tear, and the collection of baseline clinical scores.

### 5.2.3 MRI acquisition

MRI data were acquired at Torbay Hospital using a General Electric 1.5T Signa HD system (General Electric, Fairfield, CT, USA) with an 8 channel head coil and maximum 23mT.m$^{-1}$ gradient capability.

Structural MRI data were acquired using a T1-weighted 3D inversion recovery prepared fast spoiled gradient echo (FSPGR) sequence (MPRAGE equivalent, matrix 256 x 265, 1x1x1mm resolution, 170 axial slices, TE: 3.76ms, TR: 9.3s, flip angle: 13°). Diffusion-weighted MRI data were acquired using a SE EPI sequence (matrix 256 x 256, 0.94 x 0.94 x 2.5mm resolution, 50 axial slices, TE: 93.6ms, TR: 13000ms, bandwidth: 1953Hz, flip angle 90°) with 60 isotropically distributed diffusion directions (b-value: 1000s.mm$^{-2}$) and 6 b=0 images.

### 5.2.4 Clinical measures

The primary indicator of shoulder function employed in this study was the Oxford Shoulder Score (OSS). This is a well-validated 12-item patient-reported questionnaire-based metric of shoulder function (Dawson et al., 1996; Dawson et al., 2009). The OSS applied in this thesis uses the new system of scoring, with a range from 0 to 48, where a score of 0 represents the most severe symptoms, and a score of 48 represents normal function (Oxford Shoulder Score, Isis Outcomes, University of Oxford, Oxford).The OSS is applied commonly in clinical settings worldwide (Huber et al., 2004; Cloke et al., 2005; Rosenberg and Soudry, 2006; Flinkkilä et al., 2006; Berendes et al., 2010; Tuğay et al., 2011), as well as in studies of rotator cuff trauma and treatment, including the large United Kingdom Rotator Cuff Study randomised control trial (RCT) (Gwilym et al., 2011; Carr et al., 2014). A full version of the Oxford shoulder Score questionnaire can be found in Appendix B.

### 5.2.5 MRI analysis

#### 5.2.5.1 Grey matter voxel-based morphometry analysis

VBM was used to assess differences in the distribution of grey matter across the entire brain in the patient group compared with the control group using T1-weighted images. The VBM analysis was undertaken as outlined in section 2.7.5.1 using

FSL-VBM (Douaud et al., 2007), an optimised VBM protocol (Good et al., 2001), to produce a modulated spatially-normalised grey matter map for all thirty-seven subjects, with isotropic smoothing using a kernel with a FWHM of 2mm. The study specific template used in this analysis was constructed from a group of thirty-two subjects, with an even split between patients and controls.

VBM analysis was performed on the native images and images left-right flipped to achieve consistent ipsilateral/contralateral orientation relative to the side of tear. The native analysis used structural T1-weighted images in their original left-right orientation to address the question of wholebrain grey matter change. The flipped analysis addressed the potential for grey matter changes contralateral to the side of the rotator cuff tear, and therefore T1-weighted images were left-right flipped in 10/21 patients such that the left hemisphere was consistently contralateral to the side of the tear; T1-weighted images from 8/16 age and gender matched control participants were also left-right flipped.

The statistical analysis approach used in voxel-wise group comparison must include full-correction for multiple comparisons. Therefore in the comparison of grey matter maps, permutation-based non-parametric inference was applied within the framework of a GLM implemented using Randomise in FSL (Nichols and Holmes, 2002; Winkler et al., 2014) (5000 permutations). The GLM design compared the patient group with the control group (two-tailed, $p < 0.05$), adjusted for the following covariates: age, the presence of bilateral tear, and dominant hand. Statistical maps were subject to threshold free cluster enhancement: a cluster-based thresholding approach that estimates cluster-like local spatial support in the data and uses this to define an initial cluster-forming threshold (Smith and Nichols, 2009). This approach combats the problem of defining arbitrary cluster-forming thresholds and the impact of spatial smoothness seen previously in cluster-based thresholding of voxel-wise statistical maps.

#### 5.2.5.2 White matter analysis

Diffusion-weighted MRI data were used for white matter analysis. After correction for eddy-current induced distortion, maps of FA and RD were calculated using FSL DTIfit (Behrens et al., 2003), a part of the FDT in FSL (Smith et al., 2004). In order to investigate white matter tracts associated with regions of grey matter structural difference identified during VBM analysis, multi-fibre probabilistic tractography was performed (Probtrackx2, FDT) (Behrens et al., 2007) using a reference diffusion-weighted MRI dataset collected independently in Oxford. This dataset was composed of fifteen subjects [Mean age: 30.1 ± 4.71; two female; two left-handed], acquired using a Siemens Sonata 1.5T scanner at the Oxford Centre for Magnetic Resonance, Oxford, UK, with a maximum gradient strength of 40mT/m. Three sets of whole head EPI data were acquired with 60 isotropically distributed diffusion directions (b-value: 1000s.mm$^{-2}$) and 8 b=0 images, and an isotropic resolution of 1.5mm. The benefits of using this separate dataset for tractography included its higher spatial resolution and isotropic voxel dimensions.

The results of the probabilistic tractography guided the ROI analysis of the patient and control diffusion-weighted MRI data. A ROI representing the anatomically relevant tract(s) and a control tract were extracted from the John Hopkins University white matter tractography atlas (Mori et al., 2008). These tracts were subject to a threshold of 30% of the maximum voxel value. The tract ROIs were resampled from MNI-152 standard space to individual subject diffusion space using a combination of non-linear warps and linear transformation matrices calculated in FNIRT (Andersson et al., 2007a; Andersson et al., 2007b) and FLIRT (Jenkinson and Smith, 2001; Jenkinson et al., 2002) respectively. The tract ROIs were then used to calculate average diffusion metrics in the patients and control subjects. The diffusion metrics of interest in this case were FA and RD. FA is applied broadly in the study of white matter structure. As discussed in section 2.5.2, RD focuses on diffusion perpendicular to the principal eigenvector, and has the potential to provide insight into patterns of

diffusion influenced by differences in related structures, such as myelin and axonal structure (Song et al., 2005; Budde et al., 2009).

### 5.2.6 Statistics

All statistical analysis and graphing were undertaken using JMP (Version 11.0, SAS Institute, Cary, NC, USA) and Statistics Package for the Social Sciences (Version 19.0, IBM Corporation, Armork, NY, USA). All correlation metrics represent Pearson correlation coefficients (two-tailed).

| Subject ID | Group | Age | Trial shoulder | Bilateral tear | Gender | Dominant hand | OSS |
|---|---|---|---|---|---|---|---|
| 1 | P | 68 | R | Y | M | R | 24 |
| 2 | P | 83 | L | Y | F | R | 20 |
| 3 | P | 82 | L | N | M | L | 23 |
| 4 | P | 73 | L | N | M | R | 26 |
| 5 | P | 85 | R | N | F | L | 16 |
| 6 | P | 75 | R | N | M | R | 29 |
| 7 | P | 81 | R | N | M | R | 37 |
| 8 | P | 84 | R | N | F | R | 27 |
| 9 | P | 82 | R | N | M | R | 38 |
| 10 | P | 73 | L | N | M | R | 31 |
| 11 | P | 68 | L | N | M | L | 24 |
| 12 | P | 64 | L | N | M | R | 43 |
| 13 | P | 78 | L | N | M | R | 27 |
| 14 | P | 86 | R | N | M | R | 18 |
| 15 | P | 65 | R | N | M | R | 37 |
| 16 | P | 82 | R | N | M | R | 36 |
| 17 | P | 80 | R | N | M | R | 26 |
| 18 | P | 84 | R | N | M | R | 30 |
| 19 | P | 80 | L | Y | M | R | 30 |
| 20 | P | 64 | L | Y | M | R | 37 |
| 21 | P | 66 | L | Y | M | R | 26 |
| 22 | C | 83 | - | - | M | R | 48 |
| 23 | C | 69 | - | - | M | R | 48 |
| 24 | C | 68 | - | - | M | R | 47 |
| 25 | C | 68 | - | - | F | R | 48 |
| 26 | C | 80 | - | - | M | R | 48 |
| 27 | C | 67 | - | - | F | R | 48 |
| 28 | C | 80 | - | - | F | R | 48 |
| 29 | C | 66 | - | - | F | R | 48 |
| 30 | C | 66 | - | - | F | R | 48 |
| 31 | C | 75 | - | - | M | R | 45 |
| 32 | C | 70 | - | - | F | R | 48 |
| 33 | C | 68 | - | - | F | R | 48 |
| 34 | C | 75 | - | - | M | R | 48 |
| 35 | C | 72 | - | - | M | L | 48 |
| 36 | C | 83 | - | - | M | L | 48 |
| 37 | C | 74 | - | - | M | R | 48 |

Table 5.1: *Summary of patient and control subject demographic information and clinical scores.* Y: yes, N: no, R: right, L: left, P: patient, C: control, OSS: Oxford Shoulder Score.

## 5.3 Results

There was no statistically significant difference between the two groups under study in terms of age ($t(35) = 1.592$, $p = 0.12$; two-tailed) or handedness ($\chi^2(1) = 0.025$, $p = 0.87$). All MRI data were visually inspected to check for the presence of excessive subject motion. All subjects were included in analysis of structural T1-weighted and diffusion-weighted MRI data.

### 5.3.1 Native space grey matter voxel-based morphometry results

VBM comparison of patient and control subjects in their native left-right orientation demonstrated significant differences in grey matter density (controls > patients) in the posterior division of the right superior temporal gyrus (STG), directly adjacent to the temporoparietal junction (TPJ), and in the right posterior hippocampus, including the cornu ammonis, subiculum and dentate gyrus (Figures 5.2 and 5.3 and table 5.2). The anatomical location of these results was confirmed using the Harvard-Oxford Cortical Structural Atlas and Juelich Histological Atlas where appropriate (Eickhoff et al., 2005; Desikan et al., 2006; Eickhoff et al., 2006; Eickhoff et al., 2007). No regions demonstrated a significant difference in grey matter density for the opposite contrast (patients > controls).

Measures of average grey matter density were extracted from both VBM clusters for both patients and controls. In the patient group, there was a strong positive correlation between grey matter density in the posterior right STG VBM cluster and the OSS: $r(19) = 0.548$, $p = 0.0102$ (Figure 5.4). This suggests that reduced shoulder function in the patient group is associated with reduced grey matter density in the posterior right STG VBM cluster. There was no significant correlation between grey matter density in the right hippocampus cluster and the OSS in the patient group: $p > 0.05$.

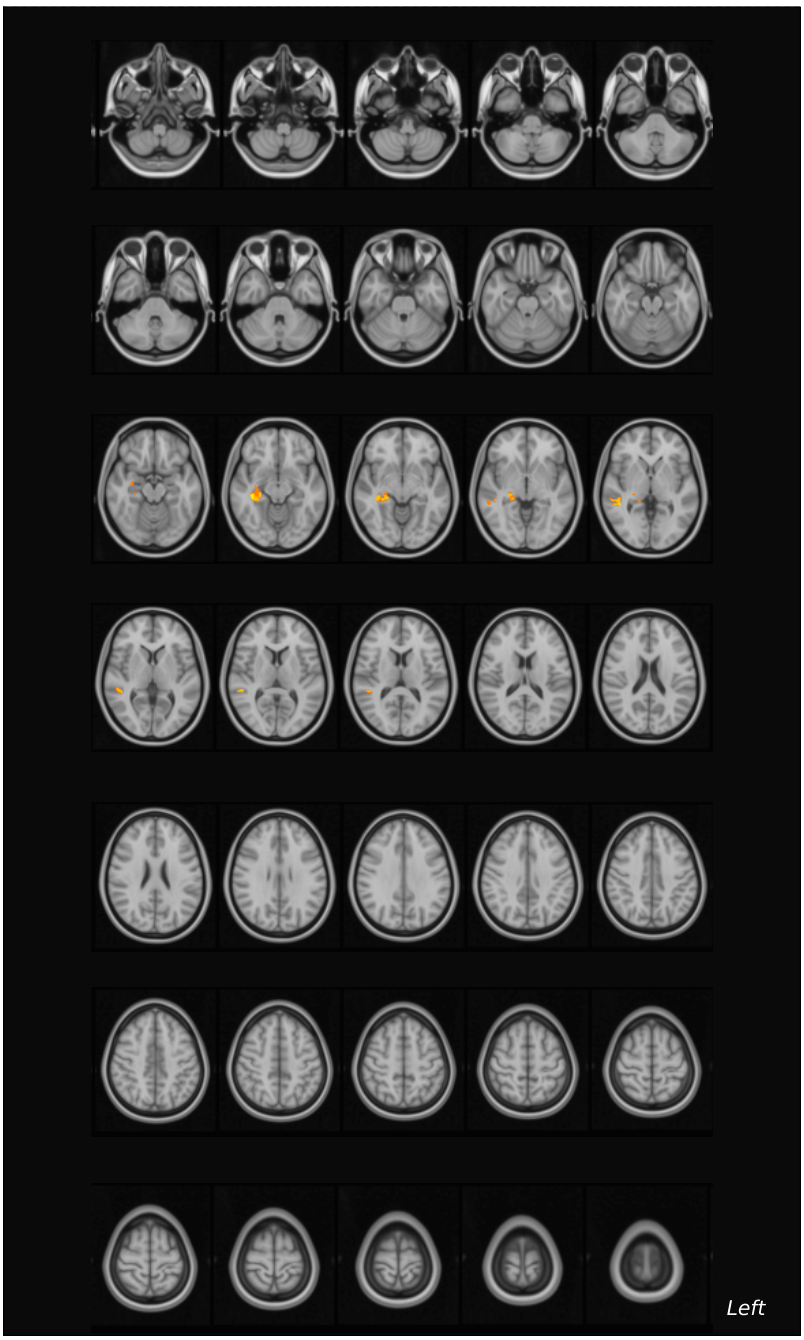


Figure 5.2: *Patients with chronic disuse of the upper limb show localised differences in grey matter density compared to control subjects.* Patients show lower grey matter density localised to right posterior hippocampus and posterior right STG, identified using a VBM approach implemented in FSL. Data overlaid on T1-weighted MNI-152 standard space brain.

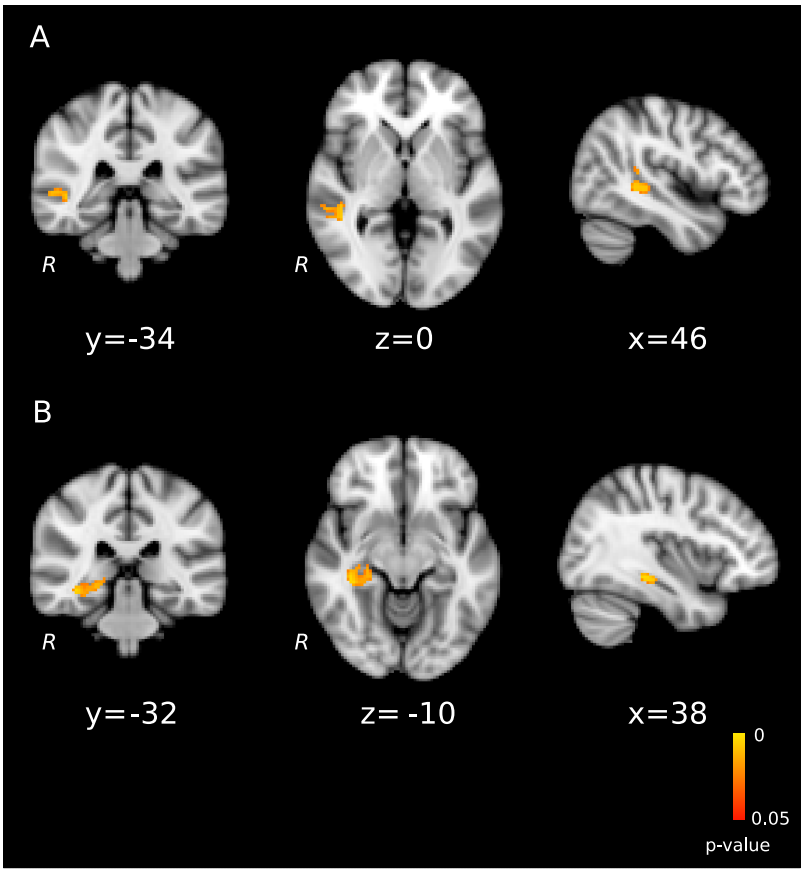


Figure 5.3: *Clusters of reduced grey matter density in patients compared to control subjects.* Two distinct clusters of reduced grey matter intensity were observed in patients compared to control subjects, the first in posterior right superior temporal gyrus at the TPJ (A), and the second in posterior right hippocampus (B). Coordinates shown indicate peak voxels in voxel coordinates given in MNI-152 coordinate standard space (mm).

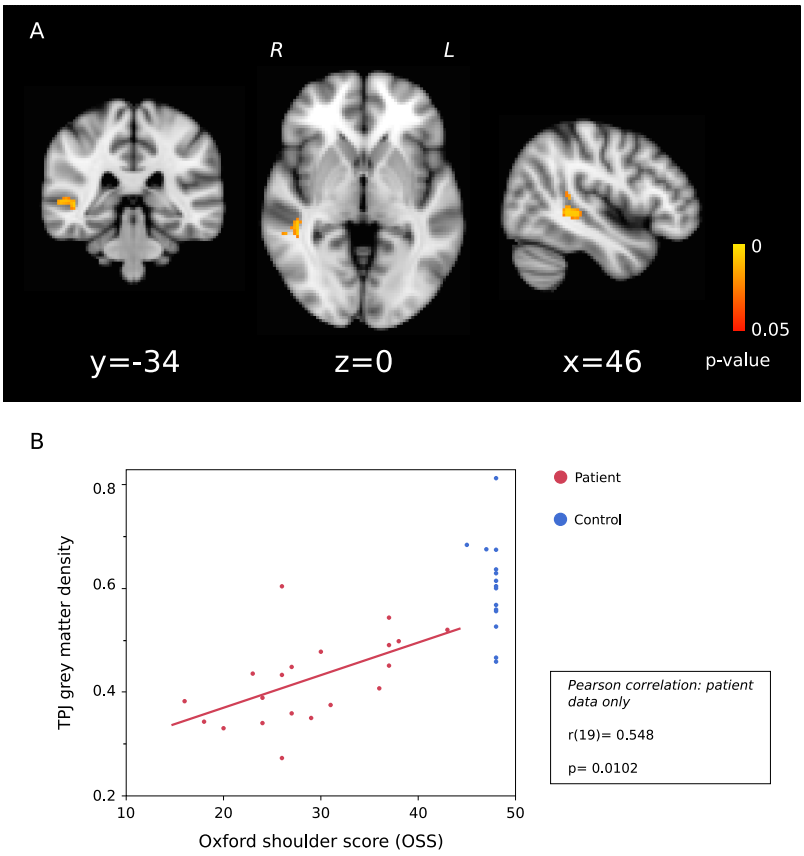


Figure 5.4: *Grey matter density in posterior right STG is strongly correlated with shoulder function in patients.* In the patient group, there was a strong positive correlation between grey matter density in the posterior right STG VBM cluster and the OSS: $r(19) = 0.548$, $p = 0.0102$. Voxel coordinates given in MNI-152 coordinate standard space (mm).

| Cortical region | Side | MNI (mm) | | | Maximum $t$-value |
|---|---|---|---|---|---|
| | | $x$ | $y$ | $z$ | |
| Posterior division of right temporal gyrus | R | 46 | -34 | 0 | 4.65 |
| Posterior hippocampus | R | 38 | -32 | -10 | 5.49 |

Table 5.2: *Summary of significant clusters from grey matter VBM analysis.* Regions showing significantly reduced grey matter density in patients compared with controls. Corrected $p$-value $<0.05$

### 5.3.2 Grey matter voxel-based morphometry results relative to the side of tear

VBM comparison of the patient and control subjects after reorientation of the data such that the left hemisphere was consistently contralateral to the side of the tear, revealed no differences in grey matter density between patients and control subjects in the primary sensorimotor cortex ipsilateral or contralateral to the side of the rotator cuff tear. More focused comparison of grey matter density in the primary sensorimotor cortex ipsilateral and contralateral to the side of the tear was performed. Independently-derived functional ROIs of the left and right hand and arm area were used to extract average measures of grey matter density (Figure 5.5A). These data were analysed using a mixed-design ANOVA with a between-subject categorical factor of group (patient and control), within-subject categorical factors of ROI (arm or hand) and side (ipsilateral or contralateral to tear), and a dependent variable of grey matter density. There was no significant interaction between group and side. Further, there was no significant main effect of group on grey matter density within the grey matter ROIs, confirmed with post-hoc independent sample $t$-tests, which found no significant difference in the grey matter density of the left arm area or left hand area in patients compared with control subjects (all $p >0.05$) (Figure 5.5). These results suggest that there was no statistically significant difference in grey matter density within the sensorimotor ROIs comparing patients with control subjects.

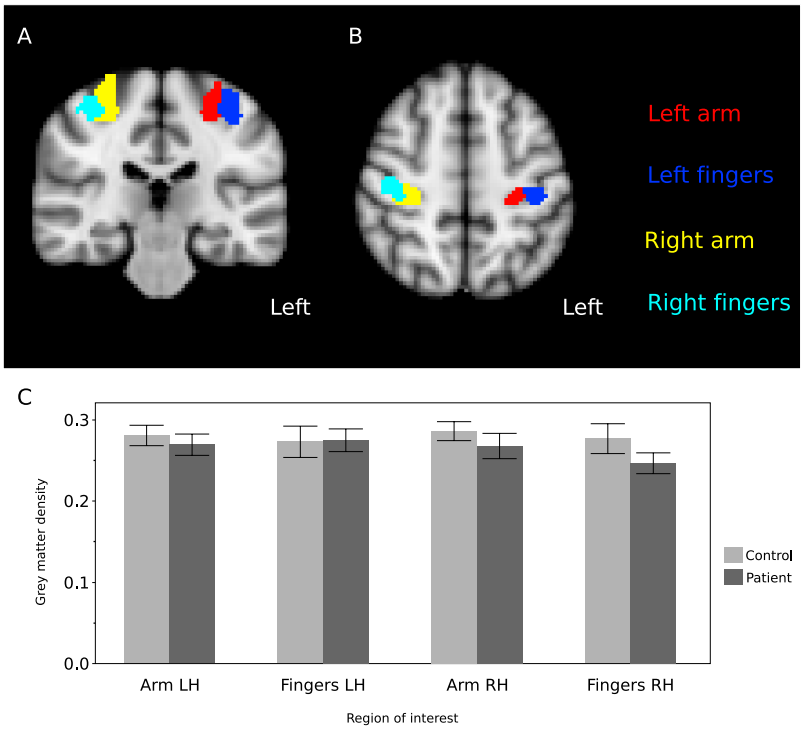


Figure 5.5: *Grey matter density in sensorimotor cortex contralateral to rotator cuff tear shows no difference in grey matter density in patients compared with control subjects.* A. ROI analysis of grey matter density used independently-derived functional maps of the arm and hand regions of sensorimotor cortex ipsilateral (right) and contralateral (left) to the side of rotator cuff tear. B. There was no significant difference in grey matter density, ipsilateral or contralateral to the tear, in patients compared with control subjects. LH: left hemisphere, RH: right hemisphere.

### 5.3.3 White matter results

Multi-fibre probabilistic tractography was undertaken in a subset of independently acquired control diffusion-weighted MRI data, described in section 5.2.5.2, using the VBM-derived cluster in posterior right STG as a seed. Tractography outputs from the sixteen independently acquired control subjects were non-linearly coregistered and averaged in MNI-152 standard space. At a threshold of 30% of the maximum, the tractography outputs demonstrated a dominant pattern of connectivity between the posterior right STG and the right superior longitudinal fasciculus (SLF) (Figures 5.6 and 5.7). ROI analysis of the patient and control diffusion metric maps was therefore undertaken using the right SLF from the John Hopkins University white matter tractography atlas (Mori et al., 2008), with an additional mask of the right CST as a control (Figure 5.8A).

Measures of average FA and RD were extracted from the right SLF and right CST ROIs for patients and controls. These data were analysed using a mixed-design ANOVA with a between-subject categorical factor of group (patient and control), a within-subject categorical factor of tract (SLF and CST), and a dependent variable of diffusion metric. There was a statistically significant interaction between group and tract on the diffusion metric RD: $F(1,35) = 9.416$, $p < 0.005$, partial $\eta^2 = 0.212$ (Figure 5.8). A post-hoc independent-sample $t$-test showed a significant difference in RD in the right SLF in patients compared with controls ($t(35) = 2.506$, $p = 0.017$; two-tailed). No such interaction was seen for the diffusion metric FA.

In the patient group, there was a strong negative correlation between RD in the right SLF and the OSS: $r(19) = -0.657$, $p = 0.0012$ (Figure 5.9). This suggests that reduced shoulder function is associated with reduced integrity in the right SLF. There was no significant correlation between RD in the right CST and the OSS in the patient group: $p > 0.05$.

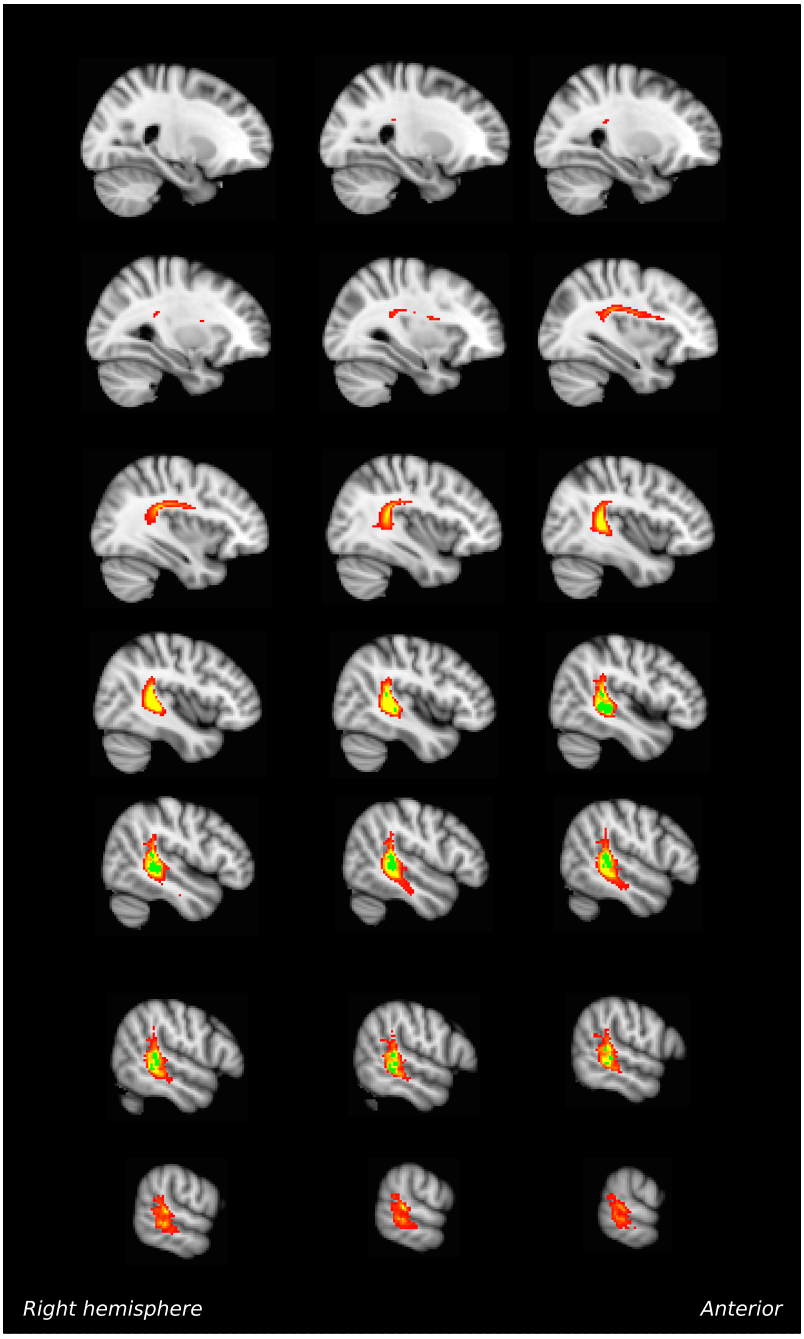


Figure 5.6: *Probabilistic tractography seeded in posterior right superior temporal gyrus VBM cluster.* Results of multi-fibre probabilistic tractography undertaken in an independently-acquired set of diffusion-weighted MRI. Tracts shown represent the average tractography output (red/yellow) from fifteen subjects, with the VBM cluster in posterior right STG as a common seed (green). Average tract shown on successive sagittal T1-weighted slices in MNI-152 standard space with a threshold at 30% of the maximum.

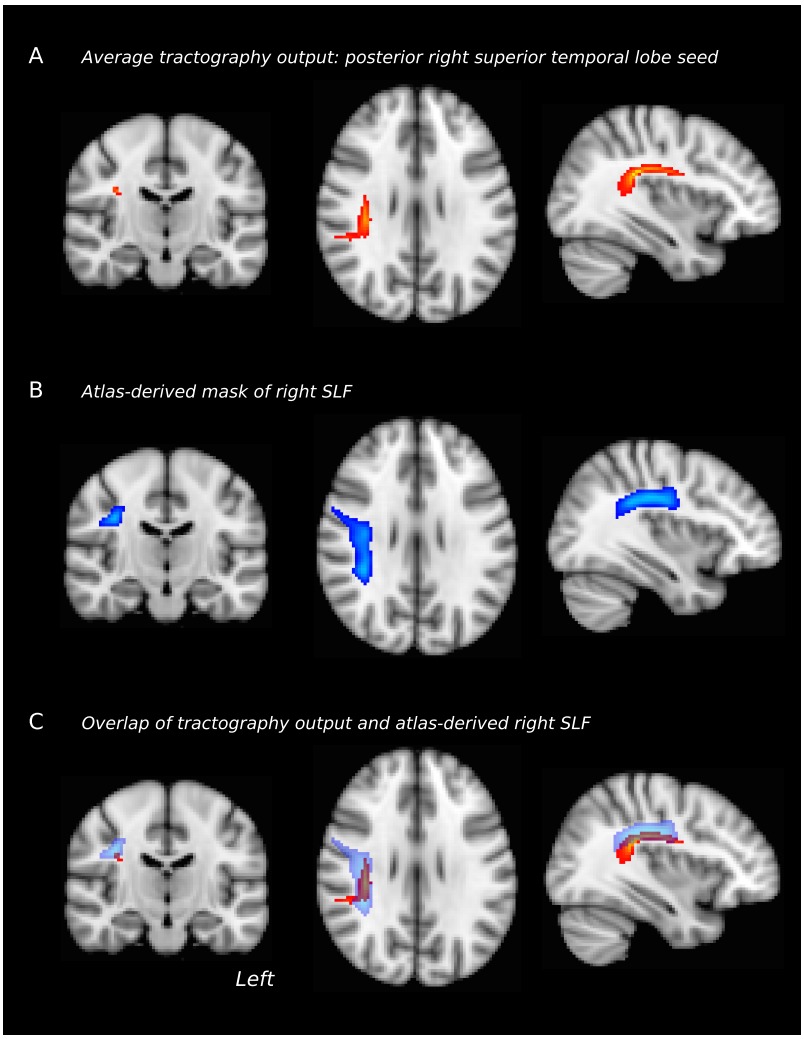


Figure 5.7: *Posterior right superior temporal gyrus VBM cluster shows strong anatomical connectivity to right superior longitudinal fasciculus.* A. Results of probabilistic tractography seeded in posterior right STG VBM cluster, run in an independently-acquired control population (threshold at 30% maximum; as in figure 5.6). B. Mask of right SLF from the John Hopkins University white matter tractography atlas (Mori et al., 2008) with a threshold at 30% of the maximum. C. Overlap of tractography-derived and atlas-derived tractography suggests connectivity between posterior right STG VBM cluster and right SLF.

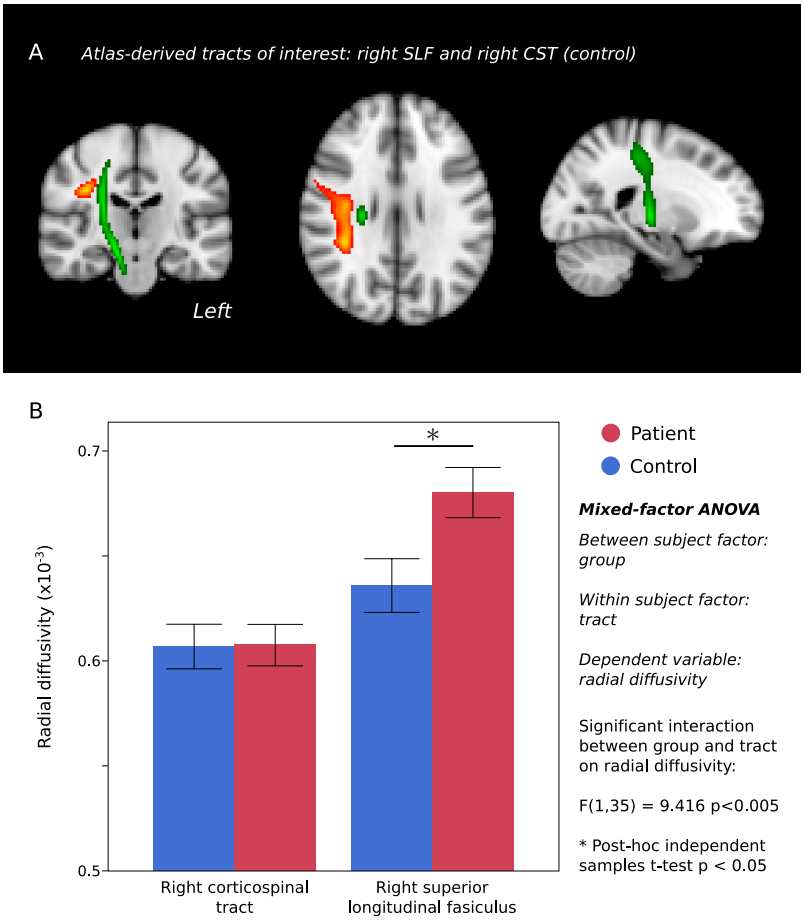


Figure 5.8: *Right superior longitudinal fasciculus shows reduced white matter integrity in patients compared with controls.* A. Atlas-derived tract ROIs: right superior longitudinal fasciculus (STG: tract of interest; orange) and right corticospinal tract (CST: control; green). B. Results of mixed-design ANOVA with a between-subject categorical factor of group (patient and control), a within-subject categorical factor of tract (SLF and CST), and a dependent variable of radial diffusivity. There was a statistically significant interaction between the group and tract on the diffusion metric RD, $F(1,35) = 9.416$, $p < 0.005$, partial $\eta^2 = 0.212$, with a post-hoc independent-samples $t$-test showing a significant difference in RD in the right SLF in patients compared with controls ($t(35) = 2.506$, $p = 0.017$; two-tailed)

.

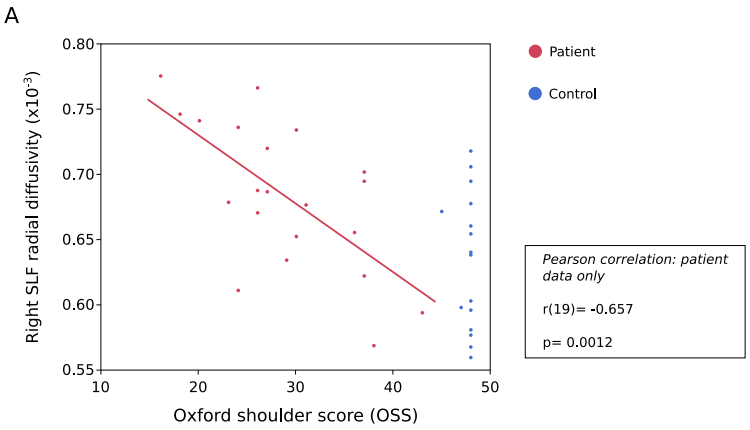


Figure 5.9: *Radial diffusivity in right superior longitudinal fasciculus is correlated with shoulder function in the patient group.* In the patient group, there was a strong negative correlation between RD in the right SLF and the OSS: $r(19)$ = -0.657, $p$ = 0.0012.

### 5.3.4 Correspondence of grey matter and white matter results

I went on to investigate the relationship between the differences in white matter and grey matter between patients and controls described above. In the patient group there was a moderate negative correlation between mean RD in the right SLF and mean grey matter density in the posterior right STG VBM cluster: $r(19)$ = -0.445, $p$ = 0.043 (Figure 5.10A). This negative correlation appeared to persist across the entire group of both patients and controls, but could not be statistically quantified with a correlation coefficient due to the mean difference between the groups (Figure 5.10B).

Next, given the degree of correlation between the grey matter density, white matter RD and OSS in the patient group, I was interested to examine whether the correlations between MRI metrics of structural integrity in the patient group was driven by the OSS score. A partial correlation showed that the relationship between mean RD in the right SLF and mean grey matter density in the posterior right STG VBM cluster did not survive after correcting for OSS: $r(18)$ = -0.134, $p$ = 0.574.

Further, a partial correlation was computed between the OSS and each of the MRI metrics, correcting for the third variable in the patient group (Table 5.3). These

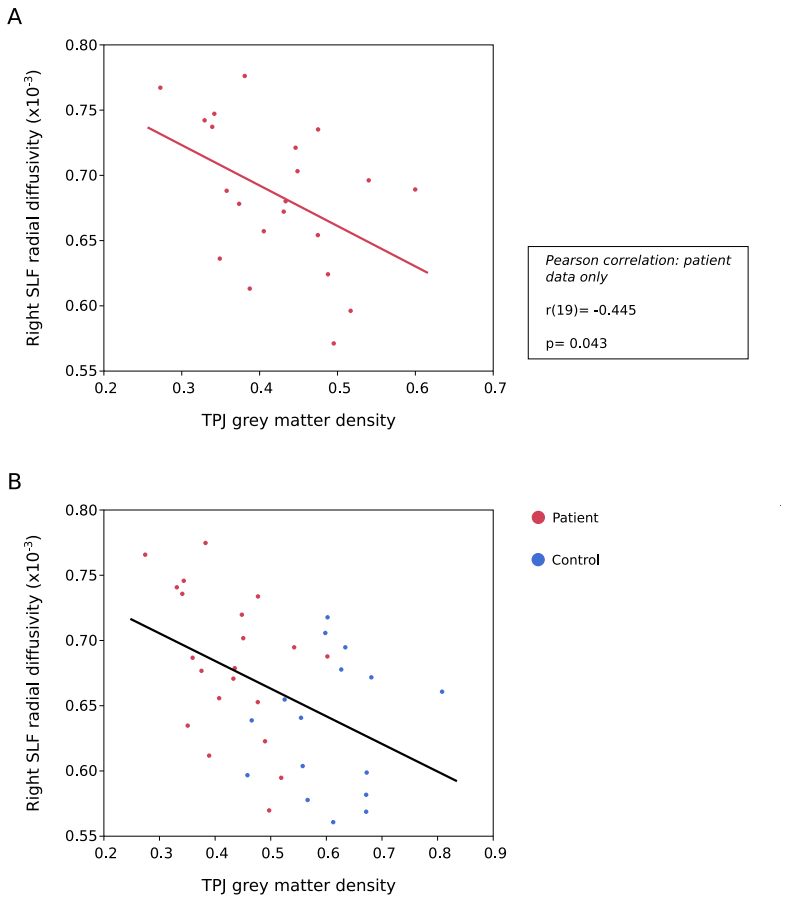


Figure 5.10: *Radial diffusivity in right superior longitudinal fasciculus is correlated with grey matter density in posterior right STG in the patient group.* A. In the patient group, there was a moderate negative correlation between RD in the right SLF and grey matter density in the posterior right STG VBM cluster: $r(19) = -0.445$, $p = 0.043$. B. The association between increased grey matter density and reduced radial diffusivity persists across the entire group under study, including both patients and control subjects.

results suggest that the relationship between shoulder function (OSS) and the integrity of the right SLF (RD) persists independent of grey matter density in the posterior right STG VBM cluster.

| Partial correlations | | | | |
|---|---|---|---|---|
| Control variable | Variable 1 | Variable 2 | Pearson $r$-value | $p$-value |
| Radial diffusivity: Right SLF | Grey matter density: Posterior right STG VBM cluster | Oxford Shoulder Score (OSS) | 0.378 | 0.100 |
| Grey matter density: Posterior right STG VBM cluster | Radial diffusivity: Right SLF | Oxford Shoulder Score (OSS) | -0.551 | 0.012 |

Table 5.3: *Partial correlations: relating behavioural measures and MRI-derived metrics.* Assessing the correlations between MRI-derived metrics and the OSS, correcting for other correlated variables.

## 5.4 Discussion

This study sought to investigate the imaging biomarkers of plasticity associated with chronic unilateral disuse of the upper limb in patients who have suffered MIRCT. Using a combination of T1-weighted and diffusion-weighted MRI, I have demonstrated evidence of localised structural differences in anatomically connected regions of grey matter (Figures 5.2 and 5.3) and white matter (Figure 5.8) in patients with chronic upper limb disuse compared to control subjects. Further, I have shown that within these localised regions in patients, the structural integrity is strongly correlated with the OSS, a behavioural measure of shoulder function and upper limb disuse (Figures 5.4 and 5.9). These results suggest not only that long-term upper limb disuse is associated with structural brain changes, but further that the degree of reduced integrity within the affected grey matter and white matter regions is associated with the severity of the disuse in the patient group.

The anatomical location of these grey matter and white matter changes in posterior right STG and SLF respectively suggest the potential for involvement of the right hemisphere lateralised ventral attention network in changes associated with long-term upper limb disuse. However, in interpreting the results in this area, it is important to remember that this region of functionally very diverse, and therefore further imaging modalities and behavioural testing will be necessary to further confirm the role of this particular brain network.

### 5.4.1 The ventral attention network

The right STG and right SLF highlighted in this study are components of the right-lateralised ventral attention network (Corbetta and Shulman, 2011b). Broadly this cortical network functions in "detecting and responding to unexpected stimuli in the environment" (MacNeilage et al., 2009), and is composed of the TPJ, ventral frontal cortex (VFC) (Vossel et al., 2014) and long association fibres including the

SLF and inferior longitudinal fasciculus (ILF) (Chechlacz et al., 2010). The posterior division of the right STG identified in the VBM results (Figures 5.2 and 5.4) is a component of the TPJ, a cortical region "defined as the posterior sector of the superior temporal sulcus (STS) and STG and the ventral part of the supramarginal gyrus (SMG)" (Corbetta et al., 2008). The SLF, which shows markers of reduced integrity in the patient population (Figure 5.8), is a large, right lateralised white matter tract, which in part links the TPJ to more rostral regions of VFC (Thiebaut de Schotten et al., 2011).

Physiologically, the ventral attention network has been implicated in stimulus-driven reorienting: response to stimuli outside of an individual's direct attention (Corbetta and Shulman, 2011a). Evidence from the fMRI literature has demonstrated broad right TPJ and VFC activity associated with unexpected and unattented stimuli (Fox et al., 2006). More recent data suggest a right laterality in TPJ activity alone, irrespective of the spatial location of the unattented cue, as well as strong resting state connectivity between right TPJ and right VFC (Shulman et al., 2009; Shulman et al., 2010), with a view of the right TPJ as an attentional circuit breaker (Corbetta et al., 2008).

The majority of evidence for right TPJ function comes from the study of pathology, specifically the effects of stroke lesion damage to the right ventral attention network. In this context, damage to the right TPJ is strongly associated with spatial neglect and hemiextinction: attentional deficits in the reorientation to stimuli. This phenomenon was first reported by Posner and colleagues (Posner et al., 1984), with a later link between lesions in the right TPJ/STG and disengagement or attentional reorientation deficits (Friedrich et al., 1998). This spatial deficit has been reported both ipsilateral and contralateral to right TPJ, consistent with the idea of right ventral attention network dominance (Rengachary et al., 2011). Further evidence from the stroke literature suggests deficits in spatial vigilance associated with right TPJ lesions, specifically in the maintenance of attention to a specific spatial location (Malhotra et al., 2009). Further imaging data from spatial neglect patients also suggests a

disruption in right ventral attention network connectivity, with evidence for reduced white matter tract integrity in non-lesioned SLF, associated with a lesion in a cortical network node (Chechlacz et al., 2010; Chechlacz et al., 2013).

### 5.4.2 Spatial attention and disuse

The pattern of reduced integrity observed in both grey matter (Figure 5.2) and white matter structures (Figure 5.8) has an anatomical distribution consistent with the right ventral attention network, and the regions commonly compromised in reports of spatial neglect (Vallar and Perani, 1986; Karnath and Rorden, 2012; Chechlacz et al., 2013).

Conversely, recent evidence from the non-human primate literature has reported an increase in grey matter density in the right TPJ, associated with tool-use learning (Quallo et al., 2009). This serial MRI study demonstrated a progressive increase in STS grey matter volume associated with two weeks of intensive daily training on a gross movement tool-based task using a rake, as well as changes in secondary somatosensory cortex and inferior parietal cortex. In a corollary of this finding, the data presented in this chapter show a reduction in grey matter density associated with upper limb disuse, correlated with the degree of disuse in patients. Following from the work of Quallo and colleagues, the anatomy of the observed grey matter and white matter results presented in this chapter are reminiscent of patterns of damage seen in neglect. However, in contrast to spatial neglect where damage to the right ventral attention network drives attentional deficits (Corbetta and Shulman, 2011a), the current data raise the possibility that an attentional bias or shift, driven by a unilateral reduction in upper limb function, has the potential to cause a loss of structural integrity in the right ventral attention network.

Clinically, these data suggest the potential for a clear neurological consequence of MIRCT, a non-neurological condition involving disuse with a high incidence in the elderly population (Clement et al., 2012). The findings presented here raise questions

regarding the potential for attentional deficits associated with long term limb disuse, and the extent to which rehabilitation of arm function is associated with adaptive neuroplasticity.

### 5.4.3 Relating grey matter and white matter integrity

The reduction in grey matter density in the right TPJ and white matter integrity assessed by RD in the right SLF in patients are moderately negatively correlated (Figure 5.10A), suggesting that a reduction in grey matter density in the right TPJ is associated with an increase in RD in the right SLF. This relationship also appears to persist across the patient and control groups (Figure 5.10B). In the context of a cross-sectional study, it is not possible to definitely assess whether a reduction in grey matter integrity drives a reduction in white matter integrity or vice versa. However, in partial correlation analysis assessing the relationship between grey and white matter integrity measures and the OSS in patients, it was clear that while the association between white matter RD and OSS persisted when correcting for grey matter density, the association between grey matter density and OSS correcting for white matter RD did not (Table 5.3). This provides some tentative evidence for a more robust association between the metric of white matter integrity and the OSS, a metric of shoulder disuse.

Evidence from comparative imaging/histology studies suggests a link between increased white matter RD and a local reduction in myelination (Song et al., 2005; Klawiter et al., 2011). Independent of synaptic plasticity, it is increasingly evident that activity-dependent changes in myelination may occur in long-range white matter tracts (Fields, 2005). In a recent study of individual cortical pyramidal neurons, Tomassy and colleagues demonstrated distinct longitudinal patterns of myelination along the axonal processes, differing between individual cells (Tomassy et al., 2014). Further, they related the myelination profiles of these axons to the relative presence of adjacent oligodendrocyte precursor cells. There is strong evidence for

activity-dependent axon-oligodendrocyte signals affecting white matter remodelling independent of synaptic processes occurring in grey matter (Wake et al., 2011). It could therefore be argued that inactivity of the right ventral attention network due to unilateral limb disuse may mediate reductions in right SLF myelination seen in the patients compared with controls.

### 5.4.4 Right posterior hippocampus and spatial localisation

VBM analysis revealed a significant reduction in grey mater density in the right posterior hippocampus in patients compared with control subjects (Figure 5.3B). The right posterior hippocampus has previously been implicated in spatial representation of the environment (Maguire et al., 2000), but typically in allocentric rather than egocentric space (Duarte et al., 2014). In the context of this literature, the grey matter difference observed in this chapter in right posterior hippocampus is in keeping with the other findings in the right ventral attention network. The hippocampal result again might suggest that a reduction in attention on the side of upper limb disuse could drive an inherent bias in spatial representations and memory. Given the resolution of structural imaging data acquired in this study, and the complex architecture of the hippocampus, a more detailed morphometric imaging approach would be required to make more specific statements regarding the hippocampal subunits responsible for the reduced grey matter density seen in upper limb disuse patients.

### 5.4.5 Limitations and future directions

There are a few limitations in this study. Firstly, the cross-sectional design of this study limits the ability to make causal inferences regarding the nature of the differences and their relationship with upper limb disuse, making only observational conclusions possible. However, this work investigates a previously unexplored patient population of high prevalence in the ageing population; the results presented herein

therefore provide strong evidence for a more detailed longitudinal study to investigate the potential for brain change associated with functional improvements in limb use. Longitudinal data (from patients only) is presented in Chapter 6.

Secondly, due to the inherent difficulties in acquiring high resolution diffusion MRI data from a 1.5T clinical scanner in the district general hospital, the diffusion data was not of sufficient quality to allow for tractography to be performed. Therefore, the diffusion analysis presented in this chapter was ROI based, however, it was heavily informed by the results of the whole-brain VBM analysis performed on T1-weighted structural data.

In order to firmly implicate the structural differences observed in this study in right ventral attention network, further analysis and data acquisition will be necessary. Resting state functional connectivity or network analysis would provide a useful adjunct. It might be reasonable to hypothesise that reduced connectivity within the right ventral attention network might be observed in the patient group compared with the control group. Given the clinical nature of this study, it would also be valuable to collect some behavioural data in a separate cohort to investigate the potential for subtle deficits in visuospatial attention in the patient group compared with control subjects, as recently reported in the ageing population more generally (Benwell et al., 2014).

The gender split in the patient group compared with the control group was slightly imbalanced. While MIRCT is a common shoulder pathology in the elderly population, it typically presents in the 7th or 8th decade. The recruitment of age and gender matched controls in this population for an imaging study presents a unique challenge, given the need for MRI compatibility and no history of a neurological disorder. We have attempted to minimise this bias as far as possible, and match in other characteristics including age and handedness. Given the link between hormonal differences and structural differences in brain morphology seen in males and females (Witte et al., 2010), the fact that the female subjects involved in the study were

15-30 years postmenopausal based on average statistics (McKinlay, 1996) renders this consideration somewhat less relevant than in a study of younger individuals.

In terms of future directions, the results presented in this chapter suggest a link between disuse of the upper limb and structural differences in the right ventral attention network. In order to substantiate this speculative link, behavioural characterisation of egocentric and allocentric attention in the patient population compared to controls could offer a valuable insight.

## 5.5 Conclusions

The data presented in this chapter provide evidence for structural differences in the right ventral attention network when comparing patients with unilateral chronic disuse in the upper limb with control subjects. Specifically, the patient group being studied showed reduced grey matter density in the posterior right STG component of the TPJ, and increased RD in the white matter of the right SLF; both of these metrics are suggestive of reduced structural integrity. Further, the markers of grey matter and white matter structure show a strong correlation with a behavioural measure of limb use in the patient group, suggesting a potential usage-dependent pattern of structural change associated with the severity of disuse. The data provide novel insights into the nature of chronic disuse and the potential neurological consequences of conditions not traditionally considered in a neurological context.

# 6 | Assessing the imaging markers of functional recovery after chronic upper limb disuse

*Motor disuse and immobilisation are associated with changes in the sensorimotor network in the short-term, as outlined in Chapter 1. The data presented in Chapter 5 suggest that long-term disuse of the upper limb is associated with structural differences in grey matter and white matter regions associated with sensory integration and the body schema. In this chapter I present preliminary analysis of an ongoing clinical trial, which seeks to investigate whether rehabilitation techniques to improve function in a disused limb are associated with structural changes in the brain. This study is part of a collaboration with Torbay Hospital, where the data are acquired. In this chapter I present a longitudinal analysis assessing the potential for grey matter and white matter change associated with an exercise rehabilitation programme designed improve function in the limb through compensatory or adaptive behaviour using intact muscle groups.*

## 6.1 Introduction and rationale

As discussed in section 1.5.2.3, programmes of motor rehabilitation have been broadly applied in the literature to promote adaptive plasticity in the human brain, commonly in chronic stroke patients. The potential for specific rehabilitation techniques to counteract or negate processes of maladaptive plasticity associated with the post-stroke period has been extensively studied (Murphy and Corbett, 2009). The results

of the cross sectional analysis presented in Chapter 5 provide tentative evidence for a potential process of maladaptive plasticity associated with chronic disuse of the upper limb following massive irreparable rotator cuff tear (MIRCT). It remains unclear whether overcoming the motor disuse of the affected limb could promote some kind of adaptive plasticity in areas related to those identified in Chapter 5.

Non-surgical interventions for rotator cuff tear in general are designed to improve function in the affected limb through compensatory or adaptive behaviour using intact muscle groups. Such non-surgical approaches have yielded mixed results in the treatment of rotator cuff tear when compared with a surgical repair (Ejnisman et al., 2009). However, in the case of MIRCT, where a surgical intervention is not feasible, behavioural rehabilitation programmes have offered encouraging results, with clinically significant improvements in outcome scores (Ainsworth and Lewis, 2007). In a randomised placebo controlled clinical trial, Ainsworth and colleagues reported that a supervised programme of targeted rehabilitation produced significant improvements in the ability of patients to use the upper limb affected by MIRCT (Ainsworth et al., 2009). The rehabilitation programme in this case included exercises designed to redress the imbalance of muscle function induced by the MIRCT, including proprioceptive training, and strengthening of the anterior deltoid and teres minor to compensate for dysfunction in the injured rotator cuff. The rehabilitation programme involves biweekly one hour sessions with a physiotherapist, with a progressive programme of exercises to be completed daily at home for a period of 30 minutes. The total duration of the rehabilitation was three months. In this study improvements in shoulder function were observed at the end of the rehabilitation period (3 months), but the functional gains did not persist at the 12 month followup.

Building upon the data presented in Chapter 5, here I present a preliminary analysis of a large longitudinal MRI dataset which seeks to identify adaptive plasticity associated with a targeted exercise based rehabilitation programme designed improve function in the limb affected after a period of chronic disuse following MIRCT. More specifically, I apply a longitudinal analysis in MIRCT patients, assessing grey matter density

derived from T1-weighted MRI and measures of white matter integrity from diffusion-weighted MRI before and after a comprehensive supervised rehabilitation intervention, as studied by Ainsworth and colleagues. I aim to identify regions in which there is grey matter or white matter change when comparing scans acquired before and after the rehabilitation intervention. Further, I aim to relate these changes to improvements in clinical measures of shoulder function.

## 6.2 Methods

This study was undertaken as part of a collaboration between the University of Oxford and Torbay Hospital, South Devon Healthcare NHS Foundation Trust. This chapter represents preliminary analysis of the patient data acquired before and after a rehabilitation intervention. The full study design is presented in figure 6.1. A control group of age-matched participants have also been recruited. Actual and projected scan figures are presented in table 6.1.

### 6.2.1 Participants

This chapter considers data from eighteen patients with MIRCT for whom scans at the baseline (0 month) and the first followup (4 month) have been acquired (figure 6.1 and table 6.1). Patients were recruited from the orthopaedics outpatient clinic at Torbay Hospital in accordance with local NHS Research Ethic Committee approval [South-West NRES REC: 10/HO102/35; Mean age: 78.4 ± 6.95; three female; three left-handed]. Exclusion criteria are outlined in section 5.2.1.

| Scan timepoint | 0 months | 4 months | 12 months |
|---|---|---|---|
| *Patient* | 21 acquired<br>0 pending | 18 acquired<br>1 pending | 14 acquired<br>5 pending |
| *Control* | 18 acquired<br>0 pending | - | 3 acquired<br>14 pending |

Table 6.1: *Actual and projected scan figures for longitudinal exercise rehabilitation study.* Time points refer to the outline shown in figure 6.1.

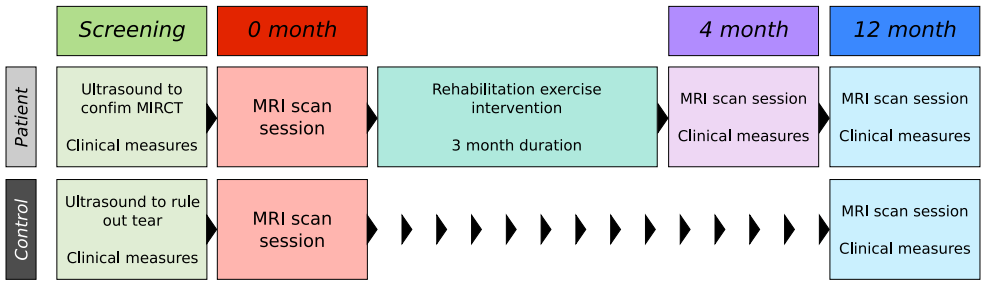


Figure 6.1: *Overview of longitudinal rehabilitation study design.* This chapter presents a preliminary analysis of data from a large patient-control longitudinal study investigating the neuroplastic effects of an exercise-based rehabilitation intervention to combat chronic disuse of the upper limb. The analysis in this chapter is concerned with comparing the patient MRI data (row one) collected at 0 months (red) and 4 months (purple).

### 6.2.2 Experimental design

Patients attended an initial screening session prior to their first MRI scan session. The screening consisted of a clinical examination of the shoulder, including an ultrasound to confirm or rule out the presence of a rotator cuff tear, and the collection of baseline clinical scores. Patients then undertook a baseline MRI scan session (0 month) immediately prior to the start of the rehabilitation intervention. This scan was followed by the supervised exercise rehabilitation intervention. Patients returned for two further followup sessions for an MRI scan and the collection of clinical measures. The first followup session took place four months after the baseline scan session, and therefore one month after the last rehabilitation session; the one month delay included time for the participant to undertake their final set of exercises at home, and to schedule the scan 4 month session, given the constraints acquiring data on a scanner system used principally to run a clinical service. The second followup session took place 12 months after the baseline scan session to assess the long-term stability of changes in shoulder function, in line with the study reported by Ainsworth and colleagues previously (Ainsworth et al., 2009). Control subjects were scanned at baseline (0 months) and at one followup session (12 months).

### 6.2.3 Exercise rehabilitation intervention

The exercise rehabilitation intervention consisted of a three month programme of supervised sessions and exercises performed by the participant in the home, as reported previously (Ainsworth, 2006). For an initial period of four weeks, patients attended an outpatients physiotherapy clinic at Torbay District General Hospital for weekly 30 minute sessions with a consultant physiotherapist. Thereafter patients attended the hospital for 30 minute sessions at two week intervals for the remainder of the three month period. At each session, patients were taught a progressive series of exercises, to be practiced at home two or three times per day. Patient progress was monitored by the same physiotherapist on each visit in order to qualitatively assess good compliance with the programme.

The programme began with patient education regarding the nature of the injury and shoulder function. Initial sessions focused on posture correction to improve the resting position of the glenoid fossa (shoulder socket). This stage was followed by exercises designed to engage healthy muscles to functionally compensate for rotator cuff dysfunction, including stretching and strengthening exercises. The final stages of the programme included exercises to improve proprioceptive abilities in the shoulder, followed by activities designed to ease day-to-day function, including education on alternative movements useful for undertaking common tasks, such as using the arm as a short lever rather than a long lever to reduce strain on the shoulder joint.

### 6.2.4 MRI acquisition

MRI data were acquired at Torbay Hospital using a General Electric 1.5T Signa HD system (General Electric, Fairfield, CT, USA) with an 8 channel head coil and maximum 23mT.m$^{-1}$ gradient capability. T1-weighted structural and diffusion-weighted MRI data were acquired at all scan sessions. Full details of scan parameters are given in section 5.2.3.

### 6.2.5 Clinical measures

The primary indicator of shoulder function employed in this study was the Oxford Shoulder Score (OSS), as outlined in section 5.2.4 and shown in full in Appendix B. Briefly, this well-validated clinical score ranges from 0 to 48, where 0 represents the most severe shoulder symptoms, and 48 represents normal function. An additional measurement of ongoing pain was also acquired using the Brief Pain Inventory (BPI) short-form questionnaire (Cleeland and Ryan, 1994), with a range from 0 to 100, where 100 represents the more severe pain imaginable. The BPI score was used in the analysis of behavioural improvement in shoulder function. The BPI short-form questionnaire can be found in Appendix C.

### 6.2.6 Longitudinal grey matter voxel-based morphometry

VBM analysis was performed using a modified version of FSL-VBM (Douaud et al., 2007), designed to incorporate the specific analysis considerations discussed in section 2.7.5.2 regarding longitudinal analysis of structural MRI data. The FSL-VBM tools were therefore used to created a modulated spatially-normalised grey matter map for all time points, using an unbiased intermediate template generated for each subject for registration purposes. All analyses were performed on native images representing true left/right orientation, as per the results presented in Chapter 5.

In this preliminary analysis the grey matter maps for each subject were compared using a voxel-wise paired sample $t$-test, to test the hypothesis that the difference in grey matter intensity between the two time points is different from 0. The statistical analysis approach used in voxel-wise group comparison must include full-correction for multiple comparisons. Therefore in the comparison of grey matter maps, permutation-based non-parametric inference was applied within the framework of a GLM, implemented using Randomise in FSL (Nichols and Holmes, 2002; Winkler et al., 2014) (5000 permutations). Statistical maps were subject to threshold free cluster

enhancement: a cluster-based thresholding approach that estimates cluster-like local spatial support in the data and uses this measure to define an initial cluster-forming threshold (Smith and Nichols, 2009), as discussed in section 5.2.5.1.

### 6.2.7 Longitudinal white matter analysis

In light of the white matter differences seen in MIRCT patients compared to control subjects at baseline in cross-sectional analysis presented in Chapter 5 (Figure 5.8), I performed a similar ROI analysis, assessing changes in the diffusion metrics of FA and RD in the right SLF (tract of interest), and the right CST (control tract).

### 6.2.8 Statistics

All statistical analysis and graphing were undertaken using JMP (Version 11.0, SAS Institute, Cary, NC, USA) and Statistics Package for the Social Sciences (Version 19.0, IBM Corporation, Armork, NY, USA). All correlation metrics represent Pearson correlation coefficients.

## 6.3 Results

This chapter considers data from eighteen patients who have completed MRI scans at the 0 month and 4 month time points. Data from the 12 month followup time point were not available at the time of writing, therefore no control participants were included in this longitudinal analysis. All MRI data were visually inspected to check for the presence of excessive subject motion. No MRI data were excluded from the analysis. Clinical measures at the 4 month time point were missing for one patient at the time of writing.

### 6.3.1 Changes in clinical measures

The patient group showed a significant increase in the OSS, reflecting a clinical improvement in shoulder function, when comparing measures taken at baseline (0 month) and following the exercise rehabilitation intervention at the first followup (4 month): paired samples $t$-test: $t(16) = 6.430$, $p < 0.0001$ (Figure 6.2A), with the mean score increasing from 29.1 to 37.1, representing an overall mean improvement of 14.6% of the maximum OSS score. 14/18 patients showed a $> 10\%$ improvement in shoulder score; 3/18 patients showed a reduction in the OSS; followup clinical scores were missing for one patient.

The patient group also showed a significant reduction in the BPI derived pain metric, representing an improvement, when comparing measures taken at baseline (0 month) and following the exercise rehabilitation intervention at the first followup (4 month): paired samples $t$-test: $t(16) = -2.745$, $p < 0.01$.

There was a moderate negative correlation between the change in OSS and the change in BPI measurement: $r(16) = -0.434$, $p = 0.0408$ (Figure 6.2B), such that greater improvements in shoulder score were associated with greater reductions in pain.

### 6.3.2 Grey matter changes

Within-subject paired comparison of grey matter density across the two time points under study revealed regions showing significant increases in grey matter density over time (Figure 6.3 and table 6.3). These changes were found in three distinct regions: right STG at the level of the TPJ, right orbitofrontal cortex (OFC) and bilaterally in the insular cortex (Figure 6.3). No regions of significant decrease in grey matter density were seen.

The region of increased grey matter density identified in the right STG at the level of the TPJ was directly adjacent to the region of the right STG in identified in baseline comparison of MIRCT patients and controls in Chapter 5, in which patients showed lower grey matter density than controls (Figure 6.4).

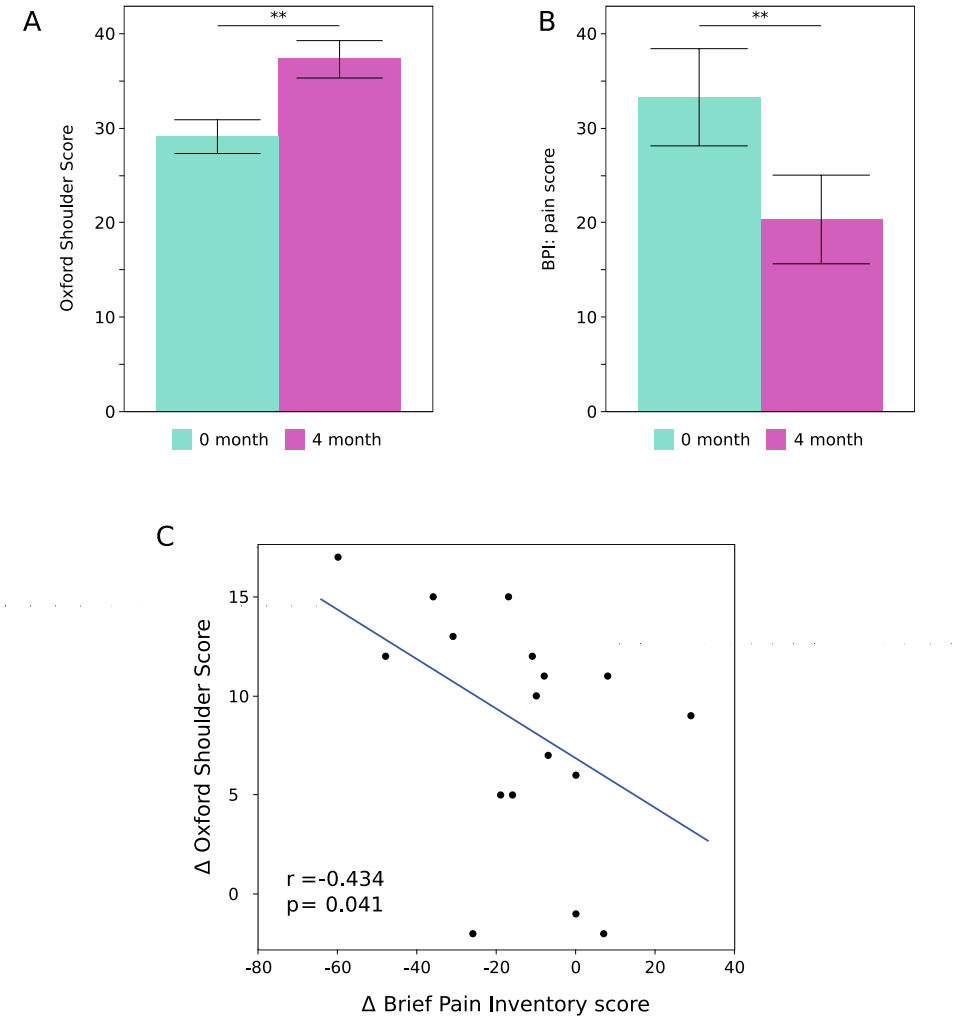


Figure 6.2: *The exercise rehabilitation intervention results in improvements in shoulder function.* A. Patients demonstrated a significant improvement in shoulder function, as quantified by the OSS, comparing measures taken at baseline (0 month) and the first followup (4 month) : paired samples $t$-test: $t(16) = 6.430$, $p < 0.0001$. This finding is consistent with the results of an RCT applying the same exercise rehabilitation intervention (Ainsworth et al., 2009). B. Patients demonstrated a significant reduction in their reported pain scores, as quantified by the BPI, comparing measures taken at baseline (0 month) and the first followup (4 month): paired samples $t$-test: $t(16) = -2.745$, $p < 0.01$. C. The degree of change in the OSS after the intervention showed a moderate negative correlation with the change in the BPI over the same period, suggesting that improvement in shoulder function was associated with a reduction in shoulder pain. ** $p < 0.01$.

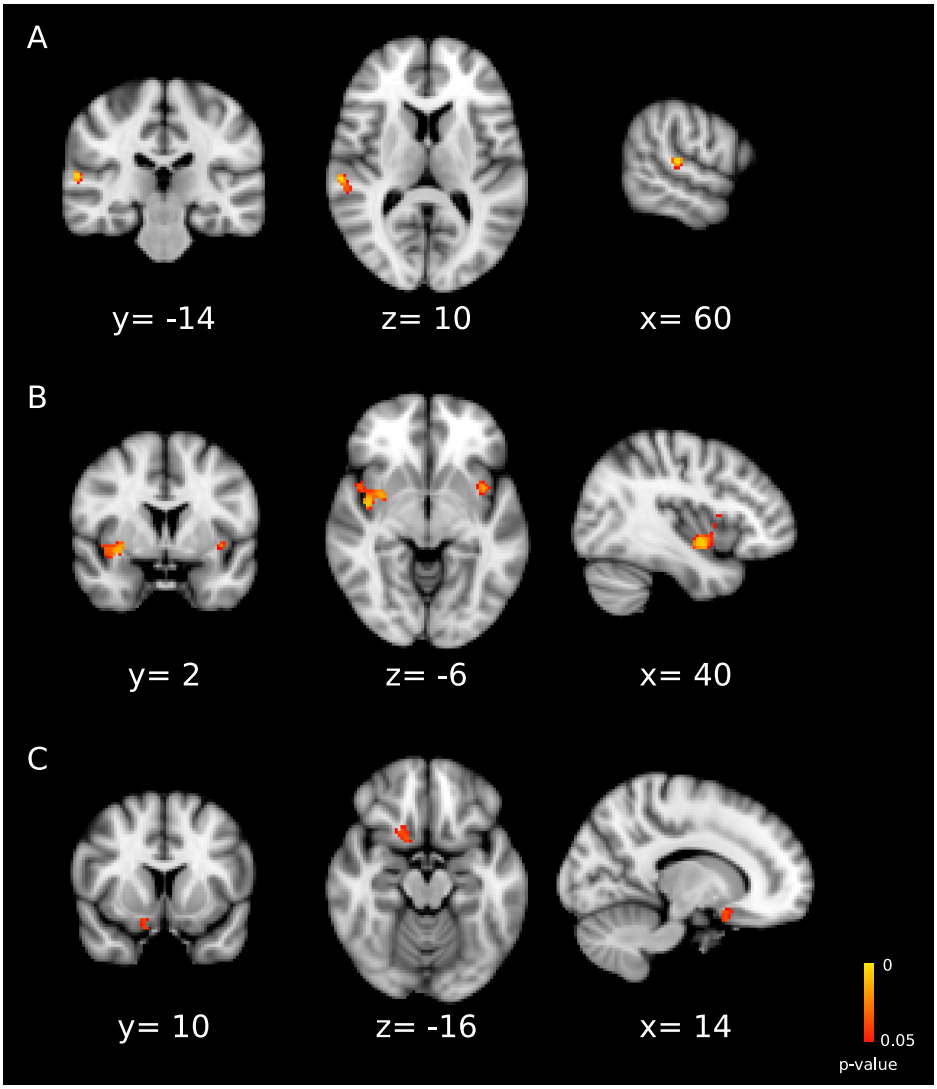


Figure 6.3: *The exercise rehabilitation intervention is associated with localised increases in grey matter density.* Increased grey matter density over the period of the exercise rehabilitation intervention were observed in (A) the posterior right STG, (B) bilateral insular cortex, and (C) right OFC. Full details are provides in table 6.3. Voxel coordinates given in MNI-152 coordinate standard space (mm).

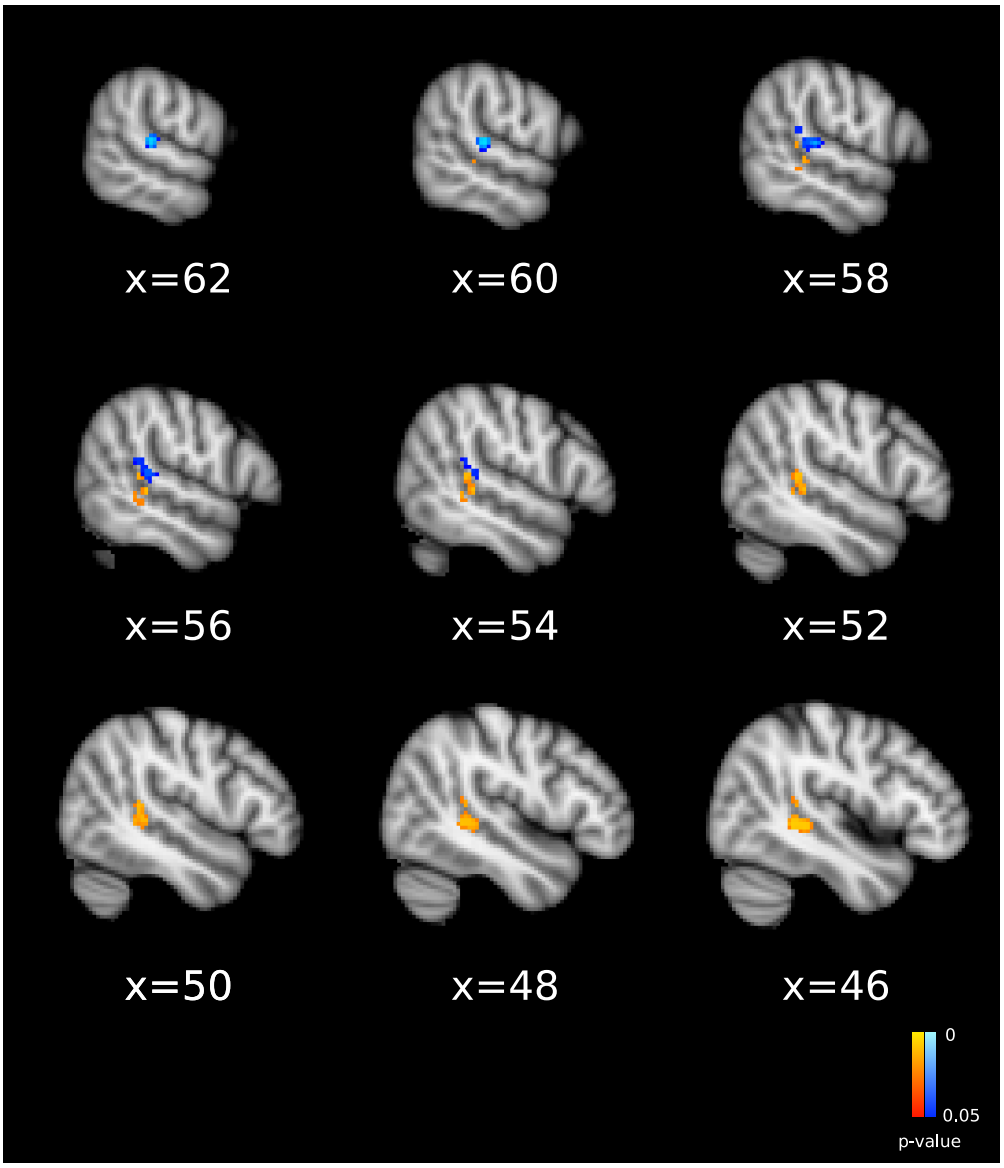


Figure 6.4: *Comparison of grey matter voxel-based morphometry results identified in cross-sectional and longitudinal analysis.* The TPJ VBM cluster identified in Chapter 5 (orange-yellow), in which patients show lower grey matter density than control subjects at baseline, is located directly adjacent to the TPJ VBM cluster identified with longitudinal VBM analysis (blue), in which patients show an increase in grey matter density when comparing measures taken at baseline (0 month) and following the exercise rehabilitation intervention at the first followup (4 month). Data show in MNI-standard space; voxel coordinates given in MNI-152 coordinate standard space (mm).

| Cortical region | Side | MNI (mm) | | | Maximum $t$-value |
|---|---|---|---|---|---|
| | | $x$ | $y$ | $z$ | |
| Posterior division of right STG | R | 60 | -14 | 10 | 10.18 |
| Insular cortex | L/R | 40 | 2 | -6 | 8.10 |
| Orbitofrontal cortex | R | 14 | 10 | -16 | 5.60 |

Table 6.2: *Summary of significant clusters from longitudinal grey matter VBM analysis.* Regions showing significant increases in grey matter density comparing pre-intervention (0 month) and post-intervention (4 month) scans. MNI-152 coordinate standard space (mm). Corrected p-value <0.05. STG: superior temporal gyrus.

### 6.3.3 Longitudinal white matter results

Measures of average FA and RD were extracted from the right SLF and right CST ROIs for at both the baseline (0 month) and first followup (4 month) time points. These data were analysed using a mixed-design ANOVA with a between-subject categorical factor of time (0 month and 4 month), a within-subject categorical factor of tract (SLF and CST), and a dependent variable of diffusion metric. There was no statistically significant interaction between time and tract on the diffusion metrics RD ($p = 0.657$) or FA ($p = 0.694$).

### 6.3.4 Relating behavioural and grey matter changes

Fourteen of the seventeen patients included in the behavioural analysis showed an improvement in OSS after the exercise rehabilitation intervention (Table 6.3). In those patients who did respond to the intervention, there was a moderate positive correlation between the change in the OSS metric, and the change in the average grey matter density in the significant cluster located in the STG at the TPJ: $r(13) = 0.509$, $p = 0.032$. The same correlation across rehabilitation responders and non-responders was not significant: $r(17) = 0.288$, $p = 0.133$. This finding provides some initial evidence to suggest that the greater the improvement in shoulder function during the intervention, the greater the change in grey matter density in this region.

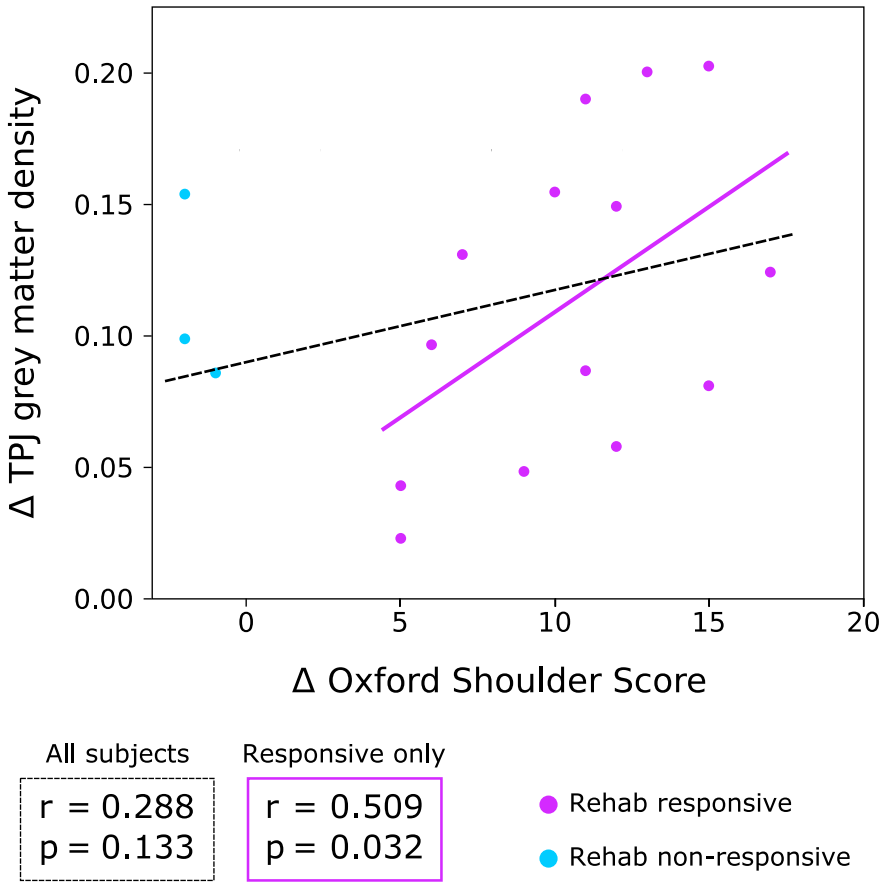


Figure 6.5: *Greater increases in shoulder function are associated with greater improvements in right STG grey matter density in rehabilitation responders.* There is a moderate correlation providing initial evidence to suggest a link between the magnitude of improvement in shoulder function and the magnitude of the increase in grey matter density in the right TPJ identified by longitudinal VBM analysis (Figure 6.3). The same correlation was not significant across both rehabilitation responders and non-responders.

| Subject ID | Age | Gender | OSS 0 month (pre) | OSS 4 month (post) | Change in OSS |
|---|---|---|---|---|---|
| 2 | 83 | F | 20 | 19 | -1 |
| 3 | 82 | M | 23 | 29 | 6 |
| 4 | 73 | M | 26 | 24 | -2 |
| 5 | 85 | F | 16 | 27 | 11 |
| 6 | 75 | M | 29 | 38 | 9 |
| 7 | 81 | M | 37 | 42 | 5 |
| 8 | 84 | F | 27 | 42 | 15 |
| 10 | 82 | M | 38 | 45 | 7 |
| 12 | 68 | M | 24 | 36 | 12 |
| 14 | 64 | M | 43 | 48 | 5 |
| 15 | 78 | M | 27 | 39 | 12 |
| 16 | 86 | M | 18 | 35 | 17 |
| 17 | 65 | M | - | - | - |
| 18 | 82 | M | 36 | 47 | 11 |
| 19 | 80 | M | 26 | 41 | 15 |
| 20 | 84 | M | 30 | 43 | 13 |
| 21 | 80 | M | 30 | 40 | 10 |
| 22 | 64 | M | 37 | 35 | -2 |

Table 6.3: *Summary of OSS changes associated with exercise rehabilitation intervention.* OSS: Oxford Shoulder Score.

## 6.4 Discussion

This chapter presents a preliminary analysis aiming to identify imaging markers of adaptive plasticity associated with improvement in shoulder function and arm use in patients who have experienced chronic disuse of the upper limb as a result of MIRCT. The data presented in this chapter replicate the finding from an RCT presented by my clinical collaborators, demonstrating a significant improvement in shoulder function following a tailored exercise rehabilitation intervention (Figure 6.2) (Ainsworth et al., 2009). However, this work significantly extends upon the clinical finding, providing initial evidence for localised increases in grey matter density from longitudinal analysis of structural MRI data acquired before and after the intervention (Figure 6.3). These increases in grey matter density are located in posterior right STG at the level of the TPJ, bilateral insular cortex, and right OFC. Right TPJ was a region identified in cross-sectional comparison of MIRCT patients and control subjects in Chapter 5; the TPJ cluster identified in the present chapter lies directly adjacent to,

but not overlapping, the cluster identified from cross-sectional comparison at baseline (Figure 6.4). The magnitude of the grey matter increase in the TPJ region showed a marginally significant correlation with the magnitude of improvement in shoulder function (Figure 6.5). Taken together, these findings provide encouraging initial evidence to support a potential role of the right TPJ and its associated right ventral attention network as a region of adaptive plasticity associated with gains in upper limb function following a period of chronic disuse. This will be further substantiated by analysis of the full dataset and comparison with control subjects.

### 6.4.1 Plasticity and the right ventral attention network

The region of significant grey matter change identified in right TPJ is directly adjacent to the region of reduced grey matter intensity identified in MIRCT patients prior to any treatment intervention (figure 5.3A). As discussed in section 5.4.1, the rTPJ is a component of the right ventral attention network and is strongly implicated in attention and the integration of multi sensory stimuli in body perception (Corbetta and Shulman, 2011b). Recent evidence from healthy control subjects has demonstrated right lateralised patterns of activation in the TPJ associated with left/right discrimination tasks (Auer et al., 2008). Further work from Haggard's group applied repetitive transcranial magnetic stimulation (rTMS) over rTPJ, reporting increased ambiguity in perception tasks involving discrimination of proprioceptive and visuo-tactile stimuli (Tsakiris et al., 2008). They argue that rTPJ plays a role in egocentric body perception and the distinction between corporeal and non-corporeal stimuli. Further evidence from the non-human primate literature supports this idea, demonstrating a localised increase in grey matter density in rTPJ associated with intensive learning of a new task designed to integrate a novel tool into the body schema (Quallo et al., 2009). Taken together, these findings concur with the observations made in this study: increased grey matter density in rTPJ following the exercise rehabilitation intervention after a period of upper-limb disuse (Figure 6.3), the magnitude of which correlates with the degree of functional improvement (Figure 6.5).

These results suggest that regaining shoulder use drives adaptive plasticity in the rTPJ; the exercise rehabilitation intervention drives changes in the cortical regions associated with body perception as the previously disused arm is reintegrated into the body schema.

### 6.4.2 Orbitofrontal cortex and sensory reinforcers

OFC is typically considered in the context of decision making and the sensory reinforcers that can exert influence on our choices (Wallis, 2007; Kringelbach, 2005). Evidence from fMRI has demonstrated distinct patterns of activation in different regions of OFC in response to pleasant touch and pain stimuli (Rolls et al., 2003a), arguing for a separation of the affective aspects of touch from the perception of the touch stimuli themselves. A broad meta-analysis of the fMRI literature involving the OFC has revealed a medial versus lateral and posterior versus anterior axis in the apparent functions of the region (Kringelbach and Rolls, 2004). This meta-analysis argued that the more posterior regions of OFC, discussed in this chapter, represent the identity and intensity of a sensory stimulus, which may act as a primary reinforcer in decision making (Craig et al., 2000; Araujo et al., 2003). The activity in this posterior region does not encode the hedonic or affective value.

In contrast, the more affective or emotive aspects of these sensory stimuli, and their influence on decision making, appears to be represented more anteriorly within the OFC, either in medial OFC in the case of pleasant stimuli, or the lateral OFC in the case of punishing or unpleasant stimuli (O'Doherty et al., 2001; Rolls et al., 2003b).

In the context of this literature and the grey matter increase observed in the posterior OFC (Figure 6.3), it is possible that regaining function in the previously disused limb may result in adaptive changes in the encoding of sensory inputs to the OFC originating from the previously disused limb. This change could potentially result from the shift in afferent input, from painful to innocuous stimuli, as the limb itself

is reintegrated into daily use and the overall body representation or schema of the patient.

### 6.4.3 Insular cortex and changes in pain

In this study we show evidence for bilateral increases in grey matter density in the anterior division of insular cortex after the exercise rehabilitation intervention. The insular cortex is a structurally and functionally diverse region of the brain, which functions broadly in multimodal integration of stimuli in an emotion of motivational context. The insula can be divided functionally and on the basis of its connectivity profile into broad anterior and posterior divisions. While the posterior division exhibits connectivity with the primary and secondary sensorimotor cortices, the anterior division displays greater connectivity with the cingulate and other frontal regions (Deen et al., 2011). Various lines of study have implicated the anterior insula in emotional processing in general, specifically the emotional processing of pain stimuli (Baliki et al., 2009; Starr et al., 2009; Wiech et al., 2010).

In the context of the observed reduction in clinical pain scores across the period of the intervention (Figure 6.2B), the increased grey matter density reported here in anterior insula is in keeping with previous studies of pain relief, which report lower grey matter density in insular cortex associated with chronic musculoskeletal pain in comparison with control subjects. This literature also reports longitudinal increases in bilateral anterior insula grey matter density associated with surgical or non-surgical interventions to reduce pain levels (Rodriguez-Raecke et al., 2009; Baliki et al., 2012). It is possible that these changes in the anterior regions relate to reductions in the unpleasantness or affective component of the pain, rather than nociception itself (Baliki et al., 2009; Starr et al., 2009).

### 6.4.4 Limitations and future directions

The results presented in this chapter represent preliminary analysis of an ongoing study, outlined in figure 6.1 and table 6.1. The data presented in this chapter provide

compelling initial evidence for longitudinal plastic change in localised cortical regions, which will be further substantiated with longitudinal analysis involving comparison to an age matched control group, the MRI data from which are currently being acquired. It is important to validate the grey matter changes observed in the MIRCT group in this chapter by comparing them to the ongoing grey matter changes seen in healthy control subjects who are not receiving the exercise rehabilitation intervention. However, in general one would expect a trend towards age-related decline in grey matter density in the control subjects, rather than the focal increase in grey matter density observed here. There is therefore cause to be optimistic in the interpretation of these preliminary longitudinal results. This additional analysis may shed further light on the non-responsive rehabilitation group, particularly considering their shoulder function at 12 months, and whether their lack of response represents a general decline not seen in the rehabilitation responsive group.

Further analysis on the final dataset will also consider the stability of any plastic change induced by the exercise rehabilitation intervention. Data from the RCT investigating the same intervention suggest that behavioural gains in shoulder function are observed directly after the intervention, but diminish over the following nine months (Ainsworth et al., 2009). By assessing longitudinal changes in imaging data at the 12 month scan, it will be possible to ascertain whether the pattern of behavioural gain and loss is mirrored in grey matter change.

## 6.5 Conclusions

The results presented in this chapter provide preliminary evidence for localised plastic change in cortical grey matter associated with recovery of upper limb function in MIRCT patients following an exercise rehabilitation intervention. The right STG at the level of the TPJ, right OFC and bilateral insular cortex all showed increased grey matter density following the intervention. Furthermore, the region of grey matter change in the TPJ was located directly adjacent to a region identified in cross-sectional

comparison of MIRCT patients with control subjects. The magnitude of the change in grey matter density in the TPJ cluster identified showed a correlation with the degree of improvement in shoulder function. Taken together, these results provide encouraging evidence for plastic change associated with the exercise rehabilitation intervention, suggesting that in regaining use of the previously disused limb, patients are promoting structural change in cortical regions responsible for body representation and spatial attention.

# 7 Investigating candidate imaging biomarkers of motor function in sub-acute stroke

*The studies presented thus far in this thesis have considered sensorimotor plasticity driven by processes extrinsic to the brain, such as altered use or disuse. However, as discussed in Chapter 1, neuroplasticity is also prompted by changes in the brain itself, for example in response to pathological insults such as stroke. The ability to relate imaging markers with motor function and recovery after stroke is of particular interest. As a first step to identifying candidate biomarkers to predict the extent of motor recovery, in this chapter I seek to investigate how multimodal imaging markers relate to measures of motor function at the sub-acute stage of stroke recovery. The data presented in this chapter form a part of an ongoing multi-centre clinical trial. On completion of the trial, these data will be used in predictive modelling to better characterise the sub-acute stage of stroke recovery.*

## 7.1 Introduction and rationale

As discussed in section 1.4, the sensorimotor network exhibits a considerable propensity for plastic change, both as a result of changing sensory inputs, and altered motor outputs. Such usage-dependent plasticity has formed the basis of studies presented in this thesis, from short-term changes in fine-grain organisation (Chapter 4), to longer-term evidence of neuroplasticity in the context of arm disuse (Chapters 5 and 6). Beyond such longer-term usage-dependent remapping whose origin is extrinsic

to the brain, there is also evidence for neuroplasticity associated with changes in the brain itself. A key example of such plasticity in seen in stroke, where there is evidence for compensatory changes in brain structure and function following focal damage (Section 1.5.2.1).

Around 80% of patients experience motor impairment after stroke, leaving many with a long-term disability (Jørgensen et al., 1995). The nature of disability can range from total hemiplegia to spasticity, and often more focal loss of fine motor abilities in the affected hand (Langhorne et al., 2009). Only around 1/3 of stroke survivors regain any degree of functional dexterity in the hand (Kwakkel et al., 2003), which is particularly debilitating, impeding independent living in the long-term.

A key aim in clinical studies of stroke is to identify predictors of motor recovery, and tailor programmes of rehabilitation accordingly. At a basic level, the degree of motor disability at the acute or sub-acute stage of stroke offers an indication of long term motor recovery, with greater disability early on associated with poorer outcomes in the long term at the group level (Kwakkel and Kollen, 2007; Chen and Winstein, 2009; Patel et al., 2000). However, the predictive power of such information at the level of individual patients is limited, and therefore more robust predictors are needed.

The advent of advanced MRI techniques has provided a number of potential imaging markers, which could be related to functional deficits in stroke patients (Farr and Wegener, 2010). MRI can provide a range of markers, which can be used in different ways to investigate stroke pathology. Imaging surrogates typically refer to imaging markers that are used to relate the extent of pathology or damage in the brain to clinical or behavioural metrics of dysfunction. Imaging surrogates are typically applied in cross-sectional correlative analysis, commonly in the study of chronic stroke. Imaging surrogates are therefore not strictly predictive. In contrast, imaging predictors refer to metrics typically measured at the more acute stages of stroke, which can be used to foresee the course of recovery, and potentially to inform treatment choices (Stinear, 2010; Farr and Wegener, 2010). Imaging predictors demonstrate the ability

to statistically predict outcome metrics, measured some time later, using a valid test of prediction, such as a bootstrapping approach. The distinction between surrogates and true predictors is important in the discussion of the stroke literature, where studies frequently refer to the predictive value of imaging metrics from cross-sectional analysis alone, which is not strictly accurate.

Various imaging markers have demonstrated a relationship with motor recovery after stroke. A study conducted by Chen and colleagues demonstrated the motor recovery after six months of recovery could be correlated with the lesion profile at one month, a metric which encompassed a combination of lesion sizes and primary location (Chen et al., 2000). Diffusion-weighted MRI metrics have also demonstrated predictive value, with a recent study demonstrating a link between reductions in the apparent diffusion coefficient in the CST of acute stroke patients and poor motor recovery at three months post-stroke (DeVetten et al., 2010). Such predictions have also been made using task fMRI measures; a recent study from Marshall and colleagues demonstrates the value of cortical activation patterns during a simple motor task at the acute stage of stroke in predicting the degree of motor recovery at the three month time point (Marshall et al., 2009).

The predictive value of these imaging measures at the very acute stage of stroke recovery is encouraging for the tailoring of motor rehabilitation interventions. As discussed in section 1.5.2.2, recent evidence from animal models and clinical studies supports the existence of a unique window of post-stroke plasticity at the acute stage, in which behavioural rehabilitative gains can be maximised. However, undertaking the detailed imaging discussed in these predictive studies at the acute stage of stroke recovery is potentially unfeasible in the clinical setting. Nevertheless, a greater understanding of the brain early after the event is vital to better promoting such adaptive plasticity and associated functional gains in motor abilities.

As a first step to identifying candidate biomarkers to predict motor recovery outcome, in this chapter I seek to investigate how multimodal imaging markers relate to

measures of motor function at the sub-acute stage of stroke recovery, when patients are more stable and detailed MRI acquisition is more feasible. More specifically, I apply a combination of diffusion-weighted, structural and resting-state fMRI to derive imaging measures of integrity in the sensorimotor network at the sub-acute stage of stroke recovery (14-60 days post-stroke) and relate these to behaviour measures of motor function and integrity in the motor system. These measures were chosen as they are relatively easy to implement across clinical platforms, and therefore are potentially feasible for measurement in clinical centres.

The data presented in this chapter form a part of an ongoing multi-centre clinical trial investigating the potential for the plastic change at the sub-acute stage of stroke recovery. This chapter aims to identify candidate imaging markers and their relationship to measures of motor function at baseline, which may be useful in future longitudinal analysis and predictive modelling.

## 7.2 Methods

The data presented in this chapter form part of the ongoing FAST INdICATE trial (http://fastindicate.com/home) investigating the clinical efficacy of functional strength training for upper limb motor recovery early after stroke (Pomeroy et al., 2014).

### 7.2.1 Patients

The inclusion and exclusion criteria were as follows: patients aged 18 years or over, recruited 14-60 days after a cerebral infarction affecting cortical and/or subcortical regions. A degree of voluntary muscle contraction adequate to achieve the early stages of prehension was necessary, quantified by motricity index of $> 11/33$ (Section 7.2.3). Patients exhibiting symptoms of spatial neglect or motor dyspraxia in the non-paretic limb were excluded.

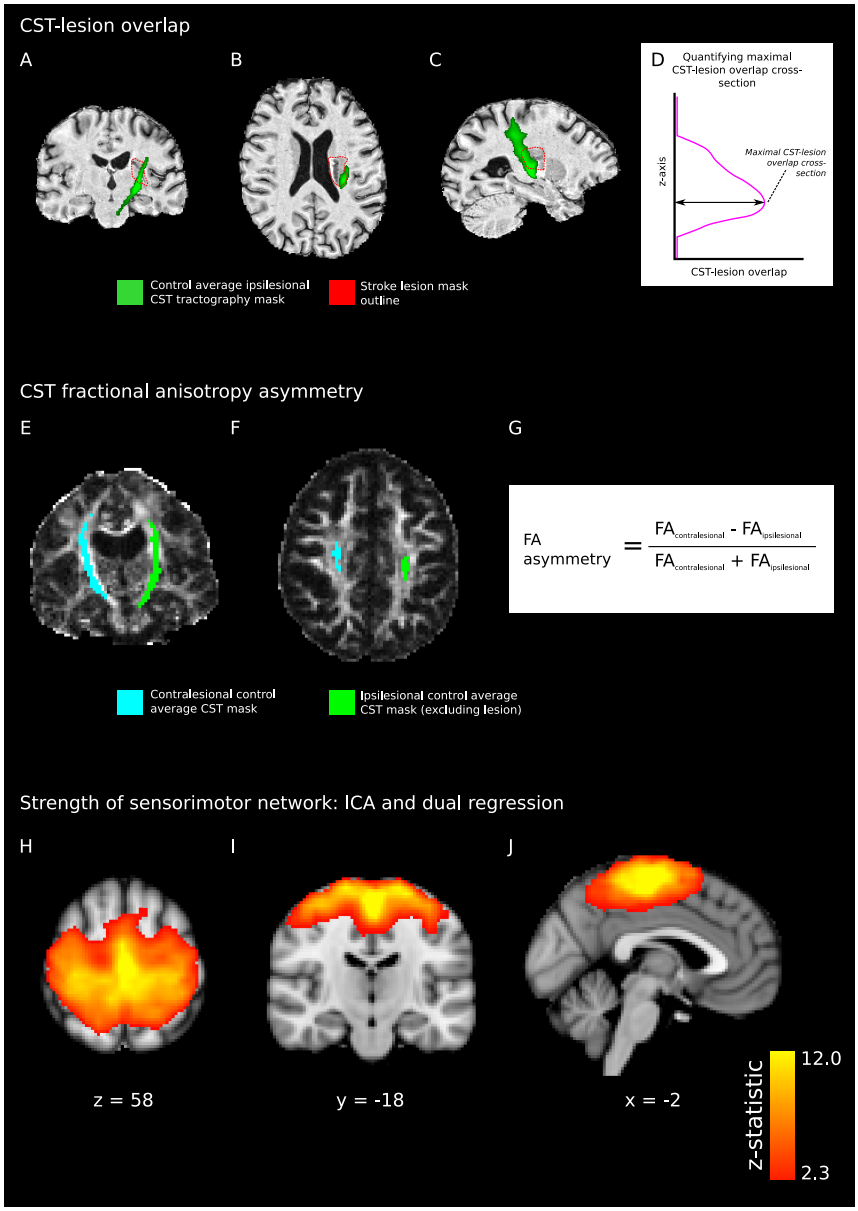


Figure 7.1: *Overview of candidate imaging markers in the sensorimotor network.* This chapter considers multimodal imaging metrics and their relationship with motor function at the sub-acute stage of stroke. Structural imaging metrics (A-C) aim to capture the degree of disruption to the CST (green) by the stroke lesion (red outline), providing a measure of CST-lesion overlap, as well the maximal area of overlap between the lesion mask and the CST masks in a single axial slice: CST-lesion cross-section (D). Diffusion-weighted MRI provides a measure of CST integrity in the ipsilesional hemisphere using a metric of asymmetry (G), which compares the ipsilesional FA in the non-lesioned regions of the CST (E/F; green) to the FA in the contralesional CST (E/F; blue). Resting state fMRI analysed using ICA and dual regression provides a measure of strength or connectivity within the sensorimotor resting state network (H-J).

At the time of writing, 135 patients had been recruited to this multi-centre study. The study is recruiting from three centres and aiming to acquire serial MRI on National Health Service (NHS) scanners. Of those recruited to date, 49 have received baseline MRI (Birmingham: 8, Norwich: 28, Staffordshire: 13). Given the low numbers of scans available from Birmingham and Staffordshire, analysis for this chapter is restricted to patient data acquired from Norwich. At the time of writing, the limited availability of baseline measures of motor function from the clinical trials unit further constrained the analysis to fourteen patients in total.

Fourteen patients at the sub-acute stage of recovery from ischaemic stroke are considered in this chapter. These patients were recruited through the clinical service at Norfolk and Norwich University Hospitals Trust [Mean age: 71.3 ± 7.63; eight female].

### 7.2.2 MRI acquisition

MRI data presented in this chapter were acquired at the Clinical Imaging and Research Centre at the Norfolk and Norwich University Hospitals Trust and the University of East Anglia using a General Electric Discovery MR750w 3.0T system (General Electric, Fairfield, CT, USA).

Structural MRI data were acquired using a T1-weighted 3D inversion recovery prepared FSPGR sequence (MPRAGE equivalent, matrix 256 x 265, 1x1x1mm resolution, 206 axial slices, TE: 3.7ms, TR: 9.1s, flip angle: 8°). Proton-density/T2-weighted images were acquired using a dual-echo fast spin echo (FSE) sequence (matrix 256 x 256, 0.7 x 0.7 x 3.0mm resolution, 50 axial slices, $TE_1$: 13ms, $TE_2$: 105ms, TR: 4670ms).

Diffusion-weighted MRI data were acquired using a two-dimensional SE EPI sequence (matrix 128 x 128, 2x2x2mm resolution, 62 axial slices, TE: 50.0ms, TR: 17000ms, flip angle 90°) with 64 isotropically distributed diffusion directions (b-value: 1500s.mm$^{-2}$) and 4 b=0 images.

Resting state BOLD fMRI data were acquired using a two-dimensional GE EPI sequence (matrix 64 x 64, 3x3x3mm resolution, 48 axial slices, TE: 30.0ms, TR: 3000ms, flip angle 90°, 200 measurements; 10 minute acquisition).

### 7.2.3 Motor function measures

#### 7.2.3.1 Wolf motor function test

Each patient undertook the Wolf motor function test (WMFT) on the same day as the MRI session. This 15-item test has been designed for use with stroke survivors. The test assesses both the time taken to produce a set of movements, and the quality of the movements themselves. The movements are based around 15 functional tasks, from simple actions (e.g. placing forearm on table) and complex tasks (e.g. turning key in lock). The WMFT has been rigorously validated and shows a high degree of reliability (Wolf et al., 2001; Morris et al., 2001).

#### 7.2.3.2 Pinch grip measures

Maximal pinch grip measures were also collected on the same day as the MRI session using a digit pinch analyser (MIE Medical, Leeds, UK). The position of the upper limb was standardised across subjects (Fasoli et al., 2002). Participants were instructed to "squeeze as hard as you can" with the index finger and thumb of their stroke affected hand. Measurements were repeated three times, separated with rest intervals. An average of the three trials repeat measures was calculated.

### 7.2.4 TMS measures

Patients attended attended a TMS session on the same day as the MRI session. TMS was applied using a standard figure of eight coil and stimulator (Magstim, Whitland, UK). Single pulses of TMS were applied over the hand and arm representation in the primary motor cortex of the stroke affected hemisphere. Motor output was monitored

using EMG recordings of MEPs on the first interosseous muscle of the hand. During TMS, with their arm supported and palm facing upwards, patients were asked to extend their wrist, raising their palm away from the table.

TMS was used to measure the active motor threshold, which was defined as the minimum single pulse stimulator intensity required to elicit an MEP of greater than 200mV on more than five out of 10 trials during muscle contraction of 20% of maximum voluntary output. Single pulse TMS measurements used in combination with the recording of MEPs have been shown previously to provide a useful measure of corticospinal tract integrity and motor excitability (Ridding and Rothwell, 1997; Ward et al., 2003).

### 7.2.5 MRI analysis

#### 7.2.5.1 Data aligment relative to stroke hemisphere

In order to achieve uniform ipsilesional/contralesional laterality in the MRI data, images were left-right flipped such that stroke lesions were consistently located in the left hemisphere. Hereafter the left hemisphere is therefore referred to as ipsilesional, and the right hemisphere is referred to as contralesional. T1/T2-weighted structural MRI and functional MRI data were aligned this way prior to any analysis. Diffusion-weighted MRI data were aligned this way after the diffusion parameter maps had been calculated (Section 7.2.5.4).

#### 7.2.5.2 Image registration

All image registration was undertaken using MRI images after the alignment process described in the previous section. Within-subject image registration was undertaken using FLIRT (Jenkinson and Smith, 2001; Jenkinson et al., 2002). Structural proton-density/T2-weighted and MPRAGE images were co-registered (Degrees of freedom: 6, cost function: normalised correlation). MPRAGE and b=0 images from the

diffusion-weighted MRI acquisition were co-registered (Degrees of freedom: 6, cost function: normalised correlation).

MPRAGE images were registered to MNI-152 standard space using a combination of non-linear warps and linear transformation matrices calculated in FNIRT (Andersson et al., 2007a; Andersson et al., 2007b) and FLIRT (Jenkinson and Smith, 2001; Jenkinson et al., 2002) respectively.

#### 7.2.5.3 Lesion masking

The stroke lesion was manually segmented using the proton-density and T2-weighted images using FSLView according to previous imaging guidelines. Lesion masks were resampled into MPRAGE structural space for further analysis (Figure 7.1A-D). Regions underlying lesion masks were excluded from inter-subject registration calculations, as outlined in section 2.7.6.2.

#### 7.2.5.4 Diffusion-weighted MRI analysis

Diffusion-weighted MRI data were used to quantify the integrity of the CST bilaterally. After correction for eddy-current induced distortion, maps of FA and RD were calculated using FSL DTIfit (Behrens et al., 2003), a part of the FDT in FSL (Smith et al., 2004). In order to define a template of the CST, multi-fibre probabilistic tractography was performed (Probtrackx2, FDT) (Behrens et al., 2007) using a separate diffusion-weighted MRI dataset acquired independently in Oxford. This dataset was composed of fifteen subjects [Mean age: 30.1 ± 4.71; two female; two left-handed], acquired using a Siemens Sonata 1.5T scanner at the Oxford Centre for Magnetic Resonance, Oxford, UK, with a maximum gradient strength of 40mT/m. Three sets of whole head EPI data were acquired with 60 isotropically distributed diffusion directions (b-value: 1000s.mm$^{-2}$) and 8 b=0 images, and an isotropic resolution of 1.5mm. Tractography was undertaken to trace both the left and right CST. On both sides, the tractography was run twice in each control subject, with

masks of the primary motor cortex and the medullary pyramids as reciprocal seeds and waypoints. The resulting tractography outputs were normalised and averaged within subject to produce a single left and right CST tract. These tracts were resampled into MNI-152 standard space using non-linear warps calculated in FNIRT (Andersson et al., 2007a; Andersson et al., 2007b). An average left and right CST tract was calculated, and thresholded at 30% of the maximum, and binarised to provide template masks of the CST for further analyses.

**CST-lesion overlap and cross-section** Average CST masks were used to quantify the degree of overlap between the stroke lesion and the typical path of this white matter structure. The lesion masks from individual subjects were resampled into MNI-152 standard space (interpolation: nearest neighbour) using non-linear warps calculated in FNIRT (Andersson et al., 2007a; Andersson et al., 2007b). CST-lesion overlap was calculated in $mm^3$ (Figure 7.1A-C), as well as a measure of CST-lesion cross-section in $mm^2$. The CST-lesion cross-section measure was calculated as the maximum area of overlap between the lesion mask and the CST masks in a single axial slice (Figure 7.1D).

**Diffusion metrics in the CST** Average CST masks were resampled into diffusion space of individual subjects using non-linear warps calculated in FNIRT (Andersson et al., 2007a; Andersson et al., 2007b). A measure of average FA was calculated in the contralesional CST mask, and in the ipsilesional CST mask, excluding the regions overlapping with the lesion mask (Figure 7.1E-G). Average values of ipsilesional and contralesional FA were used to calculate the asymmetry therein (Stinear et al., 2007) using the following equation:

$$FA\ asymmetry = \frac{FA_{contralesional} - FA_{ipsilesional}}{FA_{contralesional} + FA_{ipsilesional}}$$

#### 7.2.5.5 Resting state fMRI analysis

Resting state fMRI analysis was undertaken using Multivariate Exploratory Linear Optimized Decomposition into Independent Components (MELODIC), part of FSL (Smith et al., 2004; Beckmann et al., 2005; Jenkinson et al., 2012). Standard pre-processing was run on individual subject data, including MCFLIRT motion correction, brain extraction, spatial smoothing with a Gaussian kernel of 6mm FWHM and a high pass temporal filter of 150s. Registration between BOLD EPI images and MPRAGE structural images was undertaken using FLIRT (Jenkinson and Smith, 2001; Jenkinson et al., 2002), and optimised with BBR (Greve and Fischl, 2009). MPRAGE structural images were registered to MNI-152 standard space using FNIRT (Andersson et al., 2007a; Andersson et al., 2007b), to allow for group level analysis in a common space. Group-level analysis was undertaken using dual regression, described previously in imaging studies (Filippini et al., 2009).

The use of ICA to derive a measure of sensorimotor network strength has been described previously (Stagg et al., 2014). The analysis can be divided into three steps. First, the data from all patients were concatenated and decomposed using ICA into 25 resting state networks, identified by spatial cross-correlation with established network maps (Beckmann et al., 2005). The map of the sensorimotor network from the group-average analysis (Figure 7.1H-J) was used to generate subject-specific versions of the spatial maps, and associated timeseries, using dual regression as follows (Filippini et al., 2009). First, for each subject, the group-average set of spatial maps is regressed (as spatial regressors in a multiple regression) into the subject's 4D space-time dataset. This results in a set of subject-specific timeseries, one per group-level spatial map. Next, those timeseries are regressed (as temporal regressors, again in a multiple regression) into the same 4D dataset, resulting in a set of subject-specific spatial maps, one per group-level spatial map.

The single-subject maps of the sensorimotor network were then masked by the group-average map of the sensorimotor network. For each subject, the average beta value

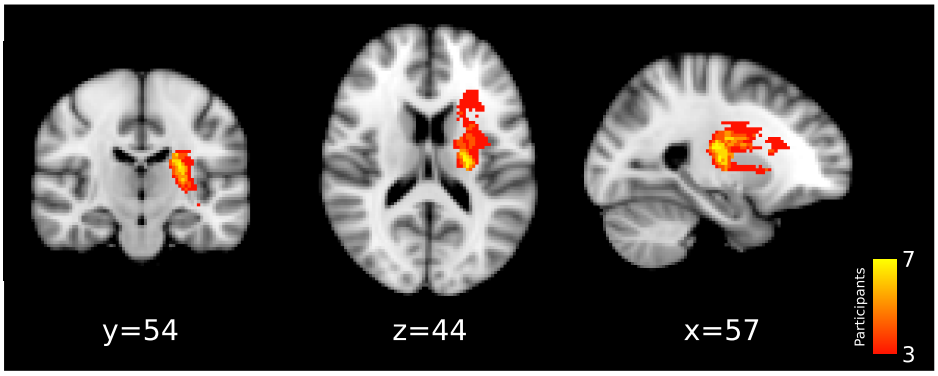


Figure 7.2: *Overview of the ischaemic lesion location in the patient group.* A summary of the lesion location in the patient group, flipped such that the ipsilesional side is consistently the left hemisphere. Lesions are shown in MNI-152 standard space. Colour scale represents number of patients in which a voxel is included in the lesion mask, with a colour-bar maximum of seven for clarity; 14 patients included in the construction of the lesion map.

within this group-mask was taken as a metric of the strength of functional connectivity within the sensorimotor network.

### 7.2.6 Statistics

All statistical analysis and graphing were undertaken using JMP (Version 11.0, SAS Institute, Cary, NC, USA) and Statistics Package for the Social Sciences (Version 19.0, IBM Corporation, Armork, NY, USA). All correlation metrics represent Pearson correlation coefficients (two-tailed).

## 7.3 Results

All MRI data were visually inspected to check for the presence of excessive subject motion. No MRI data were excluded from the analysis. Lesion mapping revealed a focus of ischaemic damage in the posterior limb of the internal capsule in the patient population under study, summarised in figure 7.2.

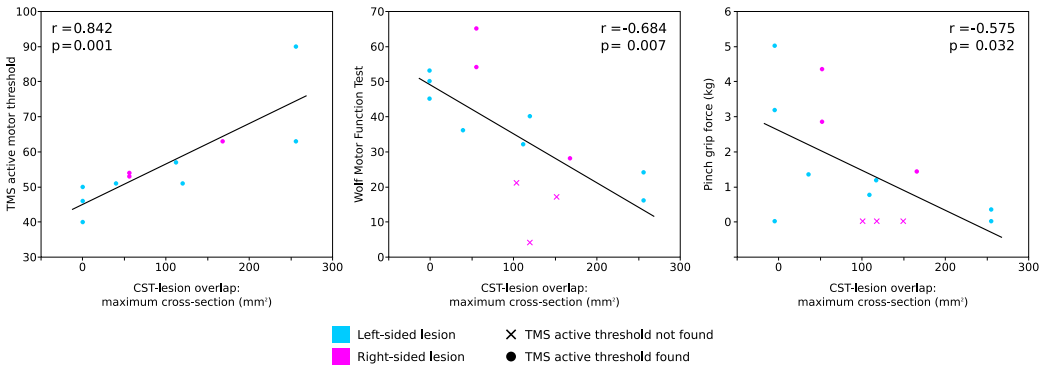


Figure 7.3: *Correlations between CST-lesion cross-section and measures of motor function.* Strong correlations were observed between CST-lesion cross-section and measures of motor function. The correlations between CST-lesion cross-section and both TMS motor threshold and WMFT score are both significant when adjusting for multiple comparisons (Bonferonni corrected $p$ <0.017.

### 7.3.1 CST-lesion overlap measures

It is not clear how best to calculate the effect of lesions on the CST. Therefore, two different measures of overlap between the CST and the stroke lesion were calculated: the total volume of CST-lesion overlap, referred to hereafter as CST-lesion overlap (Figure 7.1A-C), measured in $mm^3$, and CST-lesion cross-section (Figure 7.1D), measured in $mm^2$.

CST-lesion cross-section showed individually significant strong correlations with all three measures of motor function (Figure 7.3). There was a strong positive correlation between CST-lesion cross-section and TMS motor threshold: $r(9) = 0.842$, $p = 0.001$, such that patients who had larger cross-sectional overlaps, and therefore greater CST damage, also had higher TMS thresholds. There was a strong negative correlation between CST-lesion cross-section and the total WMFT score: $r(12)$ = -0.648, $p$ = 0.007, such that patients who had larger cross-sectional overlaps in the CST also exhibited poorer motor skills in the WMFT. There was a strong negative correlation between CST-lesion cross-section and pinch grip force: $r(12)$ = -0.575, $p$ = 0.032, such that patients who had larger cross-sectional overlaps in the CST also showed lower maximal pinch grip scores. The correlations between CST-lesion cross-section

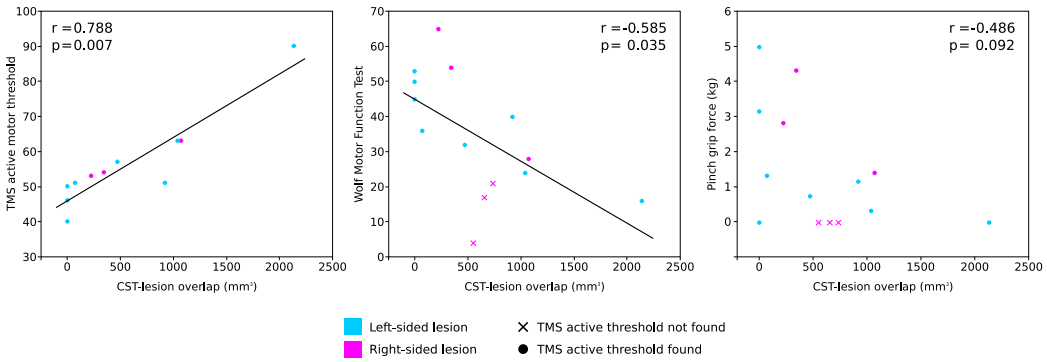


Figure 7.4: *Correlations between CST-lesion overlap and measures of motor function.* Strong correlations were observed between CST-lesion overlap and both TMS motor threshold and WMFT score. Only the correlation between CST-lesion overlap and TMS motor threshold was significant when adjusting for multiple comparisons (Bonferonni corrected $p < 0.017$).

and both TMS motor threshold and WMFT score are both significant when adjusting for multiple comparisons (Bonferonni corrected p< 0.017).

CST-lesion overlap showed a strong positive correlation with TMS motor threshold: $r(9) = 0.788$, $p = 0.007$, such that greater disruption to the CST was associated with higher TMS thresholds (Figure 7.4). CST-lesion overlap also showed a strong negative correlation with the total WMFT score: $r(12) = -0.585$, $p = 0.035$, such that greater disruption to the CST was associated with poorer motor performance in the WMFT. There was a trend toward a negative correlation between CST-lesion overlap and pinch grip force: $r(12) = -0.486$, $p = 0.092$. Only the correlation between CST-lesion overlap and TMS motor threshold was significant when adjusting for multiple comparisons (Bonferonni corrected p< 0.017) (Figure 7.4).

Total lesion volume was also correlated with behavioural metrics using non-parametric correlation coefficients. No correlations were significant.

### 7.3.2 CST FA asymmetry

CST FA asymmetry showed a negative correlation with pinch grip force: $r(12) = -0.586$, $p = 0.028$ (Figure 7.5). However, this correlation was not significant when adjusting for multiple comparisons (Bonferonni corrected $p < 0.017$).

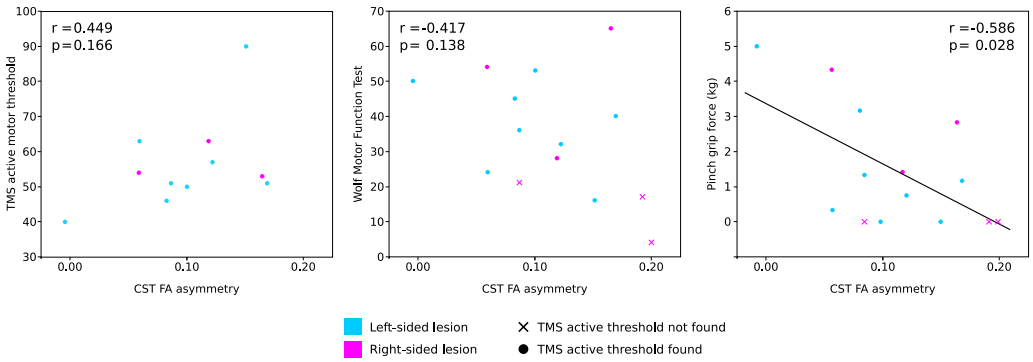


Figure 7.5: *Correlations between CST FA asymmetry and measures of motor function.* CST FA asymmetry showed a strong correlation with pinch grip force only. This correlation was not significant when adjusting for multiple comparisons (Bonferonni corrected p< 0.017).

### 7.3.3 Sensorimotor network strength

A measure of the strength of the sensorimotor network was derived from analysis of resting-state fMRI data, as outlined in section 7.2.5.5. The strength of the sensorimotor network showed a strong negative correlation with the total WMFT score: $r(12)$ = -0.625, $p$ = 0.017. The strength of the sensorimotor network also showed a strong negative correlation with pinch grip force: $r(12)$ = -0.608, $p$ = 0.021. Only the correlation between the strength of the sensorimotor network and the total WMFT score was significant when adjusting for multiple comparisons (Bonferonni corrected p< 0.017) (Figure 7.6).

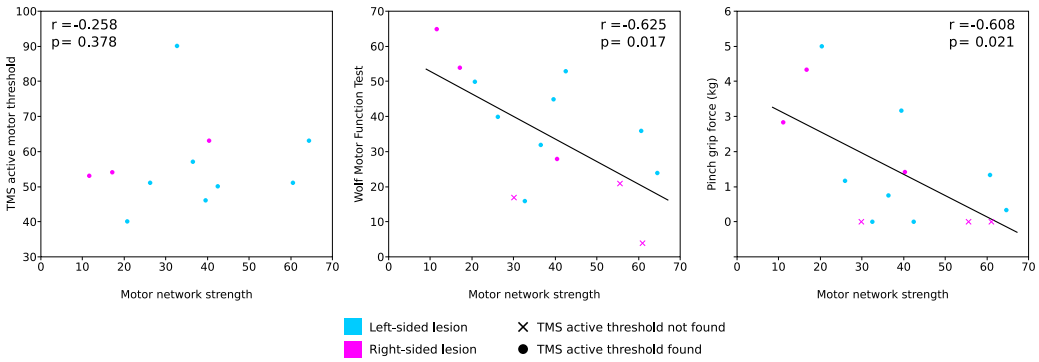


Figure 7.6: *Correlations between strength of the sensorimotor network and measures of motor function.* The strength of the sensorimotor network, derived from resting-state fMRI analysis (Section 7.2.5.5) showed a strong negative correlation with both total WMFT score, and with pinch grip force. Only the correlation between the strength of the motor network and total WMFT score was significant when adjusting for multiple comparisons (Bonferonni corrected $p$ <0.017).

## 7.4 Discussion

This chapter aimed to assess the relationship between a variety of multimodal neuroimaging markers and behavioural measures of motor function or integrity in the motor system at the sub-acute stage of stroke recovery. This work forms an initial validation of imaging markers early after stroke for potential use in longitudinal analysis of an ongoing clinical trial spanning the period of 14 days to 60 days post-stroke (http://fastindicate.com/home). The data in this chapter broadly demonstrate relationships between measures of motor function, including clinical scores, and imaging markers of integrity in the sensorimotor system, derived from a combination of MRI modalities. These markers range from structural metrics relating directly to the ischaemic lesion, as well as broader metrics of functional connectivity, relating to the off-target effects of the stroke lesion across the entire sensorimotor network. Equally, the measures of motor function range from TMS-derived metrics providing a neurophysiological measure of CST integrity to broader clinical motor scores, which encompass of qualitative aspects of motor performance across a range of tasks. The diversity in these measures is reflected in the results presented in this chapter, which, as might be expected, demonstrate that each imaging marker shows stronger

association with specific measures of motor function.

### 7.4.1 Structural measures of CST disruption

The degree of overlap between the CST and stroke lesion demonstrated a strong correlation with the three measures of motor function: maximal pinch grip, WMFT score and TMS active motor threshold in the paretic hand (Figures 7.3 and 7.4). These data suggest that greater the disruption of the CST by the stroke lesion is associated with a higher TMS active motor threshold in the paretic hand, a lower overall score on the WMFT, and a low maximum pinch grip force in the paretic hand. These correlations were seen for both the CST-lesion overlap (Figure 7.4) and for the CST-lesion cross-section (Figure 7.3).

In the context of disconnection between the primary motor cortex and descending motor tracts, the CST-lesion cross-section metric is arguably a more intuitive measure of white matter disruption, less prone to outlying values resulting from extensive lesion volume seen in figure 7.4. This finding is consistent with previous work with a mixture of 24 sub-acute and chronic stroke patients, which assessed volume based and cross-section based metrics of CST disruption (Pineiro et al., 2000). This study suggested a strong linear correlation between the cross-sectional area of the corticospinal tract disrupted by a stroke lesion a behavioural measure of motor function.

The results presented here go further, demonstrating not only a relationship between CST-lesion cross-section and motor function (WMFT and the maximal pinch grip), but also a very strong positive correlation between CST-lesion cross-section area and the TMS-derived active motor threshold. This demonstrates a strong association between the degree of disruption to the descending motor system, and the ability of a single pulse of TMS directed at the primary motor cortex to elicit movement in the hand. The strong association between the measure of structural connectivity from the MRI data, neurophysiological measures of white matter connectivity, and motor function tests raises CST-lesion cross-section as a strong candidate structural

imaging marker for upper limb function at the sub-acute stage. Given the degree of correlation between CST-lesion cross-section and the TMS active motor threshold in the upper limb, there is potential for TMS alone as a tool to interrogate the integrity of the CST, where imaging is not feasible or available in the clinical setting.

The relative merits of CST-lesion overlap and CST-lesion cross-section are much debated (Pineiro et al., 2000; Zhu et al., 2010; Sterr et al., 2010). In this relatively small study, CST-lesion cross-section shows a stronger correlation with all three behavioural measurements. It remains unclear to what extent CST-lesion cross-section would generalise to motor function beyond the upper limb; evidence from studies of locomotion suggest that the relationship between CST disruption by stroke lesions and lower limb motor function are not readily apparent, perhaps due to the relatively bilateral innervation of the proximal muscles of the lower limb (Dawes et al., 2007; Jayaram et al., 2012).

### 7.4.2 Sensorimotor network connectivity and stroke

The data presented in this chapter demonstrate a strong negative correlation between the strength of the sensorimotor network and motor function at the sub-acute stage of stroke, represented by both WMFT and maximum pinch grip force (Figure 7.6), such that greater strength of the sensorimotor network is associated with poorer clinical and behavioural measures of motor function. It is well-established that motor deficits after a stroke are accompanied by imbalance in task-evoked cortical activity (Grefkes et al., 2008), the severity of which has been linked to motor impairment (Ward et al., 2003). Evidence from longitudinal studies suggests that movement related overactivity in the contralesional hemisphere is frequently associated with poor motor recovery in chronic stroke patients (Laible et al., 2012).

Resting state analysis at the acute stage of stroke recovery ($< 8$ days) has reported reduced interhemisphic functional connectivity between the primary motor cortices, and increased connectivity between ipsilesional motor cortex and premotor areas

compared with control subjects; the magnitude of both of these phenomena was associated with the severity of the motor deficits in hand function (Rehme et al., 2014). Recent resting state fMRI studies of chronic stroke patients support increased connectivity within the sensorimotor network in stroke patients compared with age matched controls (Wang et al., 2014), as reported in this chapter at the sub-acute stage. However, increased inter-hemispheric connectivity at the chronic stage of stroke recovery has also recently been associated with improved motor function in the hand (Chen and Schlaug, 2013); the exact role of cortico-cortical connectivity in long-term stroke recovery remains unclear.

The functional metric considered in this chapter is based on resting state rather than task-evoked activity. Although the basis for resting state correlations in the BOLD signal is still debated (Fox and Raichle, 2007; Heuvel and Hulshoff Pol, 2010; Lu and Stein, 2014), it is widely accepted that resting state network strength provides some measure of functional connectivity across a distributed network. The metric of resting state network strength has been reported previously to be negatively correlated with the degree of GABAergic inhibitory activity within the sensorimotor network in healthy individuals (Stagg et al., 2014). This work suggests that the strength of a resting state network in part reflects inhibitory GABAergic tone. In the current chapter, there is a strong association between increased strength of the sensorimotor network and poor motor function, concurring with previous studies at the chronic stage of recovery (Wang et al., 2014). This finding is consistent with reports of perturbed interhemispheric inhibition in the brain after stroke. The literature suggests that imbalance in cortical activity, potentially via degeneration of transcallosal fibres (Wang et al., 2012), leads to disinhibition of the contralesional cortex (Hummel and Cohen, 2006). While beneficial initially (Rehme et al., 2014), it is argued that this increased contralesional activity suppresses the ipsilesional hemisphere in the long term, leading to poor motor function (Ward et al., 2003; Wang et al., 2014).

In the context of this evidence, I hypothesise that the association between increased

strength or connectivity of the sensorimotor network and poorer motor function may reflect the phenomenon of disinhibition at the sub-acute stage of stroke. When individuals with poor motor function attempt to make movements, the cortical imbalance and increased connectivity in the network (Wang et al., 2014) leads to deficits in effective motor outflow, and as a result, an impaired ability to make controlled movements. The idea of disinhibition in the motor network is further supported by a recent magnetic resonance spectroscopy study, which demonstrated lower levels of inhibitory GABA in the primary motor cortex of chronic stroke patients compared with controls participants (Blicher et al., 2014).

### 7.4.3 Diffusion measures of CST integrity

Changes in diffusion MRI-derived metrics have been well reported in the stroke literature, and the degree of change in the ipsilesional CST has been broadly associated with both changes in functional connectivity, as well as motor function and the potential for motor improvement (Stinear et al., 2007; Jayaram et al., 2012). The data presented in this chapter demonstrate a correlation between CST FA laterality and pinch grip score, but no such association between FA laterality and TMS active motor threshold or WMFT. Evidence from the acute stroke literature suggests that the apparent diffusion coefficient in the CST of acute stroke patients is decreased in those patients who subsequently experience poor motor recovery (DeVetten et al., 2010). However, this reduction in those who recovered poorly was greatest at seven days post-stroke, and the difference was not seen at 30 days onwards. In the context of this literature, it is possible that changes in diffusion metrics associated with Wallerian degeneration in the CST are greatest early after stroke, and in the chronic stages. However, the ongoing changes associated with recovery and remodelling may mask any potential relationship between diffusion MRI-derived measures of CST integrity and motor function.

### 7.4.4 Limitations and future directions

This chapter represents a small preliminary analysis of a dataset from the ongoing FAST INdICATE trial. This trial is a large, multi-centre randomised clinical trial, including the acquisition of imaging data at three centres, using three different scanner platforms. At the time of writing, only small datasets were available from each clinical site, and therefore a large group analysis was not feasible. Furthermore, given the issue of randomisation and blinding in the trial, there was no possibility of followup behavioural data being released prior to the trial end point to facilitate predictive analysis of baseline scan data. Longitudinal analysis will be undertaken at the trial end point. This analysis will consist of both a comparative analysis of the cortical and behavioural changes associated with the rehabilitation interventions under study and a more multimodal connectomics approach to assess how motor recovery is associated with changes in the function and structural connectivity of the brain as a whole. Furthermore, predictive modelling analysis will assess to what extent these connectomics-based imaging metrics at baseline might be useful as predictors of recovery and respond to rehabilitation as patients progress from the sub-acute to chronic stages.

## 7.5 Conclusions

This chapter sought to investigate candidate imaging markers and their relationship to measures of motor function at the sub-acute stage of stroke recovery. The analysis approach considered a multi-modal array of imaging measures, as well as a range of metrics of motor function and integrity in the descending motor system.

The correlations presented in this chapter provide encouraging initial evidence for the potential utility of CST-lesion cross-section and sensorimotor network strength as candidate markers of motor function at the sub-acute stage of stroke. The data presented here provide a strong impetus for these markers to be investigated further

in the large dataset currently being compiled as a part of the FAST INdICATE trial. This further study will determine both the predictive value of these imaging markers in terms of motor outcomes, and it will also provide an insight into the nature of reorganisation and remodelling at the sub-acute stage of stroke, prior to the onset of the chronic stages of recovery at six months and beyond.

# 8 Conclusions and future directions

*This chapter outlines the main findings presented in this thesis, and assesses the overall conclusions that can be drawn from the data therein. This chapter also considers the additional questions that have been raised by the work contained in this thesis, and what future work might be warranted to address these questions. Finally, general conclusions are outlined, including the potential future relevance of the findings presented in this thesis to specific populations and patient groups.*

## 8.1 Overview of the thesis

This thesis comprises a series of experiments designed to investigate experience-dependent and usage-dependent plasticity in the sensorimotor network of the human brain. It has employed a variety of MRI modalities in order to investigate the propensity for both short-term and long-term neuroplastic phenomena, particularly considering subtle peripheral manipulations or deficits, and their potential to shape the sensorimotor network.

In Chapter 3, I sought to develop a rapid and easily-implemented paradigm to map the sensory representations of the digits in the primary somatosensory cortex at the single-subject level. The ability to map this organisation within the primary somatosensory cortex was crucial for the subsequent study described in Chapter 4, investigating short-term plasticity. In order to map the digit representations at the single-subject level, I applied high-resolution fMRI at 7.0 tesla using an atypical

phase-encoding paradigm. I specifically aimed to develop a mapping paradigm that was easily implemented in the scanner, could be undertaken in a short fMRI run, produced reproducible maps over time, and which concurred with more traditional mapping techniques from a block design and GLM analysis. The results of this work demonstrated that the 10 minute phase-encoding paradigm that I designed was able to consistently resolve maps of digit representations on the postcentral gyrus. These maps showed a high concordance with the results of a more traditional block design, but yielded greater specificity in resolving the smooth topography present in the sensory regions of the anatomical hand knob. Furthermore, the maps showed a high degree of spatial reproducibility, even over an interval as long as four weeks. The paradigm developed in Chapter 3 provided a valuable tool for longitudinal studies of plasticity.

In Chapter 4, I applied the digit mapping paradigm developed in Chapter 3 to investigate the potential for short-term experience-dependent plasticity in the primary somatosensory cortex digit somatotopy. This chapter involved a longitudinal experiment to assess the effects of a manipulation in which participants had the index and middle fingers of their right hand glued together for a period of 24 hours. I assessed the potential for alterations in the overlap of adjacent digit representations as a result of this manipulation. The results of the within-subject analysis demonstrated a propensity for functional reorganisation of fine-grain primary somatosensory cortex topography over a period of just one day. There was a marked shift in the cortical overlap of adjacent digits after the glued manipulation, which was not seen across the control condition. Specifically, gluing together digit two (index finger) and digit three (middle finger) induced a reduction in the cortical overlap of the digit three (middle finger) and digit four (ring finger) representations, and an increase in the cortical overlap of the digit four and digit five (little finger) representations. This off-target experience-dependent plastic change raised fundamental questions regarding the organisation of the primary somatosensory cortex, and has implications in the study of a range of specific populations groups, including patients with focal hand

dystonia and the ageing population who show compromised dexterity.

In Chapter 5, I presented the results of a study undertaken in collaboration with Torbay Hospital. This work aimed to investigate the imaging markers of plasticity associated with chronic unilateral disuse of the upper limb following massive irreparable rotator cuff tear. In this chapter I applied a cross-sectional analysis to compare grey matter and white matter structure in this patient group with an age-matched control group. Furthermore, I sought to relate any observed differences in imaging metrics to clinical measures of upper limb use in the patient group. The results presented in this chapter provided clear evidence for structural differences in both grey matter and white matter in the right ventral attention network when comparing patients and controls. Specifically, the patient group showed reduced grey matter density in the posterior right STG component of the TPJ, and increased RD in the white matter of the right SLF; both of these metrics are suggestive of reduced structural integrity. Furthermore, the markers of grey matter and white matter structure showed a strong correlation with a behavioural measure of limb use in the patient group, suggestive of a usage-dependent pattern of structural change associated with the severity of disuse.

The work presented in Chapter 6 built upon the cross-sectional analysis presented in Chapter 5. In this chapter I outlined a preliminary analysis of a large longitudinal MRI dataset which sought to identify adaptive plasticity associated with a targeted exercise based rehabilitation programme designed improve function in the limb after a period of chronic disuse. The results of longitudinal grey matter analysis demonstrated localised increases in grey matter density after the exercise rehabilitation intervention, notably in the right TPJ, located directly adjacent to a region identified in cross-sectional comparison of MIRCT patients with control subjects in Chapter 5. In patients who demonstrated improvements in upper limb function, the magnitude of the change in grey matter density in the TPJ cluster showed a positive correlation with the degree of improvement in shoulder function. In combination with Chapter 5, this work provided encouraging evidence for components of the right ventral attention

network in long term disuse, and the potential for adaptive plasticity therein as patients regain upper limb use.

As a contrast to the experience-dependent and usage-dependent plasticity under study in the majority of this thesis, in Chapter 7 I considered plasticity in the context of sub-acute stroke. In this chapter I analysed a subset of a large dataset currently being acquired as a part of the large multi-centre FAST INdICATE trial (http://fastindicate.com/home). I applied a combination of diffusion-weighted, structural and resting-state fMRI analysis to derive imaging measures of integrity in the sensorimotor network at the sub-acute stage of stroke recovery (14-60 days post-stroke). I related these imaging metrics to behaviour measures of motor function and integrity in the motor system. All of the imaging metrics and behavioural measures were chosen as they are relatively easy to implement across clinical platforms, and therefore are potentially feasible for measurement in clinical centres. The data presented in this chapter provided encouraging initial evidence for the potential utility of CST-lesion cross-sectional overlap and sensorimotor network strength as candidate markers of motor function at the sub-acute stage of stroke.

## 8.2 Future directions

The work in this thesis raises a number of areas that warrant further study. This further work incorporates direct extensions of the studies presented in the thesis, as well as new experiments, which would build upon the findings presented here.

### 8.2.1 Behavioural correlates of digit remapping

The data presented in Chapter 4 provide evidence for short-term remapping of the primary somatosensory cortex after a 24 hour gluing manipulation. The manipulation involved the attachment of digit two (index finger) and digit three (middle finger) on the right hand, which resulted in a reduction in the overlap between the cortical

representations of digit three (middle finger) and digit four (ring finger), and an increase in the overlap between the cortical representations of digit four (ring finger) and digit five (little finger).

The remapping phenomenon occurred in the cortical representations of digits adjacent to those involved in the manipulation. This finding raises the potential that some altered use in the digits not involved in the glued intervention drove the short-term plastic change observed. In particular, it is possible that rather than driving synergistic use of digits two and three, the gluing manipulation induced altered patterns of use, which freed digit four from synergistic movement with digit three, and allowed it to be used in greater combination with digit five.

In order to further investigate these off-target effects, behavioural testing of sensory and motor function in the hand would be potentially informative. This work would mirror the design presented in figure 4.1, with behavioural testing in place of the imaging sessions. A test of sensory discrimination between adjacent digits would provide a potentially useful measure of cortical overlap. A temporal order judgement task using tactile stimuli might provide such a metric of sensory function behaviourally (Shore et al., 2005). In such a task, suprathreshold tactile stimuli would be presented to adjacent digit pairs at varying intervals, requiring participants to judge which stimulus came first. The temporal interval at which the two stimuli become indistinguishable would provide a potential surrogate measure of shared cortical representation, which could be compared across the control and glued conditions. A similar motor task could also be undertaken, such as a four-choice button reaction task, assessing the speed and accuracy of rapid button presses made by the different digits, considering patterns in the confusion between fingers, and investigating the effect of prior button press (adjacent vs. non-adjacent) on the speed and accuracy of the subsequent press (Lachnit and Pieper, 1990; Arunachalam et al., 2005).

### 8.2.2 Modifying digit mapping paradigms

The ability to undertake mapping of digit somatotopy in individual subjects has considerable applications for the study of plasticity and ageing. The paradigm presented in Chapter 3 provides a rapid and reproducible means of producing these maps using fMRI at 7.0 tesla with an easily implemented motor task. Movement of the digits in mapping provides a rich array of sensory stimulation, particularly in comparison of to the air puff stimuli (Stringer et al., 2014) or the piezoelectric stimuli (Sanchez-Panchuelo et al., 2010; Besle et al., 2013a) applied previously. While this mapping technique was well-suited to the longitudinal experiment presented in Chapter 4, cross-sectional studies involving more varied populations may necessitate greater control over the movement stimuli used in mapping. Specifically, across different age ranges or patient groups, it is likely that active movements will be undertaken at different rates and with a different degree of force or exertion. In order to standardise this movement and allow for comparison of cortical digit representations across a wide range of individuals, a passive movement paradigm would better deliver uniform sensory stimulation of the hand.

The development of a passive movement paradigm to map digit representations would build upon the work presented in this thesis, and allow for further studies of somatotopy in a range of population and patient groups. This work would first require the development of an MRI compatible device able to individuate passive movements in the fingers, most likely using pneumatics to drive movement in the scanner. Further work would be required to modify the fMRI acquisition to optimise the clarity of maps acquired. This work would provide a valuable tool to build on the data presented in this thesis, and investigate digit somatotopy in the broader context of health and ageing.

### 8.2.3 Spatial attention, the body schema and disuse

The results outlined in Chapters 5 and 6 strongly implicate plasticity in the right TPJ and right ventral attention network in chronic unilateral disuse. The right ventral

attention network is broadly involved in attention and the integration of multi sensory stimuli in body perception (Corbetta and Shulman, 2011b). Whilst evidence from both cross-sectional and longitudinal MRI analysis implicate this region, the scope of the original project did not include tests to assess spatial attention or the body schema.

A useful adjunct to the longitudinal study presented in Chapter 6 would be to investigate changes in the body schema and spatial attention using behavioural tests. The likely deficits in this patient population will be subtle in comparison to those observed in other groups with attentional deficits, such as spatial neglect. The selection of attentional tests will therefore require careful consideration. Previous work in patients with chronic unilateral arm pain assessed the body schema using a laterality discrimination task involving rotated images of hands (Schwoebel et al., 2002). This task involved mental rotation of the hand presented to assess its laterality. The study demonstrated that response times were longer for judgements involving the hand ipsilateral to the painful arm; an unfamiliarity which suggests a disconnect between the affected arm and the body schema.

The assessment of alterations in spatial attention or the body schema would offer considerable insight into the nature of disuse. A greater understanding of the nature of any attentional deficit would be highly informative in developing rehabilitation paradigms that address not only the musculoskeletal pathology, but also which help to reintegrate the disused body part into the brain's representation of the body.

## 8.3 General conclusions

The sensorimotor network exhibits a considerable propensity for both experience-dependent and usage-dependent plasticity. The work contained in this thesis has spanned the scope of this plasticity, from short-term changes in the fine-grain functional architecture of the primary somatosensory cortex presented in Chapters 3

and 4, to the effects of long-term disuse on higher-order cortical regions responsible for multi-sensory integration, the body schema and attention, presented in Chapters 5 and 6. This work provides strong evidence for the effects of subtle peripheral changes in sensory and motor function on the structural and functional architecture of the sensorimotor network.

The results presented in this thesis provide a strong impetus to investigate further the propensity for plastic change as a result of peripheral changes in sensory and motor function. Particularly interesting is the potential for alterations in the peripheral anatomy associated with ageing, surgical intervention or disease to drive plastic changes in the brain; a cycle which may further impair sensory and motor function in the long term.

# Bibliography


Abbott, L. F. and S. B. Nelson (2000). "Synaptic plasticity: taming the beast." In: *Nat. Neurosci.* 3 Suppl, pp. 1178–1183.

Ada, L., S. Dorsch, and C. G. Canning (2006). "Strengthening interventions increase strength and improve activity after stroke: a systematic review." In: *Aust J Physiother* 52.4, pp. 241–248.

Adamson, J., A. Beswick, and S. Ebrahim (2004). "Is stroke the most common cause of disability?" In: *J Stroke Cerebrovasc Dis* 13.4, pp. 171–177.

Ainsworth, R. (2006). "Physiotherapy rehabilitation in patients with massive, irreparable rotator cuff tears." In: *Musculoskeletal Care* 4.3, pp. 140–151.

Ainsworth, R. and J. S. Lewis (2007). "Exercise therapy for the conservative management of full thickness tears of the rotator cuff: a systematic review." In: *Br J Sports Med* 41.4, pp. 200–210.

Ainsworth, R., J. Lewis, and V. Conboy (2009). "A prospective randomized placebo controlled clinical trial of a rehabilitation programme for patients with a diagnosis of massive rotator cuff tears of the shoulder". In: *Shoulder & Elbow* 1.1, pp. 55–60.

Allard, T., S. A. Clark, W. M. Jenkins, and M. M. Merzenich (1991). "Reorganization of somatosensory area 3b representations in adult owl monkeys after digital syndactyly." In: *J. Neurophysiol.* 66.3, pp. 1048–1058.

Alloway, K. D. and H. Burton (1986). "Bicuculline-induced alterations in neuronal responses to controlled tactile stimuli in the second somatosensory cortex of the cat: a microiontophoretic study." In: *Somatosens Res* 3.3, pp. 197–211.

Alloway, K. D. and H. Burton (1991). "Differential effects of GABA and bicuculline on rapidly- and slowly-adapting neurons in primary somatosensory cortex of primates." In: *Exp Brain Res* 85.3, pp. 598–610.

Amassian, E. V. and H. Weiner (1966). "Monosynaptic and polysynaptic activation of pyramidal tract neurons by thalamic stimulation". In: *The Thalamus*. Ed. by D. P. Purpura and M. D. Yahr. New York: Columbia University Press, pp. 256–281.

Andersson, J. L., M. Jenkinson, and S. Smith (2007a). "Non-linear optimisation FMRIB Technical report TR07JA1". In: *FMRIB Analysis Group of the University of Oxford*.

Andersson, J. L., M. Jenkinson, and S. Smith (2007b). "Non-linear registration, aka Spatial normalisation FMRIB technical report TR07JA2". In: *FMRIB Analysis Group of the University of Oxford*.

Araujo, I. E. T. de, E. T. Rolls, M. L. Kringelbach, F. McGlone, and N. Phillips (2003). "Taste-olfactory convergence, and the representation of the pleasantness of flavour, in the human brain." In: *Eur J Neurosci* 18.7, pp. 2059–2068.

Arunachalam, R., V. S. Weerasinghe, and K. R. Mills (2005). "Motor control of rapid sequential finger tapping in humans." In: *J. Neurophysiol.* 94.3, pp. 2162–2170.

Ashburner, J. and K. J. Friston (2000). "Voxel-based morphometry—the methods". In: *NeuroImage* 11.6, pp. 805–821.

Astrup, J., B. K. Siesjö, and L. Symon (1981). "Thresholds in cerebral ischemia - the ischemic penumbra." In: *Stroke* 12.6, pp. 723–725.

Auer, T., A. Schwarcz, M. Aradi, Z. Kalmár, C. Pendleton, I. Janszky, R. A. Horváth, C. Szalay, T. Dóczi, S. Komoly, and J. Janszky (2008). "Right-left discrimination is related to the right hemisphere." In: *Laterality* 13.5, pp. 427–438.

Augustine, G. J., M. P. Charlton, and S. J. Smith (1985). "Calcium entry and transmitter release at voltage-clamped nerve terminals of squid." In: *J. Physiol. (Lond.)* 367, pp. 163–181.

Baliki, M. N., P. Y. Geha, and A. V. Apkarian (2009). "Parsing pain perception between nociceptive representation and magnitude estimation." In: *J. Neurophysiol.* 101.2, pp. 875–887.

Baliki, M. N., B. Petre, S. Torbey, K. M. Herrmann, L. Huang, T. J. Schnitzer, H. L. Fields, and A. V. Apkarian (2012). "Corticostriatal functional connectivity predicts transition to chronic back pain". In: *Nat. Neurosci.* 15.8, pp. 1117–1119.

Bara-Jimenez, W., M. J. Catalan, M. Hallett, and C. Gerloff (1998). "Abnormal somatosensory homunculus in dystonia of the hand". In: *Ann Neurol.* 44.5, pp. 828–831.

Barbas, H. and D. N. Pandya (1987). "Architecture and frontal cortical connections of the premotor cortex (area 6) in the rhesus monkey." In: *J. Comp. Neurol.* 256.2, pp. 211–228.

Barfuss, H., H. C. Fischer, D. Hentschel, R. Ladebeck, and J. Vetter (1988). "Whole-body MR imaging and spectroscopy with a 4-T system." In: *Radiology* 169.3, pp. 811–816.

Barker, A. T., R. Jalinous, and I. L. Freeston (1985). "Non-invasive magnetic stimulation of human motor cortex." In: *Lancet* 1.8437, pp. 1106–1107.

Basser, P. J., J. Mattiello, and D. LeBihan (1994). "Estimation of the effective self-diffusion tensor from the NMR spin echo." In: *J Magn Reson B* 103.3, pp. 247–254.

Bassolino, M., M. Bove, M. Jacono, L. Fadiga, and T. Pozzo (2012). "Functional effect of short-term immobilization: Kinematic changes and recovery on reaching-to-grasp". In: *Neuroscience* 215, pp. 127–134.

Beaulieu, C. (2002). "The basis of anisotropic water diffusion in the nervous system - a technical review." In: *NMR Biomed.* 15.7-8, pp. 435–455.

Beaulieu, C., F. R. Fenrich, and P. S. Allen (1998). "Multicomponent water proton transverse relaxation and T2-discriminated water diffusion in myelinated and nonmyelinated nerve." In: *Magnetic Resonance Imaging* 16.10, pp. 1201–1210.

Beckmann, C. F., M. DeLuca, J. T. Devlin, and S. M. Smith (2005). "Investigations into resting-state connectivity using independent component analysis". In: *Philosophical Transactions of the Royal Society B: Biological Sciences* 360.1457, pp. 1001–1013.

Behrens, T. E. J., H. Johansen-Berg, S. Jbabdi, M. F. S. Rushworth, and M. W. Woolrich (2007). "Probabilistic diffusion tractography with multiple fibre orientations: What can we gain?" In: *NeuroImage* 34.1, pp. 144–155.

Behrens, T. E. J., M. W. Woolrich, M. Jenkinson, H. Johansen-Berg, R. G. Nunes, S. Clare, P. M. Matthews, J. M. Brady, and S. M. Smith (2003). "Characterization and propagation of uncertainty in diffusion-weighted MR imaging". In: *Magn. Reson. Med.* 50.5, pp. 1077–1088.

Behzadi, Y. and T. T. Liu (2006). "Caffeine reduces the initial dip in the visual BOLD response at 3 T." In: *NeuroImage* 32.1, pp. 9–15.

Benwell, C. S. Y., G. Thut, A. Grant, and M. Harvey (2014). "A rightward shift in the visuospatial attention vector with healthy aging". In: *Front. Aging Neurosci.* 6.

Berendes, T., P. Pilot, J. Willems, H. Verburg, and R. te Slaa (2010). "Validation of the Dutch version of the Oxford Shoulder Score." In: *J Shoulder Elbow Surg* 19.6, pp. 829–836.

Besle, J., R.-M. Sanchez-Panchuelo, R. Bowtell, S. T. Francis, and D. Schluppeck (2013a). "Event-related fMRI at 7T reveals overlapping cortical representations for adjacent fingertips in S1 of individual subjects". In: *Hum. Brain Mapp.* 35.5, pp. 2027–2043.

Besle, J., R.-M. Sanchez-Panchuelo, R. Bowtell, S. T. Francis, and D. Schluppeck (2013b). "Single-subject fMRI mapping at 7 T of the representation of fingertips in S1: a comparison of event-related and phase-encoding designs." In: *J. Neurophysiol.* 109.9, pp. 2293–2305.

Betz, G. (1874). "Anatomischer Nachweis zweier Gehirncentra". In: *Centralblatt für die medizinischen Wissenschaften* 12.1, pp. 578–599.

Biernaskie, J., G. Chernenko, and D. Corbett (2004). "Efficacy of rehabilitative experience declines with time after focal ischemic brain injury." In: *J. Neurosci.* 24.5, pp. 1245–1254.

Binkofski, F. and G. Buccino (2006). "The role of ventral premotor cortex in action execution and action understanding." In: *J. Physiol. Paris* 99.4-6, pp. 396–405.

Björkman, A., A. Weibull, B. Rosén, J. Svensson, and G. Lundborg (2009). "Rapid cortical reorganisation and improved sensitivity of the hand following cutaneous anaesthesia of the forearm." In: *Eur J Neurosci* 29.4, pp. 837–844.

Blicher, J. U., J. Near, E. Næss-Schmidt, C. J. Stagg, H. Johansen-Berg, J. F. Nielsen, L. Østergaard, and Y.-C. L. Ho (2014). "GABA Levels Are Decreased After Stroke and GABA Changes During Rehabilitation Correlate With Motor Improvement." In: *Neurorehabilitation and Neural Repair*.

Bliss, T. V. P. and T. Lømo (1973). "Long-lasting potentiation of synaptic transmission in the dentate area of the anaesthetized rabbit following stimulation of the perforant path." In: *J. Physiol. (Lond.)* 232.2, pp. 331–356.

Boake, C., E. A. Noser, T. Ro, S. Baraniuk, M. Gaber, R. Johnson, E. T. Salmeron, T. M. Tran, J. M. Lai, E. Taub, L. A. Moye, J. C. Grotta, and H. S. Levin (2007). "Constraint-induced movement therapy during early stroke rehabilitation." In: *Neurorehabilitation and Neural Repair* 21.1, pp. 14–24.

Bolzoni, F., C. Bruttini, R. Esposti, and P. Cavallari (2012). "Hand immobilization affects arm and shoulder postural control." In: *Exp Brain Res* 220.1, pp. 63–70.

Bosnell, R. A., C. Wegner, Z. T. Kincses, T. Korteweg, F. Agosta, O. Ciccarelli, N. De Stefano, A. Gass, J. Hirsch, H. Johansen-Berg, L. Kappos, F. Barkhof, L. Mancini, F. Manfredonia, S. Marino, D. H. Miller, X. Montalban, J. Palace, M. Rocca, C. Enzinger, S. Ropele, A. Rovira, S. Smith, A. Thompson, J. Thornton, T. Yousry, B. Whitcher, M. Filippi, and P. M. Matthews (2008). "Reproducibility

of fMRI in the clinical setting: Implications for trial designs". In: *NeuroImage* 42.2, pp. 603–610.

Breakefield, X. O., A. J. Blood, Y. Li, M. Hallett, P. I. Hanson, and D. G. Standaert (2008). "The pathophysiological basis of dystonias." In: *Nat Rev Neurosci* 9.3, pp. 222–234.

Broca, P. (1861). "Perte de la Parole, Ramollissement Chronique et Destruction Partielle du Lobe Antérieur Gauche du Cerveau". In: *Bull Soc Anthropol* 2, pp. 235–238.

Brodmann, K. (1909). *Broadmann's Localisation in the Cerebral Cortex*. New York: Springer.

Brown, C. E., K. Aminoltejari, H. Erb, I. R. Winship, and T. H. Murphy (2009). "In vivo voltage-sensitive dye imaging in adult mice reveals that somatosensory maps lost to stroke are replaced over weeks by new structural and functional circuits with prolonged modes of activation within both the peri-infarct zone and distant sites." In: *J. Neurosci.* 29.6, pp. 1719–1734.

Brown, P. B., T. M. Brushart, and L. A. Ritz (1989). "Somatotopy of digital nerve projections to the dorsal horn in the monkey." In: *Somatosens Mot Res* 6.3, pp. 309–317.

Buch, E. R., R. B. Mars, E. D. Boorman, and M. F. S. Rushworth (2010). "A network centered on ventral premotor cortex exerts both facilitatory and inhibitory control over primary motor cortex during action reprogramming." In: *J. Neurosci.* 30.4, pp. 1395–1401.

Budde, M. D., J. H. Kim, H.-F. Liang, R. E. Schmidt, J. H. Russell, A. H. Cross, and S.-K. Song (2007). "Toward accurate diagnosis of white matter pathology using diffusion tensor imaging". In: *Magn. Reson. Med.* 57.4, pp. 688–695.

Budde, M. D., M. Xie, A. H. Cross, and S. K. Song (2009). "Axial Diffusivity Is the Primary Correlate of Axonal Injury in the Experimental Autoimmune Encephalomyelitis Spinal Cord: A Quantitative Pixelwise Analysis". In: *J. Neurosci.* 29.9, pp. 2805–2813.

Bunker, T. (2002). "Rotator cuff disease". In: *Current Orthopaedics* 16.3, pp. 223–233.

Bütefisch, C., H. Hummelsheim, P. Denzler, and K. H. Mauritz (1995). "Repetitive training of isolated movements improves the outcome of motor rehabilitation of the centrally paretic hand." In: *Journal of the Neurological Sciences* 130.1, pp. 59–68.

Cajal, S. R. Y. (1894). "The Croonian Lecture: La fine structure des centres nerveux". In: *Proceedings of the Royal Society of London* 55.331-335, pp. 444–468.

Caminiti, R., S. Ferraina, and P. B. Johnson (1996). "The sources of visual information to the primate frontal lobe: a novel role for the superior parietal lobule." In: *Cereb. Cortex* 6.3, pp. 319–328.

Campbell, A. W. (1905). *Histological Studies on the Localisation of Cerebral Function*. Cambridge University Press.

Carmichael, S. T., I. Archibeque, L. Luke, T. Nolan, J. Momiy, and S. Li (2005). "Growth-associated gene expression after stroke: evidence for a growth-promoting region in peri-infarct cortex." In: *Exp. Neurol.* 193.2, pp. 291–311.

Carr, A. J., J. L. Rees, C. R. Ramsay, R. Fitzpatrick, A. C. Gray, J. Moser, J. Dawson, H. Bruhn, C. D. Cooper, D. J. Beard, and M. K. Campbell (2014). "Protocol for the United Kingdom Rotator Cuff Study (UKUFF): a randomised controlled trial of open and arthroscopic rotator cuff repair." In: *Bone Joint Res* 3.5, pp. 155–160.

Celnik, P. A., F. Hummel, M. Harris-Love, R. Wolk, and L. G. Cohen (2007). "Somatosensory Stimulation Enhances the Effects of Training Functional Hand Tasks in Patients With Chronic Stroke". In: *Arch Phys Med Rehabil* 88.11, pp. 1369–1376.

Chechlacz, M., P. Rotshtein, W.-L. Bickerton, P. C. Hansen, S. Deb, and G. W. Humphreys (2010). "Separating neural correlates of allocentric and egocentric neglect: distinct cortical sites and common white matter disconnections." In: *Cogn Neuropsychol* 27.3, pp. 277–303.

Chechlacz, M., P. Rotshtein, P. C. Hansen, S. Deb, M. J. Riddoch, and G. W. Humphreys (2013). "The central role of the temporo-parietal junction and the superior longitudinal fasciculus in supporting multi-item competition: Evidence from lesion-symptom mapping of extinction". In: *Cortex* 49.2, pp. 487–506.

Chee, M. W. L. and W. C. Choo (2004). "Functional imaging of working memory after 24 hr of total sleep deprivation." In: *J. Neurosci.* 24.19, pp. 4560–4567.

Chen, C. L., F. T. Tang, H. C. Chen, C. Y. Chung, and M. K. Wong (2000). "Brain lesion size and location: effects on motor recovery and functional outcome in stroke patients." In: *Arch Phys Med Rehabil* 81.4, pp. 447–452.

Chen, J. L. and G. Schlaug (2013). "Resting state interhemispheric motor connectivity and white matter integrity correlate with motor impairment in chronic stroke." In: *Front Neurol* 4, p. 178.

Chen, S.-Y. and C. J. Winstein (2009). "A systematic review of voluntary arm recovery in hemiparetic stroke: critical predictors for meaningful outcomes using the international classification of functioning, disability, and health." In: *J Neurol Phys Ther* 33.1, pp. 2–13.

Cisek, P. and J. F. Kalaska (2004). "Neural correlates of mental rehearsal in dorsal premotor cortex." In: *Nature* 431.7011, pp. 993–996.

Clark, W. E. and T. P. Powell (1953). "On the thalamo-cortical connexions of the general sensory cortex of Macaca." In: *Proc. R. Soc. Lond., B,* 141.905, pp. 467–487.

Classen, J., J. Liepert, S. P. Wise, M. Hallett, and L. G. Cohen (1998). "Rapid plasticity of human cortical movement representation induced by practice." In: *J. Neurophysiol.* 79.2, pp. 1117–1123.

Claude, B. M. (1856). "Physiological analysis of the properties of the muscular and nervous systems by means of curare". In: *C. R. Acad. Sci. (Paris)* 43, pp. 825–829.

Cleeland, C. S. and K. M. Ryan (1994). "Pain assessment: global use of the Brief Pain Inventory." In: *Ann. Acad. Med. Singap.* 23.2, pp. 129–138.

Clement, N. D., Y. X. Nie, and J. M. McBirnie (2012). "Management of degenerative rotator cuff tears: a review and treatment strategy". In: *Sports Med Arthrosc Rehabil Ther Technol* 4.1, p. 48.

Cloke, D. J., S. E. Lynn, H. Watson, I. N. Steen, S. Purdy, and J. R. Williams (2005). "A comparison of functional, patient-based scores in subacromial impingement." In: *J Shoulder Elbow Surg* 14.4, pp. 380–384.

Clower, W. T. and G. E. Alexander (1998). "Movement sequence-related activity reflecting numerical order of components in supplementary and presupplementary motor areas." In: *J. Neurophysiol.* 80.3, pp. 1562–1566.

Collingridge, G. L., S. Peineau, J. G. Howland, and Y. T. Wang (2010). "Long-term depression in the CNS." In: *Nat Rev Neurosci* 11.7, pp. 459–473.

Corbetta, M., G. Patel, and G. L. Shulman (2008). "The reorienting system of the human brain: from environment to theory of mind." In: *Neuron* 58.3, pp. 306–324.

Corbetta, M. and G. L. Shulman (2011a). "Spatial Neglect and Attention Networks". In: *Annu. Rev. Neurosci.* 34.1, pp. 569–599.

Corbetta, M. and G. L. Shulman (2011b). "Spatial neglect and attention networks." In: *Annu. Rev. Neurosci.* 34, pp. 569–599.

Craig, A. D., K. Chen, D. Bandy, and E. M. Reiman (2000). "Thermosensory activation of insular cortex." In: *Nat. Neurosci.* 3.2, pp. 184–190.

Cramer, S. C. (2008). "Repairing the human brain after stroke: I. Mechanisms of spontaneous recovery." In: *Ann Neurol.* 63.3, pp. 272–287.

Dale, A. M., B. Fischl, and M. I. Sereno (1999). "Cortical surface-based analysis. I. Segmentation and surface reconstruction." In: *NeuroImage* 9.2, pp. 179–194.

Darian-Smith, C. and C. D. Gilbert (1994). "Axonal sprouting accompanies functional reorganization in adult cat striate cortex." In: *Nature* 368.6473, pp. 737–740.

Davare, M., M. Andres, G. Cosnard, J.-L. Thonnard, and E. Olivier (2006). "Dissociating the role of ventral and dorsal premotor cortex in precision grasping." In: *J. Neurosci.* 26.8, pp. 2260–2268.

Dawes, H., C. Enzinger, H. Johansen-Berg, M. D. Bogdanovic, C. Guy, J. Collett, H. Izadi, C. Stagg, D. Wade, and P. M. Matthews (2007). "Walking performance and its recovery in chronic stroke in relation to extent of lesion overlap with the descending motor tract". In: *Exp Brain Res* 186.2, pp. 325–333.

Dawson, J., R. Fitzpatrick, and A. J. Carr (1996). "Questionnaire on the perceptions of patients about shoulder surgery". In: *Journal of Bone & Joint Surgery, British Volume* 78.4, pp. 593–600.

Dawson, J., K. Rogers, R. Fitzpatrick, and A. J. Carr (2009). "The Oxford shoulder score revisited." In: *Arch Orthop Trauma Surg* 129.1, pp. 119–123.

Dechent, P. and J. Frahm (2003). "Functional somatotopy of finger representations in human primary motor cortex." In: *Hum. Brain Mapp.* 18.4, pp. 272–283.

Deecke, L. and H. H. Kornhuber (1978). "An electrical sign of participation of the mesial 'supplementary' motor cortex in human voluntary finger movement." In: *Brain Res.* 159.2, pp. 473–476.

Deen, B., N. B. Pitskel, and K. A. Pelphrey (2011). "Three systems of insular functional connectivity identified with cluster analysis." In: *Cereb. Cortex* 21.7, pp. 1498–1506.

DeFelipe, J., M. Conley, and E. G. Jones (1986). "Long-range focal collateralization of axons arising from corticocortical cells in monkey sensory-motor cortex." In: *J. Neurosci.* 6.12, pp. 3749–3766.

Delaney, R. A., A. Lin, and J. J. P. Warner (2012). "Nonarthroplasty options for the management of massive and irreparable rotator cuff tears." In: *Clinics in Sports Medicine* 31.4, pp. 727–748.

Desikan, R. S., F. Ségonne, B. Fischl, B. T. Quinn, B. C. Dickerson, D. Blacker, R. L. Buckner, A. M. Dale, R. P. Maguire, B. T. Hyman, M. S. Albert, and R. J. Killiany (2006). "An automated labeling system for subdividing the human cerebral cortex on MRI scans into gyral based regions of interest." In: *NeuroImage* 31.3, pp. 968–980.

DeVetten, G., S. B. Coutts, M. D. Hill, M. Goyal, M. Eesa, B. O'Brien, A. M. Demchuk, A. Kirton, and MONITOR and VISION study groups (2010). "Acute corticospinal tract Wallerian degeneration is associated with stroke outcome." In: *Stroke* 41.4, pp. 751–756.

Doetsch, G. S., G. P. Standage, K. W. Johnston, and C. S. Lin (1988a). "Intracortical connections of two functional subdivisions of the somatosensory forepaw cerebral cortex of the raccoon." In: *J. Neurosci.* 8.6, pp. 1887–1900.

Doetsch, G. S., G. P. Standage, K. W. Johnston, and C. S. Lin (1988b). "Thalamic connections of two functional subdivisions of the somatosensory forepaw cerebral cortex of the raccoon." In: *J. Neurosci.* 8.6, pp. 1873–1886.

Doetsch, G. S., S. D. Stoney Jr, and D. H. Hauge (1992). "Convergent inputs to single neurons in two different subdivisions of somatosensory forepaw digit cortex of the raccoon". In: *Exp. Neurol.* 115.2, pp. 250–259.

Donaldson, C., R. Tallis, S. Miller, A. Sunderland, R. Lemon, and V. Pomeroy (2009). "Effects of conventional physical therapy and functional strength training on upper limb motor recovery after stroke: a randomized phase II study." In: *Neurorehabilitation and Neural Repair* 23.4, pp. 389–397.

Donkelaar, P. van, J. F. Stein, R. E. Passingham, and R. C. Miall (1999). "Neuronal activity in the primate motor thalamus during visually triggered and internally generated limb movements." In: *J. Neurophysiol.* 82.2, pp. 934–945.

Douaud, G., S. Smith, M. Jenkinson, T. E. J. Behrens, H. Johansen-Berg, J. Vickers, S. James, N. Voets, K. Watkins, P. M. Matthews, and A. James (2007). "Anatomically related grey and white matter abnormalities in adolescent-onset schizophrenia." In: *Brain* 130.Pt 9, pp. 2375–2386.

Duarte, I. C., C. Ferreira, J. Marques, and M. Castelo-Branco (2014). "Anterior/Posterior Competitive Deactivation/Activation Dichotomy in the Human Hippocampus as Revealed by a 3D Navigation Task". In: *PLoS ONE* 9.1, e86213.

Dum, R. P. and P. L. Strick (1991). "The origin of corticospinal projections from the premotor areas in the frontal lobe." In: *J. Neurosci.* 11.3, pp. 667–689.

Dum, R. P. and P. L. Strick (2005). "Frontal lobe inputs to the digit representations of the motor areas on the lateral surface of the hemisphere." In: *J. Neurosci.* 25.6, pp. 1375–1386.

Duncan, R. O. and G. M. Boynton (2007). "Tactile hyperacuity thresholds correlate with finger maps in primary somatosensory cortex (S1)." In: *Cereb. Cortex* 17.12, pp. 2878–2891.

Dykes, R. W. and A. D. Craig (1998). "Control of size and excitability of mechanosensory receptive fields in dorsal column nuclei by homolateral dorsal horn neurons." In: *J. Neurophysiol.* 80.1, pp. 120–129.

Economo, C. von and G. N. Koskinas (1925). "Die Cytoarchitektonik der Hirnrinde des erwachsenen Menschen". In: *Springer*.

Eickhoff, S. B., S. Heim, K. Zilles, and K. Amunts (2006). "Testing anatomically specified hypotheses in functional imaging using cytoarchitectonic maps." In: *NeuroImage* 32.2, pp. 570–582.

Eickhoff, S. B., T. Paus, S. Caspers, M.-H. Grosbras, A. C. Evans, K. Zilles, and K. Amunts (2007). "Assignment of functional activations to probabilistic cytoarchitectonic areas revisited." In: *NeuroImage* 36.3, pp. 511–521.

Eickhoff, S. B., K. E. Stephan, H. Mohlberg, C. Grefkes, G. R. Fink, K. Amunts, and K. Zilles (2005). "A new SPM toolbox for combining probabilistic cytoarchitectonic maps and functional imaging data." In: *NeuroImage* 25.4, pp. 1325–1335.

Ejnisman, B., C. V. Andreoli, B. Soares, M. S. Peccin, R. J. Abdalla, F. Faloppa, and M. Cohen (2009). "Interventions for tears of the rotator cuff in adults." In: *Cochrane Database Syst Rev* 1, p. CD002758.

Elbert, T., V. Candia, E. Altenmüller, H. Rau, A. Sterr, B. Rockstroh, C. Pantev, and E. Taub (1998). "Alteration of digital representations in somatosensory cortex in focal hand dystonia". In: *Neuroreport* 9.16, p. 3571.

Engel, S. A. (2012). "The development and use of phase-encoded functional MRI designs." In: *NeuroImage* 62.2, pp. 1195–1200.

Engel, S. A., G. H. Glover, and B. A. Wandell (1997). "Retinotopic organization in human visual cortex and the spatial precision of functional MRI." In: *Cereb. Cortex* 7.2, pp. 181–192.

Facchini, S., M. Romani, M. Tinazzi, and S. M. Aglioti (2002). "Time-related changes of excitability of the human motor system contingent upon immobilisation of the ring and little fingers." In: *Clin Neurophysiol* 113.3, pp. 367–375.

Farr, T. D. and S. Wegener (2010). "Use of magnetic resonance imaging to predict outcome after stroke: a review of experimental and clinical evidence." In: *J. Cereb. Blood Flow Metab.* 30.4, pp. 703–717.

Fasoli, S. E., C. A. Trombly, L. Tickle-Degnen, and M. H. Verfaellie (2002). "Effect of instructions on functional reach in persons with and without cerebrovascular accident." In: *Am J Occup Ther* 56.4, pp. 380–390.

Ferezou, I., F. Haiss, L. J. Gentet, R. Aronoff, B. Weber, and C. C. H. Petersen (2007). "Spatiotemporal dynamics of cortical sensorimotor integration in behaving mice." In: *Neuron* 56.5, pp. 907–923.

Ferrier, D. (1875). "The Croonian Lecture.–Experiments on the Brain of Monkeys (Second Series)". In: *Philosophical Transactions of the Royal Society of London* 165, pp. 433–488.

Ferrier, D. (1886). *The Functions of the Brain*. GP Putnam's Sons. New York.

Fields, R. D. (2005). "Myelination: an overlooked mechanism of synaptic plasticity?" In: *Neuroscientist* 11.6, pp. 528–531.

Filippini, N., B. J. MacIntosh, M. G. Hough, G. M. Goodwin, G. B. Frisoni, S. M. Smith, P. M. Matthews, C. F. Beckmann, and C. E. Mackay (2009). "Distinct patterns of brain activity in young carriers of the APOE-epsilon4 allele." In: *Proc. Natl. Acad. Sci. U.S.A.* 106.17, pp. 7209–7214.

Filosa, J. A., A. D. Bonev, S. V. Straub, A. L. Meredith, M. K. Wilkerson, R. W. Aldrich, and M. T. Nelson (2006). "Local potassium signaling couples neuronal activity to vasodilation in the brain". In: *Nat. Neurosci.* 9.11, pp. 1397–1403.

Fischl, B., A. Liu, and A. M. Dale (2001). "Automated manifold surgery: constructing geometrically accurate and topologically correct models of the human cerebral cortex." In: *IEEE Trans Med Imaging* 20.1, pp. 70–80.

Flinkkilä, T., J. Ristiniemi, M. Lakovaara, P. Hyvönen, and J. Leppilahti (2006). "Hook-plate fixation of unstable lateral clavicle fractures: a report on 63 patients." In: *Acta Orthop* 77.4, pp. 644–649.

Florence, S. L. and J. H. Kaas (1995). "Large-scale reorganization at multiple levels of the somatosensory pathway follows therapeutic amputation of the hand in monkeys." In: *J. Neurosci.* 15.12, pp. 8083–8095.

Florence, S. L., H. B. Taub, and J. H. Kaas (1998). "Large-scale sprouting of cortical connections after peripheral injury in adult macaque monkeys". In: *Science* 282.5391, pp. 1117–1121.

Florence, S. L., J. T. Wall, and J. H. Kaas (1988). "The somatotopic pattern of afferent projections from the digits to the spinal cord and cuneate nucleus in macaque monkeys." In: *Brain Res.* 452.1-2, pp. 388–392.

Flourens, P. (1846). *Phrenology Examined*. Philadelphia: Hogan & Thompson.

Foerster, O. (1926). "Die Pathogenese des epileptischen Krampfanfalles". In: *Deutsche Zeitschrift f. Nervenheilkunde* 94.1, pp. 15–53.

Fogassi, L., V. Raos, G. Franchi, V. Gallese, G. Luppino, and M. Matelli (1999). "Visual responses in the dorsal premotor area F2 of the macaque monkey." In: *Exp Brain Res* 128.1-2, pp. 194–199.

Fox, M. D., M. Corbetta, A. Z. Snyder, J. L. Vincent, and M. E. Raichle (2006). "Spontaneous neuronal activity distinguishes human dorsal and ventral attention systems". In: *Proc. Natl. Acad. Sci. U.S.A.* 103.26, pp. 10046–10051.

Fox, M. D. and M. E. Raichle (2007). "Spontaneous fluctuations in brain activity observed with functional magnetic resonance imaging." In: *Nat Rev Neurosci* 8.9, pp. 700–711.

Fox, P. T., H. Burton, and M. E. Raichle (1987). "Mapping human somatosensory cortex with positron emission tomography." In: *J. Neurosurg.* 67.1, pp. 34–43.

Francis, S. T., E. F. Kelly, R. Bowtell, W. J. R. Dunseath, S. E. Folger, and F. McGlone (2000). "fMRI of the Responses to Vibratory Stimulation of Digit Tips". In: *NeuroImage* 11.3, pp. 188–202.

Friedman, D. P. and E. G. Jones (1980). "Focal projection of electrophysiologically defined groupings of thalamic cells on the monkey somatic sensory cortex." In: *Brain Res.* 191.1, pp. 249–252.

Friedman, D. P. and E. G. Jones (1981). "Thalamic input to areas 3a and 2 in monkeys." In: *J. Neurophysiol.* 45.1, pp. 59–85.

Friedrich, F. J., R. Egly, R. D. Rafal, and D. Beck (1998). "Spatial attention deficits in humans: a comparison of superior parietal and temporal-parietal junction lesions." In: *Neuropsychology* 12.2, pp. 193–207.

Friston, K. J., A. P. Holmes, K. J. Worsley, J. P. Poline, C. D. Frith, and R. S. J. Frackowiak (1995). "Statistical parametric maps in functional imaging: a general linear approach". In: *Hum. Brain Mapp.* 2.4, pp. 189–210.

Fritz, S. L., K. E. Light, T. S. Patterson, A. L. Behrman, and S. B. Davis (2005). "Active finger extension predicts outcomes after constraint-induced movement therapy for individuals with hemiparesis after stroke." In: *Stroke* 36.6, pp. 1172–1177.

Froc, D. J., C. A. Chapman, C. Trepel, and R. J. Racine (2000). "Long-term depression and depotentiation in the sensorimotor cortex of the freely moving rat." In: *J. Neurosci.* 20.1, pp. 438–445.

Frost, S. B., S. Barbay, K. M. Friel, E. J. Plautz, and R. J. Nudo (2003). "Reorganization of remote cortical regions after ischemic brain injury: a potential substrate for stroke recovery." In: *J. Neurophysiol.* 89.6, pp. 3205–3214.

Fujimoto, K., J. R. Polimeni, A. J. W. van der Kouwe, M. Reuter, T. Kober, T. Benner, B. Fischl, and L. L. Wald (2014). "Quantitative comparison of cortical

surface reconstructions from MP2RAGE and multi-echo MPRAGE data at 3 and 7 T." In: *NeuroImage* 90, pp. 60–73.

Garraghty, P. E. and N. Muja (1996). "NMDA receptors and plasticity in adult primate somatosensory cortex." In: *J. Comp. Neurol.* 367.2, pp. 319–326.

Gati, J. S., R. S. Menon, K. Ugurbil, and B. K. Rutt (1997). "Experimental determination of the BOLD field strength dependence in vessels and tissue." In: *Magn. Reson. Med.* 38.2, pp. 296–302.

Geiger, J. R. P. and P. Jonas (2000). "Dynamic Control of Presynaptic Ca2+ Inflow by Fast-Inactivating K+ Channels in Hippocampal Mossy Fiber Boutons". In: *Neuron* 28.3, pp. 927–939.

Gelnar, P. A., B. R. Krauss, N. M. Szeverenyi, and A. V. Apkarian (1998). "Fingertip Representation in the Human Somatosensory Cortex: An fMRI Study". In: *NeuroImage* 7.4, pp. 261–283.

Genovese, C. R., N. A. Lazar, and T. Nichols (2002). "Thresholding of statistical maps in functional neuroimaging using the false discovery rate." In: *NeuroImage* 15.4, pp. 870–878.

Geppert, M., Y. Goda, R. E. Hammer, C. Li, T. W. Rosahl, C. F. Stevens, and T. C. Südhof (1994). "Synaptotagmin I: a major Ca2+ sensor for transmitter release at a central synapse." In: *Cell* 79.4, pp. 717–727.

Gerloff, C. (1997). "Stimulation over the human supplementary motor area interferes with the organization of future elements in complex motor sequences". In: *Brain* 120.9, pp. 1587–1602.

González, R. G., J. A. Hirsch, M. H. Lev, P. W. Schaefer, and L. H. Schwamm (2010). "Acute Ischemic Stroke". In: *Imaging and Intervention*. Springer, p. 310.

Good, C. D., I. Johnsrude, J. Ashburner, R. N. Henson, K. J. Friston, and R. S. J. Frackowiak (2001). "Cerebral asymmetry and the effects of sex and handedness on brain structure: a voxel-based morphometric analysis of 465 normal adult human brains." In: *NeuroImage* 14.3, pp. 685–700.

Gountouna, V.-E., D. E. Job, A. M. McIntosh, T. W. J. Moorhead, G. K. L. Lymer, H. C. Whalley, J. Hall, G. D. Waiter, D. Brennan, D. J. McGonigle, T. S. Ahearn, J. Cavanagh, B. Condon, D. M. Hadley, I. Marshall, A. D. Murray, J. D. Steele, J. M. Wardlaw, and S. M. Lawrie (2010). "Functional Magnetic Resonance Imaging (fMRI) reproducibility and variance components across visits and scanning sites with a finger tapping task." In: *NeuroImage* 49.1, pp. 552–560.

Granert, O., M. Peller, C. Gaser, S. Groppa, M. Hallett, A. Knutzen, G. Deuschl, K. E. Zeuner, and H. R. Siebner (2011). "Manual activity shapes structure and function in contralateral human motor hand area." In: *NeuroImage* 54.1, pp. 32–41.

Gray, H. (1918). *Anatomy of the Human Body*. Lea & Febiger. Philadelphia and New York.

Grefkes, C., S. Geyer, T. Schormann, P. Roland, and K. Zilles (2001). "Human somatosensory area 2: observer-independent cytoarchitectonic mapping, interindividual variability, and population map." In: *NeuroImage* 14.3, pp. 617–631.

Grefkes, C., D. A. Nowak, S. B. Eickhoff, M. Dafotakis, J. Küst, H. Karbe, and G. R. Fink (2008). "Cortical connectivity after subcortical stroke assessed with functional magnetic resonance imaging." In: *Ann Neurol.* 63.2, pp. 236–246.

Greve, D. N. and B. Fischl (2009). "Accurate and robust brain image alignment using boundary-based registration". In: *NeuroImage* 48.1, pp. 63–72.

Grill-Spector, K. and R. Malach (2004). "The human visual cortex." In: *Annu. Rev. Neurosci.* 27, pp. 649–677.

Gross, J., L. Timmermann, J. Kujala, M. Dirks, F. Schmitz, R. Salmelin, and A. Schnitzler (2002). "The neural basis of intermittent motor control in humans." In: *Proc. Natl. Acad. Sci. U.S.A.* 99.4, pp. 2299–2302.

Gwilym, S. E., H. C. L. Oag, I. Tracey, and A. J. Carr (2011). "Evidence that central sensitisation is present in patients with shoulder impingement syndrome and influences the outcome after surgery." In: *J Bone Joint Surg Br* 93.4, pp. 498–502.

Hahn, E. (1950). "Spin Echoes". In: *Phys. Rev.* 80.4, pp. 580–594.

Hajnal, J. V., M. Doran, A. S. Hall, A. G. Collins, A. Oatridge, J. M. Pennock, I. R. Young, and G. M. Bydder (1991). "MR imaging of anisotropically restricted diffusion of water in the nervous system: technical, anatomic, and pathologic considerations." In: *J Comput Assist Tomogr* 15.1, pp. 1–18.

Hashman Hashemi, R., W. G. Bradley, and C. J. Lisanti (2010). *MRI: The Basics*. 3rd ed. Philadelphia: Wolters Kluwer Health.

Hebb, D. O. (1949). *The Organization of Behaviour*. New York: John Wiley and Sons Inc.

Hess, G. and J. P. Donoghue (1994). "Long-term potentiation of horizontal connections provides a mechanism to reorganize cortical motor maps." In: *J. Neurophysiol.* 71.6, pp. 2543–2547.

Heuvel, M. P. van den and H. E. Hulshoff Pol (2010). "Exploring the brain network: a review on resting-state fMRI functional connectivity." In: *Eur Neuropsychopharmacol* 20.8, pp. 519–534.

Hicks, T. P., R. Metherate, P. Landry, and R. W. Dykes (1986). "Bicuculline-induced alterations of response properties in functionally identified ventroposterior thalamic neurones." In: *Exp Brain Res* 63.2, pp. 248–264.

Hoogenraad, F. G., P. J. Pouwels, M. B. Hofman, J. R. Reichenbach, M. Sprenger, and E. M. Haacke (2001). "Quantitative differentiation between BOLD models in fMRI." In: *Magn. Reson. Med.* 45.2, pp. 233–246.

Hoover, J. E. and P. L. Strick (1999). "The organization of cerebellar and basal ganglia outputs to primary motor cortex as revealed by retrograde transneuronal transport of herpes simplex virus type 1." In: *J. Neurosci.* 19.4, pp. 1446–1463.

Hoshi, E. and J. Tanji (2000). "Integration of target and body-part information in the premotor cortex when planning action." In: *Nature* 408.6811, pp. 466–470.

Hoshi, E. and J. Tanji (2007). "Distinctions between dorsal and ventral premotor areas: anatomical connectivity and functional properties". In: *Curr. Opin. Neurobiol.* 17.2, pp. 234–242.

Hossmann, K.-A. (2012). "The two pathophysiologies of focal brain ischemia: implications for translational stroke research." In: *J. Cereb. Blood Flow Metab.* 32.7, pp. 1310–1316.

Huang, R.-S. and M. I. Sereno (2007). "Dodecapus: An MR-compatible system for somatosensory stimulation." In: *NeuroImage* 34.3, pp. 1060–1073.

Huber, W., J. G. Hofstaetter, B. Hanslik-Schnabel, M. Posch, and C. Wurnig (2004). "The German version of the Oxford Shoulder Score–cross-cultural adaptation and validation." In: *Arch Orthop Trauma Surg* 124.8, pp. 531–536.

Huffman, K. J. and L. Krubitzer (2001). "Area 3a: topographic organization and cortical connections in marmoset monkeys." In: *Cereb. Cortex* 11.9, pp. 849–867.

Hummel, F. C. and L. G. Cohen (2006). "Non-invasive brain stimulation: a new strategy to improve neurorehabilitation after stroke?" In: *Lancet Neurol* 5.8, pp. 708–712.

Huntley, G. (1997). "Correlation between patterns of horizontal connectivity and the extend of short-term representational plasticity in rat motor cortex". In: *Cerebral Cortex* 7.2, pp. 143–156.

Iadecola, C. and M. Nedergaard (2007). "Glial regulation of the cerebral microvasculature". In: *Nat. Neurosci.* 10.11, pp. 1369–1376.

*International Electrotechnical Commission* (2002). Tech. rep. Medical electrical equipment- Part 2–33: Particular requirements for the safety of magnetic resonance equipment for medical diagnosis. 60601- 2-33.

Iriki, A., C. Pavlides, A. Keller, and H. Asanuma (1989). "Long-term potentiation in the motor cortex." In: *Science* 245.4924, pp. 1385–1387.

Ito, M. (1989). "Long-term depression." In: *Annu. Rev. Neurosci.* 12, pp. 85–102.

Jablonka, J. A., O. W. Witte, and M. Kossut (2007). "Photothrombotic infarct impairs experience-dependent plasticity in neighboring cortex." In: *Neuroreport* 18.2, pp. 165–169.

Jack, C. R., R. M. Thompson, R. K. Butts, F. W. Sharbrough, P. J. Kelly, D. P. Hanson, S. J. Riederer, R. L. Ehman, N. J. Hangiandreou, and G. D. Cascino (1994). "Sensory motor cortex: correlation of presurgical mapping with functional MR imaging and invasive cortical mapping." In: *Radiology* 190.1, pp. 85–92.

Jahanshahi, M., I. H. Jenkins, R. G. Brown, C. D. Marsden, R. E. Passingham, and D. J. Brooks (1995). "Self-initiated versus externally triggered movements". In: *Brain* 118.4, pp. 913–933.

James, W. (1890). *The principles of psychology*. New York: Holt.

Jayaram, G., C. J. Stagg, P. Esser, U. Kischka, J. Stinear, and H. Johansen-Berg (2012). "Relationships between functional and structural corticospinal tract integrity and walking post stroke". In: *Clinical Neurophysiology* 123.12, pp. 2422–2428.

Jenkinson, M. and S. Smith (2001). "A global optimisation method for robust affine registration of brain images." In: *Med Image Anal* 5.2, pp. 143–156.

Jenkinson, M., P. R. Bannister, M. Brady, and S. Smith (2002). "Improved Optimization for the Robust and Accurate Linear Registration and Motion Correction of Brain Images". In: *NeuroImage* 17.2, pp. 825–841.

Jenkinson, M., C. F. Beckmann, T. E. J. Behrens, M. W. Woolrich, and S. M. Smith (2012). "FSL." In: *NeuroImage* 62.2, pp. 782–790.

Jezzard, P., P. M. Matthews, and S. M. Smith (2001). *Functional Magnetic Resonance Imaging*. An Introduction to Methods. Oxford: Oxford University Press.

Johansen-Berg, H., C. S. Baptista, and A. G. Thomas (2012). "Human Structural Plasticity at Record Speed". In: *Neuron* 73.6, pp. 1058–1060.

Johansen-Berg, H. and T. E. J. Behrens (2009). "Diffusion MRI: From quantitative measurement to in-vivo neuroanatomy". In:

Johansen-Berg, H., T. E. J. Behrens, M. D. Robson, I. Drobnjak, M. F. S. Rushworth, J. M. Brady, S. M. Smith, D. J. Higham, and P. M. Matthews (2004). "Changes in connectivity profiles define functionally distinct regions in human medial frontal cortex." In: *Proc. Natl. Acad. Sci. U.S.A.* 101.36, pp. 13335–13340.

Johansen-Berg, H., V. Christensen, M. Woolrich, and P. M. Matthews (2000). "Attention to touch modulates activity in both primary and secondary somatosensory areas." In: *Neuroreport* 11.6, pp. 1237–1241.

Johansson, R. S. and A. B. Vallbo (1979). "Tactile sensibility in the human hand: relative and absolute densities of four types of mechanoreceptive units in glabrous skin." In: *J. Physiol. (Lond.)* 286, pp. 283–300.

Jones, E. G. (1983). "Identification and classification of intrinsic circuit elements in the neocortex". In: *Dynamic aspects of neocortical function*. Ed. by G. M. Edelman, W. E. Gall, and W. M. Cowan. Chichester: Wiley, pp. 7–40.

Jones, E. G. (1984). "Laminar distribution of cortical efferent cells". In: *Cerebral cortex*. Ed. by A. Peters and E. G. Jones. New York: Plenum, pp. 521–553.

Jones, E. G. (1996). "Divergence of thalamocortical projections and limits on somatosensory cortical plasticity". In: *Somesthesis and the Neurobiology of the Somatosensory Cortex*. Ed. by O. Franzen, R. Johannsson, and L. Terenius. Basel: Birkhäuser Basel, pp. 1–15.

Jones, E. G. (2000). "Cortical and subcortical contributions to activity-dependent plasticity in primate somatosensory cortex." In: *Annu. Rev. Neurosci.* 23, pp. 1–37.

Jones, E. G., D. P. Friedman, and S. H. Hendry (1982). "Thalamic basis of place- and modality-specific columns in monkey somatosensory cortex: a correlative anatomical and physiological study." In: *J. Neurophysiol.* 48.2, pp. 545–568.

Jones, E. G. and R. Porter (1980). "What is area 3a?" In: *Brain Res.* 203.1, pp. 1–43.

Jones, E. G. and S. P. Wise (1977). "Size, laminar and columnar distribution of efferent cells in the sensory-motor cortex of monkeys." In: *J. Comp. Neurol.* 175.4, pp. 391–438.

Jones, E. G., S. P. Wise, and J. D. Coulter (1979). "Differential thalamic relationships of sensory-motor and parietal cortical fields in monkeys." In: *J. Comp. Neurol.* 183.4, pp. 833–881.

Jørgensen, H. S., H. Nakayama, H. O. Raaschou, J. Vive-Larsen, M. Støier, and T. S. Olsen (1995). "Outcome and time course of recovery in stroke. Part I: Outcome. The Copenhagen Stroke Study." In: *Arch Phys Med Rehabil* 76.5, pp. 399–405.

Ju, W., W. Morishita, J. Tsui, G. Gaietta, T. J. Deerinck, S. R. Adams, C. C. Garner, R. Y. Tsien, M. H. Ellisman, and R. C. Malenka (2004). "Activity-dependent regulation of dendritic synthesis and trafficking of AMPA receptors." In: *Nat. Neurosci.* 7.3, pp. 244–253.

Juliano, S. L. and B. L. Whitsel (1985). "Metabolic labeling associated with index finger stimulation in monkey SI: between animal variability." In: *Brain Res.* 342.2, pp. 242–251.

Kaas, J. H. (1983). "What, if anything, is SI? Organization of first somatosensory area of cortex". In: *Physiol. Rev.* 63.1, pp. 206–231.

Kaas, J. H. (1993). "The functional organization of somatosensory cortex in primates." In: *Ann. Anat.* 175.6, pp. 509–518.

Kaas, J. H., R. J. Nelson, M. Sur, C.-S. Lin, and M. M. Merzenich (1979). "Multiple representations of the body within the primary somatosensory cortex of primates". In: *Science* 204.4392, pp. 521–523.

Kamper, D. G., H. C. Fischer, E. G. Cruz, and W. Z. Rymer (2006). "Weakness is the primary contributor to finger impairment in chronic stroke." In: *Arch Phys Med Rehabil* 87.9, pp. 1262–1269.

Kaneko, F., T. Murakami, K. Onari, H. Kurumadani, and K. Kawaguchi (2003). "Decreased cortical excitability during motor imagery after disuse of an upper limb in humans." In: *Clin Neurophysiol* 114.12, pp. 2397–2403.

Karnath, H.-O. and C. Rorden (2012). "The anatomy of spatial neglect." In: *Neuropsychologia* 50.6, pp. 1010–1017.

Karni, A., G. Meyer, C. Rey-Hipolito, P. Jezzard, M. M. Adams, R. Turner, and L. G. Ungerleider (1998). "The acquisition of skilled motor performance: fast and slow experience-driven changes in primary motor cortex." In: *Proc. Natl. Acad. Sci. U.S.A.* 95.3, pp. 861–868.

Khair, M. M. and L. V. Gulotta (2011). "Treatment of irreparable rotator cuff tears". In: *Curr Rev Musculoskelet Med* 4.4, pp. 208–213.

Kim, S. W., J. K. Shim, V. M. Zatsiorsky, and M. L. Latash (2008). "Finger interdependence: linking the kinetic and kinematic variables." In: *Hum Mov Sci* 27.3, pp. 408–422.

Kirkwood, A., S. M. Dudek, J. T. Gold, C. D. Aizenman, and M. F. Bear (1993). "Common Forms of Synaptic Plasticity in the Hippocampus and Neocortex in Vitro". In: *Science* 260.5113, pp. 1518–1521.

Kirkwood, A., A. Silva, and M. F. Bear (1997). "Age-dependent decrease of synaptic plasticity in the neocortex of alphaCaMKII mutant mice." In: *Proc. Natl. Acad. Sci. U.S.A.* 94.7, pp. 3380–3383.

Klawiter, E. C., R. E. Schmidt, K. Trinkaus, H.-F. Liang, M. D. Budde, R. T. Naismith, S.-K. Song, A. H. Cross, and T. L. Benzinger (2011). "Radial diffusivity predicts demyelination in ex vivo multiple sclerosis spinal cords". In: *NeuroImage* 55.4, pp. 1454–1460.

Koch, S. P., C. Habermehl, J. Mehnert, C. H. Schmitz, S. Holtze, A. Villringer, J. Steinbrink, and H. Obrig (2010). "High-resolution optical functional mapping of the human somatosensory cortex." In: *Front Neuroenergetics* 2, p. 12.

Krainik, A., S. Lehericy, H. Duffau, M. Vlaicu, F. Poupon, L. Capelle, P. Cornu, S. Clemenceau, M. Sahel, C. A. Valery, A. L. Boch, J. F. Mangin, D. Le Bihan, and C. Marsault (2001). "Role of the supplementary motor area in motor deficit following medial frontal lobe surgery". In: *Neurology* 57.5, pp. 871–878.

Kraskov, A., N. Dancause, M. M. Quallo, S. Shepherd, and R. N. Lemon (2009). "Corticospinal Neurons in Macaque Ventral Premotor Cortex with Mirror Properties: A Potential Mechanism for Action Suppression?" In: *Neuron* 64.6, pp. 922–930.

Kringelbach, M. L. (2005). "The human orbitofrontal cortex: linking reward to hedonic experience." In: *Nat Rev Neurosci* 6.9, pp. 691–702.

Kringelbach, M. L. and E. T. Rolls (2004). "The functional neuroanatomy of the human orbitofrontal cortex: evidence from neuroimaging and neuropsychology." In: *Progress in Neurobiology* 72.5, pp. 341–372.

Kristo, G., G.-J. Rutten, M. Raemaekers, B. de Gelder, S. A. R. B. Rombouts, and N. F. Ramsey (2014). "Task and task-free FMRI reproducibility comparison for motor network identification." In: *Hum. Brain Mapp.* 35.1, pp. 340–352.

Kumar, V., A. K. Abbas, N. Fausto, and J. C. Aster (2009). *Robbins & Cotran Pathologic Basis of Disease,* Philadelphia: Elsevier.

Kwakkel, G. and B. Kollen (2007). "Predicting improvement in the upper paretic limb after stroke: a longitudinal prospective study." In: *Restor. Neurol. Neurosci.* 25.5-6, pp. 453–460.

Kwakkel, G., B. J. Kollen, J. van der Grond, and A. J. H. Prevo (2003). "Probability of regaining dexterity in the flaccid upper limb: impact of severity of paresis and time since onset in acute stroke." In: *Stroke* 34.9, pp. 2181–2186.

Kwan, H. C., W. A. MacKay, J. T. Murphy, and Y. C. Wong (1978). "Spatial organization of precentral cortex in awake primates. II. Motor outputs." In: *J. Neurophysiol.* 41.5, pp. 1120–1131.

Lachnit, H. and W. Pieper (1990). "Speed and accuracy effects of fingers and dexterity in 5-choice reaction tasks." In: *Ergonomics* 33.12, pp. 1443–1454.

Lai, S., A. L. Hopkins, E. M. Haacke, D. Li, B. A. Wasserman, P. Buckley, L. Friedman, H. Meltzer, P. Hedera, and R. Friedland (1993). "Identification of vascular structures as a major source of signal contrast in high resolution 2D and 3D functional activation imaging of the motor cortex at 1.5T: preliminary results." In: *Magn. Reson. Med.* 30.3, pp. 387–392.

Laible, M., S. Grieshammer, G. Seidel, M. Rijntjes, C. Weiller, and F. Hamzei (2012). "Association of activity changes in the primary sensory cortex with successful motor rehabilitation of the hand following stroke." In: *Neurorehabilitation and Neural Repair* 26.7, pp. 881–888.

Langer, N., J. Hanggi, N. A. Muller, H. P. Simmen, and L. Jancke (2012). "Effects of limb immobilization on brain plasticity." In: *Neurology* 78.3, pp. 182–188.

Langhorne, P., F. Coupar, and A. Pollock (2009). "Motor recovery after stroke: a systematic review." In: *Lancet Neurol* 8.8, pp. 741–754.

Laplane, D., J. Talairach, V. Meininger, J. Bancaud, and J. M. Orgogozo (1977). "Clinical consequences of corticectomies involving the supplementary motor area in man." In: *Journal of the Neurological Sciences* 34.3, pp. 301–314.

Latash, M. L. (2010). "Stages in learning motor synergies: a view based on the equilibrium-point hypothesis." In: *Hum Mov Sci* 29.5, pp. 642–654.

Le Bihan, D. and H. Johansen-Berg (2012). "Diffusion MRI at 25: Exploring brain tissue structure and function". In: *NeuroImage* 61.2, pp. 324–341.

Le Bihan, D., R. Turner, and P. Douek (1993). "Is water diffusion restricted in human brain white matter? An echo-planar NMR imaging study." In: *Neuroreport* 4.7, pp. 887–890.

Leakey, L. S., P. V. Tobias, and J. R. Napier (1964). "A new species of the genus homo from Olduvai Gorge". In: *Nature* 202, pp. 7–9.

Leakey, M. D. (1981). "Tracks and Tools". In: *Philos. Trans. R. Soc. Lond., B, Biol. Sci.* 292.1057, pp. 95–102.

Lee, C. C., C. R. Jack, and S. J. Riederer (1998). "Mapping of the central sulcus with functional MR: active versus passive activation tasks." In: *AJNR* 19.5, pp. 847–852.

Levin, M. F., J. A. Kleim, and S. L. Wolf (2009). "What do motor "recovery" and "compensation" mean in patients following stroke?" In: *Neurorehabilitation and Neural Repair* 23.4, pp. 313–319.

Li, Z.-M., S. Dun, D. A. Harkness, and T. L. Brininger (2004). "Motion enslaving among multiple fingers of the human hand." In: *Motor Control* 8.1, pp. 1–15.

Lin, W., K. Kuppusamy, E. M. Haacke, and H. Burton (1996). "Functional MRI in human somatosensory cortex activated by touching textured surfaces." In: *J Magn Reson Imaging* 6.4, pp. 565–572.

Lisman, J. E., S. Raghavachari, and R. W. Tsien (2007). "The sequence of events that underlie quantal transmission at central glutamatergic synapses." In: *Nat Rev Neurosci* 8.8, pp. 597–609.

Lisman, J. E. and A. M. Zhabotinsky (2001). "A model of synaptic memory: a CaMKII/PP1 switch that potentiates transmission by organizing an AMPA receptor anchoring assembly." In: *Neuron* 31.2, pp. 191–201.

Lo, E. H., M. A. Moskowitz, and T. P. Jacobs (2005). "Exciting, radical, suicidal: how brain cells die after stroke." In: *Stroke* 36.2, pp. 189–192.

Lømo, T. (1966). "Frequency potentiation of excitatory synaptic activity in the dentate area of the hippocampal formation". In: *Acta physiol scand* 68 (suppl. 277), p. 128.

Lu, H. and E. A. Stein (2014). "Resting state functional connectivity: its physiological basis and application in neuropharmacology." In: *Neuropharmacology* 84, pp. 79–89.

Luppino, G., M. Matelli, R. Camarda, and G. Rizzolatti (1993). "Corticocortical connections of area F3 (SMA-proper) and area F6 (pre-SMA) in the macaque monkey." In: *J. Comp. Neurol.* 338.1, pp. 114–140.

Lüscher, C., R. A. Nicoll, R. C. Malenka, and D. Muller (2000). "Synaptic plasticity and dynamic modulation of the postsynaptic membrane." In: *Nat. Neurosci.* 3.6, pp. 545–550.

Lynch, J. C., J. E. Hoover, and P. L. Strick (1994). "Input to the primate frontal eye field from the substantia nigra, superior colliculus, and dentate nucleus demonstrated by transneuronal transport." In: *Exp Brain Res* 100.1, pp. 181–186.

Lynch, P. and C. Jaffe. *Brain human lateral medial view.* Creative Commons Attribution 2.5 License.

MacNeilage, P. F., L. J. Rogers, and G. Vallortigara (2009). "Origins of the left & right brain". In: *Scientific American* 301.1, pp. 60–67.

Maendly, R., D. G. Rüegg, M. Wiesendanger, R. Wiesendanger, J. Lagowska, and B. Hess (1981). "Thalamic relay for group I muscle afferents of forelimb nerves in the monkey." In: *J. Neurophysiol.* 46.5, pp. 901–917.

Maguire, E. A., D. G. Gadian, I. S. Johnsrude, C. D. Good, J. Ashburner, R. S. J. Frackowiak, and C. D. Frith (2000). "Navigation-related structural change in the hippocampi of taxi drivers." In: *Proc. Natl. Acad. Sci. U.S.A.* 97.8, pp. 4398–4403.

Makin, T. R., J. Scholz, N. Filippini, D. Henderson Slater, I. Tracey, and H. Johansen-Berg (2013). "Phantom pain is associated with preserved structure and function in the former hand area." In: *Nat Comms* 4, p. 1570.

Maldjian, J. A., A. Gottschalk, R. S. Patel, J. A. Detre, and D. C. Alsop (1999). "The sensory somatotopic map of the human hand demonstrated at 4 Tesla." In: *NeuroImage* 10.1, pp. 55–62.

Malenka, R. C., B. Lancaster, and R. S. Zucker (1992). "Temporal limits on the rise in postsynaptic calcium required for the induction of long-term potentiation." In: *Neuron* 9.1, pp. 121–128.

Malenka, R. C. and R. A. Nicoll (1999). "Long-term potentiation–a decade of progress?" In: *Science* 285.5435, pp. 1870–1874.

Malenka, R. C. and M. F. Bear (2004). "LTP and LTD: an embarrassment of riches." In: *Neuron* 44.1, pp. 5–21.

Malhotra, P., E. J. Coulthard, and M. Husain (2009). "Role of right posterior parietal cortex in maintaining attention to spatial locations over time". In: *Brain* 132.3, pp. 645–660.

Mansfield, P. (2013). *The Long Road to Stockholm: The Story of Magnetic Resonance Imaging - An Autobiography*. Oxford: Oxford University Press.

Marcus, D. S., J. Harwell, T. Olsen, M. Hodge, M. F. Glasser, F. Prior, M. Jenkinson, T. Laumann, S. W. Curtiss, and D. C. Van Essen (2011). "Informatics and data mining tools and strategies for the human connectome project." In: *Front Neuroinform* 5, p. 4.

Margolis, D. J., H. Lütcke, K. Schulz, F. Haiss, B. Weber, S. Kügler, M. T. Hasan, and F. Helmchen (2012). "Reorganization of cortical population activity imaged throughout long-term sensory deprivation." In: *Nat. Neurosci.* 15.11, pp. 1539–1546.

Marques, J. P., T. Kober, G. Krueger, W. van der Zwaag, P.-F. Van de Moortele, and R. Gruetter (2010). "MP2RAGE, a self bias-field corrected sequence for improved segmentation and T1-mapping at high field". In: *NeuroImage* 49.2, pp. 1271–1281.

Marshall, R. S., E. Zarahn, L. Alon, B. Minzer, R. M. Lazar, and J. W. Krakauer (2009). "Early imaging correlates of subsequent motor recovery after stroke." In: *Ann Neurol.* 65.5, pp. 596–602.

Martuzzi, R., W. van der Zwaag, J. Farthouat, R. Gruetter, and O. Blanke (2014). "Human finger somatotopy in areas 3b, 1, and 2: a 7T fMRI study using a natural stimulus." In: *Hum. Brain Mapp.* 35.1, pp. 213–226.

Matelli, M., P. Govoni, C. Galletti, D. F. Kutz, and G. Luppino (1998). "Superior area 6 afferents from the superior parietal lobule in the macaque monkey." In: *J. Comp. Neurol.* 402.3, pp. 327–352.

Matelli, M., G. Luppino, and G. Rizzolatti (1985). "Patterns of cytochrome oxidase activity in the frontal agranular cortex of the macaque monkey." In: *Behav. Brain Res.* 18.2, pp. 125–136.

Matelli, M., G. Luppino, and G. Rizzolatti (1991). "Architecture of superior and mesial area 6 and the adjacent cingulate cortex in the macaque monkey". In: *J. Comp. Neurol.* 311.4, pp. 445–462.

Matsumura, M. and K. Kubota (1979). "Cortical projection to hand-arm motor area from post-arcuate area in macaque monkeys: A histological study of retrograde transport of horseradish peroxidase". In: *Neurosci. Lett.* 11.3, pp. 241–246.

McFarland, N. R. and S. N. Haber (2002). "Thalamic relay nuclei of the basal ganglia form both reciprocal and nonreciprocal cortical connections, linking multiple frontal cortical areas." In: *J. Neurosci.* 22.18, pp. 8117–8132.

McKenzie, A. L., S. S. Nagarajan, T. P. L. Roberts, M. M. Merzenich, and N. N. Byl (2003). "Somatosensory Representation of the Digits and Clinical Performance in Patients with Focal Hand Dystonia". In: *American Journal of Physical Medicine & Rehabilitation* 82.10, p. 737.

McKinlay, S. M. (1996). "The normal menopause transition: an overview". In: *Maturitas* 23.2, pp. 137–145.

Meier, J. D., T. N. Aflalo, S. Kastner, and M. S. A. Graziano (2008). "Complex organization of human primary motor cortex: a high-resolution fMRI study." In: *J. Neurophysiol.* 100.4, pp. 1800–1812.

Merzenich, M. M., J. H. Kaas, J. T. Wall, M. Sur, R. J. Nelson, and D. Felleman (1983). "Progression of change following median nerve section in the cortical representation

of the hand in areas 3b and 1 in adult owl and squirrel monkeys." In: *Neuroscience* 10.3, pp. 639–665.

Merzenich, M. M., R. J. Nelson, J. H. Kaas, M. P. Stryker, W. M. Jenkins, J. M. Zook, M. S. Cynader, and A. Schoppmann (1987). "Variability in hand surface representations in areas 3b and 1 in adult owl and squirrel monkeys." In: *J. Comp. Neurol.* 258.2, pp. 281–296.

Merzenich, M. M., R. J. Nelson, M. P. Stryker, M. S. Cynader, A. Schoppmann, and J. M. Zook (1984). "Somatosensory cortical map changes following digit amputation in adult monkeys." In: *J. Comp. Neurol.* 224.4, pp. 591–605.

Meunier, S., L. Garnero, A. Ducorps, L. Mazi res, S. p. Leh ricy, S. T zenas Du Montcel, B. Renault, and M. Vidailhet (2001). "Human brain mapping in dystonia reveals both endophenotypic traits and adaptive reorganization". In: *Ann Neurol.* 50.4, pp. 521–527.

Meyer, B. U., S. R richt, and C. Woiciechowsky (1998). "Topography of fibers in the human corpus callosum mediating interhemispheric inhibition between the motor cortices". In: *Ann Neurol.* 43.3, pp. 360–369.

Meyer, B. U., S. Röricht, H. G. von Einsiedel, F. Kruggel, and A. Weindl (1995). "Inhibitory and excitatory interhemispheric transfers between motor cortical areas in normal humans and patients with abnormalities of the corpus callosum". In: *Brain* 118.2, pp. 429–440.

Meyer, G. (1987). "Forms and spatial arrangement of neurons in the primary motor cortex of man." In: *J. Comp. Neurol.* 262.3, pp. 402–428.

Middleton, F. A. and P. L. Strick (2000). "Basal ganglia and cerebellar loops: motor and cognitive circuits." In: *Brain Res. Brain Res. Rev.* 31.2-3, pp. 236–250.

Mink, J. W. (1996). "The basal ganglia: focused selection and inhibition of competing motor programs." In: *Progress in Neurobiology* 50.4, pp. 381–425.

Mitz, A. R. and S. P. Wise (1987). "The somatotopic organization of the supplementary motor area: intracortical microstimulation mapping." In: *J. Neurosci.* 7.4, pp. 1010–1021.

Mogilner, A. (1993). "Somatosensory Cortical Plasticity in Adult Humans Revealed by Magnetoencephalography". In: *Proc. Natl. Acad. Sci. U.S.A.* 90.8, pp. 3593–3597.

Mogilner, A., J. A. Grossman, U. Ribary, M. Joliot, J. Volkmann, D. Rapaport, R. W. Beasley, and R. R. Llinás (1993). "Somatosensory cortical plasticity in adult humans revealed by magnetoencephalography." In: *Proc. Natl. Acad. Sci. U.S.A.* 90.8, pp. 3593–3597.

Molina-Luna, K., B. Hertler, M. M. Buitrago, and A. R. Luft (2008). "Motor learning transiently changes cortical somatotopy." In: *NeuroImage* 40.4, pp. 1748–1754.

Monfils, M.-H., P. M. VandenBerg, J. A. Kleim, and G. C. Teskey (2004). "Long-term potentiation induces expanded movement representations and dendritic hypertrophy in layer V of rat sensorimotor neocortex." In: *Cereb. Cortex* 14.5, pp. 586–593.

Moon, S.-K., M. Alaverdashvili, A. R. Cross, and I. Q. Whishaw (2009). "Both compensation and recovery of skilled reaching following small photothrombotic stroke to motor cortex in the rat." In: *Exp. Neurol.* 218.1, pp. 145–153.

Moore, C. I., C. E. Stern, S. Corkin, B. Fischl, A. C. Gray, B. R. Rosen, and A. M. Dale (2000). "Segregation of somatosensory activation in the human rolandic cortex using fMRI." In: *J. Neurophysiol.* 84.1, pp. 558–569.

Mori, S., K. Oishi, H. Jiang, L. Jiang, X. Li, K. Akhter, K. Hua, A. V. Faria, A. Mahmood, R. Woods, A. W. Toga, G. B. Pike, P. R. Neto, A. C. Evans, J. Zhang, H. Huang, M. I. Miller, P. C. M. van Zijl, and J. Mazziotta (2008). "Stereotaxic white matter atlas based on diffusion tensor imaging in an ICBM template." In: *NeuroImage* 40.2, pp. 570–582.

Morris, D. M., G. Uswatte, J. E. Crago, E. W. Cook, and E. Taub (2001). "The reliability of the wolf motor function test for assessing upper extremity function after stroke." In: *Arch Phys Med Rehabil* 82.6, pp. 750–755.

Moseley, M. E., Y. Cohen, J. Kucharczyk, J. Mintorovitch, H. S. Asgari, M. F. Wendland, J. Tsuruda, and D. Norman (1990). "Diffusion-weighted MR imaging of anisotropic water diffusion in cat central nervous system." In: *Radiology* 176.2, pp. 439–445.

Mountcastle, V. B. (2005). *The Sensory Hand*. Neural Mechanisms of Somatic Sensation. Harvard University Press.

Mountcastle, V. B., J. C. Lynch, A. P. Georgopoulos, H. Sakata, and C. Acuna (1975). "Posterior parietal association cortex of the monkey: command functions for operations within extrapersonal space." In: *J. Neurophysiol.* 38.4, pp. 871–908.

Muakkassa, K. F. and P. L. Strick (1979). "Frontal lobe inputs to primate motor cortex: evidence for four somatotopically organized 'premotor' areas." In: *Brain Res.* 177.1, pp. 176–182.

Mugler, J. P. and J. R. Brookeman (1990). "Three-dimensional magnetization-prepared rapid gradient-echo imaging (3D MP RAGE)." In: *Magn. Reson. Med.* 15.1, pp. 152–157.

Murphy, T. H. and D. Corbett (2009). "Plasticity during stroke recovery: from synapse to behaviour". In: *Nat Rev Neurosci* 10.12, pp. 861–872.

Murray, E. A. and J. D. Coulter (1981). "Organization of corticospinal neurons in the monkey." In: *J. Comp. Neurol.* 195.2, pp. 339–365.

Nachev, P., C. Kennard, and M. Husain (2008). "Functional role of the supplementary and pre-supplementary motor areas." In: *Nat Rev Neurosci* 9.11, pp. 856–869.

Nava, E. and B. Röder (2011). "Adaptation and maladaptation insights from brain plasticity." In: *Prog. Brain Res.* 191, pp. 177–194.

Nelson, A. J. and R. Chen (2008). "Digit somatotopy within cortical areas of the postcentral gyrus in humans." In: *Cerebral Cortex* 18.10, pp. 2341–2351.

Nelson, R. J. and J. H. Kaas (1981). "Connections of the ventroposterior nucleus of the thalamus with the body surface representations in cortical areas 3b and 1 of the cynomolgus macaque, (Macaca fascicularis)." In: *J. Comp. Neurol.* 199.1, pp. 29–64.

Nelson, R. J., M. Sur, D. Felleman, and J. H. Kaas (1980). "Representations of the body surface in postcentral parietal cortex of Macaca fascicularis." In: *J. Comp. Neurol.* 192.4, pp. 611–643.

Neri, B. R., K. W. Chan, and Y. W. Kwon (2009). "Management of massive and irreparable rotator cuff tears." In: *J Shoulder Elbow Surg* 18.5, pp. 808–818.

Nichols, T. E. and A. P. Holmes (2002). "Nonparametric permutation tests for functional neuroimaging: a primer with examples." In: *Hum. Brain Mapp.* 15.1, pp. 1–25.

Nudo, R. J. and R. B. Masterton (1990). "Descending pathways to the spinal cord, III: Sites of origin of the corticospinal tract." In: *J. Comp. Neurol.* 296.4, pp. 559–583.

Nudo, R. J., G. W. G. Milliken, W. M. W. Jenkins, and M. M. Merzenich (1996). "Use-dependent alterations of movement representations in primary motor cortex of adult squirrel monkeys." In: *J. Neurosci.* 16.2, pp. 785–807.

Nudo, R. J., E. J. Plautz, and S. B. Frost (2001). "Role of adaptive plasticity in recovery of function after damage to motor cortex." In: *Muscle Nerve* 24.8, pp. 1000–1019.

O'Doherty, J., M. L. Kringelbach, E. T. Rolls, J. Hornak, and C. Andrews (2001). "Abstract reward and punishment representations in the human orbitofrontal cortex." In: *Nat. Neurosci.* 4.1, pp. 95–102.

Ogawa, S., T. M. Lee, A. R. Kay, and D. W. Tank (1990). "Brain magnetic resonance imaging with contrast dependent on blood oxygenation." In: *Proc. Natl. Acad. Sci. U.S.A.* 87.24, pp. 9868–9872.

Ogawa, S., R. S. Menon, D. W. Tank, S. G. Kim, H. Merkle, J. M. Ellermann, and K. Ugurbil (1993). "Functional brain mapping by blood oxygenation level-dependent contrast magnetic resonance imaging. A comparison of signal characteristics with a biophysical model." In: *Biophys. J.* 64.3, pp. 803–812.

Oldfield, R. C. (1971). "The assessment and analysis of handedness: the Edinburgh inventory." In: *Neuropsychologia* 9.1, pp. 97–113.

Olman, C. A., K. A. Pickett, M.-P. Schallmo, and T. J. Kimberley (2011). "Selective BOLD responses to individual finger movement measured with fMRI at 3T". In: *Hum. Brain Mapp.* 33.7, pp. 1594–1606.

Olman, C. A. and E. Yacoub (2011). "High-field FMRI for human applications: an overview of spatial resolution and signal specificity." In: *Open Neuroimag J* 5, pp. 74–89.

Orgogozo, J. M. and B. Larsen (1979). "Activation of the Supplementary Motor Area During Voluntary Movement in Man Suggests It Works as a Supramotor Area". In: *Science, New Series* 206.4420, pp. 847–850.

Orlov, T., T. R. Makin, and E. Zohary (2010). "Topographic Representation of the Human Body in the Occipitotemporal Cortex". In: *Neuron* 68.3, pp. 586–600.

Ostry, D. J., M. Darainy, A. A. G. Mattar, J. Wong, and P. L. Gribble (2010). "Somatosensory plasticity and motor learning." In: *J. Neurosci.* 30.15, pp. 5384–5393.

Overduin, S. A., A. d'Avella, J. M. Carmena, and E. Bizzi (2012). "Microstimulation Activates a Handful of Muscle Synergies". In: *Neuron* 76.6, pp. 1071–1077.

Overduin, S. A. and P. Servos (2004). "Distributed digit somatotopy in primary somatosensory cortex." In: *NeuroImage* 23.2, pp. 462–472.

Park, C. h., W. H. Chang, S. H. Ohn, S. T. Kim, O. Y. Bang, A. Pascual-Leone, and Y. H. Kim (2011). "Longitudinal Changes of Resting-State Functional Connectivity During Motor Recovery After Stroke". In: *Stroke* 42.5, pp. 1357–1362.

Pascual-Leone, A., D. Nguyet, L. G. Cohen, J. P. Brasil-Neto, A. Cammarota, and M. Hallett (1995). "Modulation of muscle responses evoked by transcranial magnetic stimulation during the acquisition of new fine motor skills." In: *J. Neurophysiol.* 74.3, pp. 1037–1045.

Patel, A. T., P. W. Duncan, S. M. Lai, and S. Studenski (2000). "The relation between impairments and functional outcomes poststroke." In: *Arch Phys Med Rehabil* 81.10, pp. 1357–1363.

Paul, R. L., H. Goodman, and M. M. Merzenich (1972a). "Alterations in mechanoreceptor input to Brodmann's areas 1 and 3 of the postcentral hand area of Macaca mulatta after nerve section and regeneration." In: *Brain Res.* 39.1, pp. 1–19.

Paul, R. L., M. M. Merzenich, and H. Goodman (1972b). "Representation of slowly and rapidly adapting cutaneous mechanoreceptors of the hand in Brodmann's areas 3 and 1 of Macaca mulatta." In: *Brain Res.* 36.2, pp. 229–249.

Paulson, O. B., S. G. Hasselbalch, E. Rostrup, G. M. Knudsen, and D. Pelligrino (2009). "Cerebral blood flow response to functional activation". In: *J. Cereb. Blood Flow Metab.* 30.1, pp. 2–14.

Penfield, W. and E. Boldrey (1937). "Somatic motor and sensory representation in the cerebral cortex of man as studied by electrical stimulation". In: *Brain* 60.4, pp. 389–443.

Penfield, W. and H. H. Jasper (1954). *Epilepsy and the Functional Anatomy of the Human Brain*. Boston: Little Brown & Company.

Penfield, W. and T. Rasmussen (1950). *The Cerebral Cortex of Man*. New York: The Macmillan Company.

Penfield, W. and K. Welch (1951). "The Supplementary Motor Area of the Cerebral Cortex". In: *Arch NeurPsych* 66.3, pp. 289–317.

Petzold, G. C., K. M. Einhäupl, U. Dirnagl, and J. P. Dreier (2003). "Ischemia triggered by spreading neuronal activation is induced by endothelin-1 and hemoglobin in the subarachnoid space." In: *Ann Neurol.* 54.5, pp. 591–598.

Phillips, G. C. (1981). "Microarchitecture of the motor cortex in primates". In: *Progress in anatomy*. Ed. by R. J. Harrison. Cambridge University Press, pp. 61–94.

Pineiro, R., S. T. Pendlebury, S. Smith, D. E. Flitney, A. M. Blamire, P. Styles, and P. M. Matthews (2000). "Relating MRI changes to motor deficit after ischemic stroke by segmentation of functional motor pathways." In: *Stroke* 31.3, pp. 672–679.

Pineiro, R., S. Pendlebury, H. Johansen-Berg, and P. M. Matthews (2001). "Functional MRI detects posterior shifts in primary sensorimotor cortex activation after stroke: evidence of local adaptive reorganization?" In: *Stroke* 32.5, pp. 1134–1139.

Pipe, J. (2009). "Chapter 2: Pulse Sequences for Diffusion-weighted MRI". In: *Diffusion MRI: From Quantitative Measurement to In vivo Neuroanatomy*. Ed. by H. Johansen-Berg and T. E. J. Behrens. London: Elsevier Inc., pp. 11–35.

Poline, J.-B. and M. Brett (2012). "The general linear model and fMRI: Does love last forever?" In: *NeuroImage* 62.2, pp. 871–880.

Pomeroy, V. M., N. S. Ward, H. Johansen-Berg, P. van Vliet, J. Burridge, S. M. Hunter, R. N. Lemon, J. Rothwell, C. J. Weir, A. Wing, A. A. Walker, N. Kennedy, G. Barton, R. J. Greenwood, A. McConnachie, and FAST INdICATE Investigators (2014). "FAST INdiCATE Trial protocol. Clinical efficacy of functional strength training for upper limb motor recovery early after stroke: neural correlates and prognostic indicators." In: *Int J Stroke* 9.2, pp. 240–245.

Pons, T. P. and J. H. Kaas (1986). "Corticocortical connections of area 2 of somatosensory cortex in macaque monkeys: a correlative anatomical and electrophysiological study." In: *J. Comp. Neurol.* 248.3, pp. 313–335.

Pons, T. P., P. E. Garraghty, A. K. Ommaya, J. H. Kaas, E. Taub, and M. Mishkin (1991). "Massive Cortical Reorganization After Sensory Deafferentation in Adult Macaques". In: *Science* 252.5014, pp. 1857–1860.

Posner, M. I., J. A. Walker, F. J. Friedrich, and R. D. Rafal (1984). "Effects of parietal injury on covert orienting of attention." In: *J. Neurosci.* 4.7, pp. 1863–1874.

Poston, K. L. and D. Eidelberg (2012). "Functional brain networks and abnormal connectivity in the movement disorders". In: *NeuroImage* 62.4, pp. 2261–2270.

Powell, T. P. and V. B. Mountcastle (1959). "Some aspects of the functional organization of the cortex of the postcentral gyrus of the monkey: a correlation of findings obtained in a single unit analysis with cytoarchitecture." In: *Bull Johns Hopkins Hosp* 105, pp. 133–162.

Prabhu, G., H. Shimazu, G. Cerri, T. Brochier, R. L. Spinks, M. A. Maier, and R. N. Lemon (2009). "Modulation of primary motor cortex outputs from ventral premotor cortex during visually guided grasp in the macaque monkey." In: *J. Physiol. (Lond.)* 587.Pt 5, pp. 1057–1069.

Puce, A., R. T. Constable, M. L. Luby, G. McCarthy, A. C. Nobre, D. D. Spencer, J. C. Gore, and T. Allison (1995). "Functional magnetic resonance imaging of sensory and motor cortex: comparison with electrophysiological localization." In: *J. Neurosurg.* 83.2, pp. 262–270.

Pujol, J., G. Conesa, J. Deus, P. Vendrell, F. Isamat, G. Zannoli, J. L. Martí-Vilalta, and A. Capdevila (1996). "Presurgical identification of the primary sensorimotor cortex by functional magnetic resonance imaging." In: *J. Neurosurg.* 84.1, pp. 7–13.

Quallo, M. M., C. J. Price, K. Ueno, T. Asamizuya, K. Cheng, R. N. Lemon, and A. Iriki (2009). "Gray and white matter changes associated with tool-use learning in macaque monkeys." In: *Proc. Natl. Acad. Sci. U.S.A.* 106.43, pp. 18379–18384.

Raichle, M. E., A. M. MacLeod, A. Z. Snyder, W. J. Powers, D. A. Gusnard, and G. L. Shulman (2001). "A default mode of brain function". In: *Proc. Natl. Acad. Sci. U.S.A.* 98.2, pp. 676–682.

Recanzone, G. H., M. M. Merzenich, and H. R. Dinse (1992). "Expansion of the cortical representation of a specific skin field in primary somatosensory cortex by intracortical microstimulation." In: *Cereb. Cortex* 2.3, pp. 181–196.

Rehme, A. K., L. J. Volz, D.-L. Feis, I. Bomilcar-Focke, T. Liebig, S. B. Eickhoff, G. R. Fink, and C. Grefkes (2014). "Identifying Neuroimaging Markers of Motor Disability in Acute Stroke by Machine Learning Techniques." In: *Cereb. Cortex*.

Rengachary, J., B. J. He, G. Shulman, and M. Corbetta (2011). "A Behavioral Analysis of Spatial Neglect and its Recovery After Stroke". In: *Front. Hum. Neurosci.* 5.

Ridding, M. C. and J. C. Rothwell (1997). "Stimulus/response curves as a method of measuring motor cortical excitability in man." In: *Electroencephalogr Clin Neurophysiol* 105.5, pp. 340–344.

Rizzolatti, G. and G. Luppino (2001). "The cortical motor system." In: *Neuron* 31.6, pp. 889–901.

Rizzolatti, G., G. Luppino, and M. Matelli (1998). "The organization of the cortical motor system: new concepts." In: *Electroencephalogr Clin Neurophysiol* 106.4, pp. 283–296.

Rizzolatti, G., L. Fogassi, and V. Gallese (2002). "Motor and cognitive functions of the ventral premotor cortex." In: *Curr. Opin. Neurobiol.* 12.2, pp. 149–154.

Rockel, A. J., R. W. Hiorns, and T. P. Powell (1980). "The basic uniformity in structure of the neocortex." In: *Brain* 103.2, pp. 221–244.

Rodriguez-Raecke, R., A. Niemeier, K. Ihle, W. Ruether, and A. May (2009). "Brain gray matter decrease in chronic pain is the consequence and not the cause of pain". In: *J. Neurosci.* 29.44, pp. 13746–13750.

Rogalewski, A., A. Schneider, E. B. Ringelstein, and W.-R. Schäbitz (2006). "Toward a multimodal neuroprotective treatment of stroke." In: *Stroke* 37.4, pp. 1129–1136.

Rogers, B. P., J. D. Carew, and M. E. Meyerand (2004). "Hemispheric asymmetry in supplementary motor area connectivity during unilateral finger movements". In: *NeuroImage* 22.2, pp. 855–859.

Roland, P. E., E. Skinhøj, N. A. Lassen, and B. Larsen (1980). "Different cortical areas in man in organization of voluntary movements in extrapersonal space." In: *J. Neurophysiol.* 43.1, pp. 137–150.

Roll, R., A. Kavounoudias, F. Albert, R. Legré, A. Gay, B. Fabre, and J. P. Roll (2012). "Illusory movements prevent cortical disruption caused by immobilization." In: *NeuroImage* 62.1, pp. 510–519.

Rolls, E. T., J. O'Doherty, M. L. Kringelbach, S. T. Francis, R. Bowtell, and F. McGlone (2003a). "Representations of pleasant and painful touch in the human orbitofrontal and cingulate cortices." In: *Cereb. Cortex* 13.3, pp. 308–317.

Rolls, E. T., M. L. Kringelbach, and I. E. T. de Araujo (2003b). "Different representations of pleasant and unpleasant odours in the human brain." In: *Eur J Neurosci* 18.3, pp. 695–703.

Romani, G. L., S. J. Williamson, and L. Kaufman (1982). "Tonotopic organization of the human auditory cortex." In: *Science* 216.4552, pp. 1339–1340.

Rosenberg, N. and M. Soudry (2006). "Shoulder impairment following treatment of diaphysial fractures of humerus by functional brace." In: *Arch Orthop Trauma Surg* 126.7, pp. 437–440.

Rushworth, M. F. S., M. J. Buckley, P. M. Gough, I. H. Alexander, D. Kyriazis, K. R. McDonald, and R. E. Passingham (2005). "Attentional selection and action selection in the ventral and orbital prefrontal cortex." In: *J. Neurosci.* 25.50, pp. 11628–11636.

Rushworth, M. F. S., A. Ellison, and V. Walsh (2001). "Complementary localization and lateralization of orienting and motor attention". In: *Nat. Neurosci.* 4.6, pp. 656–661.

Sadato, N., M. L. Yonekura, A. Waki, H. Yamada, and Y. Ishii (1997). "Role of the supplementary motor area and the right premotor cortex in the coordination of bimanual finger movements." In: *J. Neurosci.* 17.24, pp. 9667–9674.

Sakamoto, T., L. L. Porter, and H. Asanuma (1987). "Long-lasting potentiation of synaptic potentials in the motor cortex produced by stimulation of the sensory cortex in the cat: a basis of motor learning." In: *Brain Res.* 413.2, pp. 360–364.

Salvolini, U. and T. Scarabino (2006). *High Field Brain MRI: Use in Clinical Practice*. Heidelberg: Springer.

Sanchez-Panchuelo, R. M., J. Besle, A. Beckett, R. Bowtell, D. Schluppeck, and S. T. Francis (2012). "Within-Digit Functional Parcellation of Brodmann Areas of the Human Primary Somatosensory Cortex Using Functional Magnetic Resonance Imaging at 7 Tesla". In: *J. Neurosci.* 32.45, pp. 15815–15822.

Sanchez-Panchuelo, R. M., S. T. Francis, R. Bowtell, and D. Schluppeck (2010). "Mapping human somatosensory cortex in individual subjects with 7T functional MRI." In: *J. Neurophysiol.* 103.5, pp. 2544–2556.

Sarkisov, S. A., I. N. Filimonoff, and N. S. Preobrashenskaya (1949). *Cytoarchitecture of the human cortex cerebri*. Moscow: Medgiz.

Sato, K., T. Nariai, Y. Tanaka, T. Maehara, N. Miyakawa, S. Sasaki, Y. Momose-Sato, and K. Ohno (2005). "Functional representation of the finger and face in the human somatosensory cortex: intraoperative intrinsic optical imaging". In: *NeuroImage* 25.4, pp. 1292–1301.

Sawaki, L., A. J. Butler, X. Leng, P. A. Wassenaar, Y. M. Mohammad, S. Blanton, K. Sathian, D. S. Nichols-Larsen, S. L. Wolf, D. C. Good, and G. F. Wittenberg (2008). "Constraint-induced movement therapy results in increased motor map area in subjects 3 to 9 months after stroke." In: *Neurorehabilitation and Neural Repair* 22.5, pp. 505–513.

Scarborough, P. (2009). "Stroke Statistics 2009". In: *British Heart Foundation Statistics Database*.

Schenck, J. F., C. L. Dumoulin, R. W. Redington, H. Y. Kressel, R. T. Elliott, and I. L. McDougall (1992). "Human exposure to 4.0-Tesla magnetic fields in a whole-body scanner." In: *Med Phys* 19.4, pp. 1089–1098.

Schieber, M. H. (2001). "Constraints on somatotopic organization in the primary motor cortex". In: *J. Neurophysiol.* 86.5, pp. 2125–2143.

Schieber, M. H. and M. Santello (2004). "Hand function: peripheral and central constraints on performance." In: *Journal of Applied Physiology* 96.6, pp. 2293–2300.

Schneggenburger, R. and E. Neher (2000). "Intracellular calcium dependence of transmitter release rates at a fast central synapse". In: *Nature* 406.6798, pp. 889–893.

Scholz, J., M. C. Klein, T. E. J. Behrens, and H. Johansen-Berg (2009). "Training induces changes in white-matter architecture." In: *Nat. Neurosci.* 12.11, pp. 1370–1371.

Schwark, H. D., C. F. Tennison, O. B. Ilyinsky, and J. L. Fuchs (1999). "Inhibitory influences on receptive field size in the dorsal column nuclei." In: *Exp Brain Res* 126.3, pp. 439–442.

Schweizer, R., D. Voit, and J. Frahm (2008). "Finger representations in human primary somatosensory cortex as revealed by high-resolution functional MRI of tactile stimulation." In: *NeuroImage* 42.1, pp. 28–35.

Schwoebel, J., H. B. Coslett, J. Bradt, R. Friedman, and C. Dileo (2002). "Pain and the body schema: effects of pain severity on mental representations of movement." In: *Neurology* 59.5, pp. 775–777.

Seelke, A. M. H., J. C. Dooley, and L. A. Krubitzer (2012). "The emergence of somatotopic maps of the body in S1 in rats: the correspondence between functional and anatomical organization." In: *PLoS ONE* 7.2, e32322.

Sens, E., U. Teschner, W. Meissner, C. Preul, R. Huonker, O. W. Witte, W. H. R. Miltner, and T. Weiss (2012). "Effects of temporary functional deafferentation on the brain, sensation, and behavior of stroke patients." In: *J. Neurosci.* 32.34, pp. 11773–11779.

Sereno, M. I., A. M. Dale, J. B. Reppas, K. K. Kwong, J. W. Belliveau, T. J. Brady, B. R. Rosen, and R. B. Tootell (1995). "Borders of multiple visual areas in humans revealed by functional magnetic resonance imaging." In: *Science* 268.5212, pp. 889–893.

Sherrington, C. S. (1889). "On Nerve-Tracts degenerating secondarily to Lesions of the Cortex Cerebri." In: *J Physiol* 10.5, pp. 429–432.

Sherrington, C. S. (1897). *A Text Book of Physiology.* Ed. by M. Foster.

Shibasaki, H., N. Sadato, H. Lyshkow, M. L. Yonekura, M. Honda, T. Nagamine, S. Suwazono, Y. Magata, A. Ikeda, M. Miyazaki, H. Fukuyama, R. Asato, and J. Konishi (1993). "Both primary motor cortex and supplementary motor area play an important role in complex finger movement". In: *Brain* 116.6, pp. 1387–1398.

Shima, K. and J. Tanji (2000). "Neuronal activity in the supplementary and presupplementary motor areas for temporal organization of multiple movements." In: *J. Neurophysiol.* 84.4, pp. 2148–2160.

Shimazu, H., M. A. Maier, G. Cerri, P. A. Kirkwood, and R. N. Lemon (2004). "Macaque ventral premotor cortex exerts powerful facilitation of motor cortex outputs to upper limb motoneurons." In: *J. Neurosci.* 24.5, pp. 1200–1211.

Shore, D. I., K. Gray, E. Spry, and C. Spence (2005). "Spatial modulation of tactile temporal-order judgments." In: *Perception* 34.10, pp. 1251–1262.

Shulman, G. L., S. V. Astafiev, D. Franke, D. L. W. Pope, A. Z. Snyder, M. P. McAvoy, and M. Corbetta (2009). "Interaction of stimulus-driven reorienting and expectation in ventral and dorsal frontoparietal and basal ganglia-cortical networks." In: *J. Neurosci.* 29.14, pp. 4392–4407.

Shulman, G. L., D. L. W. Pope, S. V. Astafiev, M. P. McAvoy, A. Z. Snyder, and M. Corbetta (2010). "Right hemisphere dominance during spatial selective attention and target detection occurs outside the dorsal frontoparietal network." In: *J. Neurosci.* 30.10, pp. 3640–3651.

Silver, M. A. and S. Kastner (2009). "Topographic maps in human frontal and parietal cortex." In: *Trends in Cognitive Sciences* 13.11, pp. 488–495.

Sloper, J. J. and T. P. Powell (1979). "An experimental electron microscopic study of afferent connections to the primate motor and somatic sensory cortices." In: *Philos. Trans. R. Soc. Lond., B, Biol. Sci.* 285.1006, pp. 199–226.

Smith, A. M., B. K. Lewis, U. E. Ruttimann, F. Q. Ye, T. M. Sinnwell, Y. Yang, J. H. Duyn, and J. A. Frank (1999). "Investigation of low frequency drift in fMRI signal." In: *NeuroImage* 9.5, pp. 526–533.

Smith, M. C. and P. Deacon (1984). "Topographical Anatomy of the Posterior Columns of the Spinal Cord in Man the Long Ascending Fibres". In: *Brain* 107.3, pp. 671–698.

Smith, S. M. (2002). "Fast robust automated brain extraction." In: *Hum. Brain Mapp.* 17.3, pp. 143–155.

Smith, S. M., C. F. Beckmann, N. Ramnani, M. W. Woolrich, P. R. Bannister, M. Jenkinson, P. M. Matthews, and D. J. McGonigle (2005). "Variability in fMRI: a re-examination of inter-session differences." In: *Hum. Brain Mapp.* 24.3, pp. 248–257.

Smith, S. M., M. Jenkinson, M. W. Woolrich, C. F. Beckmann, T. E. J. Behrens, H. Johansen-Berg, P. R. Bannister, M. De Luca, I. Drobnjak, D. E. Flitney, R. K. Niazy, J. Saunders, J. Vickers, Y. Zhang, N. De Stefano, J. M. Brady, and P. M. Matthews (2004). "Advances in functional and structural MR image analysis and implementation as FSL". In: *NeuroImage* 23, S208–S219.

Smith, S. M. and T. E. Nichols (2009). "Threshold-free cluster enhancement: addressing problems of smoothing, threshold dependence and localisation in cluster inference." In: *NeuroImage* 44.1, pp. 83–98.

Smith, S. M., D. Vidaurre, C. F. Beckmann, M. F. Glasser, M. Jenkinson, K. L. Miller, T. E. Nichols, E. C. Robinson, G. Salimi-Khorshidi, M. W. Woolrich, D. M. Barch, K. Ugurbil, and D. C. Van Essen (2013). "Functional connectomics from resting-state fMRI." In: *Trends in Cognitive Sciences* 17.12, pp. 666–682.

Smits, E., D. C. Gordon, S. Witte, D. D. Rasmusson, and P. Zarzecki (1991). "Synaptic potentials evoked by convergent somatosensory and corticocortical inputs in raccoon somatosensory cortex: substrates for plasticity." In: *J. Neurophysiol.* 66.3, pp. 688–695.

Snow, P. J., R. J. Nudo, W. Rivers, W. M. Jenkins, and M. M. Merzenich (1988). "Somatotopically inappropriate projections from thalamocortical neurons to the SI cortex of the cat demonstrated by the use of intracortical microstimulation." In: *Somatosens Res* 5.4, pp. 349–372.

Sommer, M. A. (2003). "The role of the thalamus in motor control." In: *Curr. Opin. Neurobiol.* 13.6, pp. 663–670.

Song, S.-K., S.-W. Sun, M. J. Ramsbottom, C. Chang, J. Russell, and A. H. Cross (2002). "Dysmyelination revealed through MRI as increased radial (but unchanged axial) diffusion of water." In: *NeuroImage* 17.3, pp. 1429–1436.

Song, S.-K., J. Yoshino, T. Q. Le, S.-J. Lin, S.-W. Sun, A. H. Cross, and R. C. Armstrong (2005). "Demyelination increases radial diffusivity in corpus callosum of mouse brain." In: *NeuroImage* 26.1, pp. 132–140.

Stagg, C. J., V. Bachtiar, U. Amadi, C. A. Gudberg, A. S. Ilie, C. Sampaio-Baptista, J. O'Shea, M. Woolrich, S. M. Smith, N. Filippini, J. Near, and H. Johansen-Berg (2014). "Local GABA concentration is related to network-level resting functional connectivity." In: *eLife* 3, e01465.

Starr, C. J., L. Sawaki, G. F. Wittenberg, J. H. Burdette, Y. Oshiro, A. S. Quevedo, and R. C. Coghill (2009). "Roles of the Insular Cortex in the Modulation of Pain: Insights from Brain Lesions". In: *J. Neurosci.* 29.9, pp. 2684–2694.

Stavrinou, M. L., S. Della Penna, V. Pizzella, K. Torquati, F. Cianflone, R. Franciotti, A. Bezerianos, G. L. Romani, and P. M. Rossini (2007). "Temporal dynamics of plastic changes in human primary somatosensory cortex after finger webbing." In: *Cereb. Cortex* 17.9, pp. 2134–2142.

Sterr, A., S. Shen, A. J. Szameitat, and K. A. Herron (2010). "The role of corticospinal tract damage in chronic motor recovery and neurorehabilitation: a pilot study." In: *Neurorehabilitation and Neural Repair* 24.5, pp. 413–419.

Stinear, C. (2010). "Prediction of recovery of motor function after stroke". In: *The Lancet Neurology* 9.12, pp. 1228–1232.

Stinear, C. M., P. A. Barber, P. R. Smale, J. P. Coxon, M. K. Fleming, and W. D. Byblow (2007). "Functional potential in chronic stroke patients depends on corticospinal tract integrity." In: *Brain* 130.Pt 1, pp. 170–180.

Stippich, C., R. Hofmann, D. Kapfer, E. Hempel, S. Heiland, O. Jansen, and K. Sartor (1999). "Somatotopic mapping of the human primary somatosensory cortex by fully automated tactile stimulation using functional magnetic resonance imaging". In: *Neurosci. Lett.* 277.1, pp. 25–28.

Strick, P. L. and J. B. Preston (1978). "Sorting of somatosensory afferent information in primate motor cortex." In: *Brain Res.* 156.2, pp. 364–368.

Stringer, E. A., P.-G. Qiao, R. M. Friedman, L. Holroyd, A. T. Newton, J. C. Gore, and L. Min Chen (2014). "Distinct fine-scale fMRI activation patterns of contra- and ipsilateral somatosensory areas 3b and 1 in humans." In: *Hum. Brain Mapp.*

Stringer, E. A., L. M. Chen, R. M. Friedman, J. C. Gatenby, and J. C. Gore (2011). "Differentiation of somatosensory cortices by high-resolution fMRI at 7 T." In: *NeuroImage* 54.2, pp. 1012–1020.

Südhof, T. C. (2004). "The synaptic vesicle cycle". In: *Annu. Rev. Neurosci.* 27.1, pp. 509–547.

Sur, M., R. J. Nelson, and J. H. Kaas (1982). "Representations of the body surface in cortical areas 3b and 1 of squirrel monkeys: Comparisons with other primates". In: *J. Comp. Neurol.* 211.2, pp. 177–192.

Swedenborg, E. (1672). *Three Transactions on the Cerebrum, trans by A Acton (1938).* Philadelphia: The Swedenborg Scientific Association.

Takada, M., A. Nambu, N. Hatanaka, Y. Tachibana, S. Miyachi, M. Taira, and M. Inase (2004). "Organization of prefrontal outflow toward frontal motor-related areas in macaque monkeys". In: *European Journal of Neuroscience* 19.12, pp. 3328–3342.

Tanji, J. and K. Shima (1994). "Role for supplementary motor area cells in planning several movements ahead". In: *Nature* 371.6496, pp. 413–416.

Teismann, I. K., S. Suntrup, T. Warnecke, O. Steinsträter, M. Fischer, A. Floel, E. B. Ringelstein, C. Pantev, and R. Dziewas (2011). "Cortical swallowing processing in early subacute stroke." In: *BMC Neurol* 11, p. 34.

Thach, W. T., H. P. Goodkin, and J. G. Keating (1992). "The cerebellum and the adaptive coordination of movement." In: *Annu. Rev. Neurosci.* 15, pp. 403–442.

Theysohn, J. M., O. Kraff, K. Eilers, D. Andrade, M. Gerwig, D. Timmann, F. Schmitt, M. E. Ladd, S. C. Ladd, and A. K. Bitz (2014). "Vestibular Effects of a 7 Tesla MRI Examination Compared to 1.5 T and 0 T in Healthy Volunteers". In: *PLoS ONE* 9.3, e92104.

Thiebaut de Schotten, M., F. Dell'Acqua, S. J. Forkel, A. Simmons, F. Vergani, D. G. M. Murphy, and M. Catani (2011). "A lateralized brain network for visuospatial attention." In: *Nat. Neurosci.* 14.10, pp. 1245–1246.

Thomas, A. G., S. Marrett, Z. S. Saad, D. A. Ruff, A. Martin, and P. A. Bandettini (2009). "Functional but not structural changes associated with learning: an exploration of longitudinal voxel-based morphometry (VBM)". In: *NeuroImage* 48.1, pp. 117–125.

Tomassini, V., S. Jbabdi, J. C. Klein, T. E. J. Behrens, C. Pozzilli, P. M. Matthews, M. F. S. Rushworth, and H. Johansen-Berg (2007). "Diffusion-Weighted Imaging Tractography-Based Parcellation of the Human Lateral Premotor Cortex Identifies Dorsal and Ventral Subregions with Anatomical and Functional Specializations". In: *J. Neurosci.* 27.38, pp. 10259–10269.

Tomassy, G. S., D. R. Berger, H.-H. Chen, N. Kasthuri, K. J. Hayworth, A. Vercelli, H. S. Seung, J. W. Lichtman, and P. Arlotta (2014). "Distinct profiles of myelin distribution along single axons of pyramidal neurons in the neocortex." In: *Science* 344.6181, pp. 319–324.

Torres-Russotto, D. and J. S. Perlmutter (2008). "Focal dystonias of the hand and upper extremity." In: *J Hand Surg Am* 33.9, pp. 1657–1658.

Triantafyllou, C., R. D. Hoge, G. Krueger, C. J. Wiggins, A. Potthast, G. C. Wiggins, and L. L. Wald (2005). "Comparison of physiological noise at 1.5 T, 3 T and 7 T and optimization of fMRI acquisition parameters." In: *NeuroImage* 26.1, pp. 243–250.

Tsakiris, M., M. Costantini, and P. Haggard (2008). "The role of the right temporo-parietal junction in maintaining a coherent sense of one's body." In: *Neuropsychologia* 46.12, pp. 3014–3018.

Tuğay, U., N. Tuğay, N. Gelecek, and M. Özkan (2011). "Oxford Shoulder Score: cross-cultural adaptation and validation of the Turkish version." In: *Arch Orthop Trauma Surg* 131.5, pp. 687–694.

Turner, R., P. Jezzard, H. Wen, K. K. Kwong, D. Le Bihan, T. Zeffiro, and R. S. Balaban (1993). "Functional mapping of the human visual cortex at 4 and 1.5 tesla using deoxygenation contrast EPI." In: *Magn. Reson. Med.* 29.2, pp. 277–279.

Turrigiano, G. (2012). "Homeostatic synaptic plasticity: local and global mechanisms for stabilizing neuronal function." In: *Cold Spring Harbor Perspectives in Biology* 4.1, a005736.

Tyler, K. L. and R. Malessa (2000). "The Goltz-Ferrier debates and the triumph of cerebral localizationalist theory". In: *Neurology* 55.7, pp. 1015–1024.

Ugurbil, K., X. Hu, W. Chen, X. H. Zhu, S. G. Kim, and A. P. Georgopoulos (1999). "Functional mapping in the human brain using high magnetic fields." In: *Philos. Trans. R. Soc. Lond., B, Biol. Sci.* 354.1387, pp. 1195–1213.

Ugurbil, K. (2012). "The road to functional imaging and ultrahigh fields". In: *NeuroImage* 62.2, pp. 726–735.

*United States Food and Drug Administration* (2003). Tech. rep. Guidance for Industry and FDA Staff: Criteria for Significant Risk Investigations of Magnetic Resonance Diagnostic Devices.

Vallar, G. and D. Perani (1986). "The anatomy of unilateral neglect after right-hemisphere stroke lesions. A clinical/CT-scan correlation study in man". In: *Neuropsychologia* 24.5, pp. 609–622.

Vaughan, J. T., M. Garwood, C. M. Collins, W. Liu, L. DelaBarre, G. Adriany, P. Andersen, H. Merkle, R. Goebel, M. B. Smith, and K. Ugurbil (2001). "7T vs. 4T: RF power, homogeneity, and signal-to-noise comparison in head images." In: *Magn. Reson. Med.* 46.1, pp. 24–30.

Vaughan, T., L. DelaBarre, C. Snyder, J. Tian, C. Akgun, D. Shrivastava, W. Liu, C. Olson, G. Adriany, J. Strupp, P. Andersen, A. Gopinath, P.-F. Van de Moortele, M. Garwood, and K. Ugurbil (2006). "9.4T human MRI: preliminary results." In: *Magn. Reson. Med.* 56.6, pp. 1274–1282.

Vidoni, E. D., N. E. Acerra, E. Dao, S. K. Meehan, and L. A. Boyd (2010). "Role of the primary somatosensory cortex in motor learning: An rTMS study". In: *Neurobiology of Learning and Memory* 93.4, pp. 532–539.

Vincent, J. L., G. H. Patel, M. D. Fox, A. Z. Snyder, J. T. Baker, D. C. Van Essen, J. M. Zempel, L. H. Snyder, M. Corbetta, and M. E. Raichle (2007). "Intrinsic functional architecture in the anaesthetized monkey brain." In: *Nature* 447.7140, pp. 83–86.

Vogt, B. A. and D. N. Pandya (1978). "Cortico-cortical connections of somatic sensory cortex (areas 3, 1 and 2) in the rhesus monkey". In: *J. Comp. Neurol.* 177.2, pp. 179–191.

Vogt, C. and O. Vogt (1919). "Allgemeine Ergebnisse unserer Hirnforschung." In: *J Psychol Neurol* 25, pp. 292–398.

Vorobiev, V., P. Govoni, G. Rizzolatti, M. Matelli, and G. Luppino (1998). "Parcellation of human mesial area 6: cytoarchitectonic evidence for three separate areas". In: *Eur J Neurosci* 10.6, pp. 2199–2203.

Vossel, S., J. J. Geng, and G. R. Fink (2014). "Dorsal and ventral attention systems: distinct neural circuits but collaborative roles." In: *Neuroscientist* 20.2, pp. 150–159.

Wake, H., P. R. Lee, and R. D. Fields (2011). "Control of Local Protein Synthesis and Initial Events in Myelination by Action Potentials". In: *Science* 333.6049, pp. 1647–1651.

Waldron, J. N., S. Ghosh, and P. Zarzecki (1989). "Multiple inputs to a population of thalamocortical neurons projecting to cat somatosensory cortex." In: *Exp Brain Res* 74.1, pp. 105–115.

Walker, A. E. and T. A. Weaver (1942). "The topical organization and termination of the fibers of the posterior columns in Macaca mulatta". In: *J. Comp. Neurol.* 76.1, pp. 145–158.

Walker, A. and R. E. Leakey (1993). *The Nariokotome Homo Erectus Skeleton.* Harvard University Press.

Wallis, J. D. (2007). "Orbitofrontal cortex and its contribution to decision-making." In: *Annu. Rev. Neurosci.* 30, pp. 31–56.

Wandell, B. A., S. O. Dumoulin, and A. A. Brewer (2007). "Visual field maps in human cortex." In: *Neuron* 56.2, pp. 366–383.

Wang, C., W. Qin, J. Zhang, T. Tian, Y. Li, L. Meng, X. Zhang, and C. Yu (2014). "Altered functional organization within and between resting-state networks in chronic subcortical infarction." In: *J. Cereb. Blood Flow Metab.* 34.4, pp. 597–605.

Wang, L. E., M. Tittgemeyer, D. Imperati, S. Diekhoff, M. Ameli, G. R. Fink, and C. Grefkes (2012). "Degeneration of corpus callosum and recovery of motor function after stroke: a multimodal magnetic resonance imaging study." In: *Hum. Brain Mapp.* 33.12, pp. 2941–2956.

Wang, X., M. M. Merzenich, K. Sameshima, and W. M. Jenkins (1995). "Remodelling of hand representation in adult cortex determined by timing of tactile stimulation". In: *Nature* 378.6552, pp. 71–75.

Ward, N. S., M. M. Brown, A. J. Thompson, and R. S. J. Frackowiak (2003). "Neural correlates of outcome after stroke: a cross-sectional fMRI study." In: *Brain* 126.Pt 6, pp. 1430–1448.

Ward, N. S. and L. G. Cohen (2004). "Mechanisms underlying recovery of motor function after stroke." In: *Arch. Neurol.* 61.12, pp. 1844–1848.

Weinrich, M. and S. P. Wise (1982). "The premotor cortex of the monkey." In: *J. Neurosci.* 2.9, pp. 1329–1345.

Weinrich, M., D. C. Good, M. Reding, E. J. Roth, D. X. Cifu, K. H. Silver, R. L. Craik, J. Magaziner, M. Terrin, M. Schwartz, and L. Gerber (2004). "Timing, intensity, and duration of rehabilitation for hip fracture and stroke: report of a workshop at the National Center for Medical Rehabilitation Research." In: *Neurorehabil Neural Repair*, pp. 12–28.

Weiss, T., W. H. R. Miltner, J. Liepert, W. Meissner, and E. Taub (2004). "Rapid functional plasticity in the primary somatomotor cortex and perceptual changes after nerve block." In: *Eur J Neurosci* 20.12, pp. 3413–3423.

Weiss, T., E. Sens, U. Teschner, W. Meissner, C. Preul, O. W. Witte, and W. H. R. Miltner (2011). "Deafferentation of the affected arm: a method to improve rehabilitation?" In: *Stroke* 42.5, pp. 1363–1370.

Werk, C. M., H. S. Klein, C. E. Nesbitt, and C. A. Chapman (2006). "Long-term depression in the sensorimotor cortex induced by repeated delivery of 10 Hz trains in vivo." In: *Neuroscience* 140.1, pp. 13–20.

Werner, G. and B. L. Whitsel (1973). "Functional Organization of the Somatosensory Cortex". In: *Handbook of Sensory Physiology*. Ed. by A. Iggo. Springer Berlin Heidelberg, pp. 621–700.

Wernicke, C. (1874). *Der aphasische Symptomencomplex*. Max Cohn & Weigert.

Wheeler-Kingshott, C. A. M. and M. Cercignani (2009). "About "axial" and "radial" diffusivities." In: *Magn. Reson. Med.* 61.5, pp. 1255–1260.

Whitsel, B. L., L. M. Petrucelli, H. Ha, and D. A. Dreyer (1972a). "The resorting of spinal afferents as antecedent to the body representation in the postcentral gyrus." In: *Brain Behav Evol* 5.4, pp. 303–341.

Whitsel, B. L., L. M. Petrucelli, and G. Sapiro (1969). "Modality representation in the lumbar and cervical fasciculus gracilis of squirrel monkeys." In: *Brain Res.* 15.1, pp. 67–78.

Whitsel, B. L., J. R. Roppolo, and G. Werner (1972b). "Cortical information processing of stimulus motion on primate skin." In: *J. Neurophysiol.* 35.5, pp. 691–717.

Wiech, K., C.-s. Lin, K. H. Brodersen, U. Bingel, M. Ploner, and I. Tracey (2010). "Anterior insula integrates information about salience into perceptual decisions about pain." In: *J. Neurosci.* 30.48, pp. 16324–16331.

Winkler, A. M., G. R. Ridgway, M. A. Webster, S. M. Smith, and T. E. Nichols (2014). "Permutation inference for the general linear model". In: *NeuroImage* 92, pp. 381–397.

Winship, I. R. and T. H. Murphy (2008). "In Vivo Calcium Imaging Reveals Functional Rewiring of Single Somatosensory Neurons after Stroke". In: *J. Neurosci.* 28.26, pp. 6592–6606.

Wise, S. P. (1985). "The primate premotor cortex: past, present, and preparatory." In: *Annu. Rev. Neurosci.* 8, pp. 1–19.

Wise, S. P. (1996). "Corticospinal efferents of the supplementary sensorimotor area in relation to the primary motor area." In: *Advances in neurology* 70, pp. 57–69.

Witte, A. V., M. Savli, A. Holik, S. Kasper, and R. Lanzenberger (2010). "Regional sex differences in grey matter volume are associated with sex hormones in the young adult human brain". In: *NeuroImage* 49.2, pp. 1205–1212.

Wolf, S. L., P. A. Catlin, M. Ellis, A. L. Archer, B. Morgan, and A. Piacentino (2001). "Assessing Wolf motor function test as outcome measure for research in patients after stroke." In: *Stroke* 32.7, pp. 1635–1639.

Wolf, S. L., D. E. Lecraw, L. A. Barton, and B. B. Jann (1989). "Forced use of hemiplegic upper extremities to reverse the effect of learned nonuse among chronic stroke and head-injured patients." In: *Exp. Neurol.* 104.2, pp. 125–132.

Wolf, S. L., C. J. Winstein, J. P. Miller, E. Taub, G. Uswatte, D. Morris, C. Giuliani, K. E. Light, D. Nichols-Larsen, and EXCITE Investigators (2006). "Effect of constraint-induced movement therapy on upper extremity function 3 to 9 months after stroke: the EXCITE randomized clinical trial." In: *JAMA* 296.17, pp. 2095–2104.

Wood, C. C., D. D. Spencer, T. Allison, G. McCarthy, P. D. Williamson, and W. R. Goff (1988). "Localization of human sensorimotor cortex during surgery by cortical surface recording of somatosensory evoked potentials." In: *J. Neurosurg.* 68.1, pp. 99–111.

Woolrich, M. W., S. Jbabdi, B. Patenaude, M. Chappell, S. Makni, T. E. J. Behrens, C. F. Beckmann, M. Jenkinson, and S. M. Smith (2009). "Bayesian analysis of neuroimaging data in FSL". In: *NeuroImage* 45.S1, S173–S186.

Woolsey, C. N., P. H. Settlage, D. R. Meyer, W. Sencer, T. Pinto Hamuy, and A. M. Travis (1952). "Patterns of localization in precentral and "supplementary" motor areas and their relation to the concept of a premotor area." In: *Res Publ Assoc Res Nerv Ment Dis* 30, pp. 238–264.

Xerri, C., M. M. Merzenich, B. E. Peterson, and W. Jenkins (1998). "Plasticity of Primary Somatosensory Cortex Paralleling Sensorimotor Skill Recovery From Stroke in Adult Monkeys". In: *J. Neurophysiol.* 79.4, pp. 2119–2148.

Yacoub, E., A. Shmuel, J. Pfeuffer, P. F. Van De Moortele, G. Adriany, P. Andersen, J. T. Vaughan, H. Merkle, K. Ugurbil, and X. Hu (2001). "Imaging brain function in humans at 7 Tesla." In: *Magn. Reson. Med.* 45.4, pp. 588–594.

Yasuda, H., M. L. Barth, D. Stellwagen, and R. C. Malenka (2003). "A developmental switch in the signaling cascades for LTP induction." In: *Nat. Neurosci.* 6.1, pp. 15–16.

Yau, J. M., C. E. Connor, and S. S. Hsiao (2013). "Representation of tactile curvature in macaque somatosensory area 2." In: *J. Neurophysiol.* 109.12, pp. 2999–3012.

Yendiki, A., K. Koldewyn, S. Kakunoori, N. Kanwisher, and B. Fischl (2014). "Spurious group differences due to head motion in a diffusion MRI study". In: *NeuroImage* 88, pp. 79–90.

Yousry, T. A., U. D. Schmid, H. Alkadhi, D. Schmidt, A. Peraud, A. Buettner, and P. Winkler (1997). "Localization of the motor hand area to a knob on the precentral gyrus. A new landmark." In: *Brain* 120 ( Pt 1), pp. 141–157.

Yousry, T. A., U. D. Schmid, A. G. Jassoy, D. Schmidt, W. E. Eisner, H. J. Reulen, M. F. Reiser, and J. Lissner (1995). "Topography of the cortical motor hand area: prospective study with functional MR imaging and direct motor mapping at surgery." In: *Radiology* 195.1, pp. 23–29.

Zarzecki, P., S. Witte, E. Smits, D. C. Gordon, P. Kirchberger, and D. D. Rasmusson (1993). "Synaptic mechanisms of cortical representational plasticity: somatosensory and corticocortical EPSPs in reorganized raccoon SI cortex." In: *J. Neurophysiol.* 69.5, pp. 1422–1432.

Zatorre, R. J., R. D. Fields, and H. Johansen-Berg (2012). "Plasticity in gray and white: neuroimaging changes in brain structure during learning". In: *Nat. Neurosci.* 15.4, pp. 528–536.

Zhang, N., F. Wang, G. H. Turner, J. C. Gore, M. J. Avison, and L. M. Chen (2010). "Intra- and inter-subject variability of high field fMRI digit maps in somatosensory area 3b of new world monkeys". In: *Neuroscience* 165.1, pp. 252–264.

Zhu, L. L., R. Lindenberg, M. P. Alexander, and G. Schlaug (2010). "Lesion load of the corticospinal tract predicts motor impairment in chronic stroke." In: *Stroke* 41.5, pp. 910–915.

Zilles, K. and K. Amunts (2010). "Centenary of Brodmann's map–conception and fate." In: *Nat Rev Neurosci* 11.2, pp. 139–145.

Zwaag, W. van der, S. T. Francis, K. Head, A. Peters, P. Gowland, P. Morris, and R. Bowtell (2009). "fMRI at 1.5, 3 and 7 T: Characterising BOLD signal changes". In: *NeuroImage* 47.4, pp. 1425–1434.

Zwart, J. A. de, A. C. Silva, P. van Gelderen, P. Kellman, M. Fukunaga, R. Chu, A. P. Koretsky, J. A. Frank, and J. H. Duyn (2005). "Temporal dynamics of the BOLD fMRI impulse response." In: *NeuroImage* 24.3, pp. 667–677.

# Appendices

# A | Edinburgh Handedness Inventory

# Edinburgh Handedness Inventory[1]

Name:_____ DOB:_____

Please indicate with a check (✓) your preference in using your left or right hand in the following tasks.

Where the preference is so strong you would never use the other hand, unless absolutely forced to, put two checks (✓✓).

If you are indifferent, put one check in each column ( ✓ | ✓).

Some of the activities require both hands. In these cases, the part of the task or object for which hand preference is wanted is indicated in parentheses.

| Task / Object | Left Hand | Right Hand |
|---|---|---|
| 1. Writing | | |
| 2. Drawing | | |
| 3. Throwing | | |
| 4. Scissors | | |
| 5. Toothbrush | | |
| 6. Knife (without fork) | | |
| 7. Spoon | | |
| 8. Broom (upper hand) | | |
| 9. Striking a Match (match) | | |
| 10. Opening a Box (lid) | | |
| Total checks: | LH = | RH = |
| Cumulative Total | CT = LH + RH = | |
| Difference | D = RH – LH = | |
| Result | R = (D / CT) × 100 = | |
| Interpretation:<br>(Left Handed: R < -40)<br>(Ambidextrous: -40 ≤ R ≤ +40)<br>(Right Handed: R > +40) | | |

[1] Oldfield, R. C. (1971). The assessment and analysis of handedness: The Edinburgh inventory. *Neuropsycholoolgia*, *9*, 97-113.

# B | Oxford Shoulder Score Questionnaire

# Oxford Shoulder Score (OSS)

English version for the United Kingdom

© Isis Innovation Limited, 1998. All rights reserved.

# PROBLEMS WITH YOUR SHOULDER

Tick (✓) one box for every question.

**1. During the past 4 weeks...**

How would you describe the **worst** pain you had from your shoulder?

| None | Mild | Moderate | Severe | Unbearable |
|---|---|---|---|---|
| ☐ | ☐ | ☐ | ☐ | ☐ |

**2. During the past 4 weeks...**

Have you had any trouble dressing yourself because of your shoulder?

| No trouble at all | A little bit of trouble | Moderate trouble | Extreme difficulty | Impossible to do |
|---|---|---|---|---|
| ☐ | ☐ | ☐ | ☐ | ☐ |

**3. During the past 4 weeks...**

Have you had any trouble getting in and out of a car or using public transport because of your shoulder?

| No trouble at all | A little bit of trouble | Moderate trouble | Extreme difficulty | Impossible to do |
|---|---|---|---|---|
| ☐ | ☐ | ☐ | ☐ | ☐ |

**4. During the past 4 weeks...**

Have you been able to use a knife and fork - at the same time?

| Yes, easily | With little difficulty | With moderate difficulty | With extreme difficulty | No, impossible |
|---|---|---|---|---|
| ☐ | ☐ | ☐ | ☐ | ☐ |

**5. During the past 4 weeks...**

Could you do the household shopping on your own?

| Yes, easily | With little difficulty | With moderate difficulty | With extreme difficulty | No, impossible |
|---|---|---|---|---|
| ☐ | ☐ | ☐ | ☐ | ☐ |

**6. During the past 4 weeks...**

Could you carry a tray containing a plate of food across a room?

| Yes, easily | With little difficulty | With moderate difficulty | With extreme difficulty | No, impossible |
|---|---|---|---|---|
| ☐ | ☐ | ☐ | ☐ | ☐ |

© Isis Innovation Limited, 1998. All rights reserved. Oxford Shoulder Score – English for the United Kingdom

**7. During the past 4 weeks...**

Could you brush/comb your hair with the affected arm?

| Yes, easily | With little difficulty | With moderate difficulty | With extreme difficulty | No, impossible |
|---|---|---|---|---|
| ☐ | ☐ | ☐ | ☐ | ☐ |

**8. During the past 4 weeks...**

How would you describe the pain you usually had from your shoulder?

| None | Very mild | Mild | Moderate | Severe |
|---|---|---|---|---|
| ☐ | ☐ | ☐ | ☐ | ☐ |

**9. During the past 4 weeks...**

Could you hang your clothes up in a wardrobe, using the affected arm?

| Yes, easily | With little difficulty | With moderate difficulty | With great difficulty | No, impossible |
|---|---|---|---|---|
| ☐ | ☐ | ☐ | ☐ | ☐ |

**10. During the past 4 weeks...**

Have you been able to wash and dry yourself under both arms?

| Yes, easily | With little difficulty | With moderate difficulty | With extreme difficulty | No, impossible |
|---|---|---|---|---|
| ☐ | ☐ | ☐ | ☐ | ☐ |

**11. During the past 4 weeks...**

How much has pain from your shoulder interfered with your usual work (including housework)?

| Not at all | A little bit | Moderately | Greatly | Totally |
|---|---|---|---|---|
| ☐ | ☐ | ☐ | ☐ | ☐ |

**12. During the past 4 weeks...**

Have you been troubled by pain from your shoulder in bed at night?

| No nights | Only 1 or 2 nights | Some nights | Most nights | Every night |
|---|---|---|---|---|
| ☐ | ☐ | ☐ | ☐ | ☐ |

**Finally, please check back that you have answered each question.**
**Thank you very much.**

© Isis Innovation Limited, 1998. All rights reserved. Oxford Shoulder Score – English for the United Kingdom

# C | Brief Pain Inventory: Short Form

STUDY ID #:_____ DO NOT WRITE ABOVE THIS LINE HOSPITAL #: _____

# Brief Pain Inventory (Short Form)

Date: ____/____/____ Time: _____

Name: _____ _____ _____

Last First Middle Initial

1. Throughout our lives, most of us have had pain from time to time (such as minor headaches, sprains, and toothaches). Have you had pain other than these every-day kinds of pain today?

1. Yes 2. No

2. On the diagram, shade in the areas where you feel pain. Put an X on the area that hurts the most.

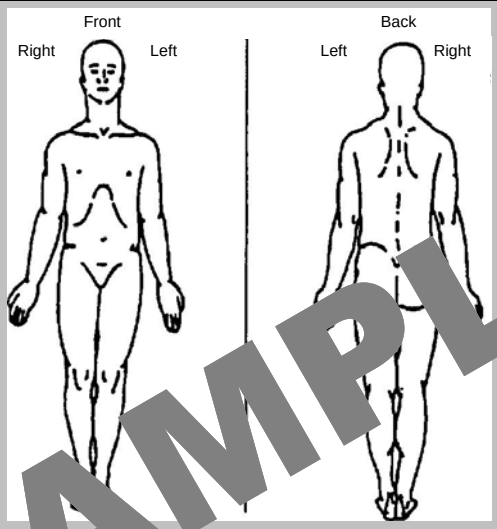


SAMPLE

3. Please rate your pain by circling the one number that best describes your pain at its worst in the last 24 hours.

| 0 | 1 | 2 | 3 | 4 | 5 | 6 | 7 | 8 | 9 | 10 |
|---|---|---|---|---|---|---|---|---|---|---|
| No Pain | | | | | | | | | | Pain as bad as you can imagine |

4. Please rate your pain by circling the one number that best describes your pain at its least in the last 24 hours.

| 0 | 1 | 2 | 3 | 4 | 5 | 6 | 7 | 8 | 9 | 10 |
|---|---|---|---|---|---|---|---|---|---|---|
| No Pain | | | | | | | | | | Pain as bad as you can imagine |

5. Please rate your pain by circling the one number that best describes your pain on the average.

| 0 | 1 | 2 | 3 | 4 | 5 | 6 | 7 | 8 | 9 | 10 |
|---|---|---|---|---|---|---|---|---|---|---|
| No Pain | | | | | | | | | | Pain as bad as you can imagine |

6. Please rate your pain by circling the one number that tells how much pain you have right now.

| 0 | 1 | 2 | 3 | 4 | 5 | 6 | 7 | 8 | 9 | 10 |
|---|---|---|---|---|---|---|---|---|---|---|
| No Pain | | | | | | | | | | Pain as bad as you can imagine |

STUDY ID #:_ _ _ _ _ _ _ _ _ _ DO NOT WRITE ABOVE THIS LINE HOSPITAL #: _ _ _ _ _ _ _ _ _ _

Date: _ _ _ _/ _ _ _ _ / _ _ _ _ Time: _ _ _ _ _ _ _ _

Name: _ _ _ _ _ _ _ _ _